Post-Variscan thermal evolution of the flanks of the southern Upper Rhine Graben: fission-track analyses and thermal modelling

Inauguraldissertation

zur

Erlangung der Würde eines Doktors der Philosophie

vorgelegt der

Philosophisch-Naturwissenschaftlichen Fakultät

der Universität Basel

von

Zoltan Timar-Geng

aus Deutschland

Basel, 2006

Genehmigt von der Philosophisch-Naturwissenschaftlichen Fakultät auf Antrag von:

Prof. Dr. A. Wetzel

Prof. Dr. B. Fügenschuh

PD Dr. Meinert Rahn

Basel, den 08.02.2005

Dekan

Acknowledgements

I am indebted to many people who have contributed to this project, in particular, my supervisor Prof. Dr. Andreas Wetzel who has been helpful in many ways from the beginning. He was one of the initiators of this research project. I would like to thank him for his careful reviews and informative discussions concerning the regional geology of the study area. I am grateful to Prof. Dr. Bernhard Fügenschuh, the co-initiator of the project, for introducing me to the subject of fission-track thermochronology and for fruitful discussions.

I would also like to thank all my friends, former and present colleagues who have helped me through the good and bad times associated with writing a PhD thesis. These include the EUCOR-URGENT team, namely Horst Dresmann, Erich Fäh, Marzio Giamboni, Kamil Ustaszewski, Pierre Dèzes, Markus Schumacher, Sebastian Hinsken, Stéphane Kock, and the other friendly people in the Bernoullianum (far too many to note by name).

A special thanks goes to Lorant Suller for his last minute review of the introductory and the conclusions parts of the thesis.

Sample preparation carried out by Laurent Cartier, Nathalie Dalcher, Johann Fleury, Jeanette Schaub, Christian Seiler and Richard Waite is greatly appreciated.

This PhD project has been supported by the Swiss National Science Foundation (Project Nos. 21-57038.99 and 20-64567.01) and carried out within the framework of the international environmental earth system dynamics research project named EUCOR-URGENT (Upper Rhine Graben: Evolution and NeoTectonics).

This thesis is dedicated in memory of Imre Timár-Geng…

Abstract

The Upper Rhine Graben (URG) is the most discernible part of the European Cenozoic rift system. Uplifted Variscan basement is exposed in the Black Forest and the Vosges and forms the flanks of the southern URG.

The impact of the Jurassic hydrothermal activity on the interpretation of fission track (FT) data from the southern URG is elaborated by means of new zircon FT analysis on samples with known U/Pb crystallisation ages. Zircon FT central ages range from 162 Ma to 247 Ma. The analysed samples experienced substantial annealing prior to Cretaceous cooling that cannot be explained by burial alone. Instead, it is suggested that circulating hydrothermal fluids with temperatures in the order of 200-250 °C are responsible for the observed thermal anomaly, which is also evidenced by vein mineralizations.

FT ages of 28 outcrop samples collected along two E-W trending transects from the Black Forest and Vosges vary from 136 Ma to 312 Ma (zircon samples) and from 20 Ma to 83 Ma (apatite samples). Broad and/or bimodal track lengths distributions indicate a complex thermal history, which was determined by inverse modelling of apatite FT parameters and tested against the observed dataset and independent geological constraints. Cooling below 120 °C in the Early Cretaceous to Palaeogene was followed by a discrete heating event during the late Eocene and subsequent cooling to surface temperature. The modelled time-temperature paths point to a total denudation of the flanks of the URG in the range of 1.0-1.7 km for a paleogeothermal gradient of 60 °C/km, and 1.3-2.2 km for a paleogeothermal gradient of 45 °C/km since the late Eocene.

Zircon and apatite FT data from four boreholes, which penetrate the Mesozoic and pre-Mesozoic sediments and crystalline basement of northern Switzerland, are also presented. Inverse thermal modelling of the apatite FT parameters reveals the low-temperature thermal history of the crystalline basement of northern Switzerland. Moderate to rapid cooling of the samples through the apatite partial annealing zone (PAZ) at the end of the Mesozoic was followed by a distinct thermal event during the Eocene and subsequent slow cooling to present-day temperatures. The Eocene heating episode coincides with the initial rifting phases of the neighbouring URG and associated volcanic activity. Crustal-scale faults of the Permo-Carboniferous Trough of northern Switzerland could have acted as major pathways for circulating hydrothermal fluids giving rise to the observed Eocene thermal event.

Table of contents

I. Introduction

by Zoltan Timar-Geng

Geological background

The Upper Rhine Graben (URG) is the most conspicuous part of a major rift system that formed in central Europe since the Cenozoic (Fig. 1). It developed by passive rifting in the foreland of the Alps in response to the build-up of compressional intraplate stresses and is an example of syn-orogenic foreland splitting (Dèzes et al., 2004). Its evolution was controlled by a repeatedly changing stress field and the reactivation of pre-existing crustal discontinuities (Schumacher, 2002).

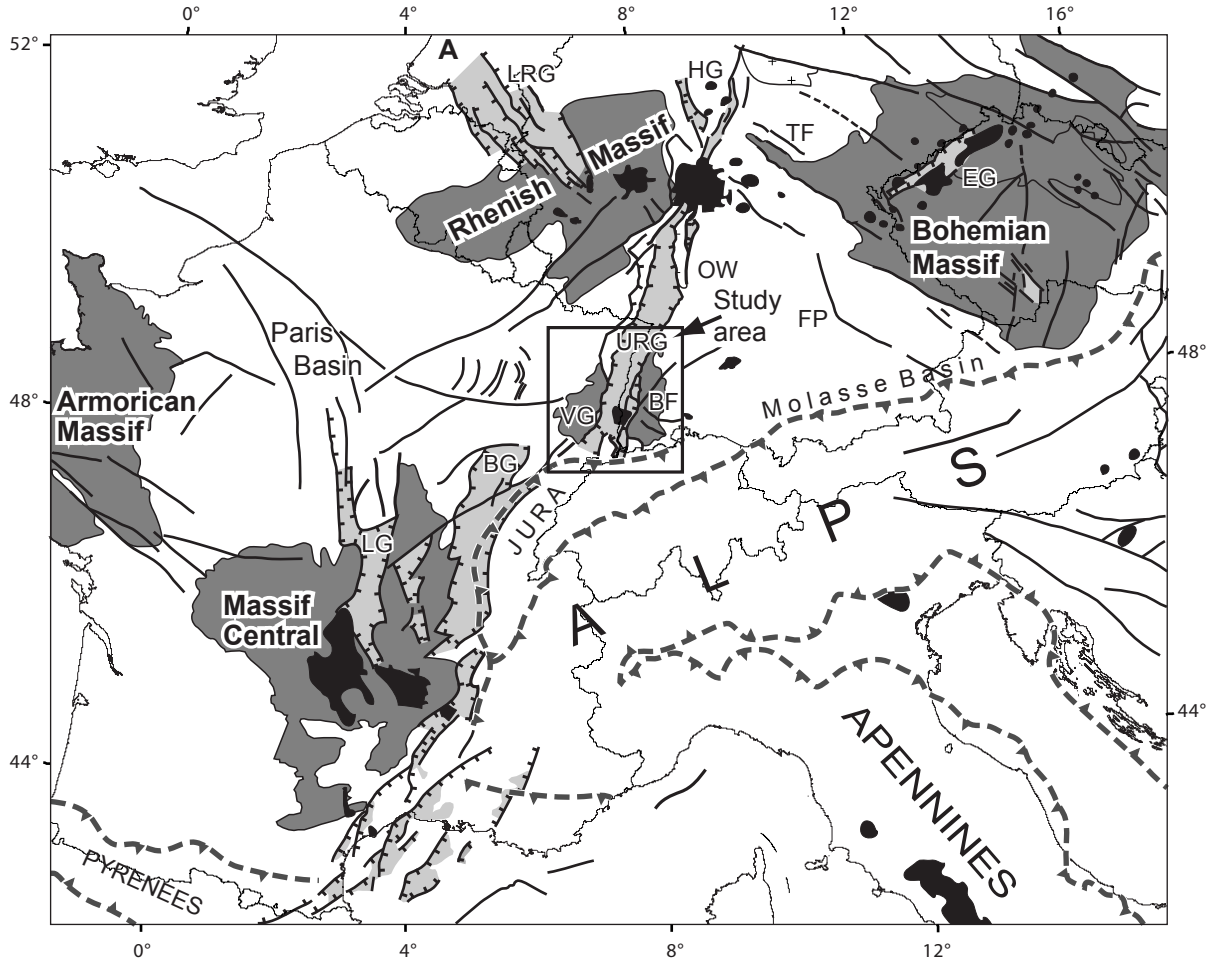

Fig. 1: *The Upper Rhine Graben as part of a major Cenozoic rift system situated in the foreland of the Alps (modified after Dèzes et al., 2004). Black lines: Cenozoic fault systems, light grey: Cenozoic rift-related sedimentary basins, dark-grey: Variscan basement outcrops, black: Cenozoic volcanic fields, dashed barbed line: Alpine deformation front, BF: Black Forest, URG: Upper Rhine Graben, VG: Vosges.*

In the last decades a great amount of geological and geophysical data has been collected evaluating the structure of the URG (e.g. Rothé and Sauer, 1967; Illies and Müller, 1970; Illies and Fuchs, 1974; Fuchs et al., 1987; Prodehl et al., 1995) and its Cenozoic development (Schumacher, 2002; Dèzes et al., 2004). Nucleation of initially separated basins started in the Middle to Late Eocene and these basins continuously merged to form the SSW-NNE striking

URG during Oligocene crustal extension (Schumacher, 2002). The Oligocene main rifting stage was contemporaneous to the northwestward propagation of the Alpine orogenic wedge into its foreland under conditions of increased collisional coupling (Schmid and Kissling, 2000; Ziegler et al., 2002). The late rifting stage is characterised by the main subsidence phase of the northern parts of the URG during the Early Miocene (Aquitanian) and uplift of the southern parts of the URG owing to lithospheric folding from the mid-Burdigalian onward (Schumacher, 2002; Dèzes et al., 2004). Ongoing neotectonic activity is clearly indicated by deformed Pliocene fluvial gravels (Giamboni et al., 2004a) and Quaternary terraces (Giamboni et al., 2004b) as well as by the well-known seismic activity as evidenced by strong historical earthquakes. Fault-plane solutions of recent earthquakes document ongoing sinistral strike-slip and oblique-slip movements in the URG as a result of NNW-SSE oriented compression (Werner and Franzke, 2001).

The onset of volcanic activity in the Paleocene (Keller et al., 2002) slightly pre-dates the initial graben formation and is contemporaneous to the onset of major Alpine crustal shortening (Schmid et al., 1996) and the initial phases of the magmatic activity of the North Atlantic Tertiary Province (Ziegler, 1990). The graben-related magmatism extending from the Middle Eocene to the Middle Miocene is characterised by rift-valley type alkaline basic magmas (Keller et al., 2002).

Much less is known about the post-Variscan, but pre-Tertiary geological history of the area, partly since most of the Mesozoic strata have been eroded. At the Permian/Triassic transition the Variscan mountain range was eroded forming a peneplained surface (Geyer and Gwinner, 1991). The subsequent Mesozoic era was characterised by relative tectonic inactivity, general subsidence and marine transgression. Almost uniform series of Triassic to Jurassic sediments were deposited discordantly on Permo-Carboniferous series or on the crystalline basement in a shallow epicontinental sea. Minor Jurassic reactivation of pre-existing basement structures resulted in synsedimentary deformation and small-scale thickness and facies changes (Wetzel et al., 2003). Many vein-type mineralisations of Mesozoic age (e.g., von Gehlen, 1987; Wernicke and Lippolt, 1997; see compilation in Wetzel et al., 2003), indicate a strong hydrothermal activity mainly in Jurassic times. Towards the end of the Jurassic large-scale domal uplift commenced (Illies, 1977; Geyer and Gwinner, 1991). Cretaceous to early Tertiary deposits are absent in the southern URG area. Based on interpolated isopach maps (Geyer and Gwinner, 1991) the thickness of the eroded Mesozoic sequence can be estimated amounting up to 1500 m. However, it is still a matter of debate, if deposited Cretaceous sediments were completely eroded during latest Cretaceous and Paleocene times (Ziegler, 1990) or they were never deposited (e.g. Geyer and Gwinner, 1991).

The Late Cretaceous to Tertiary cooling history of the southern URG area is roughly documented by available fission-track data (Michalski, 1987; Hurford and Carter, 1994; Wyss, 2001). They indicate slow overall cooling since the Middle Cretaceous.

Purpose and scope

In spite of the tremendous amount of geological and geophysical data currently available, there is still a gap of knowledge regarding some aspects of the regional geology of the URG. This PhD project aims at partly closing this gap by means of an extensive fission-track study. In doing so, the focus is on the uplifted flanks of the southern URG, the exhumed Variscan basement of the Black Forest and the Vosges (Fig. 1), as well as on the crystalline basement of northern Switzerland, which is the southern continuation of the Black Forest (Thury et al., 1994) presently covered by Mesozoic strata.

The gravels delivered from the Black Forest and the Vosges document the history of their uplift and erosion. For instance, Eo-Oligocene gravels deposited on alluvial fans along the southern URG locally already contain pebbles from the crystalline basement (Duringer, 1988). In contrast, the Jura-Nagelfluh, Miocene gravels shedded from the Black Forest to the south, contain Triassic pebbles in the basal parts. First crystalline pebbles occur during the Middle Miocene (Naef et al., 1985). Thus, gravel accumulations indicate strong uplift of the Black Forest-Vosges arch in the Middle Miocene. Several other gravel accumulations occupy various altitude levels above the Rhine valley reflecting the uplift history and changes of the drainage system (e.g., Naef et al., 1985; Duringer, 1988; Villinger, 1998). However, the dating of these gravels is not always exact because the biostratigraphic resolution in terrestrial deposits is low and chronometric age determinations are yet missing. Fission-track analysis, for example, could provide chronometric age data on cooling, uplift and erosion, and this is the main objective of this study.

The uplift and erosion history derived from gravel accumulations indicate that there is an evident time lag between initial graben subsidence (Late Eocene) and strong flank uplift (Middle Miocene). For other rift systems it has been shown that strong uplift of rift flanks nearly coincides with increased heat flux (e.g., Reading, 1986). This would imply that the strong thermal anomaly in the southern URG (e.g., Dèzes et al., 2004) was not related to initial graben formation. On the contrary, based on thermal modelling Villemin et al. (1986) suggested a two-phase heating, one at 40-30 Ma, contemporaneous to the initial rifting stage, and the second at around 10 Ma. The timing of the second phase is definitely uncertain because at that time the flanks had already started to rise rapidly. Such problems concerning the relation between exhumation and thermal evolution can be addressed by inverse thermal modelling of

apatite FT parameters.

Some other questions, which can possibly be addressed by an exhaustive FT study, are:

- Did the well documented Jurassic hydrothermal activity (Wetzel et al., 2003) affect the paleotemperature regime of the crystalline basement?
- Did a thermal anomaly form in relation to the rifting of the URG? If yes, when? In what dimension?
- Which were the rates of cooling, uplift and denudation? What was the timing of these processes?

Applied methods

The following section briefly reviews the methods applied in this thesis. It is meant to give the non-specialists a readily available overview about the methodologies used in order that they can follow the details without further reading. For a more detailed description of the techniques, the reader is referred to Wagner and van den Haute (1992), Andriessen (1995), Gallagher et al. (1998), Gleadow and Brown (2000) and Ketcham et al. (2000).

Fission-track dating

Fission tracks (FT) are linear trails of radiation damage in a crystal lattice produced by the spontaneous fission of ^{232}Th, ^{235}U and ^{238}U. They can be observed under an optical microscope after enlargement by a chemical etching treatment (Fig. 2). Since the fission half-lives of the first two isotopes are too long to produce a significant number of tracks, for all practical purposes all fission tracks are derived from fission of ^{238}U. The application of FT analysis as a geochronological method was introduced in the early 1960s (Price and Walker, 1962a; 1962b). The principles do not differ from those of other isotopic dating methods. The method is based upon the fission decay of an isotope (^{238}U) and the accumulation of "daughters" (the fission tracks).

An apparent age is calculated from the spontaneous track density observed on a polished surface. The uranium concentration is measured via a second set of fission tracks induced by a thermal neutron irradiation procedure. In terms of the analytical procedure for age determination the external detector method is in common usage (see e.g., Gallagher et al., 1998) and is also applied in this project. For this method, the age equation is written as:

$$t = (1/\lambda_d) \, \mathrm{Ln} \, (\lambda_d \, (\rho_s / \rho_i) \, \rho_d \, \zeta \, g + 1)),$$

where t is the age; ρ_s and ρ_i are the spontaneous and induced track densities; λ_d is the α decay constant of ^{238}U; ρ_d is the track density in a dosimeter (a glass of known uranium concentration) monitoring the neutron flux in the reactor; g represents the geometry factor (1/2 for the external detector method); ζ is an individual calibration factor.

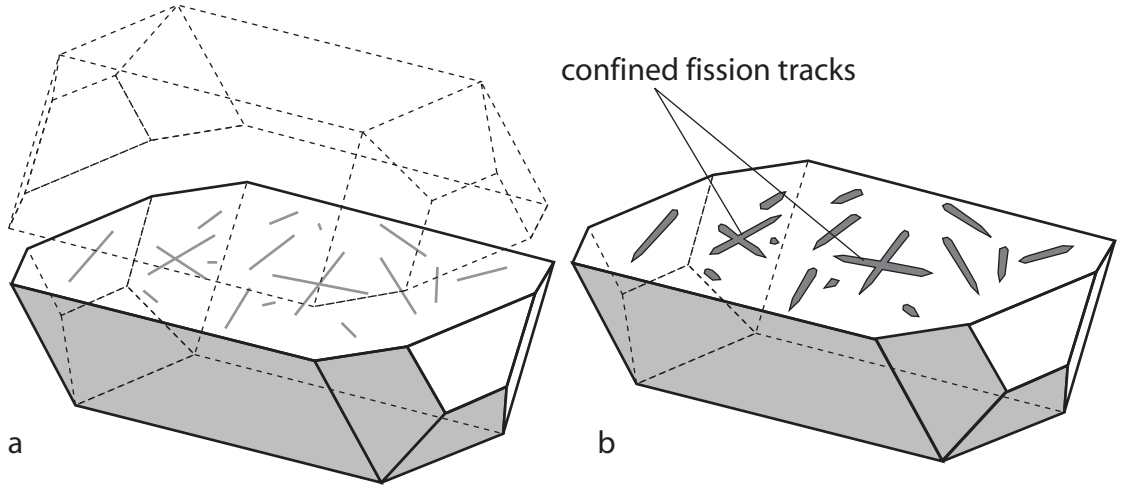

Fig. 2: *Fission tracks in an apatite crystal (after Gleadow and Brown, 2000). a) A polished surface is cut through the mineral grain, which intersects a number of spontaneous tracks. b) After chemical etching fission tracks can be observed under an optical microscope. Confined fission tracks do not intersect the surface but have been etched where they cross another track. They are used for track length measurements.*

Usually, a FT age is reported as some kind of average estimate of the individual (typically 20) single grain ages. The commonly used central age (Galbraith and Laslett, 1993) is basically the weighted mean of the log normal distribution of single grain ages. A useful graphical method for assessing the distribution of single grain ages is the radial plot (Fig. 3) introduced by Galbraith (1988, 1990). The x and y coordinates are given as:

$$x_j = 1/\sigma_j$$

$$y_j = (A_j - A_r)/\sigma_j,$$

where σ_j is the precision of the age estimate A_j, and A_r is some reference age. All data have a common normalised error. The plot also includes a circular age scale such that the age and the error of each crystal may be determined by extrapolating a line from the origin through the given data point to intercept the age scale (see Fig. 3). Thus, the more precise data plot farther from the origin allowing for the comparison of crystals of differing ages and differing precision.

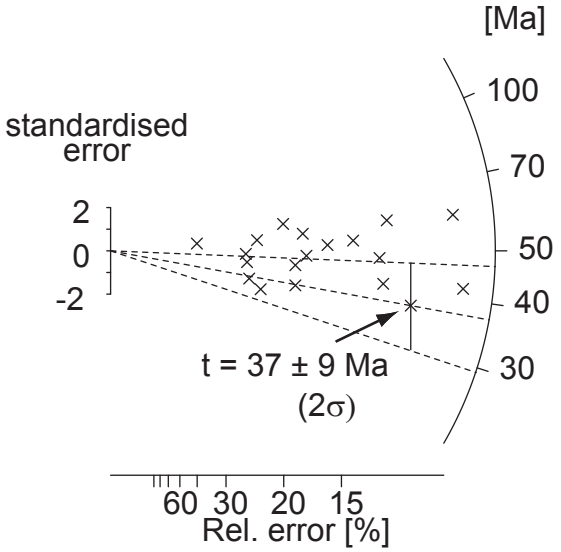

Fig. 3: *The radial plot as graphical method for comparing single-grain age estimates with different precisions (see text).*

As a consequence of the phenomenon of annealing (e.g. Naeser, 1979) a geologic meaning can rarely be ascribed to a FT age. Over a wide temperature range, also referred to as partial annealing zone (PAZ, e.g. Wagner, 1979), fission tracks progressively shorten and at even higher temperatures disappear completely. From this it follows that FT ages are always younger than the conventional radiometric ages of the host rocks. This, at first sight, bothering characteristic of the annealing process turned out to be the key point that qualifies the FT method to become a unique tool for deciphering the thermochronology of rocks. Temperature is the most important factor that causes annealing and consequently controls the degree of track shortening. As a result, the frequency distribution of track lengths yields significant thermal history information, and in practice, from the single grain age and track length data a detailed thermal history can be constructed, rather than just dating the timing of cooling below a specific closure temperature.

Different cooling history styles give rise to different track length distributions and also varying FT ages (Fig. 4). Thus, the length distribution is essential in properly interpreting the significance of the related FT age (Gleadow and Brown, 2000).

FT dating can be applied to a number of uranium-bearing minerals, but geological materials most frequently used are the accessory minerals zircon and apatite. Because of its well established annealing kinetics (see below), mainly apatite FT length distributions are used as a diagnostic tool for thermal histories.

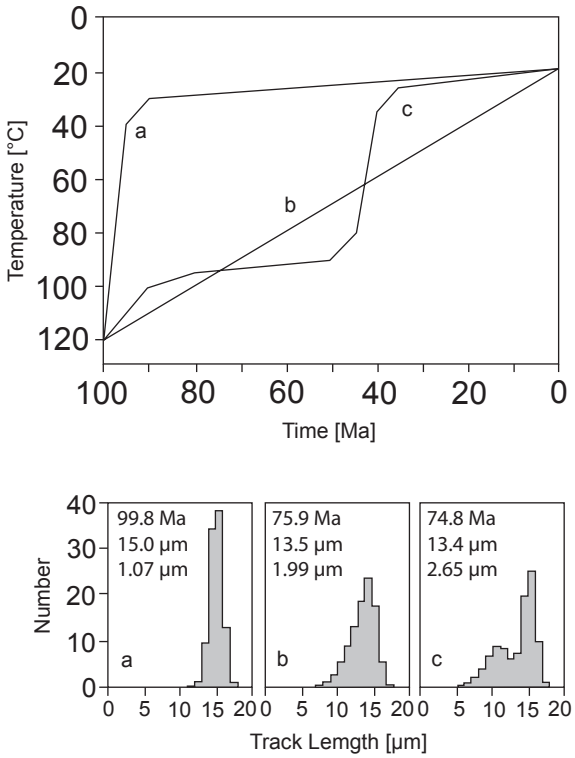

Fig. 4: *Three different cooling history styles and associated track length distributions (after Gleadow and Brown, 2000). a) An example of rapid cooling with a narrow distribution of track lengths about a mean value of 15 µm. It results in an event age closely approximating the time of major cooling. b) Steady moderate cooling resulting in a broader, skewed length distribution. The apparent age is younger and does not relate to any particular event. c) An example of a two-stage cooling history with a typical bimodal track length distribution leading to a "mixed age without any significance in terms of the timing of a discrete geological event.*

Thermal modelling

Fission tracks form and subsequently anneal as a function of time and temperature, thus the set of track lengths measured for a sample provides a continuous record of the temperatures it has experienced (Ketcham et al., 2000). Extensive studies of the annealing properties of fission tracks in apatite led to a number of numerical models, which characterise FT annealing as a function of time and temperature (e.g., Laslett et al., 1987; Carlson, 1990; Crowley et al., 1991; Laslett and Galbraith, 1996; Ketcham et al., 1999). They can be used to calculate the FT age and length distribution resulting from any given thermal history (Gleadow and Brown, 2000). The results of this forward modelling procedure can then be compared to actual observations.

In the inverse modeling approach a range of time-temperature (t-T) paths are determined that are consistent with a given set of FT data and other geological constraints (Fig. 5). This is a statistical process involving the generation of a large number of candidate t-T paths, evaluation of the goodness of fit between model predictions and the measured data, and a method for searching among the various acceptable t-T paths for the best-fitting solutions (Ketcham et al., 2000). The basic modelling approach is to enter independent constraints on the thermal history, i.e. t-T constraints through which the thermal history must pass, and have the numerical model find what thermal histories both satisfy the constraints and predict FT parameters that adequately fit the measured data.

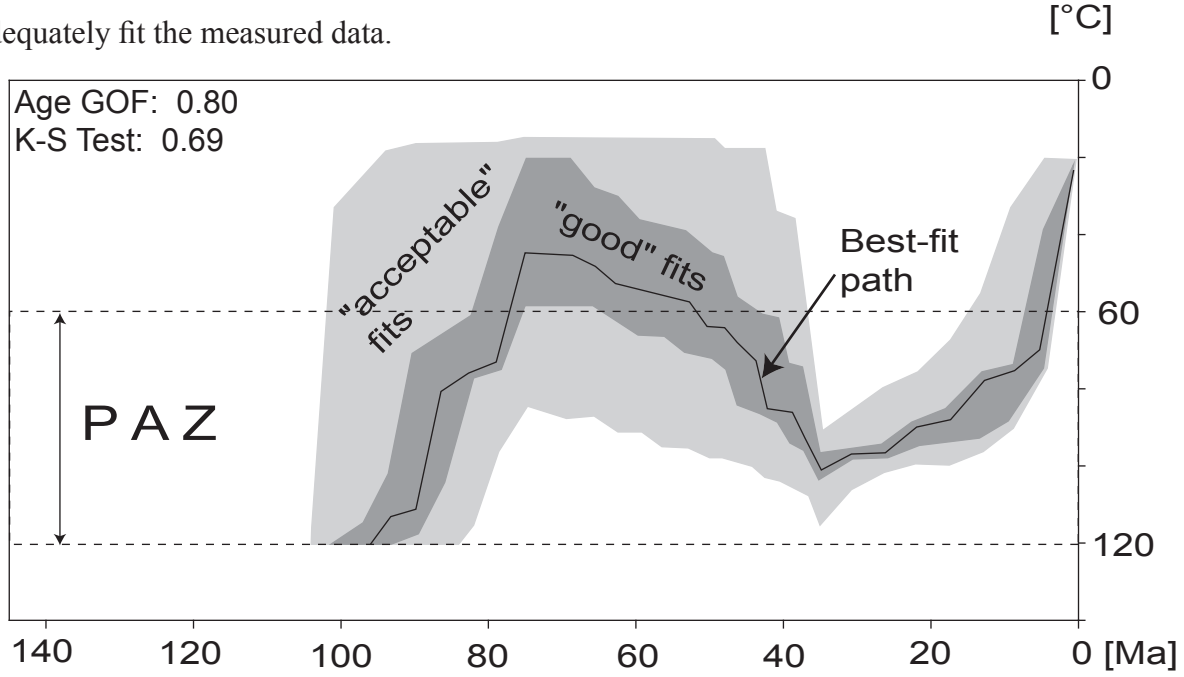

Fig. 5: Thermal modelling results as generated by the computer program AFTSolve (Ketcham et al., 2000). Confidence envelopes bound all "acceptable" (light grey) and "good" (dark grey) fits. K-S test: Kolmogorov-Smirnov test evaluating the degree of fit between FT length distributions. Age GOF: FT age goodness-of-fit test. For more details on the statistical procedures, see Ketcham et al. (2000).

It should be noted, that regardless of the annealing model and software used, a wider array of possible modelling results exists than is found by any model runs. Therefore,

independent constraints and a thorough geological understanding of the studied region are crucial for correctly interpreting the modelling results.

Organization of the thesis

This is a cumulative thesis, consisting of an introduction (Chapter I), three independent published papers (Chapters II-IV), and a summary of general conclusions (Chapter V). Chapter II focuses on the impact of the Jurassic hydrothermal activity on the interpretation of zircon FT data from the southern URG. It quantifies the timing of the observed thermal anomaly and the minimum temperature of the circulating hydrothermal fluids. In Chapter III the low-temperature thermal history of the flanks of the southern URG is determined by inverse thermal modelling of FT parameters. This article also attempts at giving an estimation of the total amount of denudation from the flanks of the URG since the Upper Eocene. Chapter IV presents the post-Variscan thermal history of the crystalline basement of northern Switzerland.

An appendix includes the raw FT data. With their help all FT analysis and thermal modelling results presented in the thesis can be reproduced.

Due to this organization a certain amount of repetition could not be avoided, even though each one of the individual units focused either on a different aspect of the thermal evolution or on a different part of the southern URG area. The contribution of the coauthors (Chapters II-IV) was restricted to careful reviews of earlier versions of the manuscripts and stimulating discussions of the results.

References:

Andriessen, P.A.M. (1995): Fission-track analysis: principles, methodology and implications for tectono-thermal histories of sedimentary basins, orogenic belts, and continental margins. Geologie en Mijnbouw 74, 1-12.

Dèzes, P., Schmid, S.M. and Ziegler, P.A. (2004): Evolution of the Alpine and Pyrenean orogens with their foreland lithosphere. Tectonophysics 389, 1-33.

Duringer, P. (1988): Les conglomérates des bordures du rift cénozoïque rhénan – dynamique sédimentaire et contrôle climatique. Thèse Université Louis Pasteur, Strasbourg, pp. 301.

Fuchs, K., Bonjer, K.-P., Gajewski, D., Lueschen, E., Prodehl, C., Sandmeier, K.-J., Wenzel, F. and Wilhelm, H. (1987): Crustal Evolution of the Rhinegraben area. 1. Exploring the lower crust in the Rhinegraben rift by unified geophysical experiments. Tectonophysics 141, 261-275.

Galbraith, R.F. (1988): Graphical display of estimates having differing standard errors.

Technometrics 30, 271-281.

Galbraith, R.F. (1990). The radial plot: graphical assesment of spread in ages. Nuclear Tracks and Radiation Measurements 17, 207-214.

Galbraith, R.F. and Laslett, G.M. (1993): Statistical models for mixed fission track ages. Nuclear Tracks Radiation Measurements 21, 459-70.

Gallagher, K., Brown, R.W. and Johnson, C. (1998): Fission track analysis and its applications to geological problems. Ann. Rev. Earth Planet. Sci. 26, 519-572.

Geyer, O.F. and Gwinner, M.P. (1991): Geologie von Baden-Württemberg. 4., neubearb. Aufl. der „Einführung in die Geologie von Baden-Württemberg". Schweizerbart, Stuttgart.

Giamboni, M., Ustaszewski, K., Schmid, S.M., Schumacher, M.E. and Wetzel, A. (2004a): Plio-Pleistocene transpressional reactivation of Paleozoic and Paleogene structures in the Rhine-Bresse transform zone (northern Switzerland and eastern France). Int. J. Earth Sci. (Geol. Rundschau) 93, 207-223.

Giamboni, M., Wetzel, A, Nivière, B. and Schumacher, M. (2004b): Plio-Pleistocene folding in the southern Rhinegraben recorded by the evolution of the drainage network (Sundgau area; northwestern Switzerland and France). Eclogae geol. Helv. 97, 17-31.

Gleadow, A.J.W. and Brown, R.W. (2000): Fission-track thermochronology and the long-term denudational response to tectonics. In: Summerfield, M.A. (Ed.): Geomorphology and Global Tectonics.

Hurford, A. and Carter, A. (1994): Regional thermo-tectonic histories of the Rhine Graben and adjacent Hercynian basement: a key to assessing the alpine influence in northwest Europe. 8th International Conference on Geochronology, Cosmochronology and Isotope Geology, abstracts, p. 148.

Illies, J.H. (1977): Ancient and recent rifting in the Rhinegraben, Geologie en Mijnbouw 56/4, 329-350.

Illies, J.H. and Fuchs, K. (eds.) (1974): Approaches to Taphrogenesis. Schweizerbart, Stuttgart, 460 pp.

Illies, J.H. and Müller, St. (eds.) (1970): Graben Problems. Schweizerbart, Stuttgart, 316 pp.

Keller, J., Kraml, M. and Henjes-Kunst, F. (2002): $^{40}Ar/^{39}Ar$ single crystal dating of early volcanism in the Upper Rhine Graben and tectonic implications. Schweiz. Mineral. Petrogr. Mitt. 82, 121-130.

Ketcham, R.A., Donelick, R.A. and Donelick, M.B. (2000): AFTSolve: a program for multi-kinetic modelling of apatite fission track data. Geol. Mater. Res. 2/1, 1-18.

Michalski, I. (1987): Apatit-Spaltspuren-Datierungen des Grundgebirges von Schwarzwald und Vogesen: Die postvariszische Entwicklung. Unpubl. doctoral dissertation, Heidelberg, pp. 125.

Naef, H., Diebold, P. and Schlanke, S. (1985): Sedimentation und Tektonik im Tertiär der Nordschweiz. Nagra Tech. Ber. 85-14. pp. 145.

Naeser, C.W. (1979): Thermal history of sedimentary basins: fission track dating of subsurface rocks. In: Scholle, P.A., Schluger, P.R. (Eds.): Aspects of Diagenesis. Soc. Econ. Paleontol. Mineral., Spec. Publ., 109-112.

Price, P.B. and Walker, R.M. (1962a): A new detector for heavy particle studies. Phys. Lett., 3, 113-115.

Price, P.B. and Walker, R.M. (1962b): Observations of charged-particle tracks in solids. J. Appl. Phys., 33, 3407-3406.

Prodehl, C., Mueller, S. and Haak, V. (1995): The European Cenozoic rift system. In: K.H. Olsen (ed.): Continental Rifts: Evolution, Structure, Tectonics, Dev. in Geotectonics 25, 133-212. Elsevier Sci., New York.

Reading, H.R. (1986): Sedimentary Environments and Facies. Blackwell, Oxford, pp. 615.

Rothé, J.P. and Sauer, K. (eds.) (1967): The Rhinegraben progress report 1967. Abh. Geol. Landesamt Baden-Wuerttemberg 6, 146 pp.

Schmid, S.M. and Kissling, E. (2000): The arc of the Western Alps in the light of geophysical data on deep crustal structure. Tectonics 19, 62-85.

Schmid, S.M., Pfiffner, O.A., Froitzheim, N., Schönborn, G. and Kissling, E. (1996): Geophysical-geological transect and tectonic evolution of the Swiss-Italian Alps. Tectonics 15/5, 1036-1064.

Schumacher, M.E. (2002): Upper Rhine Graben: Role of preexisting structures during rift evolution. Tectonics 21/1, 6-1-17.

Thury, M., Gautschi, A., Mazurek, M., Müller, W.H., Naef, H., Pearson, F.J., Vomvoris, S. and Wilson, W. (1994): Geology and Hydrology of the Crystalline Basement of Northern Switzerland. Nagra Tech. Ber. NTB 93-01. Nagra, Wettingen.

Villinger, E. (1998): Zur Flussgeschichte von Rhein und Donau in Südwestdeutschland. Jahresberichte und Mitteilungen des Oberrheinischen Geologischen Vereins, Neu Folge 80, 361-398.

von Gehlen, K. (1987): Formation of Pb-Zn-F-Ba mineralizations in SW Germany: a status report. Fortschr. Mineral. 65/1, 87-113.

Wagner, G.A. (1979): Correction and interpretation of fission track ages. In: Jäger, E. and

Hunziker, J.C. (eds.): Lectures in Isotope Geology, 170-177, Springer-Verlag, Berlin.

Wagner, G. and van den Haute (1992): Fission-Track Dating. Dordrecht, Kluwer Acad., pp. 285.

Werner, W. and Franzke, H.J. (2001): Postvariszische bis neogene Bruchtektonik und Mineralisation im südlichen Zentralschwarzwald. Z. Dt. Geol. Ges. 152, 405-437.

Wernicke, R.S. and Lippolt, H.J. (1997): (U + Th)-He evidence of Jurassic continuous hydrothermal activity in the Schwarzwald basement, Germany. Chem. Geol. 138, 273-285.

Wetzel, A., Allenbach, R. and Allia, V. (2003): Reactivated basement structures affecting the sedimentary facies in a tectonically „quiescent“ epicontinental basin: an example from NW Switzerland. Sedimentary Geology 157/1-2, 153-172.

Wyss, A. (2001): Apatit Spaltspur Untersuchungen in der Vorwaldscholle (SW-Deutschland). Unpubl. diploma thesis, Univ. Basel, pp. 69.

Ziegler, P.A. (1990): Geological Atlas of Western and Central Europe. Shell Internationale Petroleum Maatschappij – Geological Society Publishing House, 239 pp.

Ziegler, P.A., Bertotti, G. and Cloething, S. (2002): Dynamic processes controlling foreland development: the role of mechanical (de)coupling of orogenic wedges and forelands. In: Bertotti, G., Schulmann, K. and Cloething, S. (eds.): Continental Collision and the Tectono-Sedimentary Evolution of Forelands. Europ. Geophys. Soc. Stephan Mueller Spec. Publ., vol. 1, 29-91.

II. The impact of the Jurassic hydrothermal activity on zircon fission track data from the southern Upper Rhine Graben area

by Zoltan Timar-Geng, Bernhard Fügenschuh, Urs Schaltegger and Andreas Wetzel

Published in:
Schweizerische Mineralogische und Petrographische Mitteilungen 84, 257-269, 2004

Schweizerische Mineralogische und Petrographische Mitteilungen 84, 257–269, 2004

The impact of the Jurassic hydrothermal activity on zircon fission track data from the southern Upper Rhine Graben area

Zoltan Timar-Geng[1], Bernhard Fügenschuh[1], Urs Schaltegger[2]* and *Andreas Wetzel[1]*

Abstract

The influence of the Jurassic hydrothermal activity on the interpretation of fission track (FT) data from the southern Upper Rhine Graben (URG) is elaborated by means of new zircon FT analyses on samples with known U/Pb crystallisation ages. Zircon FT central ages display a wide spectrum from 162 ± 14 Ma to 247 ± 22 Ma. The combination of the U/Pb ages, independent geologic evidence (such as Mesozoic subsidence history, timing of hydrothermal activity, and apatite FT ages) and the zircon FT data unambigously indicate a Jurassic thermal overprint in the investigated area. It is suggested that circulating hydrothermal fluids with temperatures in the order of 200–250 °C were responsible for the observed thermal anomaly.

The Jurassic hydrothermal fluid migration appears to have been related to a heating event on a regional scale. Inferences from FT analyses related to burial or denudation history have to take into account how such hydrothermal events affect the FT system, including a changing geothermal gradient with time.

Keywords: Black Forest, Vosges, zircon, fission track, partial annealing zone, thermal history.

Introduction

The Upper Rhine Graben (URG) is the most perceptible part of the European Cenozoic rift system (Fig. 1) that extends from the North Sea into the western Mediterranean. Exhumed Variscan basement is exposed in the Black Forest and the Vosges and forms the flanks of the southern URG.

The emplacement age of volcanic and plutonic rocks in the Vosges was found to be very consistent in the range of 345 to 340 Ma (Schaltegger et al., 1996). In the Central Vosges the granulite-facies metamorphism was dated at about 335 Ma and amphibolite-facies retrograde overprint at about 328 Ma (Schaltegger et al., 1999). The analysed granites and rhyolites in the southern Black Forest yielded emplacement ages of 340 to 332 Ma (Schaltegger, 2000). Late Palaeozoic erosion affected the area, with the notable exception of some intramontane basins (e.g. Diebold, 1989). Thus, the base of the Mesozoic strata rests on Variscan crystalline basement.

While the URG and its Cenozoic evolution have been thoroughly studied in the past decades (e.g. Rothé and Sauer, 1967; Illies and Müller, 1970; Illies and Fuchs, 1974; Fuchs et al., 1987; Prodehl et al., 1995; Schumacher, 2002), much less is known about the Mesozoic geological history of the area. This is partly due to the fact that most of the Mesozoic strata have been eroded. After Variscan folding, uplift and subsequent denudation, the URG area became part of the central European intracontinental basin, which developed since the Permo-Triassic until the end of the Jurassic (Geyer and Gwinner, 1991). Based on interpolated isopach maps (Geyer and Gwinner, 1991) the thickness of the eroded Mesozoic deposits in the URG area is estimated to be at most 1500 m. Towards the end of the Jurassic (e.g. Geyer and Gwinner, 1991) or later (Ziegler, 1990) the URG area was uplifted above sea level.

In the outcrops of crystalline basement many vein-type mineralisations of Mesozoic age are preserved (e.g. von Gehlen, 1987; Wernicke and Lippolt, 1997; see compilation by Wetzel et al., 2003), evidencing a strong hydrothermal activity mainly in Jurassic times.

In the present study we apply zircon fission track (FT) analysis to basement samples from the Vosges and Black Forest, which were already dated by the U/Pb method (Schaltegger et al., 1996, 1999; Schaltegger, 2000) and thus, provide additional information on the thermal history of the

[1] Geologisch-Paläontologisches Institut, Universität Basel, Bernoullistrasse 32, CH-4056 Basel, Switzerland.
* Present address: Geologisches Institut, Albert-Ludwigs-Universität Freiburg, Albertstr. 23b, D-79104 Freiburg, Germany. <zoltan.timar-geng@geologie.uni-freiburg.de>
[2] Département de Minéralogie, Université de Genève, Rue des Maraîchers 13, CH-1205 Genève, Switzerland.

0036-7699/04/0084/257

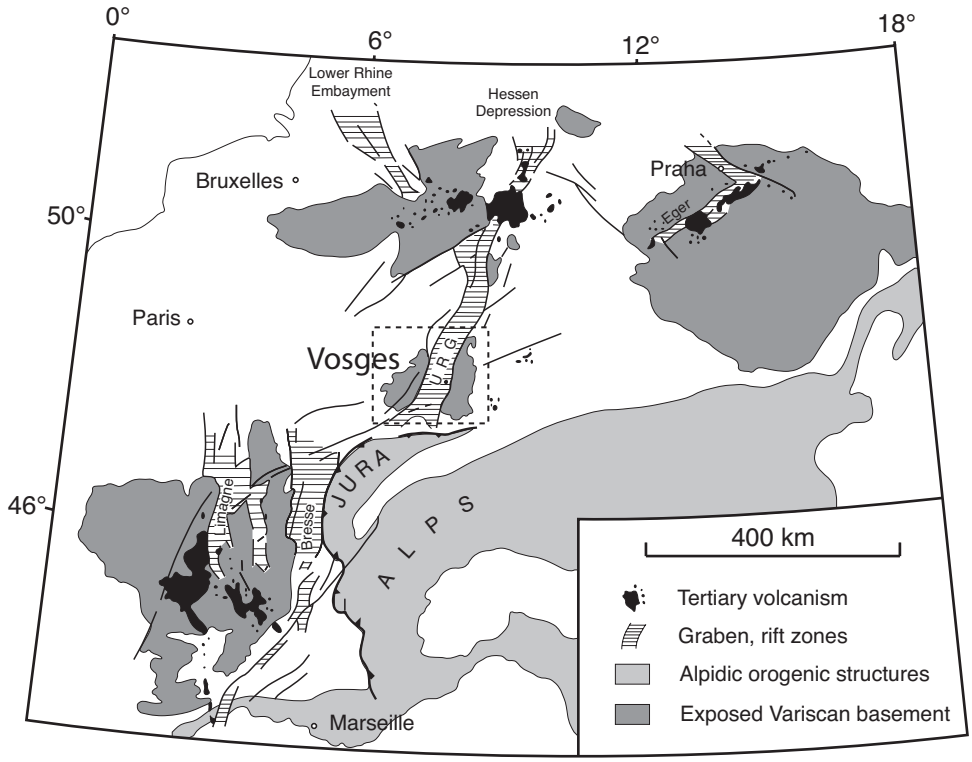

Fig. 1 The Upper Rhine Graben (URG) as part of the European Cenozoic rift system (after Prodehl et al., 1995). Black Forest and Vosges flank the Southern URG. Location of the study area is indicated by dashed square (for details see Figs. 2 and 3).

rocks. Available apatite FT data range from ~37 Ma to ~75 Ma in the Vosges, and ~29 Ma to ~107 Ma in the Black Forest (Michalski, 1987; Hurford and Carter, 1994; Wyss, 2001). Published uplift rates of the Black Forest (Wagner et al., 1989) are inferred from apatite FT data using rather simple assumptions about the paleotemperature field, i.e. constant geothermal gradients. Such an approach may lead to erroneous conclusions about the thermotectonic evolution, if convective heat transport mechanisms changed the temperature field with time. In this study we will focus on the influence of the Jurassic hydrothermal activity on the interpretation of zircon FT data from the Black Forest and Vosges.

Jurassic hydrothermal activity

In the study area, i.e. the Variscan basement of the Vosges and Black Forest, several prominent hydrothermal events have been reported previously (e.g., Wernicke and Lippolt, 1993; Lippolt and Kirsch, 1994; see compilation by Wetzel et al., 2003). Two fossil geothermal systems were identified in the intramontane troughs of Baden-Baden, northern Black Forest (Zuther and Brockamp, 1988; Brockamp et al., 1994) and Offenburg, central Black Forest (Brockamp et al., 2003). For these two well documented cases the observed thermal anomaly is clearly related to fault zones and heating effects can be studied in the adjacent rocks (e.g., Brockamp and Zuther, 1983; Brockamp et al., 1987, 1994; Tapfer, 1987; Zuther and Brockamp, 1988; Meyer et al., 2000; Brockamp et al., 2003). In the Baden-Baden trough, Upper Carboniferous, Lower Permian and Triassic sediments were hydrothermally altered during the Jurassic (Zuther and Brockamp, 1988). Vitrinite data indicate that the hydrothermal fluids reached temperatures between 240 and 290 °C (Brockamp and Zuther, 1983). This fossil geothermal system is documented by three distinct alteration zones, including from center to margin, sericitisation, albitisation and weak alteration (Zuther and Brockamp, 1988). K/Ar data on authigenic il-

lites and hydrothermally altered detrital micas reveal two major episodes of fluid migration (Brockamp et al., 1994). The first episode occurred during the Jurassic (150 Ma) and extensively altered the sediments near the fault system of Gernsbach, which is located between the Saxothuringian and Moldanubian zone. The second hydrothermal phase occurred during the Cretaceous (100 Ma) and formed the fluorite-quartz vein-type mineralisation of Käfersteige (Brockamp et al., 1994). In the Offenburg trough, central Black Forest (Brockamp et al., 2003), K/Ar data on sericites point to hydrothermal activity also during the Jurassic (145 Ma). Oxygen isotope data for sericite, sericite composition and vitrinite reflectance investigations indicate hydrothermal fluid temperatures between 150 to 210 °C (Brockamp et al., 2003).

Multiple hydrothermal activities mainly during the Jurassic can be traced around the Paleo-Atlantic all over western Europe (e.g., Mitchell and Halliday, 1976) suggesting fluid circulation on a wide regional scale. With fluid temperatures in excess of 200 °C at shallow crustal levels, and expecting a pervasive heating of the basement due to continent-wide rifting events during the opening of the North-Atlantic, these hydrothermal events should have substantially altered the paleotemperature field. Thus, interpretation of FT data assuming a constant geothermal gradient leads inevitably to erroneus results.

Fission track analysis

Zircon FT thermochronology provides insight into the low temperature thermal history of rocks between ~300 °C and ~180 °C, covering the gap between the K/Ar mica and apatite FT dating. Zircon FT analyses were carried out on 21 samples, 14 from the Vosges and 7 from the Black Forest (Figs. 2, 3). For details on lithology and localities the reader is referred to Schaltegger (2000) and Schaltegger et al. (1996, 1999).

Analytical procedure

Mineral separation and sample preparation followed standard procedures. After mounting in PFA® Teflon, zircon grains were polished and etched in a KOH–NaOH eutectic melt at 220 °C for variable times up to 12 h depending on track revelation. Thermal neutron irradiation was carried out at the Australian Nuclear Science and Technology Organisation (ANSTO) facility, Lucas Heights, Australia. All samples were analysed using the external detector method (Naeser, 1976; Gleadow, 1981). Detector micas were etched for 40 minutes in 40% HF at room temperature. Track counting was performed using an optical microscope ("Axioscope" by Zeiss) with the aid of a computer driven stage (Dumitru, 1993). Magnification was 2500 × using an oil immersion objective. Ages were determined using the zeta approach (Hurford and Green, 1982, 1983) with a zeta value of 113.49 ± 1.80 (Fish Canyon Tuff, CN1). Data processing, error calculation and graphical presentation was performed using freeware provided by I. Dunkl (2002). All ages are central ages (Galbraith and Laslett, 1993) and errors are quoted at the 1 σ confidence level. Results are given in Table 1 according to the I.U.G.S. recommendations (Hurford, 1990).

Zircon fission track partial annealing zone

In a wide temperature range, known as partial annealing zone (PAZ; Wagner and van den Haute, 1992), fission tracks gradually shorten and eventually disappear completely in response to elevated temperatures over geological timescales.

In case of the apatite FT system the temperature range of the PAZ (~120–60 °C) and the annealing kinetics are well established (e.g. Green et al., 1986; Laslett et al., 1987, Carlson et al., 1999; Donelick et al., 1999; Ketcham et al., 1999). The temperature interval over which FT partial annealing in zircon occurs is, however, still a matter of debate. Early annealing experiments performed on zircon suggest high closure temperatures (exceeding 300 °C) (Fleischer et al., 1965; Krishnaswami et al., 1974; Carpéna, 1992) and/or a very broad temperature interval of the PAZ ranging from ~170 to 390 °C (Yamada et al., 1995). Geological constraints on the stability of fission tracks in zircon generally do not confirm such high values. For rocks with a well-established cooling history it is possible to assign a "closure temperature" of the zircon FT system by interpolating the determined FT age. Such calibration yielded effective closure temperatures of ~175 °C (Harrison et al., 1979) and 240 ± 50 °C (Hurford, 1986) for the zircon FT system. Zaun and Wagner (1985) estimated the effective closure temperature to be 210 ± 20 °C on the basis of analysed zircon samples from a borehole section. They interpreted the age reduction with depth as a fossil PAZ. Deep borehole samples from the Vienna Basin revealed no partial annealing in zircons for temperatures up to ~200 °C and a heating duration of the order of 5–10 Ma (Tagami et al., 1996). This information, coupled with a relatively narrow temperature interval of ~230 to ~330 °C for the PAZ (Tagami and Shimada, 1996; Tagami et

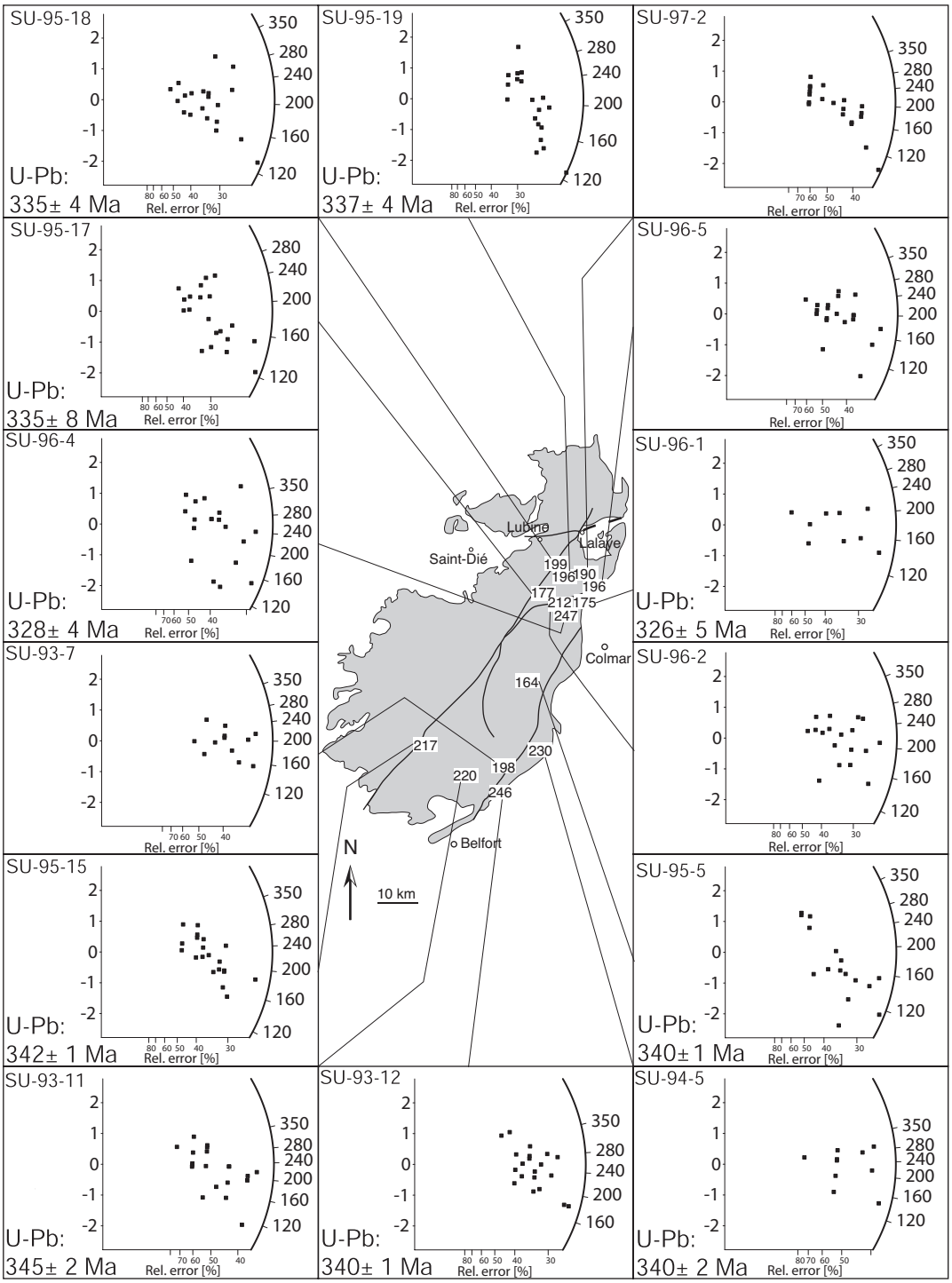

Fig. 2 Zircon FT data from the Vosges. Central ages are plotted on the map. Available U/Pb ages are inserted in the lower left corners of the corresponding radial plots.

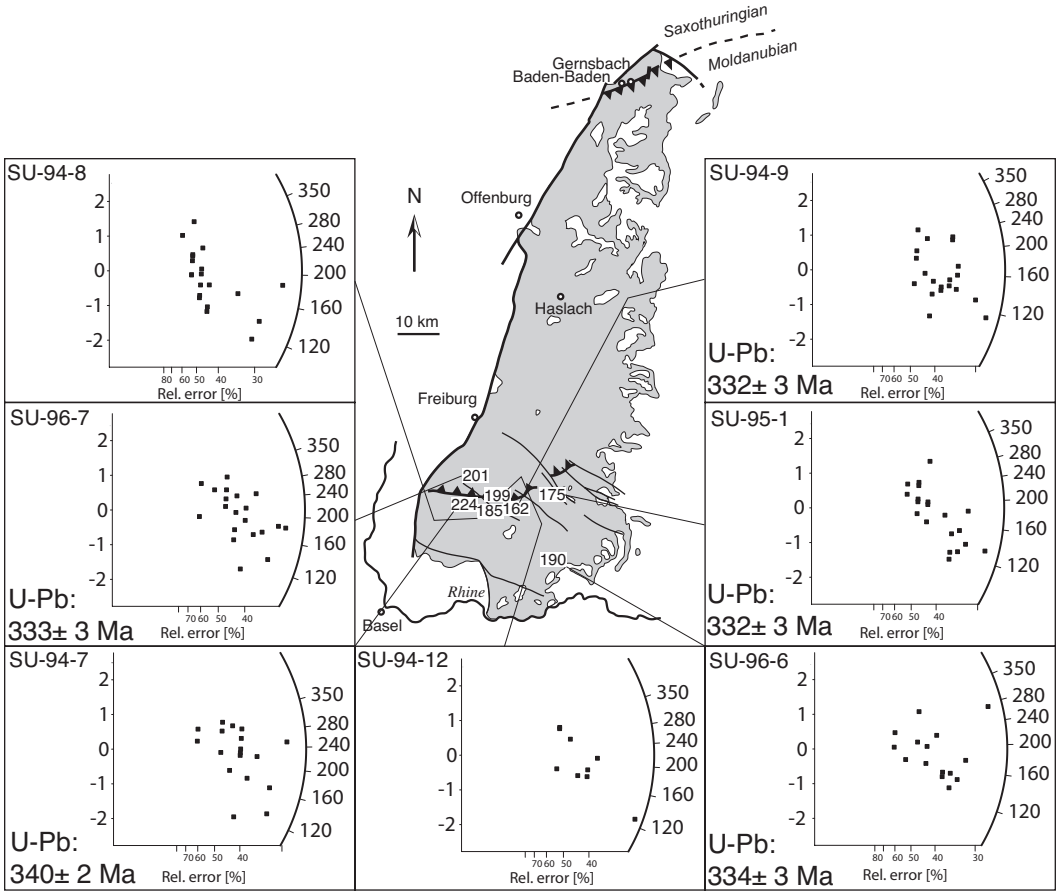

Fig. 3 Zircon FT data (central ages and radial plots) from the Black Forest. Available U/Pb ages are inserted in the lower left corners of the corresponding radial plots.

al., 1998), implies an effective closure temperature of 280 ± 50 °C. The latter value would in principle validate the results of laboratory extrapolations (Yamada et al., 1995) to geological timescales.

However, experience shows that some kinetic properties of the grains/samples in combination with different thermal histories (fast versus slow cooling) lead to distinct annealing characteristics and hence, give rise to the observed range in (zircon) FT closure temperatures.

In the case of apatite, for example, there is a clear correlation between chemistry and single-grain ages (Green et al., 1986; O'Sullivan and Parrish, 1995) and the higher resistivity of chlorine-rich apatites with respect to fluor-apatites is well known. A similar relationship seemingly exists between the density of accumulated α-recoil tracks (the damage produced by α-decay events) and the single-grain age of zircons (Kasuya and Naeser, 1988; Yamada et al., 1995). This relationship, however, strongly depends on the thermal history of the investigated rocks as the thermal stability of zircon decreases with increasing α damage (Kasuya and Naeser, 1988). Based on field and laboratory observations Rahn (2001) proposed an α damage partial annealing zone at higher temperatures than that for the fission tracks in zircons. If a sample cools rapidly through the α damage PAZ and subsequently through the zircon FT PAZ, no α damage will be present and thus the annealing of newly forming fission tracks will occur within a pristine lattice. Conversely, samples, which are heated and enter the zircon FT PAZ from the lower temperature side, will have accumulated α damage over time and the level of this damage will influence the rate of FT annealing (Rahn et al., 2004).

It seems difficult to define a generally applicable zircon FT PAZ because of the manifold dependencies of the annealing characteristics of different samples. As pointed out by Rahn (2001), it is often more appropriate to rely on a "single-grain partial annealing zone" and to define a "sample partial annealing zone" as the integral of partial annealing zones of all grains within a sample. In particular for the determination of the lower temperature boundary of the zircon FT PAZ, it is crucial to independently know the style of the thermal history, i.e. to know whether or not the sample entered the PAZ from the low temperature side. The amount of accumulated radiation damage has important implications for the temperature interval, at which zircon FT annealing occurs.

A compilation of annealing models and geologic constraints (Fig. 4) reveals a broad range for the zircon FT PAZ and reflects its various dependencies on some key parameters such as the cooling rate, the amount of accumulated α damage and consequently the style of the cooling history.

Single-grain age distributions

χ^2 statistics (Table 1) indicate that all grains analysed for individual samples belong to a single age population (Green, 1981). Thus, taking a probability of less than 5% as evidence for a mixed age population, the observed large spread in single-grain ages does not represent real differences between the apparent ages because P (χ^2) values are consistently higher than 5%. The absence of extra-Poissonian variation is also indicated by the radial plots, since all data points scatter within ± 2σ around the mean. So, from a formal statistical point of view, there is no need to further analyse the single-grain age variation. On the other hand, it has to be noted that the error on all crystals is notably high because of the low number of counted tracks. Thus, the χ^2 test may have lacked power to detect any extra-Poissonian variation due to the high standard error of the single-grain age estimates and the low number of random samples (generally 20 grains). This can be illustrated assuming we would obtain the same ratio of induced and spontaneous tracks on crystal surfaces ten times greater than the observed ones (Fig. 5). If we calculate the statistics with these new values, the χ^2 test would fail and we could deal with multiple age populations. Once again, we are fully aware that a statistically founded evaluation of the single-grain age data is not possible. However, after careful consideration of the raw data and relying on our understanding of the underlying processes, we conclude that the observed spread in single-grain ages shows extra-Poissonian variation due to different annealing

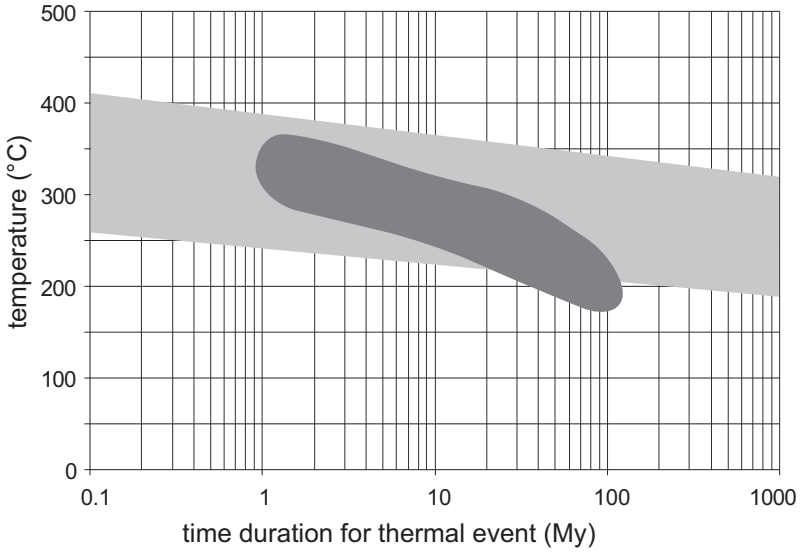

Fig. 4 Constraints on the zircon FT PAZ (modified after Rahn et al., 2004). Light grey: range of the PAZ constrained by fanning annealing models. Dark grey: PAZ derived from geologic evidence. Highest temperatures for the upper (high-temperature) boundary of the PAZ are calculated on the basis of annealing experiments with α damage-free zircon samples (Rahn et al., 2004). Lowest temperatures are derived from geologic examples with long-duration heating episodes (e.g., Zaun and Wagner, 1985).

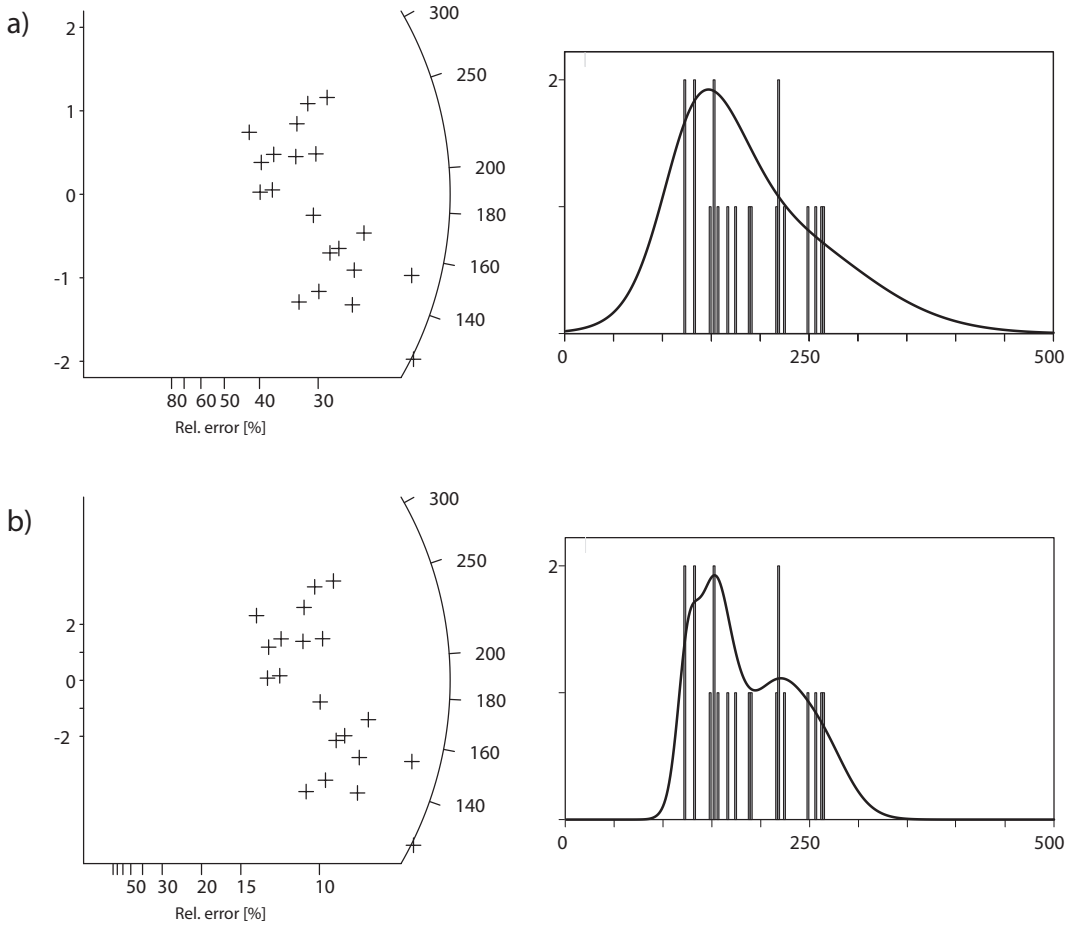

Fig. 5 (a) Radial plot and age-spectrum as probability-density diagram for one sample (SU-95-17) from the Vosges. All single-grain ages plot within ± 2σ around the mean. (b) Hypothetical plots of the same sample simulating data on ten times greater crystal surfaces ($N_s \times 10$ and $N_i \times 10$, the N_s/N_i ratio remaining the same). Under this assumption, the single-grain ages show extra-Poissonian variation.

kinetics of the individual grains. This is further evidenced by the fact that none of the samples experienced fast cooling rates and for this reason the individual grains could accumulate different amounts of α damage causing varying annealing properties of the respective grains (Rahn et al., 2004). Therefore, the following discussion is based on this *assumption*.

Analyses of single-grain age distributions of detrital zircons have been proven to provide accurate results in exhumation and provenance studies (e.g., Spiegel et al., 2000; Bernet et al., 2001; Stewart and Brandon, 2004). The underlying concept is that recycled sediments may contain zircons derived from various source regions with different thermal histories, thus displaying more than one population of zircon FT ages. However, a large spread in single-grain age distributions may also occur due to different track retentivity of the individual grains within one sample, for example owing to variable amounts of accumulated α damage (Kasuya and Naeser, 1988). Over the last decades, several attempts have been made to extract thermochronological information from FT single-grain age data from previously fully or partially annealed samples, based on differential annealing of individual grains (e.g. Green, 1989; Sobel and Dumitru, 1997; Brandon et al., 1998; Fügenschuh and Schmid, 2003). A useful concept is the interpretation of the fraction of zircons with the youngest single-grain ages as those with the lowest thermal stability because they will be the last to close on a cooling path (Brandon et al., 1998). The inference is that the youngest single-

Table 1 Zircon FT data.

Sample number	Elevation (m)	No. of crystals counted	Spontaneous tracks ρ_s (N_s)	Induced tracks tracks ρ_i (N_i)	P(χ^2) (%)	Dosimeter ρ_d(N_d)	Central age (Ma) ± 1σ
Black Forest							
SU 94-7	920	18	201 (1183)	22 (127)	81	4.31 (1590)	224 ± 22
SU 94-8	610	20	169 (1025)	21 (130)	84	4.20 (1590)	185 ± 18
SU 94-9	720	20	251 (1256)	33 (163)	94	3.75 (1590)	162 ± 14
SU 94-12	560	9	287 (462)	37 (59)	73	4.54 (1590)	199 ± 28
SU 95-1	980	20	222 (1330)	25 (148)	89	3.47 (1590)	175 ± 16
SU 96-6	580	15	297 (1059)	30 (108)	93	3.47 (1605)	190 ± 20
SU 96-7	870	20	237 (1315)	24 (133)	96	3.64 (1590)	201 ± 19
Vosges							
SU 93-7	690	12	395 (936)	38 (90)	100	3.40 (1605)	198 ± 23
SU 93-11	700	20	177 (993)	18 (99)	97	3.92 (1590)	219 ± 24
SU 93-12	460	20	418 (1959)	42 (199)	98	4.48 (1590)	246 ± 20
SU 94-5	660	10	213 (540)	20 (50)	94	3.81 (1590)	229 ± 35
SU 95-5	480	16	289 (974)	48 (161)	31	4.82 (1590)	164 ± 15
SU 95-15	890	20	260 (1556)	31 (188)	99	4.71 (1590)	217 ± 18
SU 95-17	790	20	301 (2241)	35 (260)	71	3.66 (1605)	177 ± 13
SU 95-18	400	20	246 (1907)	27 (206)	88	3.86 (1605)	199 ± 16
SU 95-19	660	19	377 (2956)	39 (305)	31	3.63 (1590)	196 ± 14
SU 96-1	290	9	390 (733)	44 (83)	97	3.53 (1605)	175 ± 21
SU 96-2	320	18	338 (1914)	33 (188)	96	3.72 (1605)	212 ± 17
SU 96-4	480	19	278 (1504)	28 (152)	40	4.48 (1590)	247 ± 22
SU 96-5	310	20	190 (935)	26 (130)	98	4.87 (1590)	196 ± 19
SU 97-2	640	20	197 (969)	22 (110)	97	3.86 (1590)	190 ± 20

Track densities (ρ) are in 10^5 tracks/cm^2, number of tracks counted (N) shown in brackets.
Analyses by external detector method using 0.5 for the $4\pi/2\pi$ geometry correction factor.
Ages calculated as central ages according to Galbraith and Laslett (1993) using dosimeter glass CN1 with ζ_{CN1} = 113.49 ± 1.80.
P(χ^2) is the probability of obtaining χ^2 value for ν degrees of freedom where ν = number of crystals – 1.

grain age represents a maximum age for the date when the sample finally left the PAZ (Fig. 6).

Results

In the Vosges, zircon FT central ages range between 164 ± 15 Ma and 247 ± 22 Ma (Fig. 2, Table 1). No regional trend can be observed.

Very similar results were obtained for the southern Black Forest with zircon FT central ages ranging between 162 ± 14 Ma and 224 ± 22 Ma (Fig. 3, Table 1), with a weak tendency for older ages to be found more to the west of the Black Forest.

Neither for the Black Forest nor for the Vosges a correlation of FT age with altitude could be observed (Fig. 7). An altitude dependence of increasing ages with elevation was not even observed for samples, derived from coherent fault bounded blocks.

Radial plots (Galbraith, 1988, 1990) of analysed samples reveal broad single-grain age variations within individual samples (Figs. 2, 3), however, all samples passed the χ^2-test (Green, 1981). Therefore, from a statistical point of view all samples are characterised by only one grain population. The single-grain ages of each sample, as depicted in the radial plots (Figs. 2, 3), display a broad range from ~340 Ma to ~100 Ma.

All single-grain ages from the Black Forest and Vosges together with the superimposed central ages (Fig. 8) reveal a maximum at ~190 Ma in the Vosges and at ~170 Ma in the Black Forest.

Discussion

Pre-Tertiary thermal event in the URG area

The samples from the Black Forest and Vosges have experienced substantial annealing, indicated by the reduced zircon FT central ages with respect to the emplacement ages. Based on independent geological evidence the post-Variscan thermotectonic evolution can be roughly reconstructed. It started with the emplacement of the magmatic rocks at the time, given by the U/Pb ages. Of special interest are samples from volcanic rocks and samples taken close to the base of the

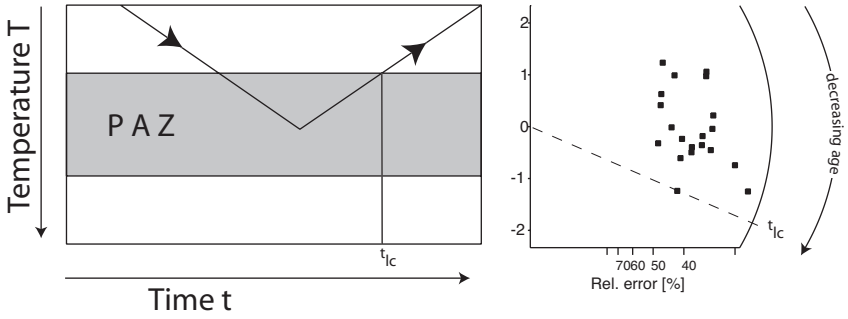

Fig. 6 Thermal history scenario with a thermal peak situated within the PAZ together with a possible single-grain age distribution (after Fügenschuh and Schmid, 2003). The youngest single-grain age corresponds to the time (t_{lc}) when the sample cools through the lower limit of the zircon PAZ. For further explanations, see text.

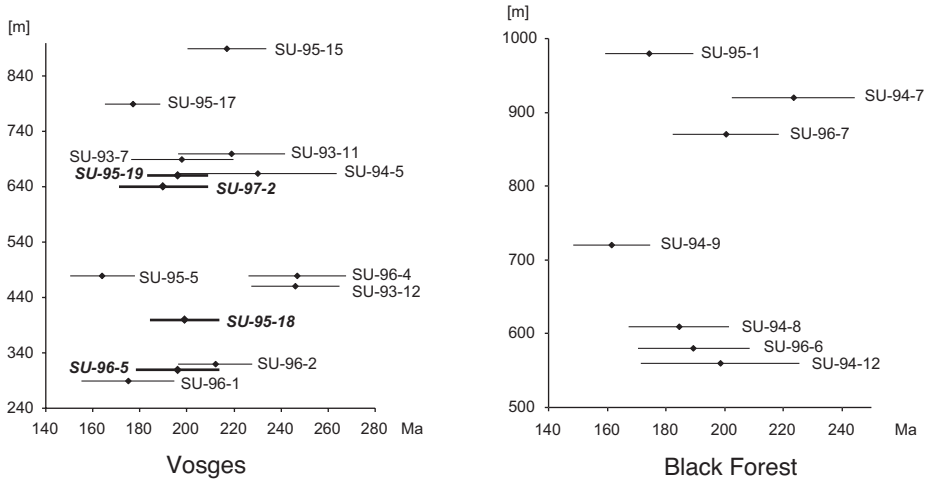

Fig. 7 Age-elevation profiles from the Vosges and the Black Forest. Four highlighted samples from the Vosges (SU 95-18, SU 95-19, SU 96-5 and SU 97-2) indicate that even samples from an apparently homogeneous block do not reveal correlation between the two parameters.

Triassic cover series (e.g. SU-96-6 from the Black Forest). In addition, the Permo-Triassic paleosurface is partly preserved in the Black Forest and has been mapped in the past decades (e.g. Paul, 1955; Wimmenauer and Schreiner, 1990). Thus it is possible to reliably estimate the thickness of the eroded pre-Mesozoic crystalline rocks to be 200 to 600 m, depending on the present elevation of the samples. For the Vosges a similar amount of eroded material is assumed. From the available apatite FT data (Michalski, 1987; Hurford and Carter, 1994; Wyss, 2001), and the youngest zircon FT single-grain ages it is clear that all samples had already cooled to temperatures below the zircon PAZ at ~100 Ma. Thus, partial annealing of the zircons must have occurred between the U/Pb ages of 330 Ma and 100 Ma.

Taking the estimated thickness of the Mesozoic sequence into account (~1500 m), the samples have experienced maximum burial of ⩽ 2100 m (thickness of the Mesozoic sediments + ⩽ 600 m eroded crystalline basement) at the end of the Mesozoic subsidence phase. Thus, elevated temperatures needed for the observed annealing due to burial alone are impossible to reconcile with the known geology of the region. Interpretation of the zircon FT data using a paleogeothermal gradient of 30 °C/km would suggest a burial of the present earth's surface of 5–6 km. Instead, the Jurassic hydrothermal fluid migration is suggested to have led to the increased paleotemperatures. The consequence of this convective heat transport seems to have been a heating event of regional extent because its effect can be detected in each of the samples.

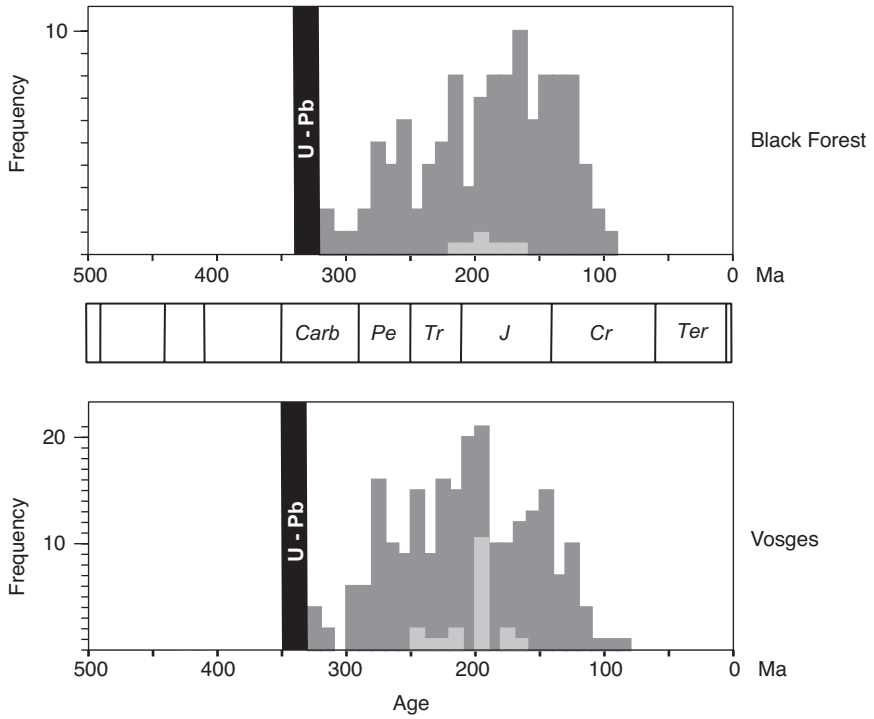

Fig. 8 Frequency distribution of central ages (light grey) and single-grain ages (dark grey) for the whole Vosges and Black Forest regions. Black bars represent the U/Pb ages of the same samples.

Since the samples entered the zircon FT PAZ from the lower temperature boundary after a prolonged period at lower temperatures, a substantial amount of α damage could be accumulated causing a decreased thermal stability of the zircon fission tracks. Thus, rather moderate temperatures of 200–250 °C would have been sufficient to cause the observed thermal anomaly. Fluid temperatures of this magnitude were reported by Brockamp and Zuther (1983) for the Baden-Baden trough based on vitrinite data. This thermal input is furthermore evidenced by paleomagnetic data from the Southern Vosges (Edel, 1997), documenting post-Permian thermal overprinting.

Zircon FT central ages and single-grain ages from the study area cluster around 190 Ma (Fig. 8). This coincides with the main hydrothermal phase (e.g. Brockamp et al., 1987, 1994; Wernicke and Lippolt, 1993; Lippolt and Kirsch, 1994; see compilation by Wetzel et al., 2003) and one of the most conspicuous subsidence pulses in the investigated area (Wetzel et al., 2003). Furthermore K–Ar data from authigenic illites in sandstones (Schaltegger et al., 1995) and from ore deposits (e.g. Bonhomme et al., 1983) in Europe scatter around 180–190 Ma. Obviously this was a time period of enhanced fluid flow (illite growth; Schaltegger et al., 1995).

Conclusions

The analysed samples experienced substantial annealing of fission tracks in zircon prior to Cretaceous cooling. Temperatures needed to allow for the observed annealing cannot be due to burial alone.

Instead, annealing is suggested to be related to a Jurassic thermal pulse, as evidenced by vein mineralisations. A thermal event is independently supported by the well-established hydrothermal activity in the investigated area, although further research is needed to determine the extent of this overprint. However, based on the present study the heating event caused by the Jurassic hydrothermal fluid migration seems to have influenced the upper crust of the southern URG area on a regional scale.

Due to the fact that samples entered the PAZ from the lower temperature boundary and were

only partially annealed, it can be assumed that a high density of α damage substantially lowered the thermal stability of the zircon fission tracks. Consequently, fluid temperatures in the order of 200–250 °C, as reported for the Jurassic hydrothermal activity in the Baden-Baden and Offenburg troughs (Brockamp and Zuther, 1983; Brockamp et al., 2003), could have been sufficient to substantially alter the palaeotemperature field in the southern URG area.

The impact of the Jurassic hydrothermal activity has important consequences on the interpretation of FT data from the URG area. Analysis of FT data using simple assumptions such as a constant paleogeothermal gradient leads inevitably to erroneous conclusions. The same is also true for the apatite FT system, especially considering that it is even more temperature-sensitive than the zircon FT system. Fluid circulation associated to Cenozoic rifting may have played a substantial role also with respect to apatite FT data. In the light of these results the interpretation of available apatite FT ages from the Black Forest as cooling ages (Michalski, 1987) is also arguable and corresponding uplift rates may have to be revised.

Acknowledgements

This work has been supported by the Swiss National Science Foundation (Project Nos. 21-57038.99 and 20-64567.01) and is a contribution to the EUCOR-URGENT project. Discussions with B. Schneider and F. Weiss about the statistical treatment of our data greatly improved the manuscript. Critical reviews by I. Dunkl, A. Hurford and an anonymous reviewer are gratefully acknowledged.

References

Bernet, M., Zattin, M., Garver, J.I., Brandon, M.T. and Vance, J.A. (2001): Steady-state exhumation of the European Alps. *Geology* **29**, 35–38.

Bonhomme, M.G., Bühmann, D. and Besnus, Y. (1983): Reliability of K/Ar-dating of clays and silifications associated with vein mineralizations in western Europe. *Geol. Rundsch*. **72**, 105–117.

Brandon, M.T., Roden-Tice, M.K. and Garver, J.I. (1998): Late Cenozoic exhumation of the Cascadia accretionary wedge in the Olympic Mountains, northwest Washington State. *Geol. Soc. Am. Bull*. **110**, 985–1009.

Brockamp, O., Clauer, N. and Zuther, M. (1994): K–Ar dating of episodic Mesozoic fluid migrations along the fault system of Gernsbach within the Moldanubian/Saxothuringian (Northern Black Forest, Germany). *Geol. Rundsch*. **83**, 180–185.

Brockamp, O., Clauer, N. and Zuther, M. (2003): Authigenic sericite record of a fossil geothermal system: the Offenburg trough, central Black Forest, Germany. *Int. J. Earth Sci*. **92**, 843–851.

Brockamp, O. and Zuther, M. (1983): Das Uranvorkommen Müllenbach/Baden-Baden, eine epigenetisch-hydrothermale Imprägnationslagerstätte in Sedimenten des Oberkarbon, Teil II: Das Nebengestein. *Neues Jahrb. Mineral. Abh*. **148**, 22–33.

Brockamp, O., Zuther, M. and Clauer, N. (1987): Epigenetic-hydrothermal origin of the sediment-hosted Müllenbach uranium deposit, Baden-Baden, W-Germany. *Monogr. Ser. Min. Dep*. **27**, 87–98.

Carlson, W.D., Donelick, R.A., and Ketcham, R.A. (1999): Variability of apatite fission track annealing kinetics I: Experimental results. *Am. Mineral.* **84**, 1213–1223.

Carpéna, J. (1992): Fission track dating of zircon: zircons from Mont Blanc granite (French-Italian Alps). *J. Geol.* **100**, 411–421.

Diebold, P. (1989): Der Nordschweizer Permokarbon-Trog und die Steinkohlenfrage der Nordschweiz. *Vjschr. natf. Ges. Zürich* **133/1**, 143–174.

Donelick, R.A., Ketcham, R.A., and Carlson, W.D., (1999): Variability of apatite fission track annealing kinetics II: Crystallographic orientation effects. *Am. Mineral.* **84**, 1224–1234.

Dumitru, T.A. (1993): A new computer-automated microscope stage system for fission-track analysis. *Nuclear Tracks and Radiation Measurements* **21**, 575–580.

Dunkl, I. (2002): Trackkey; a Windows program for calculation and graphical presentation of fission track data. *Computers Geosciences* **28/1**, 3–12.

Edel, J.-B. (1997): Les reaimantations post-permiennes dans le bassin devono-dinantien des Vosges meridionales; existence d'une phase de reaimantation au Lias, contemporaine de mineralisations d'ampleur regionale. *Comptes Rendus de l'Academie des Sciences, Paris, Serie II* **324/8**, 617–624.

Fleischer, R.L., Price, P.B. and Walker, R.M. (1965): Effects of temperature, pressure and ionization on the formation and stability of fission tracks in minerals and glasses. *J. Geophys. Res*. **70**, 1497–1502.

Fuchs, K., Bonjer, K.-P., Gajewski, D., Lueschen, E., Prodehl, C., Sandmeier, K.-J., Wenzel, F. and Wilhelm, H. (1987): Crustal Evolution of the Rhinegraben area. 1.Exploring the lower crust in the Rhinegraben rift by unified geophysical experiments. *Tectonophysics* **141**, 261–275.

Fügenschuh, B. and Schmid, S.M. (2003): Late stages of deformation and exhumation of an orogen constrained by fission-track data: A case study in the Western Alps. *Geol. Soc. Am. Bull*. **115**, 1425–1440.

Galbraith, R.F. (1988): Graphical display of estimates having differing standard errors. *Technometrics* **30**, 271–281.

Galbraith, R.F. (1990): The radial plot: graphical assesment of spread in ages. *Nuclear Tracks and Radiation Measurements* **17**, 207–214.

Galbraith, R.F. and Laslett, G.M. (1993): Statistical models for mixed fission track ages. *Nuclear Tracks Radiation Measurements* **21**, 459–70.

Geyer, O.F. and Gwinner, M.P. (1991): Geologie von Baden-Württemberg. 4., neubearb. Aufl. der "Einführung in die Geologie von Baden-Württemberg". Schweizerbart, Stuttgart.

Gleadow, A.J.W. (1981): Fission track dating methods: what are the real alternatives. *Nuclear Tracks Radiation Measurements* **5**, 3–14.

Green, P.F. (1981): A new look at statistics in fission track dating. *Nuclear Tracks and Radiation Measurements* **5**, 77–86.

Green, P.F. (1989): Thermal and tectonic history of the East Midlands shelf (onshore UK) and surrounding regions assessed by apatite fission track analysis. *J. Geol. Soc. London* **146**, 755–773.

Green, P.F., Duddy, I.R., Gleadow, A.J.W., Tingate, P.R. and Laslett, G.M. (1986): Thermal annealing of fis-

sion tracks in apatite. 1: A qualitative description. *Chem. Geol.* **59**, 237–253.

Harrison, T.M., Armstrong, R.L., Naeser, C.W. and Harakal, J.E. (1979): Geochronology and thermal history of the Coast plutonic complex, near Prince Rupert, British Columbia: *Can. J. Earth Sci.* **16**, 400–410.

Hurford, A.J. (1986): Cooling and uplift patterns in the Lepontine Alps South Central Switzerland and an age of vertical movement on the Insubric fault line. *Contrib. Mineral. Petrol.* **92**, 413–427.

Hurford, A.J. (1990): International Union of Geological Sciences Subcommission on Geochronology recommendation for the standardization of fission track dating calibration and data reporting. *Nuclear Tracks and Radiation Measurements* **17/3**, 233–236.

Hurford, A. and Carter, A. (1994): Regional thermo-tectonic histories of the Rhine Graben and adjacent Hercynian basement: a key to assessing the alpine influence in northwest Europe. 8th International Conference on Geochronology, Cosmochronology and Isotope Geology, abstracts, p. 148.

Hurford, A.J. and Green, P.F. (1982): A users' guide to fission track dating calibration. *Earth Planet. Sci. Lett.* **59/2**, 343–354.

Hurford, A.J. and Green, P.F. (1983): The zeta age calibration of fission-track dating. *Chem. Geol.* **41/4**, 285–317.

Illies, J.H. and Fuchs, K. (eds.) (1974): Approaches to Taphrogenesis. Schweizerbart, Stuttgart, 460 pp.

Illies, J.H. and Müller, St. (eds.) (1970): Graben Problems. Schweizerbart, Stuttgart, 316 pp.

Kasuya, M. and Naeser, C.W. (1988): The effect of α-damage on fission-track annealing in zircon. *Nuclear Tracks and Radiation measurements* **14**, 477–480.

Ketcham, R.A., Donelick, R.A., and Carlson, W.D. (1999): Variability of apatite fission track annealing kinetics III: Extrapolation to geological time scales. *Am. Mineral.* **84**, 1235–1255.

Krishnaswami, S., Lal, D., Prabhu, N. and MacDougall, D. (1974): Characteristics of fission tracks in zircon: applications to geochronology and cosmology. *Earth Planet. Sci. Lett.* **22**, 51–59.

Laslett, G.M., Green, P.F., Duddy, I.R. and Gleadow, A.J.W. (1987): Thermal annealing of fission tracks in apatite. 2: A quantitative analysis. *Chem. Geol.* **65**, 1–13.

Lippolt, H.J. and Kirsch, H. (1994): Isotopic investigation of post-Variscan plagioclase sericitization in the Schwarzwald gneiss massif. *Chemie der Erde* **54**, 179–198.

Meyer, M., Brockamp, O., Clauer, N., Renk, A. and Zuther, M. (2000): Further evidence for a Jurassic mineralizing event in Central Europe; K–Ar dating of hydrothermal alteration and fluid inclusion systematics in wall rocks of the Kaefersteige fluorite vein deposit in the northern Black Forest, Germany. *Mineralium Deposita* **35/8**, 754–761.

Michalski, I. (1987): Apatit-Spaltspuren-Datierungen des Grundgebirges von Schwarzwald und Vogesen: Die postvariszische Entwicklung. Unpubl. doctoral dissertation, Heidelberg, pp. 125.

Mitchell, J.G. and Halliday, A.N. (1976): Extent of Triassic/Jurassic hydrothermal ore deposits on the North Atlantic margin. *Trans. (Sect B) Inst. Min. Metall.* **85**, 159–161.

Naeser, C.W. (1976): Fission-track dating. *U. S. Geol. Surv.,* Open-File Rep. 76-190, 65 pp.

O'Sullivan, P.B. and Parrish, R.R. (1995): The importance of apatite composition and single-grain ages when interpreting fission track data from plutonic rocks: a case study from the Coast Ranges, British Columbia. *Earth Planet. Sci. Lett.* **132**, 213–224.

Paul, W. (1955): Zur Morphogenese des Schwarzwaldes (I). *Jahresheft geol. Landesamt Baden-Württ.* **1**, 395–427.

Prodehl, C., Mueller, S. and Haak, V. (1995): The European Cenozoic rift system. In: K.H. Olsen (ed.): Continental Rifts: Evolution, Structure, Tectonics. *Developments in Geotectonics* **25**, 133–212. Elsevier Sci., New York.

Rahn, M. (2001): The metamorphic and exhumation history of the Helvetic Alps, Switzerland, as revealed by apatite and zircon fission tracks. Habilitation thesis, University of Freiburg, Germany, 140 pp.

Rahn, M.K., Brandon, M.T., Batt, G.E. and Garver, J.I. (2004): A zero-damage model for fission-track annealing in zircon. *Am. Mineral.* **89**, 473–484.

Rothé, J.P. and Sauer, K. (eds.) (1967): The Rhinegraben progress report 1967. *Abh. Geol. Landesamt Baden-Wuerttemberg* **6**, 146 pp.

Schaltegger, U. (2000): U–Pb geochronology of the Southern Black Forest Batholith (Central Variscan Belt): timing of exhumation and granite emplacement. *Int. J. Earth Sci.* **88**, 814–828.

Schaltegger, U., Zwingmann, H., Clauer, N., Larque, P. and Stille, P. (1995): K–Ar dating of a Mesozoic hydrothermal activity in Carboniferous to Triassic clay minerals of northern Switzerland. *Schweiz. Mineral. Petrogr. Mitt.* **75**, 163–176.

Schaltegger, U., Schneider, J.-L., Maurin, J.C. and Corfu, F. (1996): Precise U–Pb chronometry of 345–340 Ma old magmatism related to syn-convergence extension in the Southern Vosges (Central Variscan Belt). *Earth Planet. Sci. Lett.* **144**, 403–419.

Schaltegger, U., Fanning, C.M., Günther, D., Maurin, J.C., Schulmann, K. and Gebauer, D. (1999): Growth, annealing and recrystallisation of zircon and preservation of monazite in high-grade metamorphism: conventional and in-situ U–Pb isotope, cathodoluminescence and microchemical evidence. *Contrib. Mineral. Petrol.* **134**, 186–201.

Schumacher, M.E. (2002): Upper Rhine Graben: Role of preexisting structures during rift evolution. *Tectonics* **21/1**, 6/1–17.

Sobel, E.R. and Dumitru, T.A. (1997): Thrusting and exhumation around margins of the western Tarim Basin during the India-Asia collision. *J. Geoph. Res.* **102**, 5043–5063.

Spiegel, C., Kuhlemann, J., Dunkl, I., Frisch, W., von Eynatten, H. and Balogh, K. (2000): The erosion history of the Central Alps; evidence from zircon fission track data of the foreland basin sediments. *Terra Nova* **12/4**, 163–170.

Stewart, R.J. and Brandon, M.T. (2004): Detrital-zircon fission-track ages for the „Hoh Formation"; implications for late Cenozoic evolution of the Cascadia subduction wedge. *Geol. Soc. Am. Bull.* **16**, 60–75.

Tagami, T. and Shimada, C. (1996): Natural long-term annealing of the zircon fission track system around a granitic pluton. *J. Geophys. Res.* **101/B4**, 8245–8255.

Tagami, T., Carter, A. and Hurford, A.J. (1996): Natural long-term annealing of the zircon fission-track system in Vienna Basin deep borehole samples: constraints upon the partial annealing zone and closure temperature. *Chem. Geol.* **130**, 147–157.

Tagami, T., Galbraith, R.F., Yamada, R. and Laslett, G.M. (1998): Revised annealing kinetics of fission tracks in zircon and geological implications. In: Van den Haute, P. and De Corte, F. (eds.): Advances in Fission Track Geochronology, Kluwer Academic Publishers, Dordrecht, 99–112.

Tapfer, M. (1987): Geochemical characteristics of non-strata-bound uranium mineralization of the Muellenbach Deposit (northern Schwarzwald, W. Germa-

ny). In: Proceedings of the Uranium symposium. *Monograph Series on Mineral Deposits* **27**, 99–106.
von Gehlen, K. (1987): Formation of Pb–Zn–F–Ba mineralizations in SW Germany: a status report. *Fortschr. Mineral.* **65/1**, 87–113.
Wagner, G.A., Michalski, I. and Zaun, P. (1989): Apatite fission track dating of the Central European basement. Postvariscan thermo-tectonic evolution. In: Emmermann, R. and Wohlenberg, J. (eds.): The German Continental Deep Drilling Program (KTB). Site-selection studies in the Oberpfalz and Schwarzwald. Springer-Verlag, Berlin, 481–500.
Wagner, G.A. and van den Haute, P. (1992): Fission-Track Dating. Kluwer Academic Publishers.
Wernicke, R.S. and Lippolt, H.J. (1993): Botryoidal hematite from the Schwarzwald (Germany): heterogeneous uranium distributions and their bearing on the helium dating method. *Earth Planet. Sci. Lett.* **114**, 287–300.
Wernicke, R.S. and Lippolt, H.J. (1997): (U + Th)-He evidence of Jurassic continuous hydrothermal activity in the Schwarzwald basement, Germany. *Chem. Geol.* **138**, 273–285.
Wetzel, A., Allenbach, R. and Allia, V. (2003): Reactivated basement structures affecting the sedimentary facies in a tectonically „quiescent" epicontinental basin: an example from NW Switzerland. *Sedimentary Geology* **157**, 153–172.
Wimmenauer, W. and Schreiner, A. (1990): Erläuterungen zu Blatt 8114, Feldberg. Geol. Karte Baden-Württ. 1:25 000, Stuttgart, 134 pp.
Wyss, A. (2001): Apatit Spaltspur Untersuchungen in der Vorwaldscholle (SW-Deutschland). Unpubl. diploma thesis, Univ. Basel, 69 pp.
Yamada, R., Tagami, T., Nishimura, S. and Ito, H. (1995): Annealing kinetics of fission tracks in zircon: an experimental study. *Chem. Geol.* **122**, 249–258.
Zaun, P.E. and Wagner, G.A. (1985): Fission-track stability in zircons under geological conditions. *Nuclear Tracks and Radiation Measurements* **10**, 303–307.
Ziegler, P.A. (1990): Geological Atlas of Western and Central Europe. Shell Internationale Petroleum Maatschappij – Geological Society Publishing House, 239 pp.
Zuther, M. and Brockamp, O. (1988): The fossil geothermal system of the Baden-Baden trough (Northern Black Forest, Germany). *Chem. Geol.* **71**, 337–353.

Received 12 November 2003
Accepted in revised form 8 September 2004
Editorial handling: R. Gieré

III. Low-temperature thermochronology of the flanks of the southern Upper Rhine Graben

by Zoltan Timar-Geng, Bernhard Fügenschuh, Andreas Wetzel and Horst Dresmann

Published in:
International Journal of Earth Sciences 95, 685-702, 2006

Int J Earth Sci (Geol Rundsch) (2006) 95: 685–702
DOI 10.1007/s00531-005-0059-1

ORIGINAL PAPER

Zoltan Timar-Geng · Bernhard Fügenschuh
Andreas Wetzel · Horst Dresmann

Low-temperature thermochronology of the flanks of the southern Upper Rhine Graben

Received: 6 June 2005 / Accepted: 22 October 2005 / Published online: 14 December 2005

Abstract The Upper Rhine Graben (URG) is the most perceptible part of the European Cenozoic Rift System. Uplifted Variscan basement of the Black Forest and the Vosges forms the flanks of the southern part of the graben. Apatite and zircon fission-track (FT) analyses indicate a complex low-temperature thermal history of the basement that was deciphered by inverse modelling of FT parameters. The models were tested against the observed data and independent geological constraints. The zircon FT ages of 28 outcrop samples taken along an E–W trending transect across the Black Forest and the Vosges range from 136 to 312 Ma, the apatite FT ages from 20 to 83 Ma. The frequency distributions of confined track lengths are broad and often bimodal in shape indicating a complex thermal history. Cooling below 120°C in the Early Cretaceous to Palaeogene was followed by a discrete heating episode during the late Eocene and subsequent cooling to surface temperature. The modelled time–temperature (*t*–*T*) paths point to a total denudation of the flanks of URG in the range of 1.0–1.7 km for a paleogeothermal gradient of 60°C/km, and 1.3–2.2 km for a paleogeothermal gradient of 45°C/km since the late Eocene.

Keywords Upper Rhine Graben · Black Forest · Vosges · Fission-track · Low-temperature thermal history

Z. Timar-Geng (✉) · B. Fügenschuh · A. Wetzel · H. Dresmann
Geologisch-Paläontologisches Institut, Universität Basel,
Bernoullistrasse 32, 4056 Basel, Switzerland
E-mail: zoltan.timar-geng@geologie.uni-freiburg.de
Tel.: +49-761-2036477
Fax: +49-761-2036496

Present address: Z. Timar-Geng
Geologisches Institut, Albert-Ludwigs-Universität Freiburg,
Albertstr. 23b, 79104 Freiburg, Germany

Introduction

The Upper Rhine Graben (URG) forms part of a complex Cenozoic rift system that extends over a distance of more than 1,000 km from the North Sea to the western Mediterranean (Fig. 1). The N–NE trending southern branch of the URG is flanked by uplifted Variscan basement, exposed in the Black Forest and Vosges, and limited to the south by the Swiss Jura Mountains.

In the last decades, a large amount of geological and geophysical data has been collected by evaluating the structure of the URG (e.g. Rothé and Sauer 1967; Illies and Müller 1970; Illies and Fuchs 1974; Fuchs et al. 1987; Prodehl et al. 1995) and its Cenozoic evolution (e.g. Schumacher 2002; Dèzes et al. 2004). The URG developed in the foreland of the Alps by passive rifting in response to the elevated collision-related compressional intraplate stresses (Dèzes et al. 2004). Thus, the Cenozoic uplift and exhumation history of the Black Forest and Vosges may reflect changes in the interplay between the Alpine orogenic wedge and its foreland (Schumacher 2002) as well as onset of plume-type upwelling of the sub-lithospheric mantle and thermal weakening of the foreland lithosphere (Dèzes et al. 2004). In this context, it is of particular interest to closely constrain the low-temperature thermochronology of the strongly uplifted flanks of the southern URG as this especially may reveal the timing and magnitude of distinct heating and cooling events. Furthermore, there are still some ambiguities concerning the overall picture. For example, the time lag between Late Eocene initial graben formation and Middle to Late Miocene flank uplift suggests that these two phases are not closely related. In addition, the amount of rift flank exhumation in the southern part significantly exceeds that in the north.

Fission-track (FT) analysis is a suitable method, particularly to reconstruct the low-temperature thermal history of the uppermost parts of the crust. It has

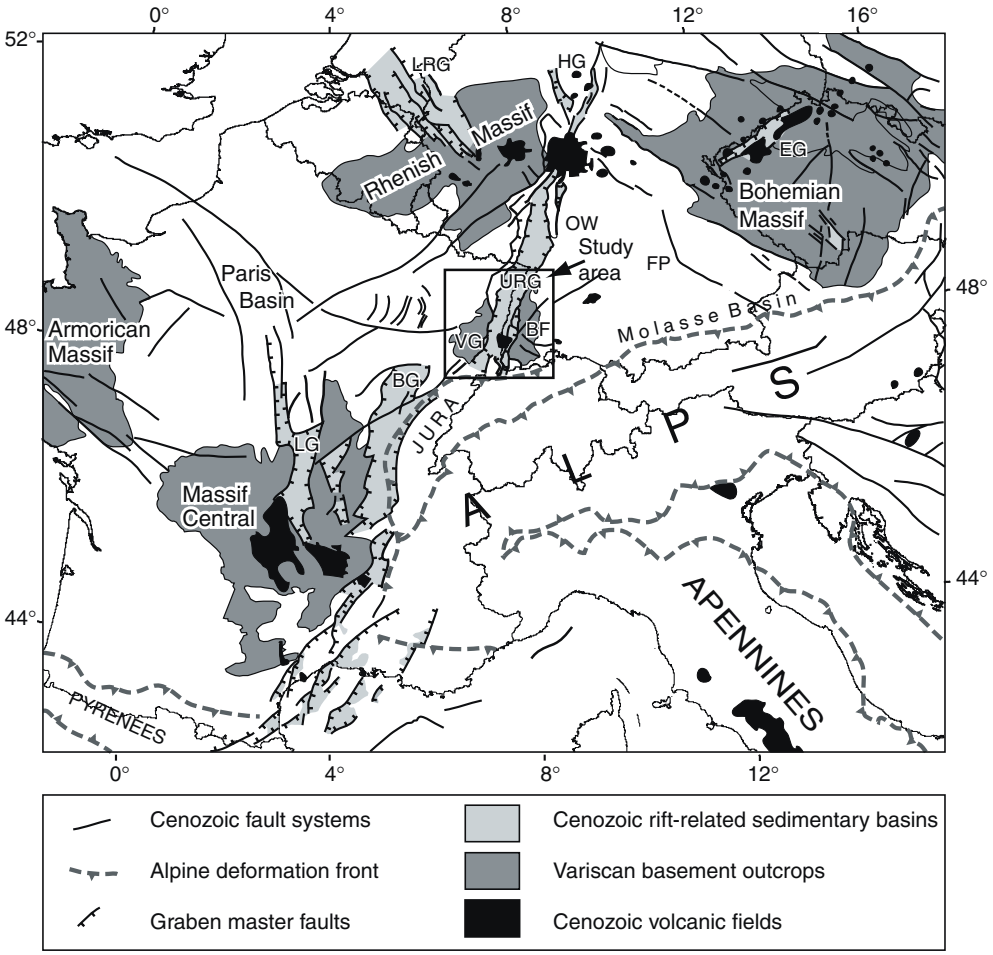

Fig. 1 The European Cenozoic Rift System in the foreland of the Alps (after Dèzes et al. 2004). *BF* Black Forest, *BG* Bresse Graben, *EG* Eger Graben, *FP* Franconian Platform, *HG* Hessian grabens, *LG* Limagne Graben, *LRG* Lower Rhine Graben, *OW* Odenwald, *URG* Upper Rhine Graben, *VG* Vosges

already been successfully applied to continental extension zones (e.g. Foster et al. 1993; Foster and Gleadow 1996; Foster and Raza 2002). Existing apatite FT data (Michalski 1987; Wagner 1990; Hurford and Carter 1994; Wyss 2001) from the southern URG area roughly document the Late Cretaceous to Tertiary cooling history of the Black Forest and Vosges. These apatite FT ages cluster around 80–100, 55–70 and 30–40 Ma and indicate slow overall cooling since the Middle Cretaceous. These early studies revealed pronounced block faulting and an increased paleogeothermal gradient, which have been related to the formation of the URG (Michalski 1987; Wagner et al. 1989; Wagner 1990). However, to provide a more comprehensive analysis, it is desirable to include the track length distributions, which have a direct record of the temperatures experienced since accumulation of the tracks. Together with the FT age, they can be used to reconstruct quantitatively the thermal history.

It is the purpose of the present investigation to elucidate the low-temperature thermal history of the flanks of the southern URG. Based on new zircon and apatite FT data from basement rocks sampled along two E–W trending transects in the Black Forest and the Vosges (Fig. 2), the thermal history was evaluated by an inverse modelling procedure.

Post-Variscan evolution

After the late Variscan consolidation of the crust, the mountain range in the today's area of the southern URG was eroded forming a peneplain at the Permian/Triassic transition (Geyer and Gwinner 1991). Compared to the late Paleozoic, the Mesozoic was a period of relative tectonic inactivity characterised by subsidence and marine transgression. A series of up to 1,500 m well-stratified Triassic to Jurassic sediments accumulated on Permo-Carboniferous sedimentary rocks or on the crystalline basement (Geyer and Gwinner 1991). Only minor Jurassic reactivation of pre-existing basement structures led to synsedimentary deformation and some variations in thickness and facies (Wetzel et al. 2003). Contemporaneous substantial hydrothermal activity is evidenced by many vein-type mineralizations of Mesozoic age (e.g. von Gehlen 1987; Wernicke and Lippolt 1997; see compilation by Wetzel et al. 2003). Zircon FT data indicate that circulating hydrothermal fluids with temperatures in the order of 200–250°C significantly altered the paleotemperature field in the upper crust during Mesozoic times (Timar-Geng et al. 2004). In the southern URG area large-scale domal uplift commenced towards the end of the Jurassic (Illies 1977; Geyer and Gwinner 1991). Cre-

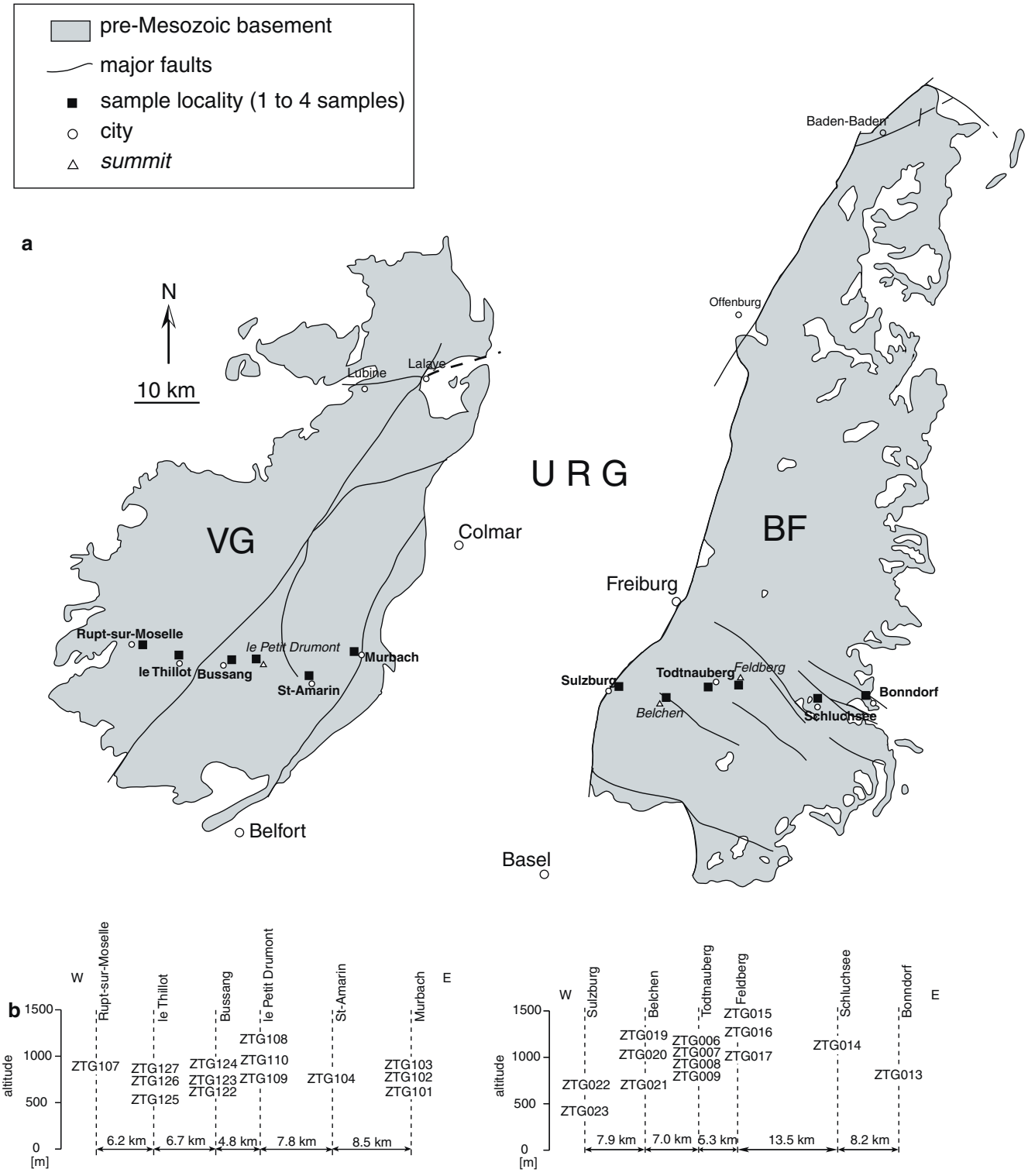

Fig. 2 **a** Outline of the outcropping Variscan basement forming the flanks of the southern Upper Rhine Graben with sample localities for fission-track analysis. *BF* Black Forest, *URG* Upper Rhine Graben, *VG* Vosges. **b** Schematic E–W profile showing the elevation of samples

taceous to Palaeogene deposits are absent in this area. However, it is still a matter of debate, if Cretaceous sediments were completely eroded during latest Cretaceous and Paleocene times (Ziegler 1990) or if they were never deposited (e.g. Geyer and Gwinner 1991).

The Cenozoic evolution of the southern URG area is characterised by renewed tectonic activity reflecting the interaction of the Alpine orogen with its foreland (Dèzes et al. 2004). Rifting and subsidence of the URG started with the nucleation of Middle to Late Eocene local basins,

which further evolved and became connected under repeatedly changing stress fields, and remained active until the present (Schumacher 2002). Middle Miocene large-scale uplift of the Black Forest and the Vosges due to lithospheric folding was controlled by NW-directed compressional stresses built up in the Alpine foreland (Dèzes et al. 2004). The volcanic activity started slightly before the initial graben formation, but remained active until Miocene times (Keller et al. 2002). The associated mantle upwelling system beneath the Alpine foreland caused thermal weakening of the lithosphere (Ziegler et al. 1995).

Neotectonic activity is clearly shown by deformed Pliocene fluvial gravels (Giamboni et al. 2004), and the elevated seismic activity as evident by strong historical earthquakes in the URG area. Fault-plane solutions of recent earthquakes document ongoing sinistral strike- and oblique-slip movements in the URG as a result of NNW–SSE oriented compression (Werner and Franzke 2001).

Fission-track thermochronology

The FT dating is a radiometric dating method to determine a FT age of uranium bearing minerals like zircon and apatite (for a detailed overview see, e.g. Gallagher et al. 1998; Gleadow and Brown 2000). The spontaneous fission of ^{238}U leaves a trail of damage in the crystal lattice (Price and Walker 1962a, b). From the number of tracks formed since the crystal for the last time cooled below the track retention temperature, a FT age can be calculated. Because of a process called annealing (e.g. Naeser 1979), a geologic meaning can rarely be ascribed to such an age. In a wide temperature range, referred to as partial annealing zone (PAZ, e.g. Wagner 1979), fission tracks gradually shorten and at even higher temperatures disappear completely over geological time. As a result, FT ages are often younger than the conventional (U-Pb and K-Ar) radiometric ages of the same samples. This, at first sight, disturbing characteristic of the annealing process turned out to be a key feature that enables the FT method to become a unique tool for deciphering the thermochronology of rocks. Temperature is the most important factor that causes annealing and, consequently, controls the degree of track shortening. Therefore, the track length distribution of a sample yields significant thermal history information over a protracted temperature range. In practice, from the single grain age and track length data a detailed thermal history can be constructed, rather than just an estimate of the timing when the sample cooled through the closure temperature.

Table 1 Zircon FT data of the Black Forest and Vosges

Sample number	Coordinates (GK3)	Elevation (m)	Rock type	Number of crystals counted	Spontaneous tracks $\rho_s(N_s)$	Induced tracks ρ_i (N_i)	$P(\chi^2)$ (%)	Dosimeter $\rho_d(N_d)$	Disp.	Central age (Ma) $\pm 1\sigma$
Black Forest										
ZTG006	3420040, 5301820	1,085	Anatectic gneiss	20	183 (1737)	15 (139)	56	4.51 (1732)	0.05	312 ± 29
ZTG007	3420005, 5301405	1,010	Anatectic gneiss	20	200 (1485)	17 (123)	89	4.18 (1605)	0.00	280 ± 28
ZTG008	3419990, 5301285	960	Anatectic gneiss	20	133 (1196)	13 (113)	96	4.44 (1705)	0.00	262 ± 27
ZTG009	3419815, 5301280	860	Anatectic gneiss	20	243 (1675)	26 (179)	67	4.90 (1882)	0.02	255 ± 22
ZTG013	3448455, 5299915	770	Granite	20	305 (2101)	55 (379)	<0.001	4.84 (1859)	0.50	146 ± 19
ZTG014	3438620, 5299295	1,100	Granite	9	274 (514)	52 (97)	63	4.57 (1755)	0.49	136 ± 16
ZTG015	3425620, 5304330	1,480	Anatectic gneiss	20	250 (1515)	23 (141)	91	4.77 (1832)	0.01	285 ± 26
ZTG016	3426215, 5303360	1,250	Orthogneiss	14	257 (834)	22 (72)	96	4.31 (1655)	0.00	277 ± 35
ZTG017	3425355, 5302705	980	Paragneiss	20	319 (2214)	27 (185)	85	3.66 (1405)	0.00	244 ± 20
ZTG019	3412965, 5299095	1,210	Anatectic gneiss	17	118 (1285)	11 (124)	46	4.70 (1805)	0.13	269 ± 28
ZTG020	3412925, 5299685	1,000	Anatectic gneiss	17	292 (1431)	27 (130)	22	4.64 (1782)	0.19	282 ± 31
ZTG021	3412150, 5300195	690	Anatectic gneiss	20	203 (1090)	23 (125)	22	4.05 (1555)	0.22	195 ± 22
ZTG022	3404790, 5301740	690	Paragneiss	20	267 (1269)	30 (143)	55	3.92 (1505)	0.07	194 ± 18
ZTG023	3403780, 5301265	400	Paragneiss	20	231 (1671)	25 (182)	39	3.99 (1532)	0.08	204 ± 18
Vosges										
ZTG101	3360955, 5310900	605	Granite	4	352 (318)	42 (38)	32	4.01 (1540)	0.10	184 ± 34
ZTG102	3360440, 5310740	760	Granite	17	341 (1015)	38 (113)	3.5	4.12 (1582)	0.32	202 ± 26
ZTG103	3360155, 5310970	850	Granite	15	313 (1000)	44 (141)	45	4.10 (1574)	0.06	163 ± 16
ZTG107	3327230, 5312175	840	Granite	6	454 (410)	55 (50)	95	3.98 (1528)	0.00	182 ± 28
ZTG108	3344305, 5309310	1,200	Granite	20	450 (1000)	45 (101)	66	4.07 (1563)	0.00	225 ± 24
ZTG109	3342910, 5310030	740	Granite	20	371 (969)	46 (120)	99	3.99 (1532)	0.00	180 ± 18
ZTG110	3343230, 5309100	960	Granite	7	460 (359)	46 (36)	89	4.15 (1594)	0.00	231 ± 41
ZTG123	3340290, 5308750	750	Granite	11	432 (727)	52 (88)	6	4.38 (1682)	0.28	200 ± 29
ZTG124	3340440, 5309340	880	Granite	4	612 (209)	59 (20)	44	4.36 (1674)	0.00	254 ± 60
ZTG125	3332465, 5308815	560	Granite	11	458 (637)	58 (81)	99	4.08 (1567)	0.00	180 ± 22
ZTG127	3333085, 5310170	825	Granite	20	408 (836)	43 (88)	96	4.13 (1586)	0.00	219 ± 25

Track densities (ρ) are in 10^5 tracks/cm^2, number of tracks counted (N) shown in brackets. Analyses by external detector method using 0.5 for the $4\pi/2\pi$ geometry correction factor. Disp. = Dispersion, according to Galbraith and Laslett (1993). Ages calculated as central ages according to Galbraith and Laslett (1993) using dosimeter glass CN1 with $\zeta_{CN1} = 113.49 \pm 1.80$ (Z. Timar-Geng). $P(\chi^2)$ is the probability of obtaining χ^2 value for v degrees of freedom where v = number of crystals−1

Table 2 Apatite FT data of the Black Forest and Vosges

Sample number	Coordinates (GK3)	Elevation (m)	Rock type	Number of crystals counted	Spontaneous tracks ρ_s (N_s)	Induced tracks ρ_i (N_i)	$P(\chi^2)$ (%)	Dosimeter ρ_d(N_d)	Disp.	Central age (Ma) $\pm 1\sigma$
Black Forest										
ZTG006	3420040, 5301820	1,085	Anatectic gneiss	20	18 (787)	48 (2084)	< 0.001	8.19 (3143)	0.30	54 ± 5
ZTG007	3420005, 5301405	1,010	Anatectic gneiss	20	7 (309)	19 (886)	0.6	8.84 (3393)	0.29	53 ± 5
ZTG008	3419990, 5301285	960	Anatectic gneiss	20	13 (827)	21 (1329)	26	7.55 (2898)	0.04	81 ± 4
ZTG009	3419815, 5301280	860	Anatectic gneiss	20	6 (345)	14 (831)	< 0.001	9.16 (3516)	0.52	83 ± 12
ZTG013	3448455, 5299915	770	Granite	20	9 (704)	17 (1408)	65	7.01 (2689)	0.02	60 ± 3
ZTG014	3438620, 5299295	1,100	Granite	20	8 (463)	32 (1794)	0.1	9.06 (3475)	0.25	42 ± 4
ZTG015	3425620, 5304330	1,480	Anatectic gneiss	20	13 (720)	43 (2479)	1.7	10.09 (3871)	0.16	51 ± 3
ZTG016	3426215, 5303360	1,250	Orthogneiss	20	20 (1251)	50 (3151)	< 0.001	6.67 (2559)	0.16	46 ± 3
ZTG017	3425355, 5302705	980	Paragneiss	20	22 (936)	69 (2919)	1.4	10.43 (4001)	0.16	56 ± 4
ZTG019	3412965, 5299095	1,210	Anatectic gneiss	20	14 (639)	41 (1870)	< 0.001	8.72 (3345)	0.24	51 ± 4
ZTG020	3412925, 5299685	1,000	Anatectic gneiss	20	6 (254)	36 (1572)	40	7.36 (2823)	0.13	20 ± 2
ZTG021	3412150, 5300195	690	Anatectic gneiss	20	4 (199)	35 (1649)	< 0.001	10.45 (4011)	0.56	27 ± 4
ZTG022	3404790, 5301740	690	Paragneiss	20	9 (320)	66 (2371)	< 0.001	9.81 (3765)	0.51	20 ± 3
ZTG023	3403780, 5301265	400	Paragneiss	20	14 (826)	76 (4540)	< 0.001	10.13 (3888)	0.26	33 ± 3
Vosges										
ZTG101	3360955, 5310900	605	Granite	20	20 (815)	92 (3760)	< 0.001	10.94 (4203)	0.26	40 ± 3
ZTG102	3360440, 5310740	760	Granite	20	17 (679)	69 (2733)	0.9	9.00 (3458)	0.17	38 ± 3
ZTG103	3360155, 5310970	850	Granite	20	21 (1173)	88 (4896)	8	11.64 (4472)	0.10	48 ± 3
ZTG104	3352140, 5307635	750	Granite	20	7 (329)	28 (1327)	6	10.58 (4065)	0.19	45 ± 4
ZTG107	3327230, 5312175	840	Granite	20	5 (236)	30 (1292)	27	11.29 (4338)	0.12	36 ± 3
ZTG108	3344305, 5309310	1,200	Granite	20	14 (673)	38 (1747)	46	10.76 (4134)	0.02	71 ± 4
ZTG109	3342910, 5310030	740	Granite	20	13 (656)	45 (2227)	3.4	10.23 (3930)	0.15	52 ± 3
ZTG110	3343230, 5309100	960	Granite	20	7 (311)	21 (955)	< 0.001	10.05 (3861)	0.37	61 ± 7
ZTG122	3339230, 5310445	640	Granite	20	4 (289)	27 (1911)	< 0.001	9.96 (3827)	0.36	26 ± 3
ZTG123	3340290, 5308750	750	Granite	20	5 (363)	23 (1514)	1.9	9.70 (3728)	0.20	40 ± 3
ZTG124	3340440, 5309340	880	Granite	20	10 (544)	29 (1569)	5	12.49 (4799)	0.16	75 ± 5
ZTG125	3332465, 5308815	560	Granite	20	10 (416)	41 (1639)	< 0.001	12.19 (4683)	0.25	61 ± 5
ZTG126	3333255, 5309805	730	Granite	20	20 (601)	59 (1819)	< 0.001	11.89 (4568)	0.33	71 ± 7
ZTG127	3333085, 5310170	825	Granite	20	13 (471)	37 (1313)	1.9	9.70 (3727)	0.20	61 ± 5

Track densities (ρ) are in 10^5 tracks/cm^2, number of tracks counted (N) shown in brackets. Analyses by external detector method using 0.5 for the $4\pi/2\pi$ geometry correction factor. *Disp.*, Dispersion, according to Galbraith and Laslett (1993). Ages calculated as central ages according to Galbraith and Laslett (1993) using dosimeter glass CN5 with $\zeta_{CN5} = 345.69 \pm 8.75$ (Z. Timar-Geng). $P(\chi^2)$ is the probability of obtaining χ^2 value for v degrees of freedom where v = number of crystals−1

In the last decades, several annealing models for apatite have been developed to characterise FT annealing as function of time and temperature (e.g. Laslett et al. 1987; Carlson 1990; Crowley et al. 1991; Laslett and Galbraith 1996; Ketcham et al. 1999). With an inverse modelling approach, including generation of candidate *t–T* paths and statistical evaluation of the goodness-of-fit between model predictions and the observed data, it is possible to determine a range of thermal histories that are consistent with both the measured FT age and track length distribution (Ketcham et al. 2000). However, it has to be kept in mind that this approach does not provide an unequivocal answer in terms of a strict mathematical inversion, but offers a wide range of *t–T* paths that could produce the measured data. It is the task of a geologist to find the "geologically reasonable" model by constraining the range of possible thermal histories based on independent geologic evidence.

Methodological details

Twenty-eight basement samples were collected for FT analysis along an E–W oriented transect across the southern Vosges and the southern Black Forest (Fig. 2 and Table. 1, 2). Apatite and zircon samples were separated by using conventional magnetic and heavy liquid techniques. After mounting in epoxy resin (apatite) and PFA® Teflon (zircon), grinding, and polishing, apatites were etched for 40 s in 6.5% HNO_3 at room temperature and zircons for 6–13 h in a KOH–NaOH eutectic melt at 220°C. Thermal neutron irradiation was performed at the Australian Nuclear Science and Technology Organisation (ANSTO) facility, Lucas Heights, Australia. External mica detectors were etched for 40 min in 40% HF at room temperature. Track counting and track length measurements were carried out under an optical microscope ("Axioscope" by Zeiss) with the aid of a computer driven stage (Dumitru 1993). The magnification applied was 1,600× using a dry objective for apatite FT analysis (both for track counting and confined track length measurement) and 2,500 × using an oil immersion objective for zircon FT analysis. Samples were dated by the external detector method (Naeser 1976; Gleadow 1981) applying the zeta approach (Hurford and Green 1982, 1983) with a zeta value of 345.69 ± 8.75 (Durango, CN5) for apatite and 113.49 ± 1.80 (Fish Canyon Tuff, CN1) for zircon. FT ages and their graphical represen-

tations were calculated and generated by using the computer program Trackkey (Dunkl 2002). All FT ages are displayed as central ages (Galbraith and Laslett 1993) and errors are quoted as $\pm 1\sigma$.

Fission-track results

Twenty-five new zircon FT ages and twenty-eight new apatite FT ages are presented according to the I.U.G.S. recommendations (Hurford 1990) together with details of the measurement in Tables 1 and 2. Zircon and apatite FT ages, radial plots (Galbraith 1988, 1990) of single grain ages, and track length distributions are shown in Figs. 3, 4, 5, 6, 7, 8 and 9. Both zircon and apatite FT ages of the samples collected on the two flanks of the southern URG are very similar and cover the entire age range found by previous studies (Michalski 1987; Hurford and Carter 1994; Wyss 2001; Timar-Geng et al. 2004).

Black Forest

Fourteen basement samples were collected along an E–W transect with a maximum elevation difference of 1,080 m in the southern Black Forest (Fig. 2).

Zircon FT central ages range from 136 ± 16 to 312 ± 29 Ma (Fig. 3 and Table 1). No regional trend is detectable in the spatial distribution of the age data. However, a vertical trend of increasing zircon FT central ages with elevation can be observed. Radial plots of zircon samples reveal broad single-grain age distributions from ~500 to ~100 Ma (Fig. 4). In all the cases except one (ZTG013), the wide spread of single-grain ages falls into the natural Poissonian variation as obtained by the applied χ^2 statistics (Table 1); $P(\chi^2)$ values higher than 5% indicate that all grains of an individual sample belong to a single age population (Green 1981).

Apatite FT central ages range from 20 ± 2 to 83 ± 12 Ma (Fig. 3 and Table 2), the youngest ages are found in the proximity of the URG. Radial plots (Fig. 5) display a large spread of the single-grain ages between ~100 and ~5 Ma. In most of the samples, several age populations are present as revealed by the χ^2 statistics (Table 2). Track length distributions differ significantly in their shape from unimodal (e.g. ZTG013, ZTG015) to clearly bimodal (e.g. ZTG006, ZTG007, ZTG008, ZTG009, ZTG023). Confined mean track lengths range between 10.5 and 12.1 μm with relatively large standard deviations of ~2 to ~3 μm.

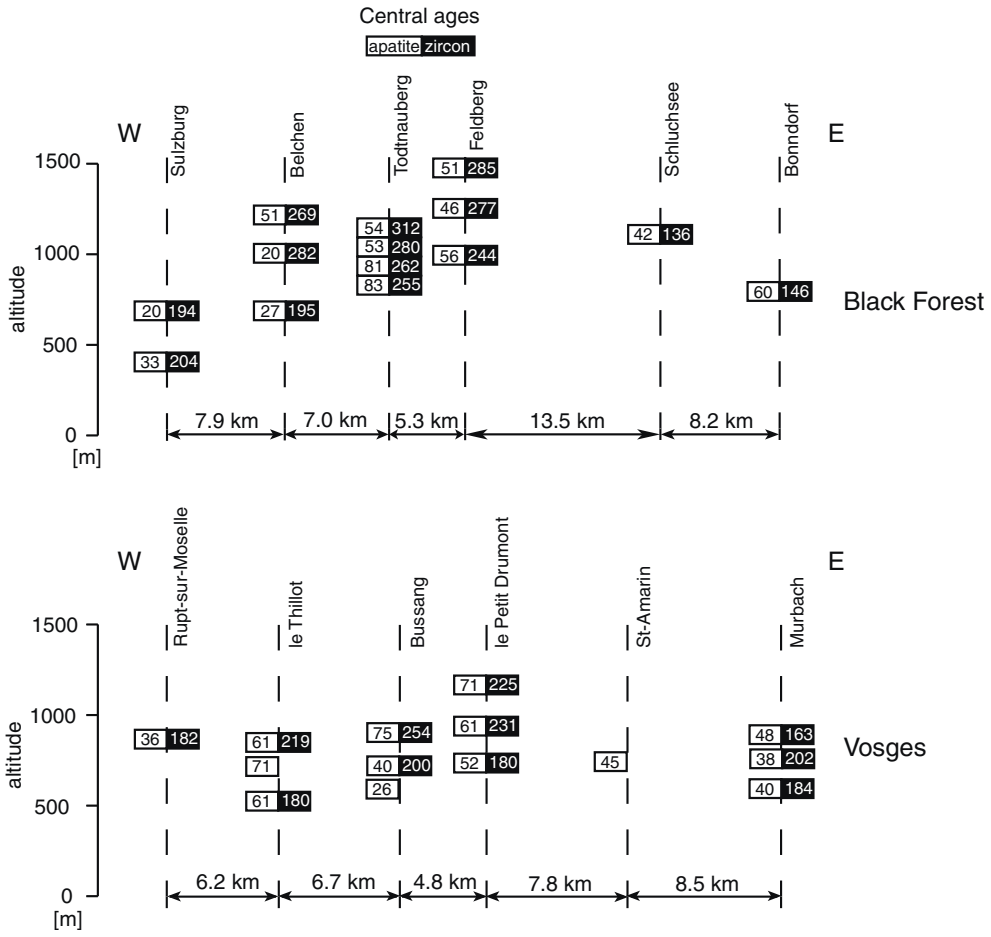

Fig. 3 Zircon (right side of bar) and apatite FT central ages (left side of bar) in Ma ordered according to the sections shown in Fig. 2b showing some of the weak vertical trends discussed in the text. Their respective errors are presented on Figs. 4, 5, 7 and 8

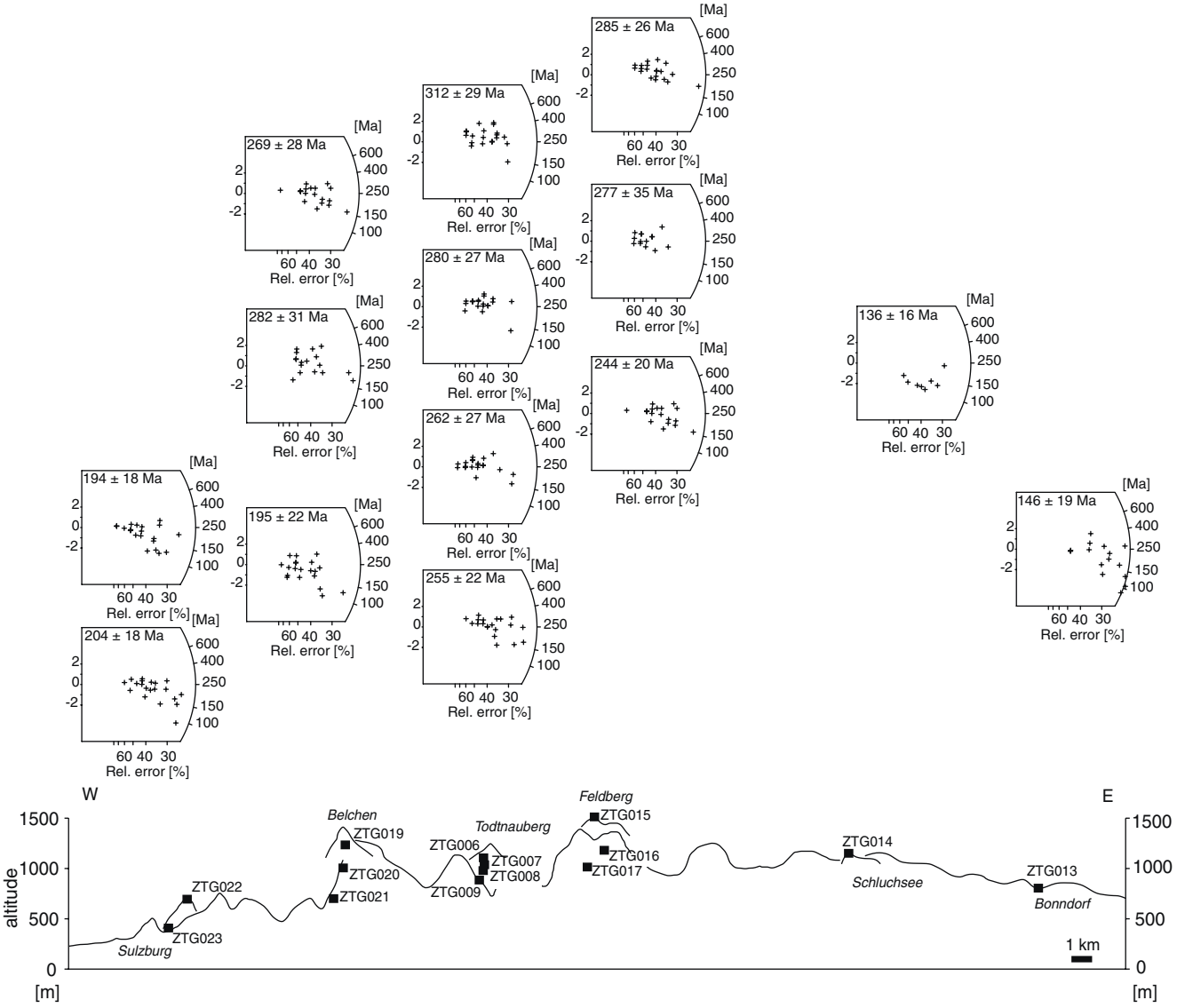

Fig. 4 Zircon FT radial plots of the Black Forest samples. An E–W topographic profile (vertical scale exaggerated by a factor of 5) with sample locations is shown at the bottom of the figure

Vosges

Along the second E–W transect in the southern Vosges, another 14 basement samples were collected with an elevation difference of 640 m (Fig. 2).

Zircon FT central ages scatter between 163 ± 16 and 254 ± 60 Ma (Fig. 3 and Table 1) without a discernible regional trend. Single-grain ages (Fig. 7) range from ~400 to ~100 Ma with no statistical indication of an extra-Poissonian variation (except ZTG102, Table 1).

Apatite FT central ages range from 26 ± 3 to 75 ± 5 Ma (Fig. 3 and Table 2) and are evenly distributed over the entire area. The vertical FT age profiles show a weak tendency to increase with an increase in elevation. Radial plots (Fig. 8) reveal a spread of the single-grain ages from ~100 to ~10 Ma. In most of the cases, $P(\chi^2)$ values are lower than 5% (Table 2), thus indicating an extra-Poissonian variation among single-grain ages within individual samples. Bimodality in the track length distributions (Fig. 9) is less pronounced than in the Black Forest, but most of them are relatively broad. Confined mean track lengths range from 10.1 to 12.7 μm; their standard deviations are somewhat lower than in the Black Forest ranging from 1.7 to 2.3 μm.

Thermal modelling of apatite FT data

Thermal modelling of the FT parameters was carried out with the help of the computer programme AFTSolve (Ketcham et al. 2000) by using the Laslett et al. (1987) algorithm and an initial track length of 16.3 μm. By adopting the inverse modelling approach (for details see Ketcham et al. 2000) after careful selection of fitting

692

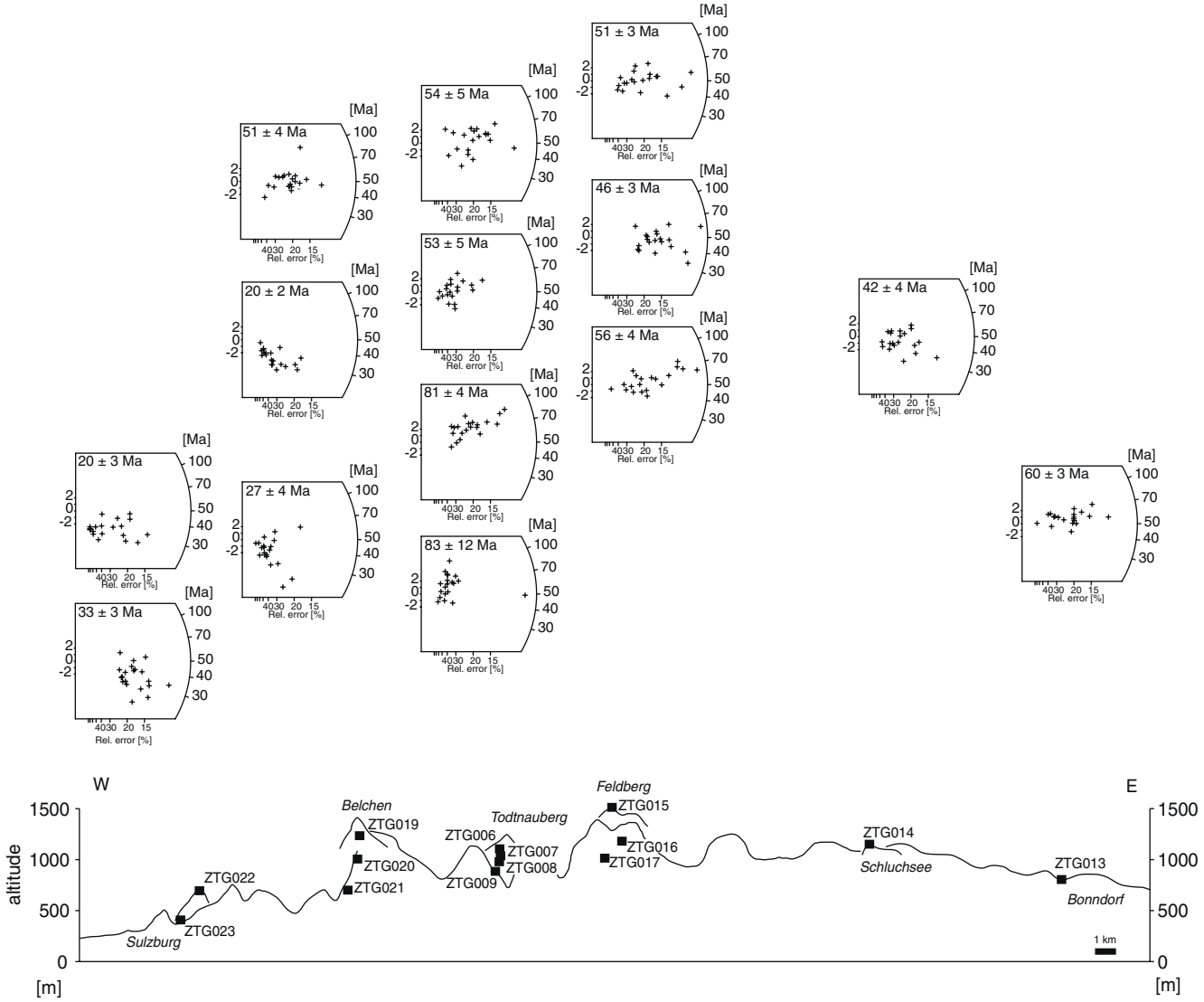

Fig. 5 Apatite FT radial plots of the Black Forest samples. An E–W topographic profile (vertical scale exaggerated by a factor of 5) with sample locations is shown at the bottom of the figure

conditions, i.e. time–temperature (t–T) constraints that all cooling paths must pass through, thermal history information from apatite FT data could be derived, resulting in two differing portions of the t–T space and a best-fit path (Figs. 10, 11). The outer envelope bounds all models that provide statistically "acceptable" fits (Kolmogorov–Smirnov probability ≥0.05) and the inner envelope bounds all models that provide statistically "good" fits (Kolmogorov–Smirnov probability ≥0.5). For an exact description of the underlying statistical tests, the reader is referred to Ketcham et al. (2000). Modelling of the FT parameters was an iterative process as model runs were gradually refined by forcing limitations on the t–T paths as suggested by consecutive modelling results and geological observations. Modelling details are listed in Appendix.

Black Forest

Best-fit models of the Black Forest samples indicate that there was total annealing of apatite fission tracks in the Early Cretaceous (Fig. 10). One sample next to the eastern boundary of the URG (ZTG023) cooled below track retention temperature, i.e. ~120°C, not until the Palaeogene. Oldest tracks preserved in the best-fit models scatter between 43 Ma (ZTG023) and 125 Ma (ZTG009) and neither a regional trend nor a correlation with sample elevation is identifiable. Measured and predicted parameters of the best-fit paths are in very good agreement, with age goodness-of-fit values of up to 0.96 and Kolmogorov–Smirnov probabilities of up to 0.98. The modelled t–T paths of only one sample (ZTG013) failed to yield good fits to the measured data,

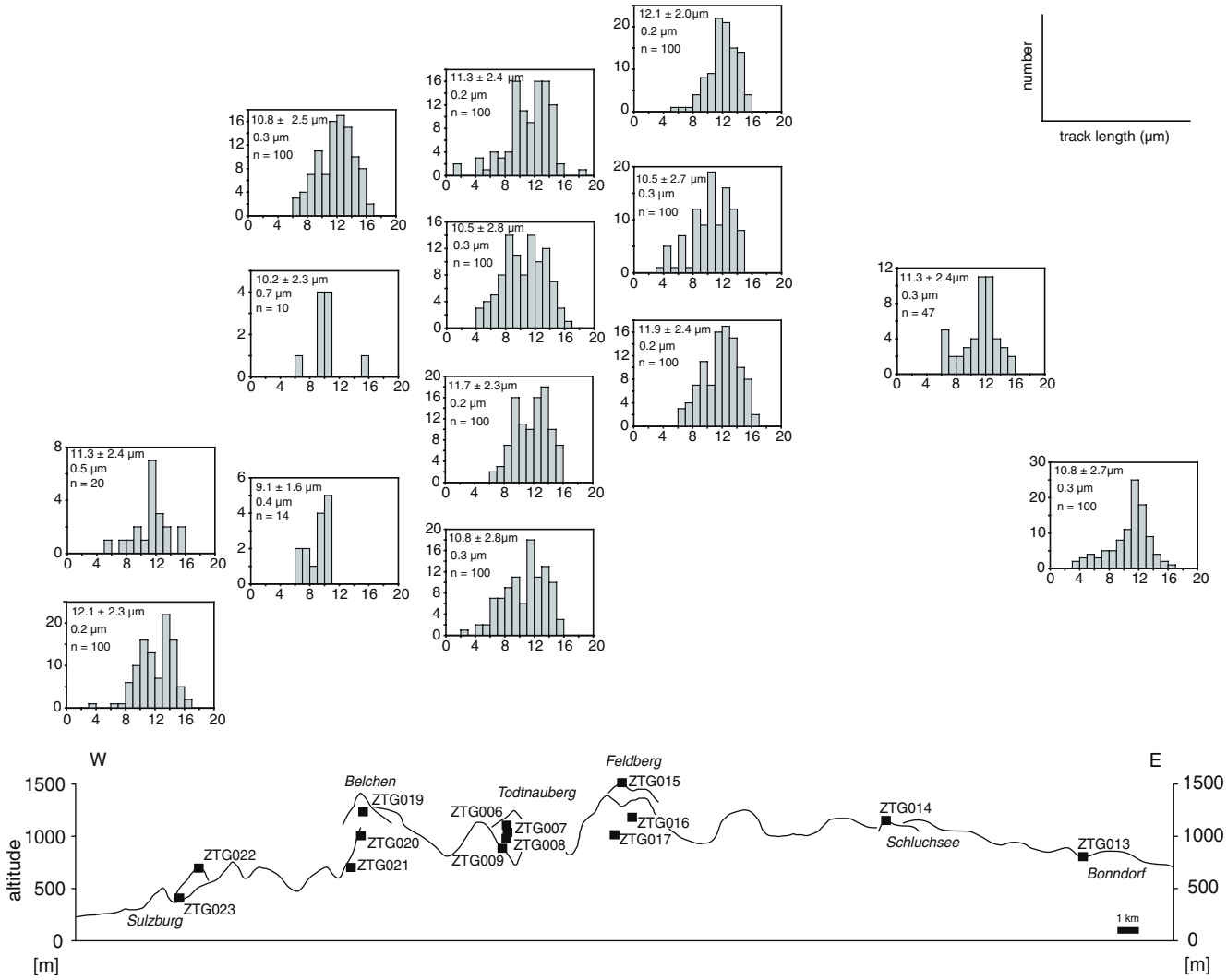

Fig. 6 Apatite FT length distributions of the Black Forest samples. An E–W topographic profile (vertical scale exaggerated by a factor of 5) with sample locations is shown at the bottom of the figure

but acceptable fits exhibit the same general shape as the best-fit paths of the other samples.

The modelled best-fit t–T paths exhibit very similar thermal histories for all samples. Most samples cooled below the closure temperature of the apatite FT system in the Early Cretaceous. After moderate to slow cooling below ~60°C, a distinct heating event occurred in the late Eocene. This was followed firstly by slow, and then by accelerated cooling from the Miocene onwards.

Vosges

All of the samples experienced temperatures greater than 120°C in the Early Cretaceous and some of them also in the Palaeogene (Fig. 11). Best-fit models reveal oldest preserved tracks in apatite ranging between 128 Ma (ZTG124) and 37 Ma (ZTG122). Samples closer to the URG and from lower altitudes seemingly cooled later below the track retention temperature—with some exceptions (e.g. ZTG107)—than samples further to the W and from higher altitudes. Evaluation of the statistical goodness-of-fit of modelled FT length distributions and ages to the observed data results in values between 0.69 and 0.98.

Most of the best-fit models display a two-phase cooling history, very similar to the ones obtained for the Black Forest samples. Cooling of the samples through the apatite PAZ in a time span ranging from the Early Cretaceous to the Palaeogene was followed by an Eocene heating event. The subsequent cooling phase is characterised by rapid late-stage cooling from the late Miocene onwards.

Interpretation and discussion

A question of open debate concerning the regional geology of the URG area is whether Cretaceous sediments were deposited and subsequently completely ero-

694

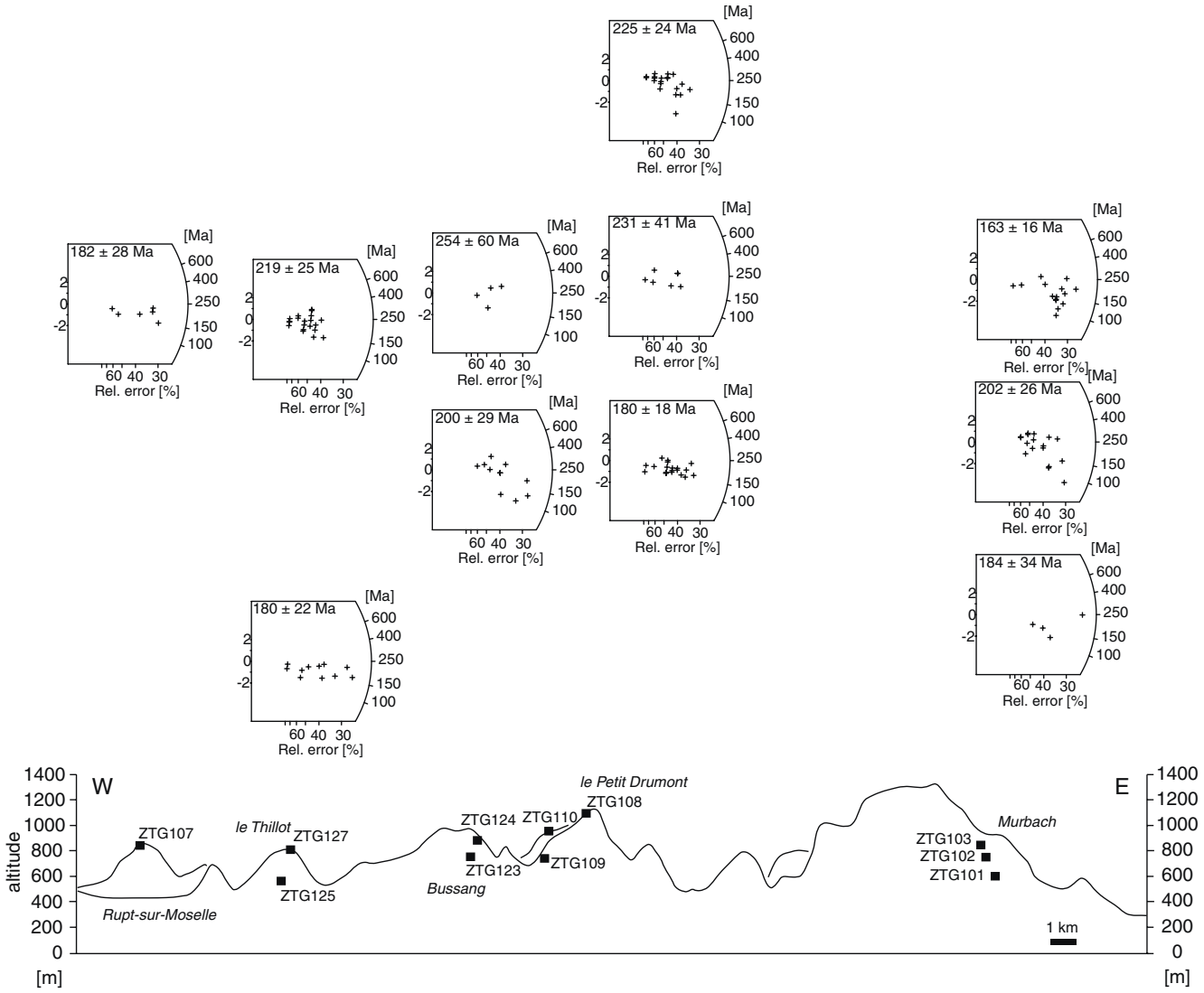

Fig. 7 Zircon FT radial plots of the Vosges samples. An E–W topographic profile (vertical scale exaggerated by a factor of 5) with sample locations is shown at the bottom of the figure

ded during the latest Cretaceous to the Paleocene (Ziegler 1990) or never existed (e.g. Geyer and Gwinner 1991). FT thermochronology can potentially contribute to the solution of this question, since it provides information on both paleotemperature and timing. The zircon FT data, particularly the existence of many grains with pre-Mesozoic ages, indicate that the sampled crustal segments never reached the critical temperature for complete track loss, i.e. ~330°C (Tagami and Shimada 1996; Tagami et al. 1998), after post-Variscan peneplanation. Zircon FT central ages as well as single-grain ages scatter significantly. χ^2 statistics (Table 1) indicate that the observed large spread in single-grain ages generally does not represent a real difference to the respective apparent age because $P(\chi^2)$ values are (with exception of the sample ZTG102) consistently higher than 5% (Green 1981). However, due to the low number of random samples (20 counted grains or fewer) and the high standard errors of single-grain age estimates the χ^2 approach may lack power to detect any extra-Poissonian variation (Timar-Geng et al. 2004). Thus, the observed high spread may reflect different track retentivity of the individual grains within one sample, for instance due to variable amounts of accumulated α damage (Kasuya and Naeser 1988). Based on this assumption, the zircons with the youngest single-grain ages can be interpreted as having the lowest thermal stability because they are the last to close on a cooling path (Brandon et al. 1998). The youngest single-grain age represents the maximum age dating the passage of the sample through the cool limit of the zircon FT PAZ (Fügenschuh and Schmid 2003). Continuous hydrothermal activity in the Jurassic (e.g. Wernicke and Lippolt 1997; Wetzel et al. 2003) caused substantial annealing of fission tracks in zircon (Timar-Geng et al. 2004) and a long residence time within the PAZ. This is also suggested by the broad distribution of zircon single-grain ages in the present dataset. Based on these observations it can be inferred that the sampled

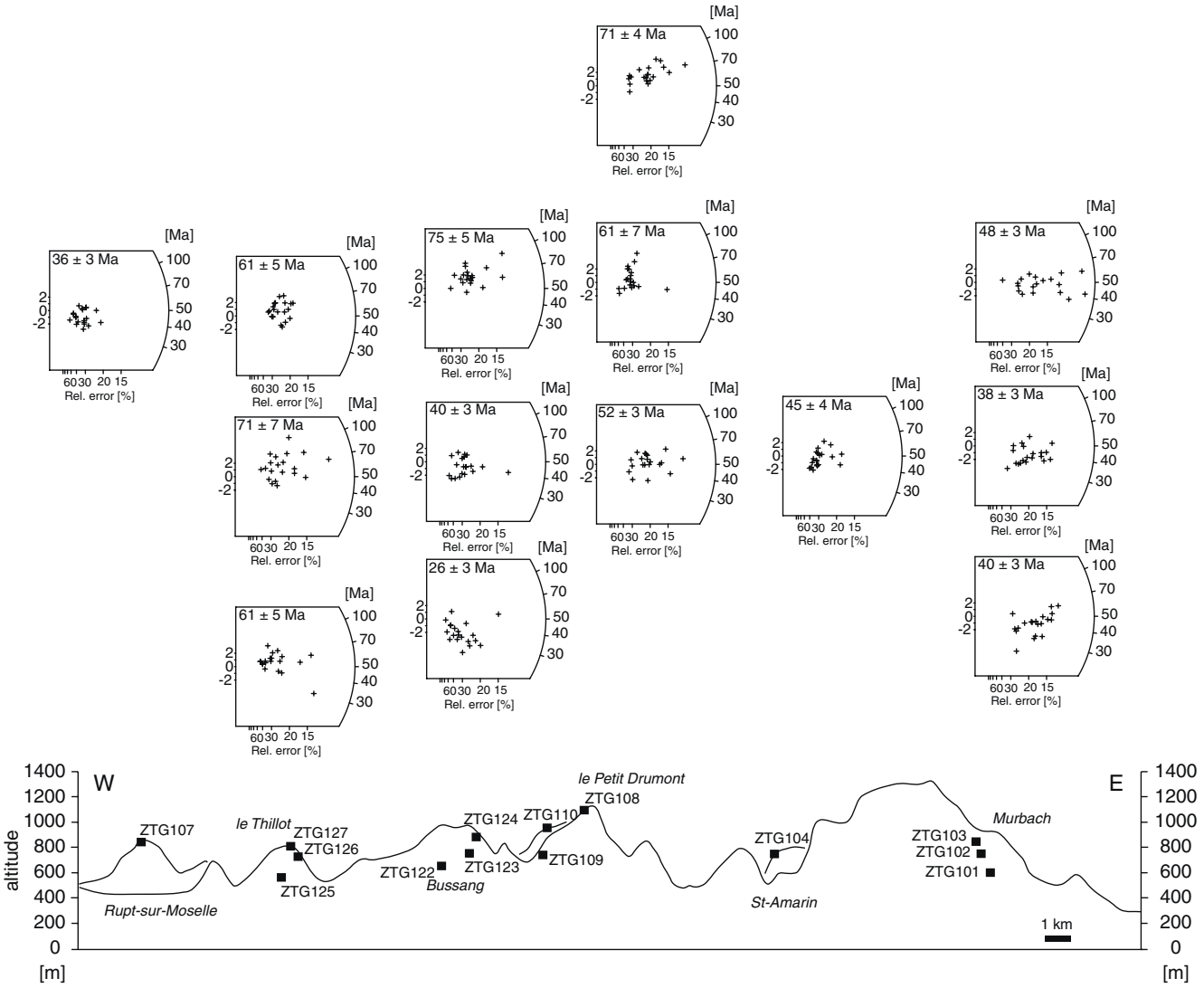

Fig. 8 Apatite FT radial plots of the Vosges samples. An E–W topographic profile (vertical scale exaggerated by a factor of 5) with sample locations is shown at the bottom of the figure

level of the crust cooled below ~230°C (the cool limit of the zircon PAZ after Tagami et al. 1998) during the Early Cretaceous. Since the Permo-Triassic paleosurface is partly preserved in the southern Black Forest (e.g. Paul 1955; Wimmenauer and Schreiner 1990), it can be assumed that no significant erosion of the pre-Mesozoic basement has been occurred. Taking a generous estimate of ~1,500 m Mesozoic sediment cover, based on interpolated isopach maps (e.g. Geyer and Gwinner 1991), it is obvious that the observed paleotemperatures in the Early Cretaceous cannot be due to burial alone (see also Timar-Geng et al. 2004), even not if a hypothetical kilometre-scale thick Upper Jurassic to Lower Cretaceous pile of sediments is assumed (Fig. 12).

The *t*–*T* path between ~230°C, given by the youngest cluster of zircon FT single-grain ages, and ~120°C, marking the entrance of the samples into the apatite PAZ, is only poorly constrained. However, it appears that the Cretaceous must have been a period of accelerated cooling, since some of the modelled *t*–*T* paths enter the apatite PAZ already at the end of the Early Cretaceous. This could have been caused primarily by the cessation of the hydrothermal activity in the area in combination with the uplift-induced erosion of the so-called "Rhenish Shield" (Cloos 1939).

From the Early Cretaceous onwards, the thermal history of the flanks of the southern URG is tightly constrained by the apatite FT modelling results. Best-fit models display a fairly common *t*–*T* path for all samples with a two-phase cooling history. It starts with entering the apatite PAZ in Early Cretaceous to Palaeogene times depending on the position of the samples. Overall cooling is interrupted by a distinct heating event in the late Eocene that is invariably recorded by all samples. Subsequent cooling to surface temperatures is characterised by an accelerated rate from the Miocene onwards. This can reflect amplified erosion due to uplift of the Vosges–Black Forest area owing to lithospheric

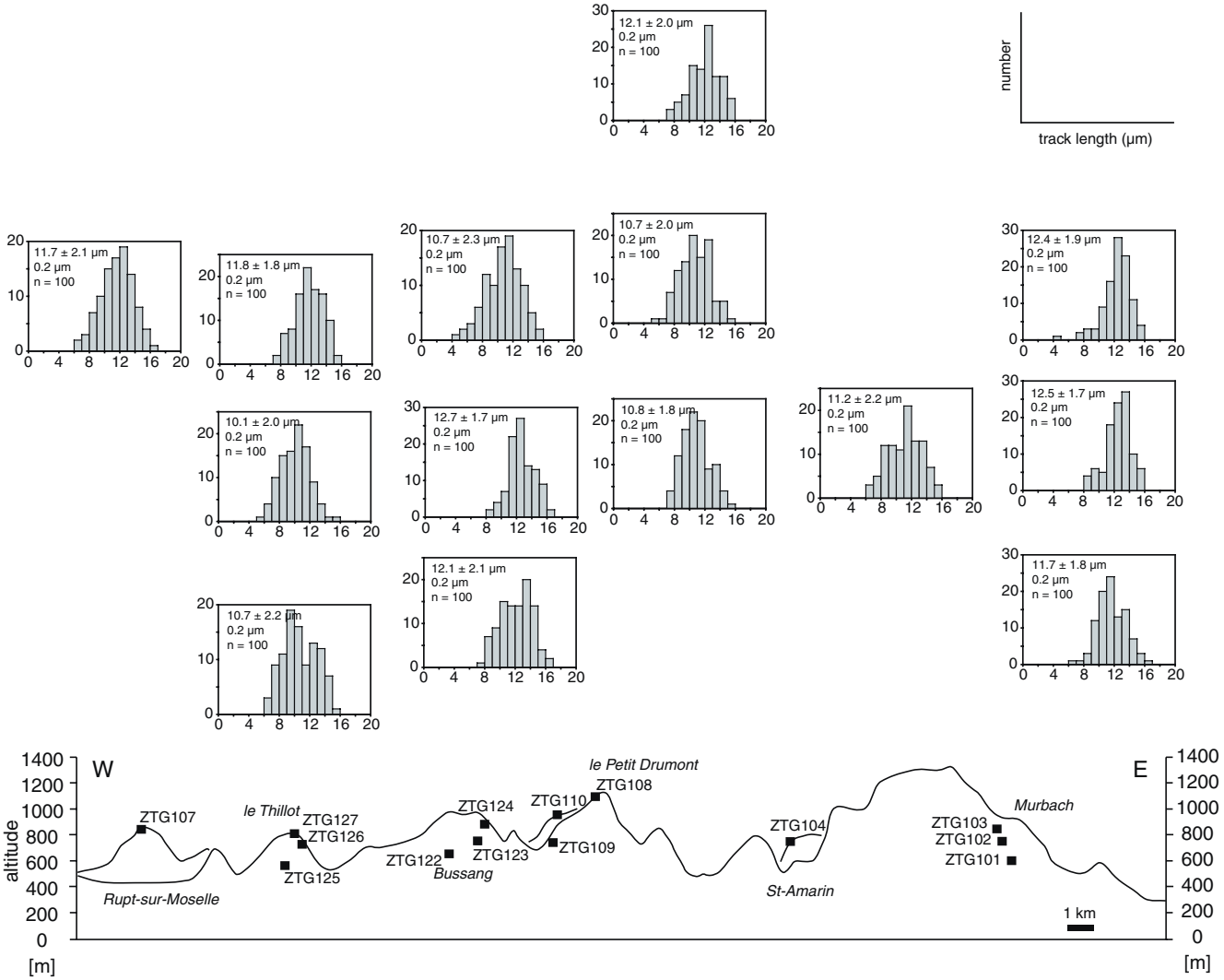

Fig. 9 Apatite FT length distributions of the Vosges samples. An E–W topographic profile (vertical scale exaggerated by a factor of 5) with sample locations is shown at the bottom of the figure

folding (Dèzes et al. 2004). However, this late cooling episode can also be an artefact of the Laslett et al. (1987) annealing model (e.g. Ketcham et al. 2000) and should be considered with caution. In contrast, the other parts of the *t–T* paths, especially the timing of entry into the PAZ and the temperature maximum and timing of a transient heating episode, are well reconstructed by thermal modelling studies (Gleadow and Brown 2000). A complex cooling history is also evidenced by the frequent bimodal distributions of apatite FT lengths (e.g. the Todtnauberg profile in the Black Forest; Fig. 6). One generation of tracks is severely annealed (with track lengths of 8–10 µm) due to the Eocene thermal episode and a second generation formed after the temperature peak has longer tracks in the range of 12–14 µm.

To gain information on the denudation history of the flanks of the URG, two transects with an elevation difference of 640–1,080 m were sampled. Such a vertical reference frame can be used to estimate the rate of denudation (Gallagher et al. 1998). Samples collected over considerable relief often yield apatite FT ages that display a positive correlation with sample elevation (e.g. Wagner et al. 1977). For high denudation rates, such as in active orogenic belts, the gradients of the age–elevation profiles correspond closely to the denudation rates (Gleadow and Brown 2000). For low denudation rates, these linear profiles are replaced by concave-upwards curves and are interpreted as representing prolonged residence in the PAZ. In this case, the age–elevation profiles are not related to denudation rate. An important pre-requisite in order to obtain information on denudation from such profiles is that the samples were taken within a single tectonic unit. Another essential requirement is that the samples cover a significant range of vertical relief that may render possible to contain a complete frozen paleo-PAZ. Unfortunately, none of these preconditions are fulfilled in this study and the apatite FT age–elevation profiles (Fig. 13) show substantial disturbance. Even though, a tendency towards increasing ages with increasing elevation is recognizable

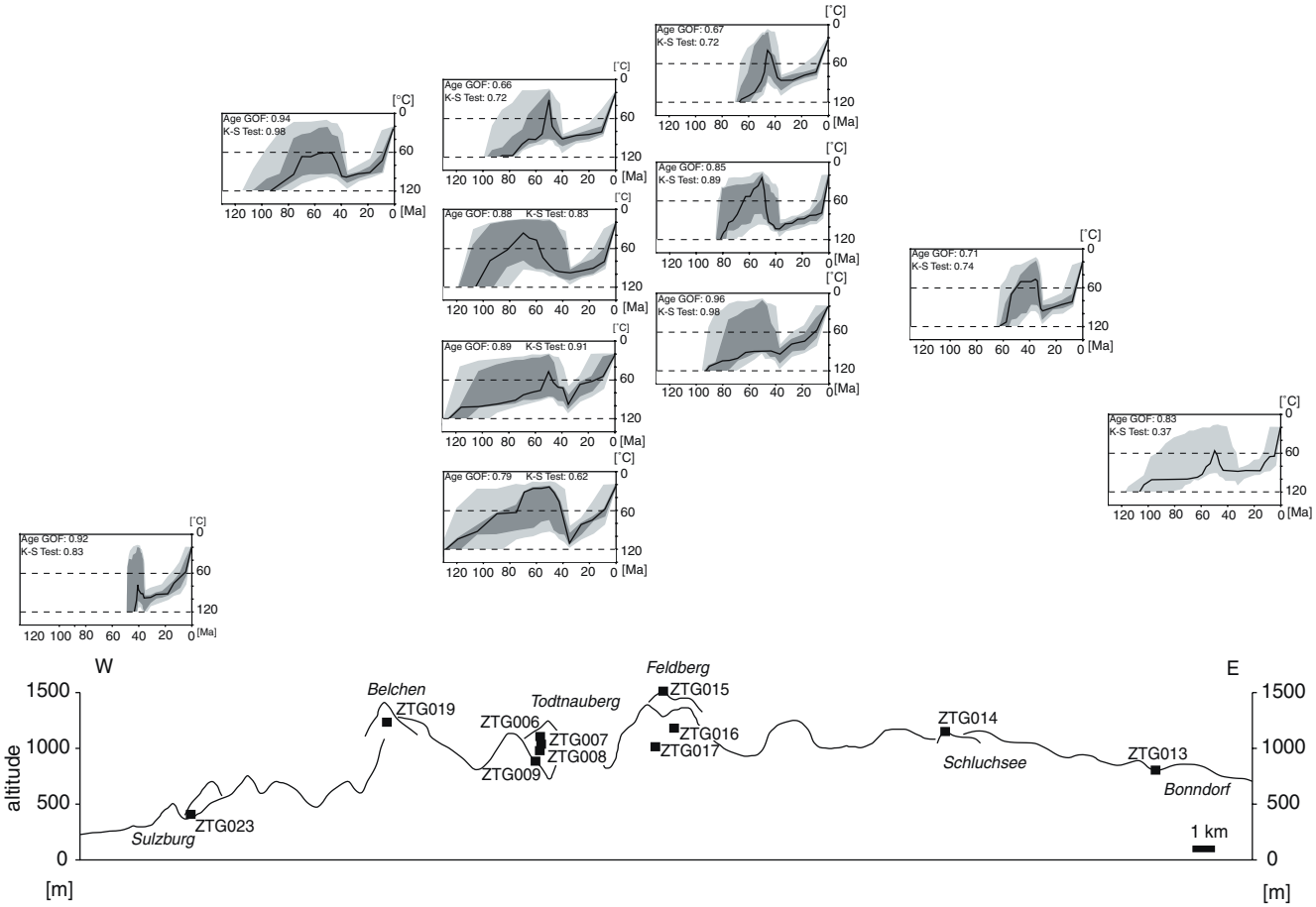

Fig. 10 Modelled best-fit *t–T* paths and two envelopes covering the statistically "acceptable" fits (light grey) and "good" fits (dark grey) from the Black Forest. K–S test: Kolmogorov–Smirnov test evaluating the degree of fit between FT length distributions. Age GOF: FT age goodness-of-fit test. For methodological details, see Ketcham et al. (2000). An E–W topographic profile (vertical scale exaggerated by a factor of 5) with sample locations is shown at the bottom of the figure

(Fig. 13). However, in the present case the distribution of FT age with elevation points to progressive annealing as a result of increasing temperature and it is not associated to any cooling rate. For a sound interpretation of the data in terms of a quantitative assessment of amount and rate of denudation, both FT age and length measurements have to be incorporated. Temperature and timing of the thermal maximum prior to the final cooling to surface temperatures are quite well determined from modelling studies (Gleadow and Brown 2000). These paleotemperature estimates can be used to derive constraints on the amount of denudation (e.g. Raab et al. 2002). Temperature can be equated to burial depth using the following equation:

$$D = (T - T_s)/G$$

where D is the thickness of the denuded section (km), T, the modelled paleotemperature (°C], T_s, the surface temperature (°C) and G, the geothermal gradient (°C/km). Despite the considerable variation among the observed apatite FT ages, the modelled thermal histories suggest a common timing for the onset of the last cooling phase in the late Eocene. These *t–T* points can be used to estimate the amount of denudation since the late Eocene (Table 3). Modelling of the apatite FT parameters suggest a distinct heating episode in the late Eocene contemporaneous to the initial rifting phase of the URG (e.g. Schumacher 2002) and associated volcanic activity (Keller et al. 2002). This clearly points to a possible elevated paleogeothermal gradient during this time. The denudation estimates for gradients of 45 and 60°C/km are given in Table 3. For the latter case, they range between 1.0 and 1.7 km correlating quite well with the present elevation of the samples (Fig. 14). Conversely, taking into account up to 1,500 m, Mesozoic sedimentary rocks based on geological observations and the fact that only minor amounts of crystalline basement are being eroded, the observed annealing requires elevated paleotemperatures in the late Eocene.

Minor differences in the amount of denudation can be explained by Tertiary differential block movements. For example, in the eastern Vosges, N–NE trending Paleozoic discontinuities were reactivated as normal faults during the E–W extension in the Oligocene (Edel and Fluck, 1989).

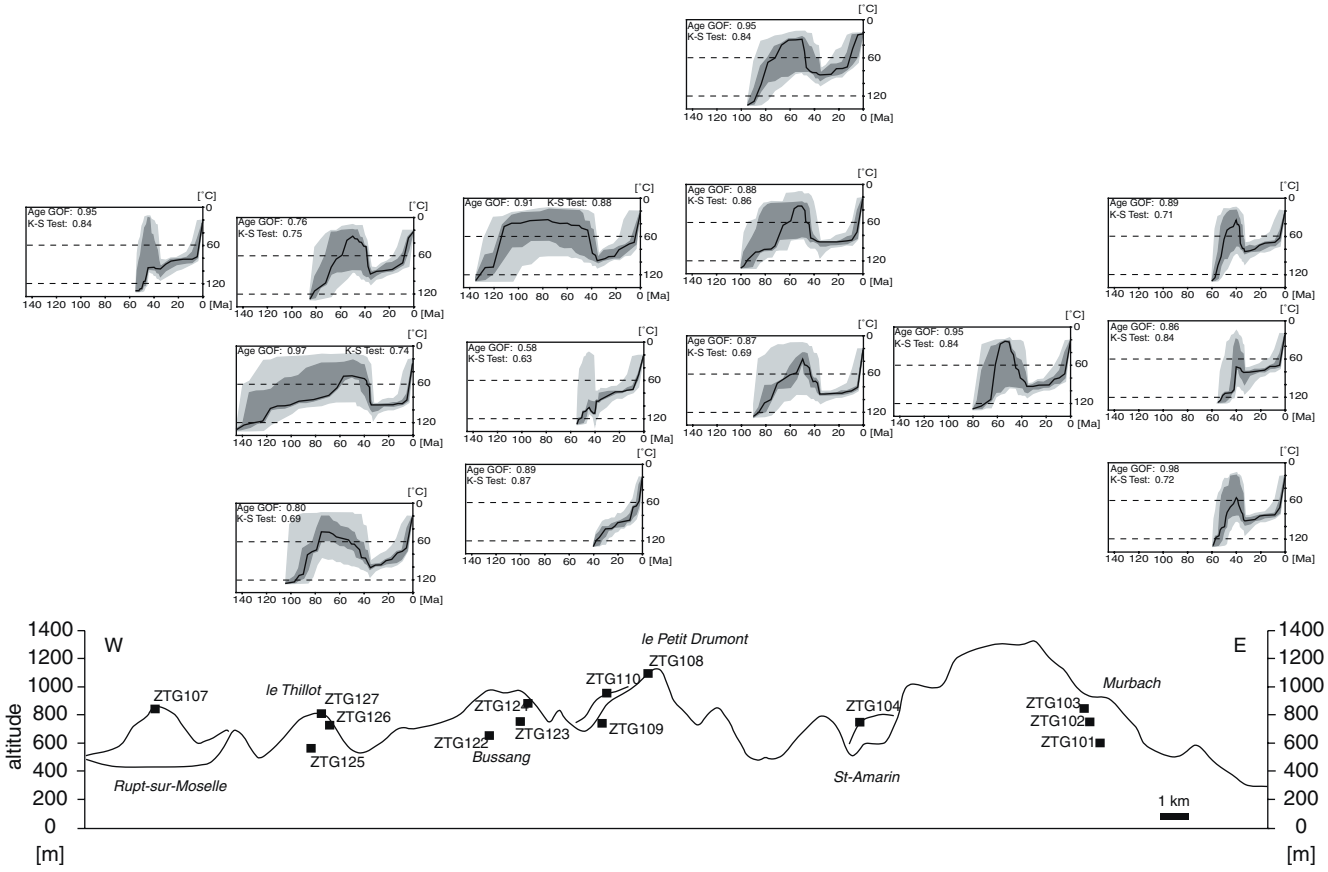

Fig. 11 Modelled best-fit *t*–*T* paths and two envelops covering the statistically "acceptable" fits (light grey) and "good" fits (dark grey) from the Vosges. K–S test: Kolmogorov–Smirnov test evaluating the degree of fit between FT length distributions. Age GOF: FT age goodness-of-fit test. For methodological details, see Ketcham et al. (2000). An E–W topographic profile (vertical scale exaggerated by a factor of 5) with sample locations is shown at the bottom of the figure

It may be worthwhile noting explicitly that it is inappropriate to interpret the measured apatite FT ages in the URG as cooling ages, particularly, because one of several requirements, a steady-state paleogeothermal gradient, is definitively not met throughout the low-temperature thermal history of the southern URG. The FT age–elevation profiles do not result from simple linear cooling in the upper crust.

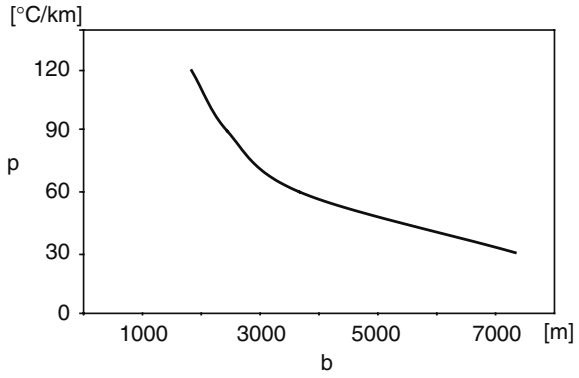

Fig. 12 Relationship between the paleogeothermal gradient (*p*) and the hypothetical burial (*b*) of the present earth's surface for the Early Cretaceous. Paleotemperature: ~230°C (the cool limit of the zircon PAZ after Tagami et al. 1998); assumed surface temperature: 10°C. The FT results cannot be explained by burial depth, since such high values up to 7 km are impossible to reconcile with the known geology of the URG area

Conclusions

The FT data demonstrate that the flanks of the southern URG have experienced a complex thermal history with repeatedly changing paleogeothermal gradients. Using an inverse modelling approach, the low-temperature thermal history of the area could be determined that is consistent with the measured FT dataset and independent geological observations.

Interpreting the youngest cluster of zircon FT single-grain ages as the approximate date of cooling through the cool limit of the zircon FT PAZ, and interpolating the thickness of the Mesozoic sedimentary rocks from adjacent regions into the study area, it can be inferred that not even a hypothetical kilometre-thick cover of Upper Jurassic to Lower Cretaceous sediments could have caused the observed very high paleotemperatures.

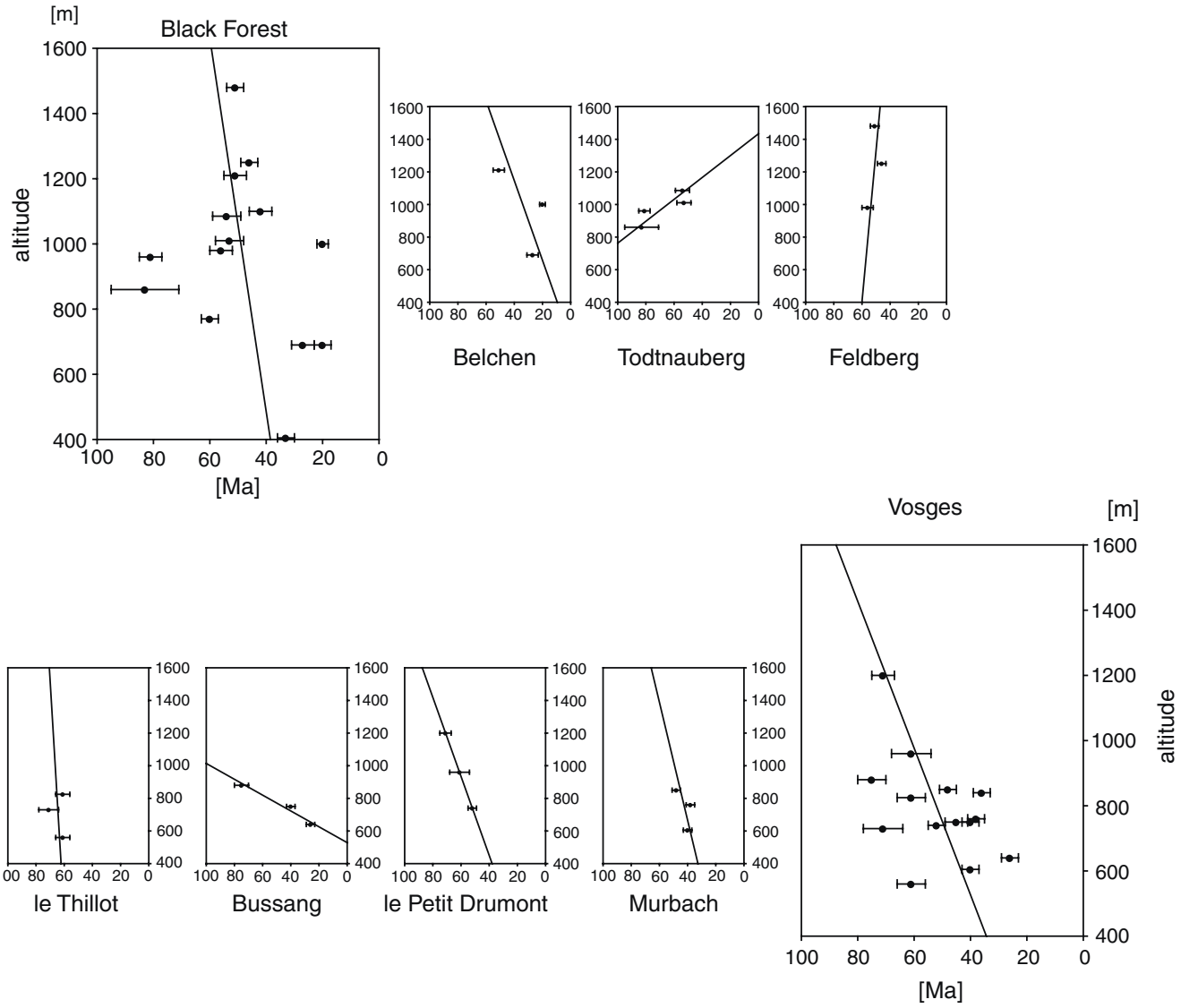

Fig. 13 Apatite FT age versus elevation profiles from the Black Forest and Vosges

The reason for the observed thermal anomaly is ascribed to one or (very probably) repeated Mesozoic hydrothermal episodes (see also Timar-Geng et al. 2004). Thus, the question regarding the thickness of the Cretaceous sediments in the southern URG area cannot be answered on the basis of FT analysis alone.

Modelling results provided a comprehensive thermal history of the study area from the Early Cretaceous to present. It is characterised by complex cooling with a transient heating episode in the late Eocene. This heating phase is contemporaneous to the initial rifting stage of the URG and associated with increased volcanic activity.

Based on best-fit t–T paths and a tentative estimation of the prevailing paleogeothermal gradient in the late Eocene, the total amount of the denuded section from the flanks of the URG could be estimated. It amounts to 1.0–1.7 km for a paleogeothermal gradient of 60°C/km and 1.3–2.2 km for a paleogeothermal gradient of 45°C/km, respectively.

Apatite FT central ages from the URG area not only record cooling due to tectonic uplift alone, but also due to decreasing hydrothermal activity. Therefore, no uplift rates based an age–elevation profiles can be derived. Convective heat transport seems to have played an important role throughout the post-Variscan thermotectonic evolution of the region. Therefore, only the thermal modelling approach can offer a meaningful interpretation of the growing amount of FT data.

Acknowledgements This work has been supported by the Swiss National Science Foundation (Project Nos. 21-57038.99 and 20-64567.01). We thank M. Brix, U.A. Glasmacher and M. Rahn for their constructive comments and suggestions that substantially improved the manuscript.

Table 3 Total amount of denudation for paleogeothermal gradients of 45 and 60°C/km since the late Eocene

Samples	Timing of T_{max} (Ma)	T_{max} (°C)	D (km) for $G = 45$°C/km	D (km) for $G = 60$°C/km
Black Forest				
ZTG006	40	90	1.6	1.2
ZTG007	36	97	1.7	1.3
ZTG008	36	96	1.7	1.3
ZTG009	36	110	2.0	1.5
ZTG013	33	88	1.5	1.1
ZTG014	30	93	1.6	1.2
ZTG015	35	83	1.4	1.1
ZTG016	38	103	1.8	1.4
ZTG017	37	92	1.6	1.2
ZTG019	36	99	1.8	1.3
ZTG023	35	96	1.7	1.3
Vosges				
ZTG101	33	90	1.6	1.2
ZTG102	33	80	1.3	1.0
ZTG103	33	80	1.3	1.0
ZTG104	36	91	1.6	1.2
ZTG107	35	96	1.7	1.3
ZTG108	35	84	1.4	1.1
ZTG109	36	92	1.6	1.2
ZTG110	36	88	1.5	1.1
ZTG122	38	120	2.2	1.7
ZTG123	40	111	2.0	1.5
ZTG124	36	98	1.7	1.3
ZTG125	35	103	1.8	1.4
ZTG126	34	91	1.6	1.2
ZTG127	35	88	1.5	1.1

Appendix

Modelling details

This appendix (Table. 4, 5) contains information about parameters used for inverse modelling. The time for the first constraint was chosen based on the consideration that this time should be somewhat earlier than the FT age of the oldest and thus most resistant apatite grains to allow for age reduction by partial annealing (Ketcham et al. 2000). Thus, the temperature for the first constraint was set at ~130°C providing that there are no fission tracks present as an initial condition. Modelled t–T paths were initially defined to be non-monotonic, aiming at finding solutions by the program, particularly any possible heating events and their timing. The initial model runs also constrain the time of cooling below the track retention temperature, which can be used as initial constraints for subsequent model runs. In a next step, the new initial constraint and additional intermediate constraints were used to better evaluate individual heating and cooling events. Model runs were so gradually refined by forcing restrictions on the t–T paths as suggested by consecutive modelling results and geological observations.

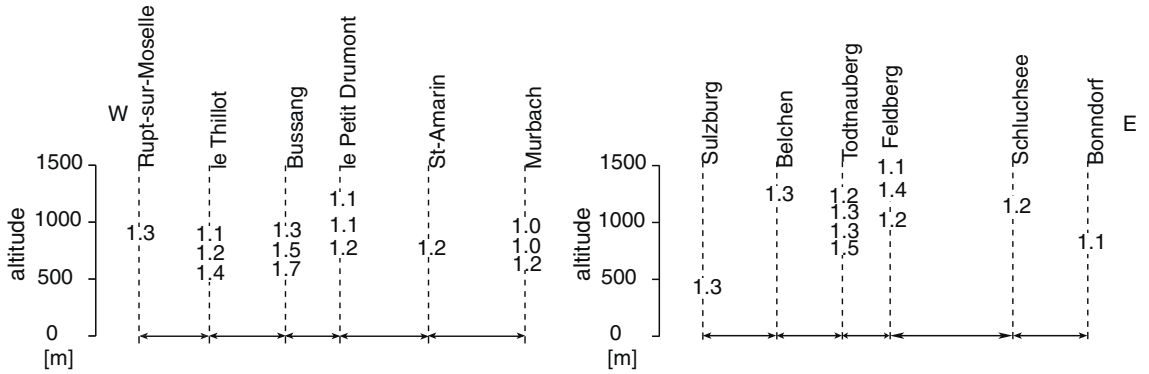

Fig. 14 Amount of denudation since the late Eocene for an assumed paleogeothermal gradient of 60°C/km. Values ordered according to the schematic profiles from Fig. 2b

Table 4 Modelling details of the Black Forest samples

Samples	Constraints (Ma, °C–°C)	Iterations	Nodal points
ZTG-0-06	(0.0, 20–20)(40, 115–60)(50, 109–17)(71, 110–16)(100, 131–131)	10,000	17
ZTG-0-07	(0.0, 20–20)(35, 124–63)(50, 122–16)(70, 120–17)(121, 130–130)	10,000	21
ZTG-0-08	(0.0, 20–20)(35, 124–44)(50, 105–20)(75, 127–20)(131, 130–130)	10,000	21
ZTG-0-09	(0.0, 20–20)(35, 124–58)(50, 122–16)(75, 124–17)(135, 131–131)	20,000	17
ZTG-0-13	(0.0, 20–20)(32, 126–40)(50, 99–18)(75, 124–20)(121, 130–130)	50,000	33
ZTG-0-14	(0.0, 20–20)(30, 131–14)(35, 129–13)(50, 129–16)(65, 133–133)	10,000	17
ZTG-0-15	(0.0, 20–20)(35, 115–40)(45, 110–7)(50, 115–11)(70, 129–129)	10,000	17
ZTG-0-16	(0.0, 20–20)(37, 127–57)(50, 115–16)(75, 131–18)(85, 131–131)	50,000	33
ZTG-0-17	(0.0, 20–20)(37, 129–37)(50, 109–10)(75, 133–14)(95, 127–127)	10,000	17
ZTG-0-19	(0.0, 20–20)(35, 132–35)(50, 105–11)(75, 125–13)(115, 127–127)	10,000	21
ZTG-0-23	(0.0, 20–20)(35, 133–45)(40, 125–17)(48, 129–129)	50,000	25

Table 5 Modelling details of the Vosges samples

Samples	Constraints (Ma, °C–°C)	Iterations	Nodal points
ZTG-1-01	(0.0, 20–20)(33, 129–47)(40, 103–17)(50, 130–20)(60, 130–130)	50,000	33
ZTG-1-02	(0.0, 20–20)(33, 129–59)(40, 130–16)(55, 128–128)	50,000	25
ZTG-1-03	(0.0, 20–20)(33, 105–49)(40, 87–16)(60, 129–129)	50,000	25
ZTG-1-04	(0.0, 20–20)(35, 128–41)(50, 128–16)(80, 129–129)	10,000	25
ZTG-1-07	(0.0, 20–20)(35, 131–28)(45, 106–14)(55, 132–132)	40,000	25
ZTG-1-08	(0.0, 20–20)(35, 131–16)(50, 102–17)(95, 131–131)	10,000	25
ZTG-1-09	(0.0, 20–20)(35, 112–64)(50, 93–11)(91, 127–127)	100,000	25
ZTG-1-10	(0.0, 20–20)(35, 124–34)(50, 105–8)(75, 129–16)(101, 131–131)	20,000	33
ZTG-1-22	(0.0, 20–20)(40, 127–127)	10,000	33
ZTG-1-23	(0.0, 20–20)(35, 127–14)(40, 129–16)(45, 127–16) (55, 127–127)	30,000	33
ZTG-1-24	(0.0, 20–20)(35, 130–45)(50, 127–18)(75, 127–16) (135, 129–129)	10,000	33
ZTG-1-25	(0.0, 20–20)(35, 125–46)(50, 127–14)(75, 126–15)(105, 125–125)	10,000	33
ZTG-1-26	(0.0, 20–20)(33, 118–65)(40, 110–17)(50, 102–12) (100, 107–12)(145, 132–132)	100,000	49
ZTG-1-27	(0.0, 20–20)(35, 129–49)(50, 129–13)(85, 129–129)	10,000	25

References

Brandon MT, Roden-Tice MK, Garver JI (1998) Late Cenozoic exhumation of the Cascadia accretionary wedge in the Olympic Mountains, northwest Washington State. Geol Soc Am Bull 110:985–1009

Carlson WD (1990) Mechanisms and kinetics of apatite fission-track annealing. Am Mineral 75:1120–1139

Cloos H (1939) Hebung-Spaltung-Vulkanismus. Geologische Rundschau 30:401–527

Crowley KD, Cameron M, Schaefer RL (1991) Experimental studies of annealing etched fission tracks in fluorapatite. Geochimica et Cosmochimica Acta 55:1449–1465

Dèzes P, Schmid SM, Ziegler PA (2004) Evolution of the Alpine and Pyrenean orogens with their foreland lithosphere. Tectonophysics 389:1–33

Dumitru TA (1993) A new computer-automated microscope stage system for fission-track analysis. Nucl Tracks Radiat Meas 21:575–580

Dunkl I (2002) TRACKKEY: a Windows program for calculation and graphical presentation of fission track data. Comput Geosci 28:3–12

Edel JB, Fluck P (1989) The upper Rhenish Shield basement (Vosges, Upper Rhinegraben and Schwarzwald): Main structural features deduced from magnetic, gravimetric and geological data. Tectonophysics 169:303–316

Foster DA, Gleadow AJW (1996) Structural framework and denudation history of the flanks of the Kenya and Anza Rifts, East Africa. Tectonics 15:258–271

Foster DA, Gleadow AJW, Reynolds SJ, Fitzgerald PF (1993) The denudation of metamorphic core complexes and the reconstruction of the Transition Zone, west central Arizona: constraints from apatite fission track thermochronology. J Geophys Res 98:2167–2185

Foster DA, Raza A (2002) Low-temperature thermochronological record of exhumation of the Bitterroot metamorphic core complex, northern Cordilleran Orogen. Tectonophysics 349:23–36

Fuchs K, Bonjer K-P, Gajewski D, Lueschen E, Prodehl C, Sandmeier K-J, Wenzel F, Wilhelm H (1987) Crustal Evolution of the Rhinegraben area. 1. Exploring rhe lower crust in the Rhinegraben rift by unified geophysical experiments. Tectonophysics 141:261–275

Fügenschuh B, Schmid SM (2003) Late stages of deformation and exhumation of an orogen constrained by fission-track data: a case study in the Western Alps. Geol Soc Am Bull 115:1425–1440

Galbraith RF (1988) Graphical display of estimates having differing standard errors. Technometrics 30:271–281

Galbraith RF (1990) The radial plot: graphical assessment of spread in ages. Nucl Tracks Radiat Meas 17:207–214

Galbraith RF, Laslett GM (1993) Statistical models for mixed fission track ages. Nucl Tracks Radiat Meas 21:459–470

Gallagher K, Brown RW, Johnson C (1998) Fission track analysis and its applications to geological problems. Ann Rev Earth Planet Sci 26:519–572

Geyer OF, Gwinner MP (1991) Geologie von Baden-Württemberg. 4., neubearb Aufl der "Einführung in die Geologie von Baden-Württemberg". Schweizerbart, Stuttgart

Giamboni M, Ustaszewski K, Schmid SM, Schumacher ME, Wetzel A (2004) Plio-Pleistocene transpressional reactivation of Paleozoic and Paleogene structures in the Rhine-Bresse transform zone (northern Switzerland and eastern France). Int J Earth Sci 93:207–223

Gleadow AJW (1981) Fission track dating: what are the real alternatives. Nucl Tracks Radiat Meas 5:3–14

Gleadow AJW, Brown RW (2000) Fission-track thermochronology and the long-term denudational response to tectonics. In: Summerfield MA (ed) Geomorphology and global tectonics. Wiley, New York, pp 57–75

Green PF (1981) A new look at statistics in fission track dating. Nucl Tracks Radiat Meas 5:77–86

Hurford AJ (1990) International Union of Geological Sciences Subcommission on Geochronology recommendation for the standardization of fission track dating calibration and data reporting. Nucl Tracks Radiat Meas 17:233–236

Hurford A, Carter A (1994) Regional thermo-tectonic histories of the Rhine Graben and adjacent Hercynian basement: a key to assessing the alpine influence in northwest Europe. In: 8th International Conference on Geochronology, Cosmochronology and Isotope Geology, abstracts, p 148

Hurford AJ, Green PF (1982) A users' guide to fission track dating calibration. Earth Planet Sci Lett 59:343–354

Hurford AJ, Green PF (1983) The zeta age calibration of fission-track dating. Chem Geol 41:285–317

Illies JH (1977) Ancient and recent rifting in the Rhinegraben. Geologie en Mijnbouw 56:329–350

Illies JH, Fuchs K (eds) (1974) Approaches to taphrogenesis. Schweizerbart, Stuttgart, p 460

Illies JH, Müller S (eds) (1970) Graben problems. Schweizerbart, Stuttgart, p 316

Kasuya M, Naeser CW (1988) The effect of α-damage on fission-track annealing in zircon. Nucl Tracks Radiat Meas 14:477–480

Keller J, Kraml M, Henjes-Kunst F (2002) $^{40}Ar/^{39}Ar$ single crystal dating of early volcanism in the Upper Rhine Graben and tectonic implications. Schweiz Mineral Petrogr Mitt 82:121–130

Ketcham RA, Donelick RA, Carlson WD (1999) Variability of apatite fission-track annealing kinetics III: Extrapolation to geological time scales. Am Mineral 84:1235–1255

Ketcham RA, Donelick RA, Donelick MB (2000) AFTSolve: a program for multi-kinetic modelling of apatite fission track data. Geol Mater Res 2:1–18

Laslett GM, Galbraith RF (1996) Statistical modelling of thermal annealing of fission tracks in apatite. Geochim Cosmochim Acta 60:5117–5131

Laslett GM, Green PF, Duddy IR, Gleadow AJW (1987) Thermal annealing of fission tracks in apatite 2. A quantitative analysis. Chem Geol (Isot Geosci Sect) 65:1–13

Michalski I (1987) Apatit-Spaltspuren-Datierungen des Grundgebirges von Schwarzwald und Vogesen: Die postvariszische Entwicklung. Doctoral dissertation, Heidelberg, p 125

Naeser CW (1976) Fission-track dating. US Geol Surv Open-File Rep 76–190, pp 65

Naeser CW (1979) Thermal history of sedimentary basins: fission track dating of subsurface rocks. In: Scholle PA, Schluger PR (eds) Aspects of diagenesis. Soc Econ Paleontol Mineral Spec Publ, SEPM, Tulsa OK United States, pp 109–112

Paul W (1955) Zur Morphogenese des Schwarzwaldes (I). Jh geol Landesamt Baden-Württ 1:395–427

Price PB, Walker RM (1962a) A new detector for heavy particle studies. Phys Lett 3:113–115

Price PB, Walker RM (1962b) Observations of charged-particle tracks in solids. J Appl Phys 33:3407–3406

Prodehl C, Mueller S, Haak V (1995) The European Cenozoic rift system. In: Olsen KH (ed) Continental rifts: evolution, structure, tectonics. Developments in geotectonics 25. Elsevier, New York, pp 133–212

Raab MJ, Brown RW, Gallagher K, Carter A, Weber K (2002) Late Cretaceous reactivation of major crustal shear zones in northern Namibia: constraints from apatite fission track analysis. Tectonophysics 349:75–92

Rothé JP, Sauer K (eds) (1967) The Rhinegraben progress report 1967. Abh Geol Landesamt Baden-Württemberg 6, pp 146

Schumacher ME (2002) Upper Rhine Graben: role of preexisting structures during rift evolution. Tectonics 21:6-1-17

Tagami T, Shimada C (1996) Natural long-term annealing of the zircon fission track system around a granitic pluton. J Geophys Res 101/B4:8245–8255

Tagami T, Galbraith RF, Yamada R, Laslett GM (1998) Revised annealing kinetics of fission tracks in zircon and geological implications. In: Van den Haute P, De Corte F (eds)Advances in fission track geochronology. Kluwer, Dordrecht, pp 99–112

Timar-Geng Z, Fügenschuh B, Schaltegger U, Wetzel A (2004) The impact of the Jurassic hydrothermal activity on zircon fission track data from the southern Upper Rhine Graben area. Schweiz Mineral Petrogr Mitt 84:257–269

von Gehlen K (1987) Formation of Pb-Zn-F-Ba mineralizations in SW Germany: a status report. Fortschr Miner 65:87–113

Wagner GA (1979) Correction and interpretation of fission track ages. In: Jäger E, Hunziker JC (eds) Lectures in isotope geology. Springer, Berlin Heidelberg New York, pp 170–177

Wagner GA (1990) Apatite fission-track dating of the crystalline basement of Middle Europe: concepts and results. Nucl Tracks Radiat Meas 17:277–282

Wagner GA, Reimer GM, Jäger E (1977) Cooling ages derived by apatite fission track, mica Rb–Sr, and K–Ar dating: the uplift and cooling history of the central Alps. Mem Inst Geol Mineral Univ Padova 30:1–27

Wagner GA, Michalski I, Zaun P (1989) Apatite fission-track dating of the Central European basement: post-Variscian thermotectonic evolution. In: The German Continental Deep Drilling Program (KTB). Springer, Berlin Heidelberg New York, pp 481–500

Werner W, Franzke HJ (2001) Postvariszische bis neogene Bruchtektonik und Mineralisation im südlichen Zentralschwarzwald. Z Dt Geol Ges 152:405–437

Wernicke RS, Lippolt HJ (1997) (U + Th)-He evidence of Jurassic continuous hydrothermal activity in the Schwarzwald basement, Germany. Chem Geol 138:273–285

Wetzel A, Allenbach R, Allia V (2003) Reactivated basement structures affecting the sedimentary facies in a tectonically "quiescent" epicontinental basin: an example from NW Switzerland. Sediment Geol 157:153–172

Wimmenauer W, Schreiner A (1990) Erläuterungen zu Blatt 8114, Feldberg. Geol Karte Baden-Württ 1:25 000, Stuttgart, p 134

Wyss A (2001) Apatit Spaltspur Untersuchungen in der Vorwaldscholle (SW-Deutschland). Unpubl diploma thesis, Univ Basel, p 69

Ziegler PA (1990) Geological atlas of Western and Central Europe. Shell Internationale Petroleum Maatschappij, Geological Society Publishing House, London, p 239

Ziegler PA, Cloething S, van Wees J-D (1995) Dynamics of intraplate compressional deformation: the Alpine foreland and other examples. Tectonophysics 252:7–59

IV. The low-temperature thermal history of northern Switzerland as revealed by fission track analysis and inverse thermal modelling

by Zoltan Timar-Geng, Bernhard Fügenschuh, Andreas Wetzel and Horst Dresmann

Published in:
Eclogae Geologicae Helvetiae 99, 255-270, 2006

Eclogae geol. Helv.

DOI 10.1007/s00015-006-1191-z
Birkhäuser Verlag, Basel, 2006

The low-temperature thermal history of northern Switzerland as revealed by fission track analysis and inverse thermal modelling

ZOLTAN TIMAR-GENG[1*], BERNHARD FÜGENSCHUH[1**], ANDREAS WETZEL[1] & HORST DRESMANN[1]

Key words: Northern Switzerland, low-temperature thermochronology, fission track analysis, Nagra boreholes

ABSTRACT

New zircon and apatite fission track (FT) data from four boreholes, which penetrate the Mesozoic and pre-Mesozoic sediments and crystalline basement of northern Switzerland, are presented. Inverse thermal modelling of the measured apatite FT parameters unravels the low-temperature (below ~120 °C) thermal history of the crystalline basement of northern Switzerland. Zircon FT central and single-grain ages cluster around 250 Ma, thus maximum palaeotemperatures did not exceed ~330 °C after late-Variscan consolidation of the crystalline basement. Apatite FT central ages vary between 25 and 87 Ma. Confined mean track lengths range between 9.3 µm and 11.6 µm, suggesting substantial track annealing within all apatite samples. Modelled time-temperature paths offer a clear picture about the low-temperature thermal history of the crystalline basement of northern Switzerland: Cretaceous cooling is followed by an Eocene heating event and subsequent cooling to present-day temperatures. The Eocene heating episode is contemporaneous with the initial rifting stage of the nearby Upper Rhine Graben and the associated increasing volcanic activity. Crustal-scale faults of the Permo-Carboniferous Trough of northern Switzerland could have acted as major pathways for circulating hydrothermal fluids giving rise to the observed Middle to Late Eocene thermal event.

ZUSAMMENFASSUNG

Neue Zirkon- und Apatit-Spaltspurdaten werden aus vier Bohrungen, welche die mesozoische und pre-mesozoische Sedimentbedeckung, sowie das oberste kristalline Grundgebirge der Nordschweiz durchteufen, vorgelegt. Inverse thermische Modellierung der gemessenen Apatit-Spaltspurparameter erlaubt, die Niedrigtemperaturgeschichte (unter ~120 °C) des kristallinen Grundgebirges der Nordschweiz zu enträtseln. Die Zirkon-Spaltspuralter (Zentralalter) und die Einzelkornalter zeigen eine Häufung um 250 Ma. Daraus folgt, dass die maximalen Paläotemperaturen nach der spätvariszischen Konsolidierung des Kristallins ~330 °C nicht mehr überschritten haben. Apatit-Spaltspuralter (Zentralalter) variieren zwischen 25 und 87 Ma. Die mittleren Spaltspurlängen reichen von 9,3 µm bis 11,6 µm und weisen auf eine substantielle Ausheilung in den Apatiten hin. Die modellierten Zeit-Temperatur-Pfade bieten ein klares Bild der Niedrigtemperaturgeschichte des kristallinen Grundgebirges in der Nordschweiz: Einer kretazischen Abkühlung folgt ein eozänes Wärmeereignis und anschliessend eine Abkühlung zur heutigen Temperaturverteilung. Der eozäne Wärmepuls ist zeitgleich mit der initialen Riftingphase des nahegelegenen Oberrheingrabens und der damit verbundenen erhöhten vulkanischen Aktivität. Zum Nordschweizer Permokarbontrog-System gehörige Störungen im Krustenmassstab könnten als Fliesswege für zirkulierende Fluide gedient haben, die zum beobachteten mittel- bis späteozänen thermischen Ereignis führten.

1. Introduction

The trend and the shape of fission track (FT) age-depth (or age-elevation) profiles provide important constraints on the thermal history of crustal segments. Most commonly ages decrease with depth. In a typical foreland basin, however, detrital FT ages might record the erosion history of the hinterland (e.g., Cederbom et al. 2004), and in some rare cases FT ages represent formation ages of, for example, volcanic ashes and, hence, are consistent with the chronostratigraphy (e.g., Naeser et al. 1987). The age-depth graphs vary from nearly linear in active orogenic belts to concave-upwards in cratonic regions with extremely low cooling rates, or alternatively, in sedimentary basins with slow heating due to progressive burial (e.g., Gleadow & Brown 2000). Significant acceleration of the cooling rate after a period of relative stability leads to a compound profile with a typical "break in slope", interpreted as the onset of rapid cooling (e.g., Gleadow & Brown 2000). Moreover, vertical sections are very convenient, when time-temperature paths experienced by individual samples are modelled, because the palaeogeothermal gradient at different times can be indirectly determined. Thus, the information from a vertical

[1]Geologisch-Paläontologisches Institut, Universität Basel, Bernoullistrasse 32, CH-4056 Basel, Switzerland.
*Present address: Geologisches Institut, Albert-Ludwigs-Universität Freiburg, Albertstr. 23b, D-79104 Freiburg, Germany.
E-mail: zoltan.timar-geng@geologie.uni-freiburg.de
**Present address: Institut für Geologie und Paläontologie, Universität Innsbruck, Innrain 52, A-6020 Innsbruck, Austria.

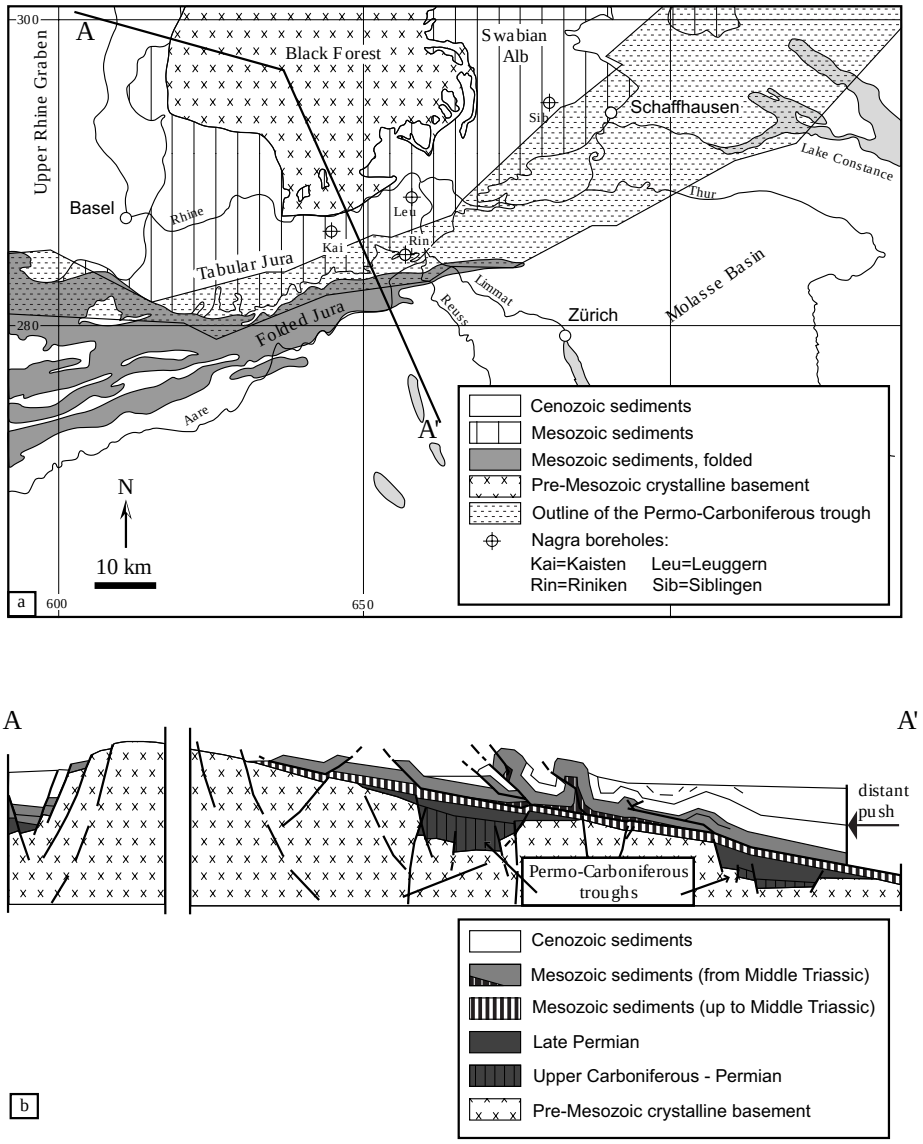

Fig. 1. (a) Tectonic sketch map and (b) schematic profile of the study area (after Thury et al. 1994).

alignment of samples is markedly better than that from any individual sample alone, provided that the samples did not experience tectonic displacements relative to each other during or after their recorded thermal histories. In regions with relatively low relief vertically aligned samples from deep boreholes are particularly favourable, since approximations to a true vertical section are possible only in mountainous regions with high relief. This sampling approach has led to many successful applications of FT analysis on borehole cores evaluating the thermal history of sedimentary basins (e.g., Gleadow et al. 1983; Green et al. 1989; Duddy 1994; Tingate & Duddy 2002; House et al. 2002) or revealing the palaeothermal anomalies in different geological settings (Green et al. 2001; Murakami et al. 2002).

Due to the lack of substantial relief in northern Switzerland, the analysis of borehole samples, in addition to surface samples, is essential for a sound determination of the thermal history of the region.

In the course of an extensive geological investigation program for the assessment of the feasibility and safety of a repository for radioactive waste, Nagra (Swiss National Cooperative for the Disposal of Radioactive Waste) carried out several drillings in central northern Switzerland. Results are summarised in a number of reviews (e.g., Thury et al. 1994; Müller et al. 2002; Nagra 2002). In addition, the burial and the associated thermal history of the Molasse basin have been investigated by, for instance, Schegg & Leu (1998), and Nagra (2002). Applying a 1D basin modelling approach, Nagra (2002) postulated two heating events for the crystalline basement and the Mesozoic cover, a first one during the Early Cretaceous and a second one in the Late Miocene. These heating events are supported by available apatite FT modelling results (Mazurek et al. 2006).

This paper presents new zircon and apatite FT data from four of the Nagra boreholes (Fig. 1) and uses these data as input parameters for modelling the time-temperature paths experienced by the samples. The focus lies on the pre-Mesozoic crystalline basement and the Permo-Carboniferous Trough of northern Switzerland. The differences between the new results and the previous FT modelling results related to the thermal history of the Molasse basin (Mazurek et al. 2006) are also discussed. Finally, also the relationship to the FT results from the adjacent Upper Rhine Graben area (Timar-Geng et al. 2004; 2006) is investigated. This article provides new insights into the low-temperature thermal history of northern Switzerland and makes an important contribution to the assessment of safe disposal of radioactive waste in northern Switzerland.

2. Geological setting

Five main tectonic units are distinguished in northern Switzerland and adjacent SW Germany (Fig. 1): a) the crystalline basement, exposed in the Black Forest; b) the Permo-Carboniferous Trough of northern Switzerland which is not exposed at the surface; c) the autochtonous sedimentary cover of the Tabular Jura and the Swabian Alb; d) the sheared-off sedimentary cover comprising the Folded Jura and the Molasse Basin, and e) the Tertiary rift sediments of the Upper Rhine Graben.

The Late Palaeozoic consolidation of the crystalline basement of northern Switzerland was preceded by extensive Variscan deformation and metamorphism, accompanied by substantial magmatic activity, and the formation of the Permo-Carboniferous Trough of northern Switzerland (for details see overviews by, e.g., Thury et al. 1994; Müller et al. 2002). Well-stratified Triassic to Jurassic deposits accumulated in a shallow epicontinental sea and indicate relative tectonic stability. However, episodic reactivation of pre-existing basement structures during the Jurassic led to differential subsidence and synsedimentary deformation, documented by changes of facies and sediment thickness (Wetzel et al. 2003). Reactivated faults also acted as major conduits for hot fluids in the crystalline basement, as documented by Jurassic hydrothermal mineralisations, exposed, for example, in the nearby Black Forest and Vosges (for a compilation, see Wetzel et al. 2003). Mesozoic heating is also evidenced by palaeomagnetic data from the Vosges (Edel 1997), documenting post-Permian thermal overprinting. FT data from the southern Upper Rhine Graben area indicate that the Jurassic hydrothermal fluid migration affected the upper crust on a regional scale (Timar-Geng et al. 2004, 2006). Thus, it is very likely that substantial heating also occurred in the crystalline basement of northern Switzerland. A significant stratigraphic gap between the Upper Jurassic and middle Eocene deposits provides evidence of Cretaceous to early Tertiary erosion. However, it is still a matter of debate, how much Cretaceous sediments were deposited and subsequently eroded (e.g. Ziegler 1990).

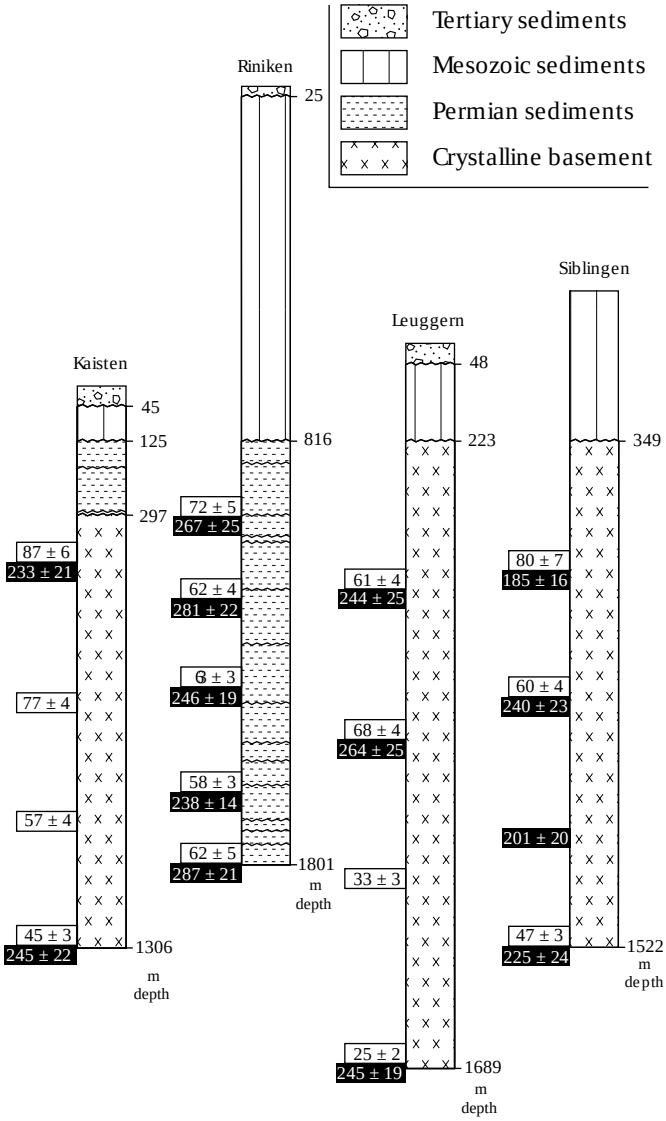

Fig. 2. Stratigraphic overview of the Nagra boreholes with zircon (in white letter on black background) and apatite FT central ages (black letter on white background). All ages are given with their 1σ error. The boreholes are leveled according to their common Mesozoic base unconformity. Waved horizontal lines indicate unconformities.

The Tertiary geological history of northern Switzerland and adjacent areas is a period of renewed tectonic activity, mainly related to Alpine orogeny. It includes the Eo-Oligocene subsidence of the Upper Rhine Graben, the subsequent updoming of the southern Black Forest, the subsidence of the Alpine foreland from the Late Oligocene onwards, and finally, the Late Miocene formation of the Jura Mountains. Ongoing tectonic activity is clearly documented for northern Switzerland and the southern Upper Rhine Graben area by the well-known increased seismicity (several strong earthquakes in historical times; see compilation by Müller et al.

Table 1. Sample details and present temperatures according to Nagra (1990; 1991a; 1991b; 1993).

Borehole	Sample No.	Depth (m)	Lithostratigraphy	Present temp. (°C)
Kaisten	Kai1	1305	Metapelite/-psammite	58
	Kai2	1009	Metapelite/-psammite	50
	Kai3	737	Metapelite/-psammite	40
	Kai4	407	Metapelite/-psammite	28
Riniken	Rin1	1797	Breccia	83
	Rin2	1628	Breccia	78
	Rin3	1381	Breccia	70
	Rin4	1181	Sandstone	65
	Rin5	992	Sandstone	58
Leuggern	Leu1	1684	Two-mica-granite	70
	Leu2	1249	Metapelite/-psammite	55
	Leu3	916	Metapelite/-psammite	42
	Leu4	567	Metapelite/-psammite	30
Siblingen	Sib1	1519	Cordierite-biotite-granite	58
	Sib2	1220	Cordierite-two-mica-granite	49
	Sib3	930	Cordierite-biotite granite	37
	Sib4	639	Cordierite-biotite-granite	32

2002) and by the deformation of Pliocene fluvial gravels (Giamboni et al. 2004a) and Quaternary terraces (Giamboni et al. 2004b).

3. Methodology

3.1 Basics of FT analysis

FT analysis of zircon and apatite is a powerful tool in assessing the thermal history of rocks in the temperature range of ~ 60–300 °C, which characterises the upper few kilometres of the crust. It is based on the spontaneous nuclear fission of ^{238}U (Price & Walker 1962a, 1962b) inducing a damage trail in the crystal, i.e. the latent fission tracks. After revelation of the latent tracks by chemical etching of polished grain-internal surfaces, the spontaneous track density may be counted. The FT age is calculated from the ratio of the spontaneous track density N_s observed on the polished surface and the induced track density N_i measured in an external detector after an irradiation procedure. A detailed overview of the principles of FT dating was provided, for instance, by Wagner & Van den Haute (1992), Gallagher et al. (1998) and Gleadow & Brown (2000).

The linear damage trails are stable over geological time only at relatively low temperatures and they become shorter by a process known as annealing at elevated temperatures. This reduction in length depends on the maximum temperature that each individual FT has experienced after its formation. Apart from other factors (e.g. chemistry, α-damage) temperature and time are clearly the most important factors for annealing of fission tracks. Since new tracks are continuously produced due to spontaneous decay, characteristic track length distributions can result depending on the thermal history to which the mineral grain has been exposed. Thus, the process of annealing is the key to the study of thermal histories by FT analysis. Modelling of FT annealing allows constraining the thermal history of rocks by matching observed and modelled FT parameters (FT age and length distribution).

3.2 Analytical details

Seventeen samples from drill cores of four Nagra boreholes were collected (Fig. 2, Table 1). After crushing and sieving, mineral separation was performed using conventional magnetic and heavy liquid techniques. Apatites were mounted in epoxy resin, zircons in PFA® Teflon. A sequence of grinding and polishing steps was carried out on the mounts in order to reveal grain-internal surfaces. Apatites were etched for 40 sec in HNO_3 (6.5 %) at room temperature, zircons for 4 to 14 h in a KOH-NaOH eutectic melt at 220 °C. Thermal neutron irradiation was carried out at the Australian Nuclear Science and Technology Organisation (ANSTO) facility, Lucas Heights, Australia. External mica detectors were etched for 40 min in HF (40 %) at room temperature. Tracks were counted and measured under an optical microscope with the aid of a computer driven stage (Dumitru 1993). Magnification used was 1600× using a dry objective for apatite FT analysis (track counting and confined track length measuring) and 2500× using an oil immersion objective for zircon FT analysis. FT ages were calculated according to the external detector method (Naeser 1976; Gleadow 1981) and the zeta approach (Hurford & Green 1982, 1983) with a zeta value of 345.69 ± 8.75 (Durango, CN5) for apatite and 113.49 ± 1.80 (Fish Canyon Tuff, CN1) for zircon. FT age and error calculation as well as the generation of the graphical representation were

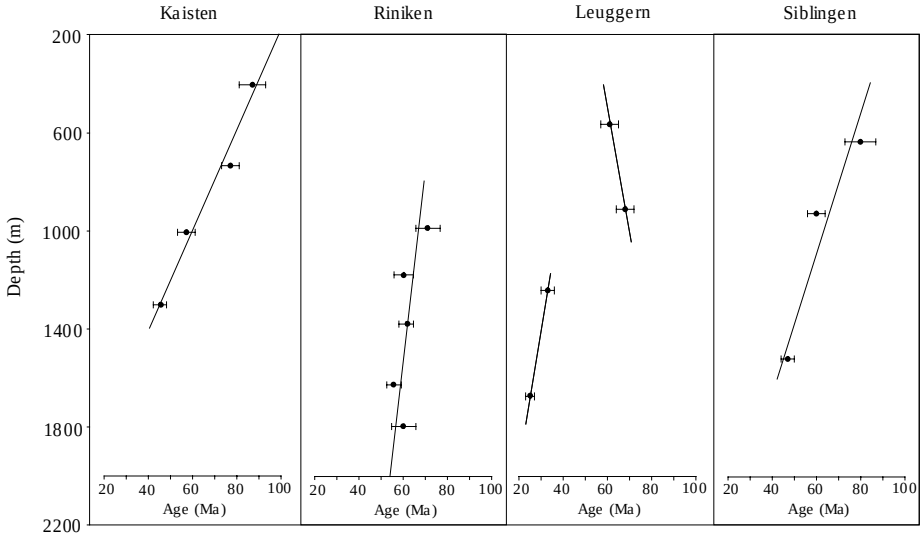

Fig. 3. Apatite FT central age (with 1σ error) versus depth graphs of the investigated Nagra boreholes. The Leuggern samples are splitted in two separate age groups as indicated by their thermal modelling results.

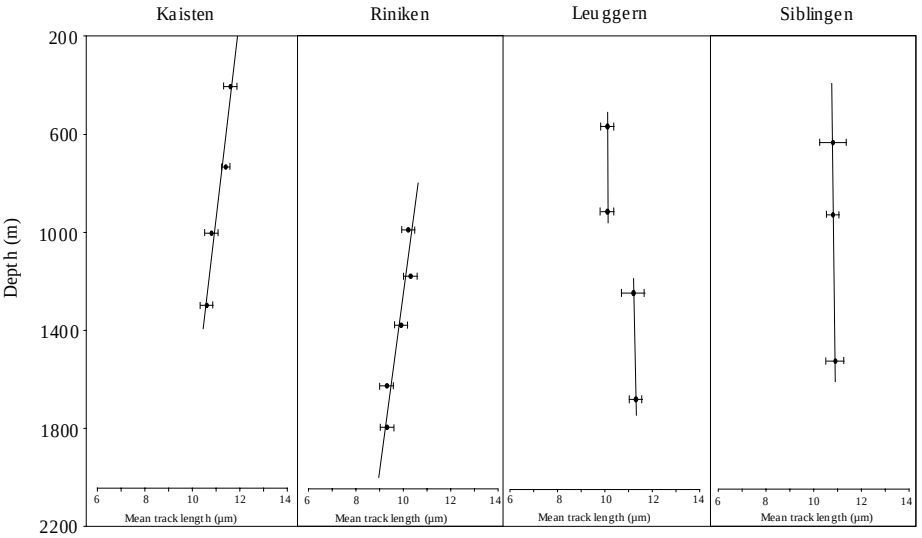

Fig. 4. Mean track length versus depth graphs of the investigated Nagra boreholes.

performed by the computer program Trackkey (Dunkl 2002). All FT ages are central ages (Galbraith & Laslett 1993) and errors are quoted as ± 1σ.

Thermal modelling of the apatite FT data was performed using the computer program AFTSolve (Ketcham et al. 2000) and the algorithm of Laslett et al. (1987), which is a numerical characterization of apatite FT annealing as a function of time and temperature. It is assumed that there is no significant difference in the annealing behaviour between the apatites of this study and the Durango apatite on which the algorithm of Laslett et al. (1987) is based. In this study an inverse modelling approach was carried out: a set of t-T paths was assessed that is consistent with the measured FT data in apatite and other geological constraints. The modelling process includes the generation of a large number of potential t-T paths and the statistical evaluation of the quality of the fit between predicted (based on each t-T path generated) and the measured FT data in apatite (for details see Ketcham et al. 2000). As a result two regions outline all "acceptable" fits (light grey regions) with a Kolmogorov-Smirnov probability of 0.05 or more and "good" fits (dark grey regions) with a Kolmogorov-Smirnov probability of 0.5 or more (Ketcham et al., 2000). The best-fit t-T path is also included in each diagram. However, it has to be noted that the envelopes do not encompass t-T fields in which *all* t-T paths pass the corresponding statistical tests.

4. Analytical results

Seventeen core samples yielded fourteen zircon and sixteen apatite ages. Both zircon and apatite FT central ages are very similar in all boreholes, zircon FT central ages in total varying between 185 ± 16 Ma and 287 ± 21 Ma (Fig. 2, Table 2) and ap-

Table 2. Zircon FT age data from four boreholes (Nagra) in Northern Switzerland

Sample number	Depth (m)	No. of crystals counted	Spontaneous tracks ρ_s (N_s)	Induced tracks ρ_i (N_i)	$P(\chi^2)$ (%)	Dosimeter ρ_d(N_d)	Central age (Ma) ± 1σ
Kaisten							
Kai 1	1305	20	237 (1812)	21 (162)	54	3.94 (1497)	245 ± 22
Kai 4	407	20	210 (1636)	19 (152)	85	3.88 (1474)	233 ± 21
Riniken							
Rin 1	1797	20	333 (2985)	27 (242)	85	4.19 (1592)	287 ± 21
Rin 2	1628	20	350 (4652)	34 (453)	29	4.15 (1577)	238 ± 14
Rin 3	1381	20	328 (2329)	31 (217)	80	4.12 (1566)	246 ± 19
Rin 4	1181	20	262 (2453)	21 (198)	88	4.08 (1550)	281 ± 22
Rin 5	992	20	307 (1672)	26 (141)	99	4.05 (1539)	267 ± 25
Leuggern							
Leu 1	1684	20	324 (2177)	32 (216)	84	4.37 (1660)	245 ± 19
Leu 3	916	20	224 (1506)	20 (137)	98	4.31 (1638)	264 ± 25
Leu 4	567	20	246 (1225)	24 (119)	99	4.26 (1619)	244 ± 25
Siblingen							
Sib 1	1519	20	361 (2103)	35 (203)	<1	4.01 (1524)	225 ± 24
Sib 2	1220	20	319 (1066)	35 (118)	99	3.99 (1516)	201 ± 20
Sib 3	930	20	318 (1451)	29 (134)	99	3.97 (1509)	240 ± 23
Sib 4	639	20	347 (1711)	41 (204)	24	3.96 (1505)	185 ± 16

Track densities (ρ) are in 10^5 tracks/cm2, number of tracks counted (N) shown in brackets.
Analyses by external detector method using 0.5 for the 4π/2π geometry correction factor.
Ages calculated as central ages according to Galbraith and Laslett (1993) using dosimeter glass CN1 with ξ_{CN1} = 113.49 ± 1.80 (Z. Timar-Geng).
$P(\chi^2)$ is the probability of obtaining χ^2 value for ν degrees of freedom where ν = number of crystals - 1.

atite FT central ages varying between 25 ± 2 Ma and 87 ± 6 Ma (Fig. 2, Table 3) with a trend of decreasing ages with depth (Fig. 3). Mean track lengths exhibit a similar decreasing tendency with increasing borehole depth (Fig. 4).

4.1 Kaisten

In the Kaisten borehole metapsammitic layers of the crystalline basement beneath 172 m sediments of the Permian trough shoulder were sampled from a depth range between 407 m and 1306 m and present-day temperatures of 28° to 58 °C (Table 1).

Two samples yielded similar zircon FT ages of 233 ± 21 Ma and 245 ± 22 Ma from the top and the bottom of the entire sampled depth range (Figs. 2, 5). Radial plots (Galbraith 1988, 1990) of both zircon samples display relatively broad single-grain age distributions from ~400 to ~130 Ma. This high scatter of single-grain ages can be explained with normal Poissonian variation as revealed by the applied χ^2 statistics (Table 2), i.e. $P(\chi^2)$ values >5% indicate that all grains analysed for individual samples may be derived from a single age population (Green 1981). However, Timar-Geng et al. (2004) showed that high standard errors of single-grain age estimates and the low number of counted grains can render the χ^2-approach unsuitable for detection of any extra-Poissonian variation due to, for instance, different annealing kinetics of the individual grains.

Apatite FT ages vary from 45 ± 3 Ma at the bottom to 87 ± 6 Ma at the top of the sampled depth range with a clear younging trend toward depth (Figs. 2, 5). Single-grain ages scatter between ~140 Ma and ~30 Ma, the two youngest samples (Kai1 and Kai2) revealing very low $P(\chi^2)$ values (Table 3), which is an indication of extra-Poissonian variation in the spread of these ages. Confined mean track lengths ranging between 10.6 µm and 11.6 µm together with standard deviations all greater than 1.4 µm (Fig. 5) clearly show substantial partial annealing of all samples. In addition, decreasing apatite FT ages correlate with decreasing track lengths.

4.2 Riniken

Riniken is the only borehole of this study that penetrates the deep Permo-Carboniferous trough of northern Switzerland (Nagra 1990). Permian breccias and sandstones were sampled from a depth range between 992 m and 1797 m (Table 1).

Zircon FT central ages scatter between 238 ± 14 Ma and 287 ± 21 Ma (Figs. 2, 6). The large spread in single-grain ages (~460 Ma to ~ 130 Ma) with a significant proportion of pre-depositional single-grain ages indicate that none of the samples experienced palaeotemperatures critical for complete annealing of fission tracks in zircon, i.e. ~330 °C (Tagami & Shimada 1996; Tagami et al. 1998) since deposition. Thus, these samples exhibit a strong inherited signal from the source region.

Table 3. Apatite FT age data from four boreholes (Nagra) in Northern Switzerland

Sample number	Depth (m)	No. of crystals counted	Spontaneous tracks ρ_s (N_s)	Induced tracks ρ_i (N_i)	$P(\chi^2)$ (%)	Dosimeter ρ_d(N_d)	Central age (Ma) ± 1σ
Kaisten							
Kai 1	1305	20	8 (620)	33 (2590)	<1	10.77 (4092)	45 ± 3
Kai 2	1009	20	15 (1040)	49 (3377)	<1	10.48 (3982)	57 ± 4
Kai 3	737	20	22 (1404)	50 (3227)	12	10.19 (3872)	77 ± 4
Kai 4	407	20	5 (463)	10 (910)	35	9.91 (3766)	87 ± 6
Riniken							
Rin 1	1797	20	13 (864)	48 (3263)	<1	13.92 (5290)	62 ± 5
Rin 2	1628	20	20 (2503)	73 (9358)	<1	13.06 (4963)	58 ± 3
Rin 3	1381	20	18 (1504)	63 (5214)	2.13	12.77 (4853)	63 ± 3
Rin 4	1181	20	12 (1080)	41 (3663)	<1	12.20 (4636)	62 ± 4
Rin 5	992	20	18 (1324)	49 (3706)	<1	11.34 (4309)	72 ± 5
Leuggern							
Leu 1	1684	20	8 (425)	66 (3463)	<1	11.24 (4271)	25 ± 2
Leu 2	1249	20	4 (141)	21 (857)	36	11.47 (4359)	33 ± 3
Leu 3	916	20	14 (727)	33 (1681)	65	9.17 (3485)	68 ± 4
Leu 4	567	20	8 (719)	20 (1895)	7	9.35 (3553)	61 ± 4
Siblingen							
Sib 1	1519	20	14 (542)	46 (1800)	39	9.05 (3439)	47 ± 3
Sib 3	930	20	21 (657)	51 (1578)	<1	8.48 (3222)	60 ± 4
Sib 4	639	20	29 (531)	51 (926)	<1	8.19 (3112)	80 ± 7

Track densities (ρ) are in 10^5 tracks/cm^2, number of tracks counted (N) shown in brackets.
Analyses by external detector method using 0.5 for the $4\pi/2\pi$ geometry correction factor.
Ages calculated as central ages according to Galbraith and Laslett (1993) using dosimeter glass CN5 with ξ_{CN5} = 345.69 ± 8.75 (Z. Timar-Geng).
$P(\chi^2)$ is the probability of obtaining χ^2 value for ν degrees of freedom where ν = number of crystals - 1.

Apatite FT central ages range between 58 ± 3 Ma and 72 ± 5 Ma (Figs. 2, 6) with only a weak tendency of decreasing ages with depth. Radial plots (Fig. 6) display a large spread in the single-grain ages, varying between ~160 Ma and ~25 Ma. In all of the samples multiple age populations are present as revealed by the χ^2 statistics (Table 3). Substantial annealing is indicated by short confined mean track lengths of 9.3 µm to 10.2 µm and standard deviations greater than 1.7 µm.

4.3 Leuggern

A two-mica granite at the bottom and paragneisses at shallower depths were sampled in the Leuggern borehole between 567 m and 1684 m depth (Table 1).

Three samples yield uniform zircon FT central ages of 245 ± 19 Ma at the bottom, 244 ± 25 Ma at the top and 264 ± 25 Ma in-between (Figs. 2, 7). Single-grain ages range between ~450 Ma and ~ 140 Ma with no statistical indication for extra-Poissonian variation (Table 2).

Apatite FT central ages vary between 25 ± 2 Ma and 68 ± 4 Ma with a striking jump in the FT ages between Leu2 and Leu3 (Fig. 7). This feature is also visible in the confined mean track lengths, the two younger samples (Leu1 and Leu2) having longer mean track lengths (11.3 µm and 11.2 µm) than the older ones (Leu3 and Leu4 with mean track lengths of 10.1 µm), but *not* in the zircon FT central ages. Standard deviations are greater than 1.8 µm. A distinction in two age groups is also reflected in the single-grain age distributions. Radial plots of the two younger samples (Leu1 and Leu2) display a single-grain age variation between ~60 Ma and ~10 Ma, while the older ones (Leu3 and Leu4) reveal a distribution of significantly older single-grain-ages from ~120 Ma to ~ 40 Ma (Fig. 7). Only Leu1 reveals a statistically founded indication for multiple age populations (Table 3).

4.4 Siblingen

Cordierite-biotite- and cordierite-two-mica-granites were sampled in the Siblingen borehole between 639 m and 1519 m depth (Table 1).

Zircon FT central ages scatter between 185 ± 16 Ma and 240 ± 23 Ma (Figs. 2, 8). There is a large spread in single-grain ages (~470 Ma to ~100 Ma), but only the sample at the bottom of the borehole (Sib1) has a $P(\chi^2)$ value lower than 5% (Table 2), thus indicating extra-Poissonian variation. Such isolated variation could be due to different annealing kinetics of the individual grains.

Apatite FT central ages range between 47 ± 3 Ma and 80 ± 7 Ma (Figs. 2, 8) with a clear tendency of decreasing ages with depth. Contrary to the zircon FT results Sib1 is the only sample showing no extra-Poissonian variation with a relatively narrow range of single-grain ages (~80 Ma to ~30 Ma). Radial

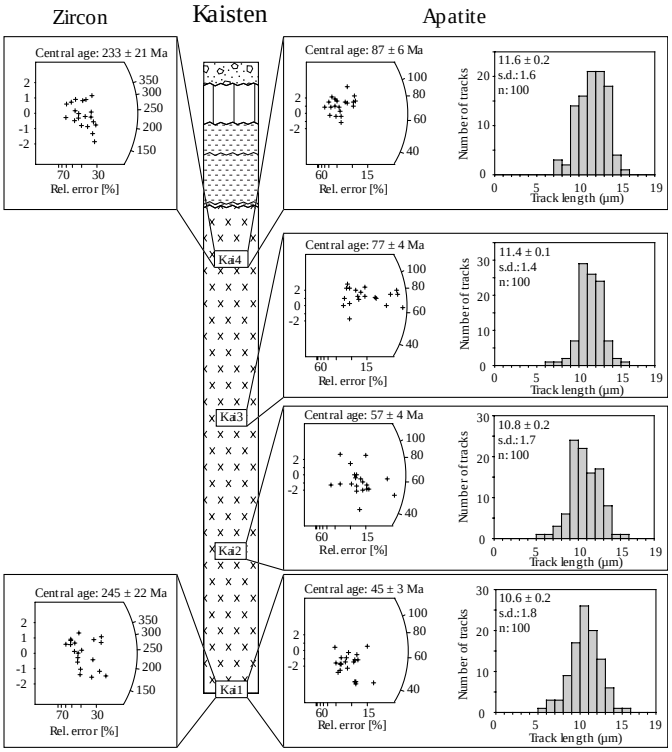

Fig. 5. Kaisten borehole: radial plots and track length distributions. For data, see Tab. 2 (zircon) and Tab. 3 (apatite). For geological unit patterns, see Fig. 2.

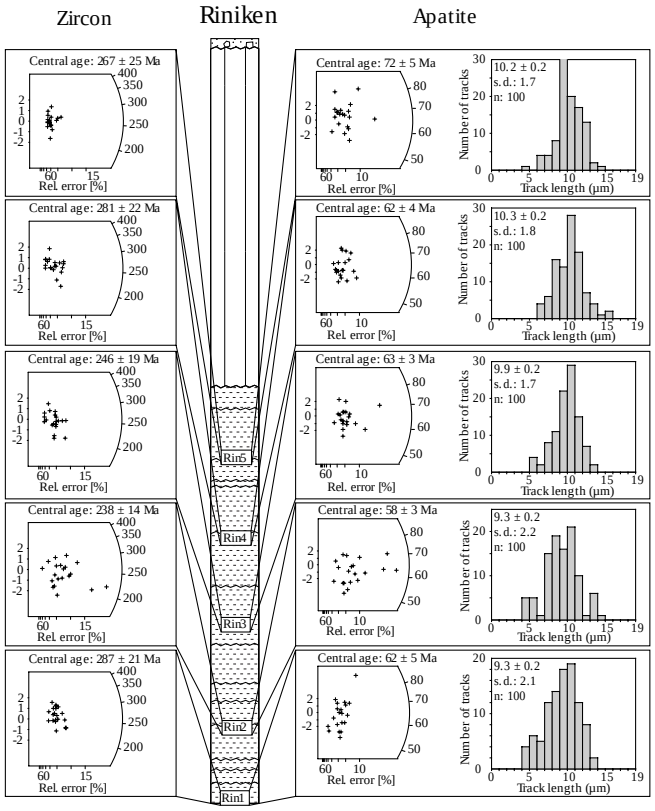

Fig. 6. Riniken borehole: radial plots and track length distributions. For data, see Tab. 2 (zircon) and Tab. 3 (apatite). For geological unit patterns, see Fig. 2.

plots of the other samples reveal single-grain ages up to ~130 Ma (Fig. 8). Confined mean track length in Sib3 (the only sample with the standard amount of 100 measurable confined horizontal tracks) is 10.8 ± 1.9 µm.

5. Thermal modelling

5.1 Modelling strategy

The low-temperature thermal history of northern Switzerland was derived using the following modelling strategy: Initial model runs were performed with only a few constraints on the time-temperature (t-T) path of each sample. The time for the first constraint was chosen on the base of the zircon FT age of the same sample and the oldest apatite single-grain age. This date should be somewhat older than the FT age of the oldest and thus most resistant apatite grains to allow for age reduction by partial annealing (Ketcham et al. 2000). The temperature for the first constraint was set at ~130 °C ensuring that there are no apatite fission tracks present as an initial condition. The last time constraint was set at the temperature at which the sample was collected (Nagra 1990, 1991a, 1991b, 1993). Modelled t-T paths were defined to be non-monotonic. This configuration is aimed at finding solutions by the program, particularly any possible heating events and their timing. This first model runs also constrain the time of cooling of the sample below the track retention temperature, which can be used as a new constraint for following model runs.

In a next step, the new initial constraint and additional intermediate constraints (Table 4) were used to better evaluate individual heating and cooling events. Thereby model runs were progressively refined by forcing restrictions on the t-T paths as suggested by successive modelling results using additional nodal points in the region of assumed thermal events. Several possibilities regarding the timing of such a heating event were tested in an effort to find the temperature peak most consistent with the measured data. In a final step a narrower search was carried out using monotonic t-T paths between two user-defined constraints. This option potentially reduces the full extent of the envelope of statistically acceptable solutions, but simultaneously disables the modelled t-T paths to bounce up and down in a geologically inappropriate fashion (Ketcham et al. 2000). An example of the modelling procedure up to the "final" result is illustrated for sample Kai2 (Fig. 9).

5.2 Model results

5.2.1 Kaisten

Modelling of the apatite FT data from the Kaisten borehole samples (Fig. 10) indicates total track annealing since the be-

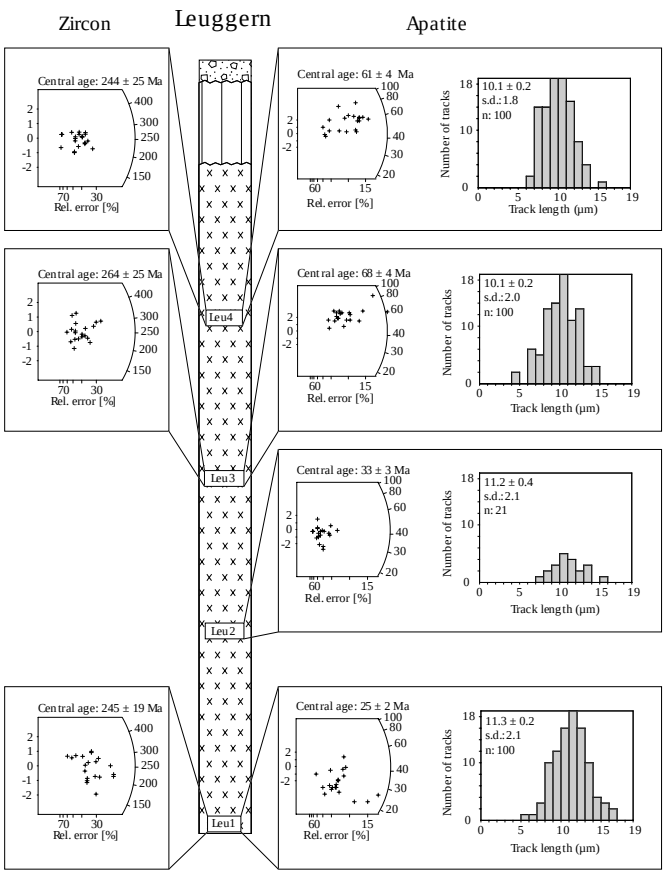

Fig. 7. Leuggern borehole: radial plots and track length distributions. For data, see Tab. 2 (zircon) and Tab. 3 (apatite). For geological unit patterns, see Fig. 2.

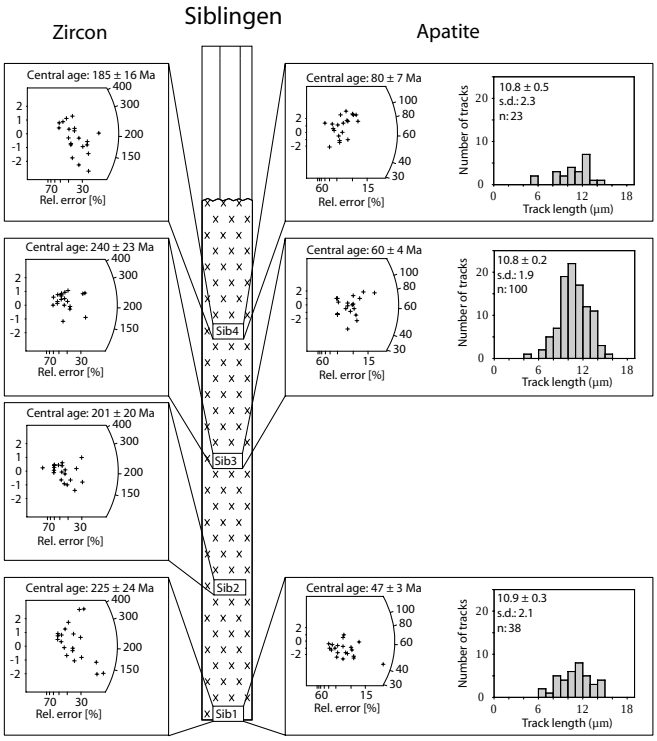

Fig. 8. Siblingen borehole: radial plots and track length distributions. For data, see Tab. 2 (zircon) and Tab. 3 (apatite). For geological unit patterns, see Fig. 2.

Table 4. Modelling details

Samples	Constraints of final models (Ma, °C-°C)	Iterations	Nodal points
Kaisten			
Kai1	(0.0, 59-59)(11, 130-40)(30, 133-40)(35, 132-39)(40,130-40)(66, 130-40)(80, 129-129)	10,250	15
Kai2	(0.0, 51-51)(9.5, 129-31)(30, 128-34)(35, 129-33)(75, 130-41)(90, 130-130)	10,000	25
Kai3	(0.0, 40-40)(4.7, 100-40)(25, 113-41)(31, 100-21)(75, 100-21)(100, 132-132)	10,000	25
Kai4	(0.0, 29-29)(5.2, 126-30)(25, 126-31)(30, 125-30)(76, 126-30)(120, 130-130)	10,250	25
Riniken			
Rin1	(0.0, 84-84)(35, 128-84)(39, 128-30)(130, 106-30)(181, 130-130)	10,250	41
Rin2	(0.0, 78-78)(35, 132-60)(40, 119-20)(75, 117-21)(141, 131-131)	100,000	41
Rin3	(0.0, 70-70)(4.8, 130-86)(35, 130-66)(41, 128-23)(75, 127-26)(121, 130-130)	500,000	49
Rin4	(0.0, 65-65)(35, 122-26)(40, 102-20)(75, 133-21)(120, 132-132)	100,000	41
Rin5	(0.0, 59-59)(4.8, 120-78)(30, 111-71)(40, 129-24)(75, 129-23)(121, 131-131)	100,000	25
Leuggern			
Leu1	(0.0, 71-71)(40, 130-130)	10,000	33
Leu2	(0.0, 56-56)(51, 131-131)	10,000	33
Leu3	(0.0, 42-42)(10, 114-13)(35, 122-9)(40, 122-9)(75, 102-14)(121, 130-130)	112,183	49
Leu4	(0.0, 30-30)(10, 95-19)(36, 128-19)(40, 127-17)(90, 98-23)(121, 131-131)	10,000	49
Siblingen			
Sib1	(0.0, 59-59)(35, 123-25)(40, 103-26)(65, 130-25)(80, 129-129)	10,000	41
Sib2	(0.0, 37-37)(35, 129-40)(41, 108-20)(75, 117-25)(100, 130-130)	150,000	41
Sib3	(0.0, 33-33)(30, 128-20)(35, 98-16)(75, 129-21)(121, 130-130)	10,000	41

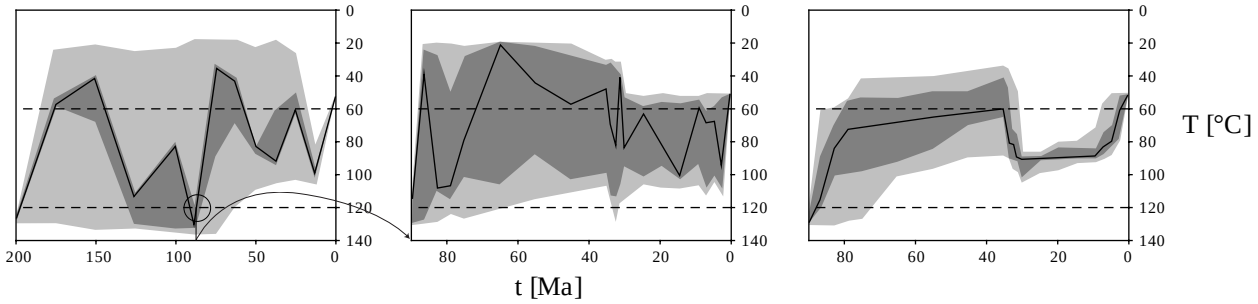

Fig. 9. Illustration of the modelling procedure (sample Kai2). From left to right: initial step with only a few constraints and non-monotonic t-T paths; intermediate step with more restrictions, as suggested by first model runs (e.g. initial constraint at 90 Ma) but still with non-monotonic t-T paths; "final" result with monotonic t-T paths between user-defined constraints.

ginning of the Mesozoic subsidence. Thus, the maximum palaeo-temperatures after post-Variscan peneplanation exceeded 120 °C. Oldest tracks preserved in the best-fit models vary from 75 Ma at the bottom of the sampled depth interval to 115 Ma at the top. This trend of increased track annealing with depth is consistent with the age data and can be interpreted in terms of increasing down-hole palaeo-temperatures. Measured and predicted parameters of the best-fit paths are in very good agreement, with age goodness-of-fit values of up to 0.98.

All four models (Fig. 10) display a two-phase cooling history since the samples cooled below the track retention temperature of ~120 °C. Moderate to rapid Cretaceous cooling through the apatite partial annealing zone (PAZ), i.e. through 120 °C to 60 °C, was followed by an Eo-Oligocene heating event and subsequent slow cooling to present-day temperatures. During the late cooling phase all samples remained within the PAZ until comparatively recent times.

5.2.2 Riniken

Best-fit models of the Riniken samples (Fig. 11) suggest that there was total annealing of fission tracks in Mesozoic times. Oldest tracks preserved in the best-fit models scatter between 113 Ma and 154 Ma. Evaluation of the statistical goodness-of-fit of modelled FT length distributions and ages to the measured data yields values between 0.63 and 0.99 (Fig. 11).

The modelled best-fit t-T paths are very similar for all samples. After Late Jurassic to Cretaceous cooling below the closure temperature of the apatite FT system a new heating phase started in the Late Eocene. After this heating event annealing temperatures persisted until recent times, which is also implied from the scarcity of very long tracks (Fig. 6).

5.2.3 Leuggern

The modelled t-T paths of the Leuggern borehole samples show two groups of markedly different shape (Fig. 12). The two upper samples (Leu3 and Leu4) experienced last resetting of the apatite FT system in Mesozoic times. Best-fit models of the two lower samples (Leu1 and Leu2) indicate total annealing during the Eocene preserving oldest tracks with an age of 37 Ma (Leu1) and 48 Ma (Leu2). Preserved oldest tracks in the best-fit models of the two other samples are significantly older (118 Ma and 121 Ma). The statistical precision of the best-fit t-T paths is especially good for the two samples with short thermal histories (Leu1 and Leu2) with goodness-of-fit values >0.95. Somewhat lower but still "good" values were obtained for the two upper samples (Fig. 12).

Modelled t-T paths of both Leu3 and Leu4 display a common thermal history. Initial cooling below track retention temperatures in Cretaceous times and subsequent residence at moderate temperatures were followed by a prominent heating event during the Eocene. After this heating episode the samples remained within the PAZ until almost recent times. Apatite FT data of the two other samples (Leu1 and Leu2) recorded only the last cooling phase since the Eocene (Fig. 12).

5.2.4 Siblingen

Best-fit models of the Siblingen borehole samples (Fig. 13) indicate total annealing of apatite fission tracks during the Cretaceous. Oldest tracks preserved in the best-fit models range from 74 Ma (bottom) to 115 Ma (top), displaying a trend of increased track annealing with depth. Excellent age goodness-of-fit values of up to 0.99 prove that measured FT data and predicted parameters of the best-fit paths are in very good agreement.

All three models (Fig. 13) exhibit very comparable thermal histories with two cooling phases separated by a distinct heating event. The first cooling phase started in Cretaceous times and is characterised by moderate to rapid cooling rates. This cooling phase is followed by a heating event during the Eocene and a subsequent slow cooling phase to present-day temperatures. During the last cooling phase annealing temperatures have been maintained until comparatively recent times.

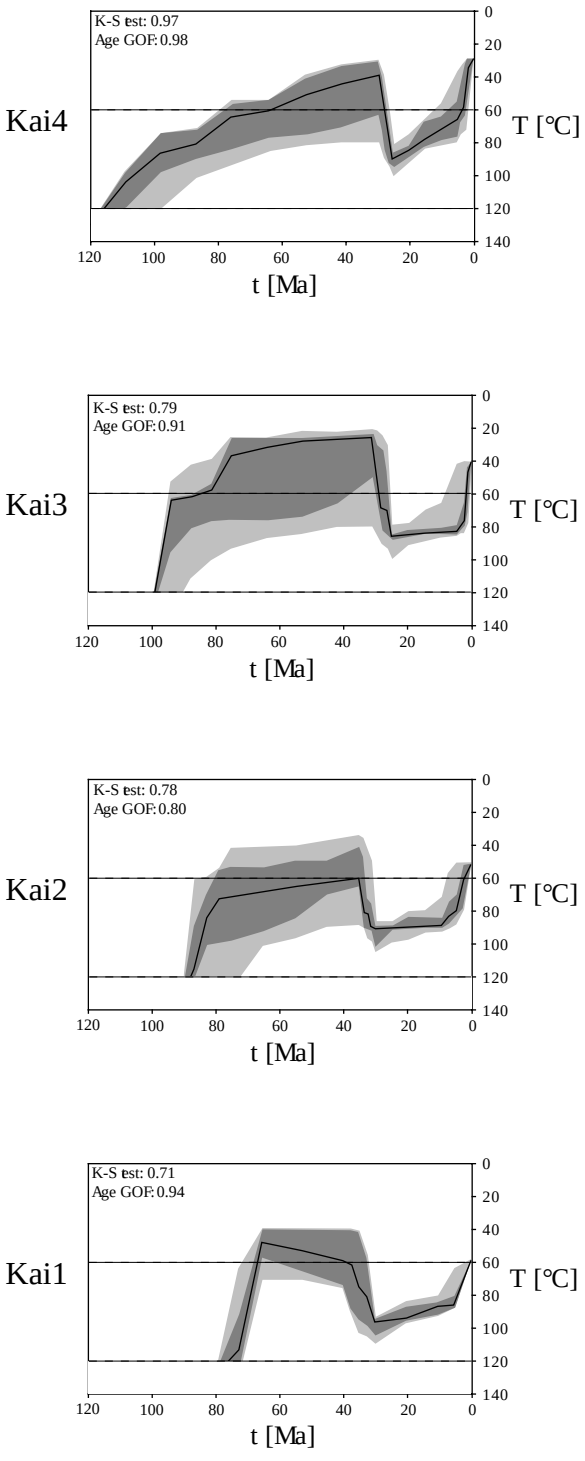

Fig. 10. Kaisten borehole: thermal modelling results. K-S test: Kolmogorov-Smirnov test evaluating the degree of fit between FT length distributions. Age GOF: FT age goodness-of-fit test. For details see Ketcham et al. (2000).

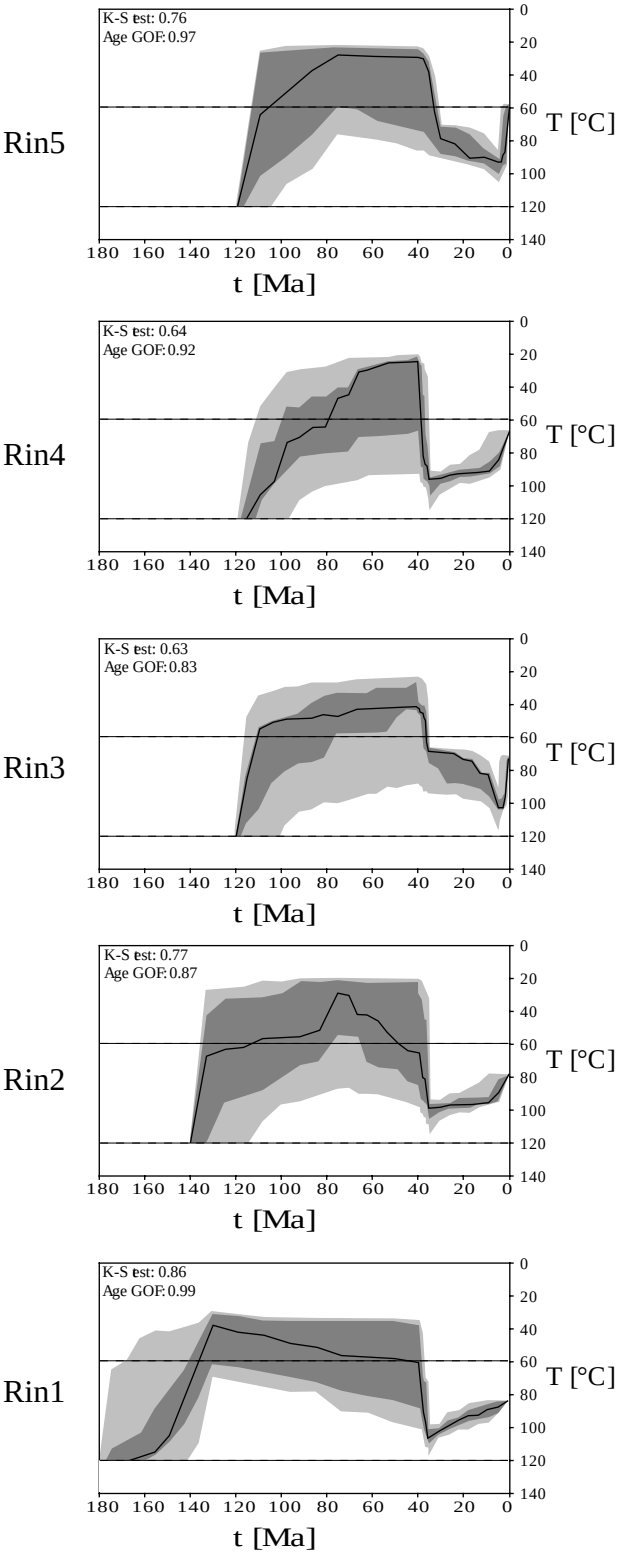

Fig. 11. Riniken borehole: thermal modelling results. For abbreviations, see Fig. 8.

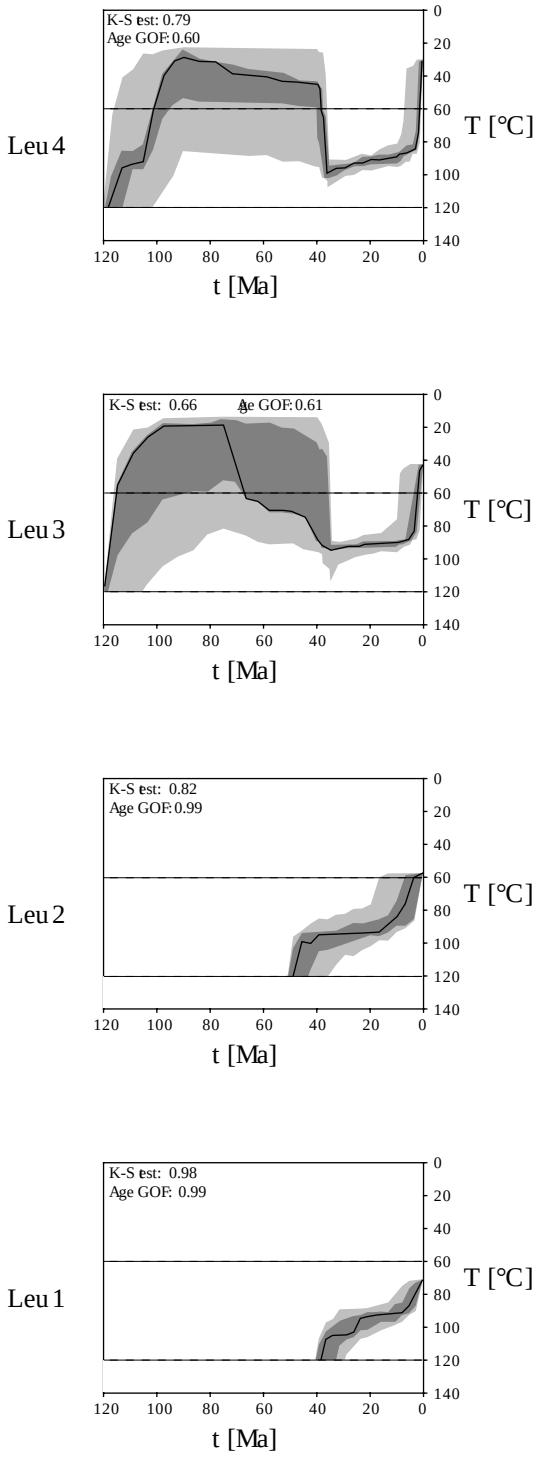

Fig. 12. Leuggern borehole: thermal modelling results. For abbreviations, see Fig. 8.

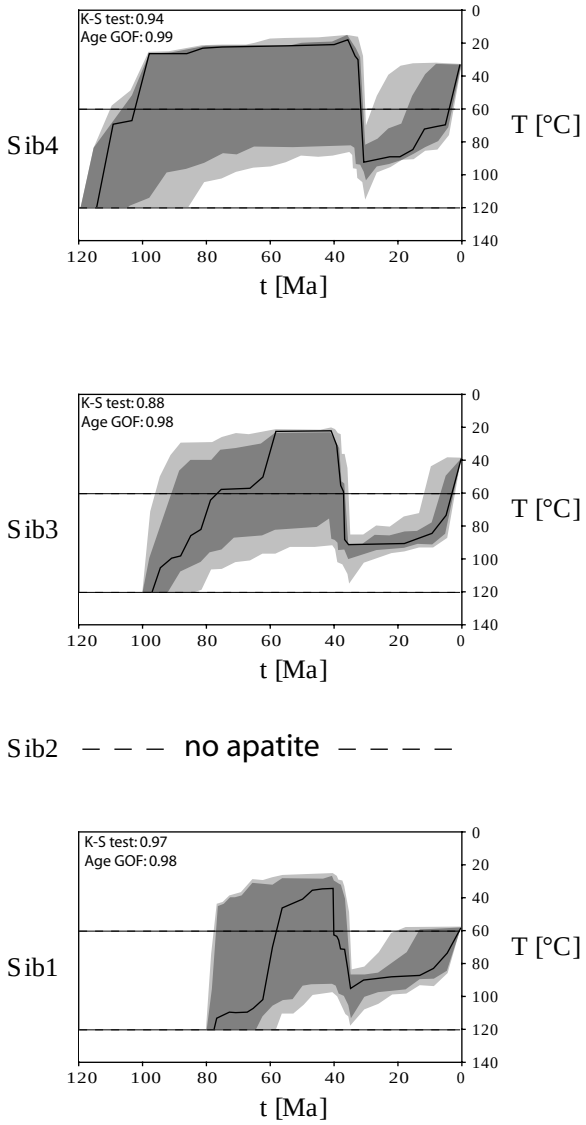

Fig. 13. Siblingen borehole: thermal modelling results. For abbreviations, see Fig. 8.

6. Discussion

The zircon FT ages indicate that in all boreholes the level of the crust sampled in northern Switzerland never experienced temperatures in excess of ~330 °C after the late Variscan consolidation of the crystalline basement, since total annealing of fission tracks in zircon is not observed. Zircon FT central ages and single-grain ages cluster at around 250 Ma and are substantially older than the central and single-grain ages from the nearby Black Forest (Fig. 14). The crystalline basement of northern Switzerland may be considered as the southern continuation of the internal zone of the Central European Variscides, now exposed in the Black Forest (e.g., Thury et al.

1994). The present-day outcrop level of the Black Forest approximately corresponds to the sampled depth range of the boreholes during Mesozoic subsidence. This can be stated because the Permo-Triassic paleosurface is partly preserved in the southern Black Forest (Paul 1955; Wimmenauer & Schreiner 1990). Primarily the Tertiary uplift of the Black Forest and the subsidence of the Alpine foreland, which was accompanied by reactivation of old fault zones in the study area (e.g., Müller et al. 2002), led to the current altitude difference between the two geographically neighbouring regions. Timar-Geng et al. (2004) interpreted the zircon FT data from the Black Forest in terms of a Jurassic heating event caused by regional-scale hydrothermal fluid migration. Obviously this thermal overprint is not observable from FT data in the borehole samples of northern Switzerland. Also, there is no other geological evidence for a main Jurassic hydrothermal phase in the crystalline basement of northern Switzerland. The youngest penetrative thermal event with a clear petrographic signature is a kaolinitic alteration and the formation of interconnected vugs in pre-existing structures with weakly constrained post-Permian ages (Mazurek et al. 1992) and authigenic illite formation in sandstones in the Jurassic (Schaltegger et al., 1995). Based on coalification and fission track data, Schegg & Leu (1998) estimated high palaeogeothermal gradients of 80–90 °C/km in northern Switzerland during the Late Palaeozoic. The zircon FT data of this study bear the signature of this regional thermal event, which also correlates with the rhyolitic volcanism known in the Black Forest. Common for both the Black Forest and the crystalline basement of northern Switzerland is the Cretaceous cooling below the zircon FT PAZ, i.e. below ~200 °C (e.g., Tagami & Shimada 1996; Tagami et al. 1998; see also discussion in Timar-Geng et al. 2004). This is inferred from the youngest single-grain age cluster dating the passage through the low-temperature boundary of the PAZ (Fügenschuh & Schmid 2003).

The apatite FT data document the low temperature (< ~120°C) thermal history of the region. The borehole samples mostly exhibit a trend of decreasing ages with depth (Fig. 3). This is a common feature in most geological settings and the shape of the age-depth graphs often reflects the thermal history of the rocks as they cooled through the PAZ (Gleadow & Brown 2000). Such age-depth profiles vary from nearly linear for high denudation rates to concave-upwards curves at low rates (Gleadow & Brown 2000). The age-depth trend of the Nagra borehole samples are approximated by a linear relationship, but a sound interpretation in terms of denudation rates is not recommended due to the measured track length distributions. In fact, thermal modelling of the FT data suggests a composite thermal history of the region with slow post-Eocene cooling and prolonged residence in the PAZ. The shape of the age-depth graph is, therefore, primarily controlled by the increase in temperature with depth and is not related to the denudation rate. There is a published apatite FT central age (160 ± 10 Ma; Mazurek et al. 2006) from the borehole Riniken from shallower depth, which is significantly older than the Riniken samples in this study. Most probably this sample did not experience total annealing but rather also contains inherited tracks.

Modelling of the apatite FT parameters provides a fairly clear picture about the low-temperature thermal history of the crystalline basement of northern Switzerland since Cretaceous times (Figs. 10–13). All t-T paths (with the exception of Leu1 and Leu2) exhibit the same general shape: moderate to rapid Cretaceous cooling through the PAZ is followed by Eocene heating in-between the PAZ and subsequent cooling to present-day temperatures. The second cooling phase is characterised by prolonged residence in the PAZ. This is also implied by strongly reduced mean track lengths (Fig. 4) and scarcity of long tracks. The two lower Leuggern borehole samples (Leu1 and Leu2) apparently experienced total track loss during the Eocene heating event. Therefore, only the last cooling phase is documented by the apatite FT parameters. It should be stated that in spite of the excellent statistical goodness-of-fit values, the modelled thermal histories need not be unique. A broad range of t-T paths may generate FT parameters that could lie behind the measured data (Ketcham et al. 2000). Furthermore, cooling phases prior to reheating are not well documented by FT data for those temperatures lying below the maximum temperature of the reheating event due to annealing of all pre-existing tracks (De Bruijne & Andriessen 2002). The maximum temperature of a reheating event is quite well determined by modelling studies (Gleadow & Brown 2000). However, due to statistical uncertainties in the evaluation of the best-fit paths, the reconstruction of palaeogeothermal gradients based on modelling results is not recommended.

Some previous apatite FT modelling studies (Nagra 2002; Mazurek et al. 2006) dealt with parts of the Swiss Molasse Basin, located only a few km further to the south of the area presented here. Combined with other methods, Mazurek et al. (2006) reconstructed a multi-stage burial history of the basin with two successive stages of heating, one in the Cretaceous and the other in the Miocene. They relate the first heating episode to Mesozoic burial *and* an increased heat flux of 85-100 mW/m^2 in the Early Cretaceous. The second heating stage was caused by maximum burial during the Miocene (Mazurek et al. 2006). The initial cooling phase of our samples into the PAZ roughly coincides with the first cooling stage after Cretaceous burial and heating presented by Mazurek et al. (2006). Thus, it appears that the same Mesozoic thermal event caused total track annealing in the sampled crustal level of the external parts of northern Switzerland, mostly north of the Permo-Carboniferous trough. However, Cretaceous heating of the internal parts of northern Switzerland postdates the peak of the Mesozoic hydrothermal alteration observed in the neighbouring Black Forest, even though a less clear record of hydrothermal activity in the crystalline basement throughout the Cretaceous is also available (see compilation by Wetzel et al. 2003). Thus, in the case of the samples presented here, increased heat flux values affect the experienced total annealing of apatite fission tracks rather than burial below Mesozoic sediments.

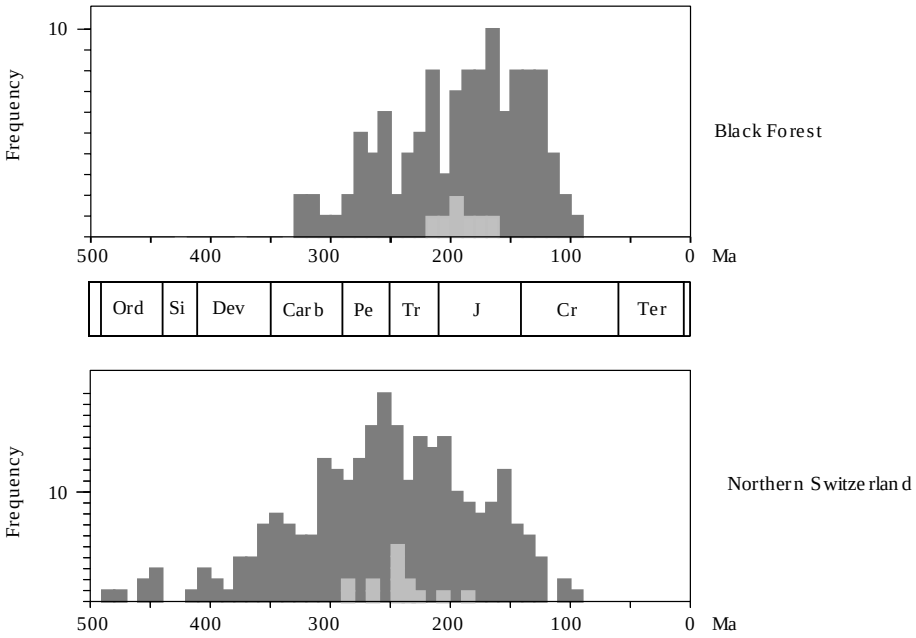

Fig. 14. Frequency distribution of central ages (light grey) and single-grain ages (dark grey) for the Black Forest (Timar-Geng et al., 2004) and northern Switzerland (this study).

The striking feature of the modelled t-T paths of the present study is a major heating event of mostly Middle to Late Eocene age, which clearly predates the second heating stage in the Molasse basin. However, this can be explained by the tectonically and palaeogeographically different settings of the two regions. The borehole samples of this study are situated outside or in a marginal position of the Molasse basin, whereas the previously analysed samples (Mazurek et al. 2006) experienced substantial burial due to the subsidence of the Alpine foreland from the Late Oligocene onwards. Consequently, the elevated temperatures during the Miocene burial phase (e.g., Mazurek et al. 2006) might have overprinted a possible Eocene thermal pulse in the more internal parts of the Molasse basin. The Eocene heating event recorded in the FT data of this study, in contrast, can be related to the initial rifting stage of the nearby Upper Rhine Graben in the foreland of the evolving Alps (e.g., Schumacher 2002). This initial rifting stage was controlled by the gradually increasing subduction resistence of the European lithosphere and the build-up of intraplate stresses (Dèzes et al. 2004), and accompanied by progressively increasing volcanic activity (e.g., Lippolt 1983; Keller et al. 2002). Reactivation of Permo-Carboniferous crustal-scale fault systems played a fundamental role during the initial, Late Eocene rifting phase of the Upper Rhine Graben (Schumacher 2002) and was also characteristic for the entire foreland of the Alps at this time (Dèzes et al. 2004). Thus, faults of the Permo-Carboniferous Trough of northern Switzerland could have also acted as major conduits for circulating hydrothermal fluids giving rise to the observed middle to Late Eocene thermal event in the crystalline basement of northern Switzerland.

A distinctly accelerated cooling towards the present-day temperature, displayed by almost all modelled t-T paths, appears to be an artefact of the Laslett et al. (1987) algorithm (e.g. Ketcham et al. 2000) and, hence, is not further discussed.

7. Conclusions

The low-temperature thermal history of the crystalline basement of northern Switzerland has been derived by FT analysis on 17 borehole samples. Inverse modelling techniques were used to provide quantitative constraints on time-temperature histories that are in agreement with the measured data.

Within the investigated borehole sections, maximum palaeotemperatures never exceeded ~330 °C since post-Variscan peneplanation. Zircon FT central and single-grain ages do not show evidence for a Jurassic hydrothermal event, as was observed in the nearby southern Black Forest (Timar-Geng et al. 2004, 2006). Instead, the zircon FT data bear the signature of elevated Late Palaeozoic palaeogeothermal gradients (Schegg & Leu 1998).

Modelling results suggest that moderate to rapid cooling of the samples through the apatite PAZ at the end of the Mesozoic was followed by a distinct thermal event during the Eocene and subsequent slow cooling to present-day temperatures. For the duration of the second cooling phase the samples remained within the PAZ until comparatively recent times or even until present.

The Eocene heating event coincides with the initial rifting phases of the neighbouring Upper Rhine Graben and associated volcanic activity. It is proposed that faults of the Permo-Carboniferous Trough of northern Switzerland could have acted as important pathways for migrating hydrothermal fluids inducing the observed middle to Late Eocene thermal anomaly in the crystalline basement of northern Switzerland.

Acknowledgements

This work was supported by the Swiss National Science Foundation (Project Nos. 21-57038.99 and 20-64567.01). We are indebted to Nagra for providing the borehole samples and unpublished data. We gratefully acknowledge the critical reading of the manuscript and the constructive comments by M. Mazurek, M. Rahn and S. Schmid. This paper is a contribution to the international EUCOR-URGENT project.

REFERENCES

CEDERBOM, C.E., SINCLAIR, H.D., SCHLUNEGGER, F. & RAHN, M.K. 2004: Climate-induced rebound and exhumation of the European Alps. Geology 32, 709–712.

DE BRUIJNE, C.H. & ANDRIESSEN, P.A.M. 2002: Far field effects of Alpine plate tectonism in the Iberian microplate recorded by fault-related denudation in the Spanish Central System. Tectonophysics 349, 161–184.

DÈZES, P., SCHMID, S.M. & ZIEGLER, P.A. 2004: Evolution of the Alpine and Pyrenean orogens with their foreland lithosphere. Tectonophysics 389, 1–33.

DUDDY, I.R. 1994: The Otway Basin: thermal, structural, tectonic and hydrocarbon generation histories. In: FINLAYSON, D.M. (Ed.): NGMA/PESA Otway Basin Symposium, Extended Abstracts Record 1994, 35–42. Australian Geological Survey Organisation, Canberra.

DUMITRU, T.A. 1993: A new computer-automated microscope stage system for fission-track analysis. Nuclear Tracks and Radiation Measurements 21, 575–580.

DUNKL, I. 2002: Trackkey; a Windows program for calculation and graphical presentation of fission track data. Computers and Geosciences 28/1, 3–12.

EDEL, J.-B. 1997: Les réaimantations post-permiennes dans le bassin dévonodinantien des Vosges méridionales; existence d'une phase de réaimantation au Lias, contemporaine de minéralisations d'ampleur régionale. Comptes Rendus de l'Academie des Sciences, Serie II. Sciences de la Terre et des Planètes 324/8, 617–624.

FÜGENSCHUH, B. & SCHMID, S.M. 2003: Late stages of deformation and exhumation of an orogen constrained by fission-track data: A case study in the Western Alps. Geol. Soc. Am. Bull. 115, 1425–1440.

GALBRAITH, R.F. 1988: Graphical display of estimates having differing standard errors. Technometrics 30, 271–281.

GALBRAITH, R.F. 1990: The radial plot: graphical assessment of spread in ages. Nuclear Tracks and Radiation Measurements 17, 207–214.

GALBRAITH, R.F. & LASLETT, G.M. 1993: Statistical models for mixed fission track ages. Nuclear Tracks Radiation Measurements 21, 459–70.

GALLAGHER, K., BROWN, R.W. & JOHNSON, C. 1998: Fission track analysis and its applications to geological problems. Ann. Rev. Earth Planet. Sci. 26, 519–572.

GIAMBONI, M., USTASZEWSKI, K., SCHMID, S.M., SCHUMACHER, M.E. & WETZEL, A. 2004a: Plio-Pleistocene transpressional reactivation of Paleozoic and Paleogene structures in the Rhine-Bresse transform zone (northern Switzerland and eastern France). Int. J. Earth Sci. 93, 207–223.

GIAMBONI, M., WETZEL, A, NIVIÈRE, B. & SCHUMACHER, M. 2004b: Plio-Pleistocene folding in the southern Rhinegraben recorded by the evolution of the drainage network (Sundgau area; northwestern Switzerland and France). Eclogae geol. Helv. 97, 17–31.

GLEADOW, A.J.W. 1981: Fission track dating: what are the real alternatives. Nucl. Tracks 5, 3–14.

GLEADOW, A.J.W. & BROWN, R.W. 2000: Fission-track thermochronology and the long-term denudational response to tectonics. In: Summerfield, M.A. (Ed.): Geomorphology and Global Tectonics. John Wiley & Sons, Chichester, United Kingdom, 57–76.

GLEADOW, A.J.W., DUDDY, I.R. & LOVERING, J.F. 1983: Fission track analysis: a new tool for the evaluation of thermal histories and hydrocarbon potential. Aust. Pet. Explor. Assoc. J. 23, 93–102.

GREEN, P.F. 1981: A new look at statistics in fission track dating. Nuclear Tracks and Radiation Measurements 5, 77–86.

GREEN, P.F., DUDDY, I.R., GLEADOW, A.J.W. & LOVERING, J.F. 1989: Apatite fission-track analysis as a paleotemperature indicator for hydrocarbon exploration. In: Naeser, N.D., McCulloh, T.H. (Eds.), Thermal History of Sedimentary Basins: Methods and Case Histories. Springer-Verlag, Berlin, 181–195.

GREEN, P.F., THOMSON, K. & HUDSON, J.D. 2001: Recognition of tectonic events in undeformed regions; contrasting results from the Midland Platform and East Midlands Shelf, central England. J. Geol. Soc. London 158, 59–73.

HOUSE, M.A., KOHN, B.P., FARLEY, K.A. & RAZA, A. 2002: Evaluating thermal history models for the Otway Basin, southeastern Australia, using (U-Th)/He and fission-track data from borehole apatites. Tectonophysics 349, 277–295.

HURFORD, A.J. & GREEN, P.F. 1982: A users' guide to fission track dating calibration. Earth Planet. Sci. Lett. 59/2, 343–354.

HURFORD, A.J. & GREEN, P.F. 1983: The zeta age calibration of fission-track dating. Chem. Geol. 41/4, 285–317.

KELLER, J., KRAML, M. & HENJES-KUNST, F. 2002: $^{40}Ar/^{39}Ar$ single crystal dating of early volcanism in the Upper Rhine Graben and tectonic implications. Schweiz. Mineral. Petrogr. Mitt. 82, 121–130.

KETCHAM, R., DONELICK, R. & DONELICK, M. 2000: AFTSolve: a program for multi-kinetic modelling of apatite fission track data. Geol. Mater. Res. 2/1, 1–18.

LASLETT, G., GREEN, P., DUDDY, I. & GLEADOW, A. 1987: Thermal annealing of fission tracks in apatite. Chem. Geol. 65, 1–13.

LIPPOLT, H.J. 1983: Distribution of volcanic activity in space and time. In: Fuchs, K., von Gehlen, K., Mälzer, M., Murawski, H. and Semmel, A. (Eds.), Plateau Uplift, The Rhenish Shield – A Case History. Springer-Verlag, Berlin, 112–120.

MAZUREK, M., MEYER, J. & PETERS, T. 1992: The crystalline basement of Northern Switzerland. Eclogae geol. Helv. 85/3, 767–769.

MAZUREK, M., HURFORD, A.J. & LEU, W. 2006: Unravelling the multi-stage burial history of the Swiss Molasse Basin: integration of apatite fission track, vitrinite reflectance and biomarker isomerisation analysis. Basin Research 18, 27–50.

MURAKAMI, M., TAGAMI, T. & HASEBE, N. 2002: Ancient thermal anomaly of an active fault system; zircon fission-track evidence from Nojima GSJ 750 m borehole samples. Geophys. Res. Lett. 29, 23.

MÜLLER, W.H., NAEF, H. & GRAF, H.R. 2002: Geologische Entwicklung der Nordschweiz, Neotektonik und Langzeitszenarien Zürcher Weinland. Nagra Tech. Ber. NTB 99–08, Nagra, Wettingen.

NAESER, C.W. 1976: Fission-track dating. Open-File Rep. – U. S. Geol. Surv. 76–190.

NAESER, C.W., MCKEE, E.H., JOHNSON, N.M. & MACFADDEN, B.J. 1987: Confirmation of a late Oligocene-early Miocene age of the Deseadan Salla beds of Bolivia. J. Geol. 95, 825–828.

NAGRA 1990: Sondierbohrung Riniken. Untersuchungsbericht. Beiträge zur Geologie der Schweiz. Geotechnische Serie 74.

NAGRA 1991a: Sondierbohrung Leuggern. Untersuchungsbericht. Beiträge zur Geologie der Schweiz. Geotechnische Serie 75.

NAGRA 1991b: Sondierbohrung Kaisten. Untersuchungsbericht. Beiträge zur Geologie der Schweiz. Geotechnische Serie 83.

NAGRA 1993: Sondierbohrung Siblingen. Untersuchungsbericht. Beiträge zur Geologie der Schweiz. Geotechnische Serie 86.

NAGRA 2002: Projekt Opalinuston-Synthese der geowissenschaftlichen Untersuchungs-ergebnisse. Nagra Technical Report NTB 02–03, Nagra, Wettingen, Switzerland.

PAUL, W. 1955: Zur Morphogenese des Schwarzwaldes (I). Jahresheft geol. Landesamt Baden-Württ. 1, 395–427.

PRICE, P.B. & WALKER, R.M. 1962a: A new detector for heavy particle studies. Phys. Lett. 3, 113–115.

PRICE, P.B. & WALKER, R.M. 1962b: Observations of charged-particle tracks in solids. J. Appl. Phys. 33, 3400–3406.

SCHALTEGGER, U., ZWINGMANN, H., CLAUER, N., LARQUE, P. & STILLE, P. 1995: K–Ar dating of a Mesozoic hydrothermal activity in Carboniferous to Triassic clay minerals of northern Switzerland. Schweiz. Mineral. Petrogr. Mitt. 75, 163–176.

SCHEGG, R. & LEU, W. 1998: Analysis of erosion events and palaeogeothermal gradients in the North Alpine Foreland Basin of Switzerland. In: S.J. Düppenbecker and J.E. Iliffe (eds.): Basin Modelling: Practice and Progress. Geol. Soc. Spec. Publ. 141, 137–155.

SCHUMACHER, M.E. 2002: Upper Rhine Graben: Role of preexisting structures during rift evolution. Tectonics 21/1, 6, 1–17.

TAGAMI, T. & SHIMADA, C. 1996: Natural long-term annealing of the zircon fission track system around a granitic pluton. J. Geophys. Res. 101/B4, 8245–8255.

TAGAMI, T., GALBRAITH, R.F., YAMADA, R. & LASLETT, G.M. 1998: Revised annealing kinetics of fission tracks in zircon and geological implications. In: P. Van den Haute and F. De Corte (eds.): Advances in Fission Track Geochronology, Kluwer Academic Publishers, Dordrecht, 99–112.

THURY, M., GAUTSCHI, A., MAZUREK, M., MÜLLER, W.H., NAEF, H., PEARSON, F.J., VOMVORIS, S. & WILSON, W. 1994: Geology and Hydrology of the Crystalline Basement of Northern Switzerland. Nagra Tech. Ber. NTB 93–01, Nagra, Wettingen.

TIMAR-GENG, Z., FÜGENSCHUH, B., SCHALTEGGER, U. & WETZEL, A. 2004: The impact of the Jurassic hydrothermal activity on zircon fission track data from the southern Upper Rhine Graben area. Schweiz. Mineral. Petrogr. Mitt. 84, 257–269.

TIMAR-GENG, Z., FÜGENSCHUH, B., WETZEL, A. & DRESMANN, H. 2006: Low-temperature thermochronology of the flanks of the southern Upper Rhine Graben. Int. J. Earth Sci. 95, 685–702

TINGATE, P.R. & DUDDY, I.R. 2002: The thermal history of the eastern Officer Basin (South Australia): evidence from apatite fission track analysis and organic maturity data. Tectonophysics 349, 251–275.

WAGNER, G.A. & VAN DEN HAUTE, P. 1992: Fission track dating. Kluwer, Dordrecht, 285pp.

WETZEL, A., ALLENBACH, R. & ALLIA, V. 2003: Reactivated basement structures affecting the sedimentary facies in a tectonically "quiescent" epicontinental basin: an example from NW Switzerland. Sedimentary Geology 157/1–2, 153–172.

WIMMENAUER, W. & SCHREINER, A. 1990: Erläuterungen zu Blatt 8114, Feldberg. Geol. Karte Baden-Württ. 1:25 000, Stuttgart, 134 pp.

ZIEGLER, P.A. 1990: Geological Atlas of Western and Central Europe. Shell Internationale Petroleum Maatschappij – Geological Society Publishing House, 239 pp.

Manuscript received November 29, 2005
Revision accepted July 4, 2006

V. Summary and conclusions

by Zoltan Timar-Geng

The Upper Rhine Graben (URG) is part of a complex Cenozoic rift system that is located in the foreland of the Alps. The southern end of the URG is flanked by uplifted Variscan basement, exposed in the Black Forest and Vosges. The post-Variscan thermal evolution of the flanks of the southern URG and the neighbouring crystalline basement of northern Switzerland was evaluated by an extensive fission-track (FT) study.

The impact of the Jurassic hydrothermal activity on the interpretation of zircon FT data was elaborated by means of new zircon FT analyses on samples with known U/Pb crystallization ages (see Chapter II). FT central ages range from 162 Ma to 247 Ma. The analysed samples experienced substantial annealing prior to Cretaceous cooling that cannot be explained by burial alone. Instead, annealing is suggested to be associated with Jurassic hydrothermal activity, as also evidenced by vein mineralizations. Since samples entered the partial annealing zone (PAZ) from the lower temperature boundary and were only partially annealed, it can be presumed that a high density of α damage significantly lowered the thermal stability of the zircon fission tracks. Thus, it is suggested that circulating hydrothermal fluids with temperatures in the order of 200 – 250 °C were sufficient to give rise to the observed thermal anomaly. This has important implications for the interpretation of FT data in areas known as having been hydrothermally altered in the past. Analysis of FT data using simple assumptions such as a constant paleogeothermal gradient leads unavoidably to erroneous conclusions. Thus, interpretation of available FT ages from the Black Forest and Vosges as cooling ages is questionable. Particularly the gradients of age-elevation profiles do not correspond to input denudation rates.

FT ages of 28 outcrop samples collected along two E-W trending transects from the Black Forest and Vosges (Chapter III) cover the whole range of ages found by previous studies. Zircon FT central ages vary from 136 Ma to 312 Ma. Apatite FT ages range between 20 Ma and 83 Ma. Broad and/or bimodal track lengths distributions indicate a complex thermal history, which was determined by inverse modelling of FT parameters and tested against the observed dataset and independent geological constraints. It provided a comprehensive thermochronological record of the study area from the Lower Cretaceous to present, characterised by a compound cooling history with a transient heating event in the Upper Eocene. This heating phase is contemporaneous to the initial rifting stage of the URG and associated with increased volcanic activity.

One open question regarding the regional geology of the URG area is whether Cretaceous sediments were deposited and subsequently eroded completely or never existed. Interpreting the youngest cluster of zircon FT single-grain ages as dating the passage of a sample through the lower limit of the zircon FT PAZ, and interpolating the known Mesozoic sediment thicknesses from surrounding regions into the study area, it can be concluded that not even a significant

amount (kilometre-scale) of Upper Jurassic to Lower Cretaceous sedimentary sequence would have been sufficient to cause the observed very high paleotemperatures. Instead of cooling on account of tectonic uplift and denudation, the cessation of the Mesozoic hydrothermal activity is suggested as reason for the Cretaceous cooling below the lower limit of the zircon FT PAZ.

Based on modelling results and on a cautious estimation of the prevailing paleogeothermal gradient the total amount of denudation from the flanks of the URG since the Upper Eocene could be estimated. It amounts to 1.0 – 1.7 km for a paleogeothermal gradient of 60 °C/km and 1.3 to 2.2 km for a paleogeothermal gradient of 45 °C/km.

In addition to the samples from the Black Forest and Vosges, FT data from four boreholes, which penetrated the pre-Mesozoic basement of the neighbouring area of northern Switzerland, were also collected (Chapter IV). Zircon FT central ages and single-grain ages cluster around 250 Ma, thus it can be concluded that maximum palaeotemperatures did not exceed ~330 °C (i.e. temperatures for complete track loss) after late-Variscan consolidation of the crystalline basement. Apatite FT central ages range between 25 Ma and 87 Ma. Confined mean track lengths range between 9.3 μm and 11.6 μm suggesting substantial annealing of all samples. Inverse modelling techniques have been used to provide quantitative constraints on the low-temperature thermochronology of the area that are permitted by the measured data. The revealed thermal history is very similar to the one obtained for the southern URG area: Cretaceous cooling is followed by an Eocene heating event and subsequent cooling to present-day temperatures. Apparent differences to earlier FT modelling results can be explained by the different paleogeographic positions of the sample localities. The Eocene heating episode is contemporaneous to the initial rifting stage of the nearby URG. Reactivated crustal-scale faults of the Permo-Carboniferous Trough of northern Switzerland could have acted as major conduits for circulating hydrothermal fluids giving rise to the observed middle to late Eocene thermal anomaly.

In general it can be concluded that the southern URG was an area with repeatedly changing paleogeothermal gradients, and convective heat transport seems to have played an important role throughout its post-Variscan thermotectonic evolution. Thus, the available FT ages cannot be interpreted as cooling ages and no denudation rates based an age-elevation profiles can be derived. Only the thermal modelling approach can offer a meaningful interpretation of the existing dataset.

Appendix

Raw FT data

Appendix

In this appendix the raw FT data are presented, subdivided into three data sets according to the three main parts of the thesis.

1. Zircon FT data from the Black Forest and the Vosges with known crystallisation ages („SU"-Samples).

The interpretation of this data set is presented in Chapter II of the thesis.

Black Forest			Sample: SU 94-7
ζ = 113.49 ± 1.8			Dated mineral: zircon
Irrad. code : BS-12	Rho_d: 4.3117		Dosimeter glass: CN1
Grid unit: 60.4 μm^2	N_d: 1590		

Cryst	N_s	N_i	Area	Rho_s	Rho_i	Age [Ma]	σ	U [ppm]
1	57	8	9	104.857	14.717	172.01	65.14	135.85
2	45	6	9	82.781	11.038	180.94	78.82	101.88
3	30	7	20	24.834	5.795	104.01	43.77	53.49
4	47	5	24	32.423	3.449	225.98	106.51	31.84
5	71	5	16	73.469	5.174	338.39	156.89	47.76
6	63	5	9	115.894	9.198	301.14	140.2	84.9
7	136	13	24	93.819	8.968	251.01	73.25	82.78
8	66	7	12	91.06	9.658	226.65	90.35	89.15
9	82	9	24	56.567	6.209	219.15	77.23	57.31
10	79	6	9	145.327	11.038	314.35	133.45	101.88
11	64	7	9	117.734	12.877	219.9	87.79	118.86
12	87	7	12	120.033	9.658	297.13	117.07	89.15
13	69	7	10	114.238	11.589	236.77	94.18	106.98
14	75	11	12	103.477	15.177	164.7	53.4	140.09
15	78	7	12	107.616	9.658	267.02	105.65	89.15
16	42	3	12	57.947	4.139	333.74	199.7	38.21
17	34	3	9	62.546	5.519	271.49	163.71	50.94
18	58	11	9	106.696	20.235	127.73	42.18	186.79

Black Forest			Sample: SU 94-8
ζ = 113.49 ± 1.8			Dated mineral: zircon
Irrad. code : BS-12	Rho_d: 4.1992		Dosimeter glass: CN1
Grid unit: 60.4 μm^2	N_d: 1590		

Cryst	N_s	N_i	Area	Rho_s	Rho_i	Age [Ma]	σ	U [ppm]
1	45	4	12	62.086	5.519	262.65	137.26	52.31
2	142	18	30	78.366	9.934	185.29	46.68	94.15
3	36	5	15	39.735	5.519	169.32	80.97	52.31
4	30	5	12	41.391	6.898	141.41	68.44	65.38
5	80	14	12	110.375	19.316	134.74	39.24	183.07
6	31	5	10	51.325	8.278	146.07	70.53	78.46
7	33	6	12	45.53	8.278	129.74	57.71	78.46
8	44	4	9	80.942	7.358	256.92	134.39	69.74
9	49	3	10	81.126	4.967	377.9	225.04	47.08
10	45	5	12	62.086	6.898	210.97	99.65	65.38

11	33	4	12	45.53	5.519	193.65	102.68	52.31
12	74	4	12	102.097	5.519	426.41	219.25	52.31
13	41	4	10	67.881	6.623	239.73	125.78	62.77
14	70	10	12	96.578	13.797	164.68	55.89	130.77
15	62	13	12	85.541	17.936	112.65	34.53	170
16	60	5	12	82.781	6.898	279.78	130.49	65.38
17	31	6	9	57.027	11.038	121.95	54.51	104.61
18	42	5	12	57.947	6.898	197.11	93.43	65.38
19	33	4	12	45.53	5.519	193.65	102.68	52.31
20	44	6	12	60.706	8.278	172.41	75.21	78.46

Black Forest — Sample: SU 94-9

ζ = 113.49 $\pm$ 1.8 — Dated mineral: zircon

Irrad. code : BS-12 — Rho_d: 3.7492 — Dosimeter glass: CN1

Grid unit: 60.4 μm^2 — N_d: 1590

Cryst	N_s	N_i	Area	Rho_s	Rho_i	Age [Ma]	σ	U [ppm]
1	33	5	8	68.295	10.348	138.91	66.79	109.85
2	71	6	9	130.611	11.038	246.96	105.25	117.17
3	61	9	12	84.161	12.417	142.61	51.1	131.82
4	51	8	9	93.819	14.717	134.22	51.2	156.23
5	46	6	6	126.932	16.556	161.08	70.08	175.75
6	66	10	12	91.06	13.797	138.91	47.32	146.46
7	32	7	6	88.3	19.316	96.53	40.38	205.05
8	80	13	12	110.375	17.936	129.61	38.95	190.4
9	101	9	9	185.798	16.556	234.44	81.85	175.75
10	42	7	9	77.263	12.877	126.4	51.74	136.7
11	53	8	8	109.685	16.556	139.43	53.05	175.75
12	47	5	8	97.268	10.348	196.94	92.83	109.85
13	83	10	10	137.417	16.556	174.21	58.54	175.75
14	98	9	9	180.28	16.556	227.59	79.56	175.75
15	69	5	16	71.399	5.174	287.1	133.24	54.92
16	49	7	16	50.704	7.243	147.23	59.65	76.89
17	81	15	16	83.816	15.522	113.87	32.19	164.77
18	52	5	9	95.659	9.198	217.55	102.06	97.64
19	76	10	12	104.857	13.797	159.69	53.93	146.46
20	65	9	9	119.573	16.556	151.85	54.19	175.75

Black Forest — Sample: SU 94-12

ζ = 113.49 $\pm$ 1.8 — Dated mineral: zircon

Irrad. code : BS-12 — Rho_d: 4.5367 — Dosimeter glass: CN1

Grid unit: 60.4 μm^2 — N_d: 1590

Cryst	N_s	N_i	Area	Rho_s	Rho_i	Age [Ma]	σ	U [ppm]
1	70	14	8	144.868	28.974	127.45	37.5	254.18
2	54	5	9	99.338	9.198	272.2	127.5	80.69
3	47	7	9	86.461	12.877	170.57	69.29	112.97
4	67	8	8	138.659	16.556	212.07	79.58	145.25
5	28	4	6	77.263	11.038	177.73	95.15	96.83
6	53	4	8	109.685	8.278	332.38	172.63	72.62
7	52	4	6	143.488	11.038	326.27	169.57	96.83
8	51	7	6	140.728	19.316	184.88	74.72	169.45
9	40	6	6	110.375	16.556	169.38	74.32	145.25

Black Forest — Sample: SU 95-1
ζ = 113.49 ± 1.8 — Dated mineral: zircon
Irrad. code : BS-12 — Rho_d: 3.4679 — Dosimeter glass: CN1
Grid unit: 60.4 μm^2 — N_d: 1590

Cryst	N_s	N_i	Area	Rho_s	Rho_i	Age [Ma]	σ	U [ppm]
1	104	11	15	114.79	12.141	183.42	58.41	139.34
2	72	8	12	99.338	11.038	174.72	65.32	126.67
3	104	6	16	107.616	6.209	332.38	139.9	71.25
4	63	10	12	86.921	13.797	122.8	41.96	158.34
5	63	6	8	130.381	12.417	203.38	87.1	142.51
6	95	14	16	98.303	14.487	132.17	38.04	166.26
7	45	5	8	93.129	10.348	174.72	82.53	118.76
8	67	9	12	92.439	12.417	144.86	51.61	142.51
9	53	5	12	73.124	6.898	205.29	96.23	79.17
10	69	5	12	95.199	6.898	266	123.45	79.17
11	55	9	15	60.706	9.934	119.15	42.99	114.01
12	56	4	12	77.263	5.519	269.78	139.85	63.34
13	49	6	9	90.14	11.038	158.74	68.82	126.67
14	51	9	12	70.364	12.417	110.56	40.11	142.51
15	48	4	9	88.3	7.358	231.92	120.89	84.45
16	66	5	9	121.413	9.198	254.66	118.36	105.56
17	78	10	12	107.616	13.797	151.69	51.15	158.34
18	76	11	16	78.642	11.382	134.55	43.59	130.63
19	55	5	16	56.912	5.174	212.91	99.65	59.38
20	61	6	12	84.161	8.278	197.02	84.5	95.01

Black Forest — Sample: SU 96-6
ζ = 113.49 ± 1.8 — Dated mineral: zircon
Irrad. code : BS-17 — Rho_d: 3.4635 — Dosimeter glass: CN1
Grid unit: 60.4 μm^2 — N_d: 1605

Cryst	N_s	N_i	Area	Rho_s	Rho_i	Age [Ma]	σ	U [ppm]
1	50	6	9	91.979	11.038	161.73	70.04	126.84
2	59	8	8	122.103	16.556	143.34	54.17	190.25
3	198	14	25	131.126	9.272	272.13	75.69	106.54
4	70	9	12	96.578	12.417	151.08	53.68	142.69
5	62	8	12	85.541	11.038	150.54	56.73	126.84
6	31	3	6	85.541	8.278	199.95	121.05	95.13
7	55	5	6	151.766	13.797	212.64	99.52	158.54
8	99	11	12	136.589	15.177	174.5	55.7	174.4
9	34	4	4	140.728	16.556	164.93	87.32	190.25
10	83	5	10	137.417	8.278	318.26	146.86	95.13
11	62	6	8	128.311	12.417	199.95	85.69	142.69
12	40	3	4	165.563	12.417	256.86	153.95	142.69
13	74	10	9	136.13	18.396	143.82	48.64	211.39
14	60	9	6	165.563	24.834	129.71	46.52	285.38
15	82	7	15	90.508	7.726	226.21	89.33	88.78

Black Forest — Sample: SU 96-7
ζ = 113.49 ± 1.8 — Dated mineral: zircon
Irrad. code : BS-12 — Rho_d: 3.6367 — Dosimeter glass: CN1

Grid unit: 60.4 μm^2 N_d: 1590

Cryst	N_s	N_i	Area	Rho_s	Rho_i	Age [Ma]	σ	U [ppm]
1	50	3	10	82.781	4.967	335.08	199.43	54.36
2	36	7	12	49.669	9.658	105.27	43.6	105.7
3	43	6	12	59.327	8.278	146.22	63.87	90.6
4	75	9	12	103.477	12.417	169.72	60.08	135.89
5	61	6	12	84.161	8.278	206.46	88.55	90.6
6	61	5	12	84.161	6.898	246.97	115.12	75.5
7	65	7	10	107.616	11.589	188.83	75.33	126.83
8	55	5	12	75.883	6.898	223.1	104.42	75.5
9	107	12	12	147.627	16.556	181.43	55.5	181.19
10	64	8	12	88.3	11.038	163.01	61.32	120.79
11	82	5	12	113.135	6.898	329.85	152.26	75.5
12	64	10	12	88.3	13.797	130.74	44.62	150.99
13	99	11	10	163.907	18.212	183.1	58.45	199.31
14	69	5	12	95.199	6.898	278.67	129.33	75.5
15	75	6	12	103.477	8.278	252.93	107.57	90.6
16	100	8	12	137.969	11.038	252.93	93.23	120.79
17	28	3	9	51.508	5.519	189.79	115.43	60.4
18	75	7	12	103.477	9.658	217.4	86.16	105.7
19	57	4	8	117.964	8.278	287.56	148.98	90.6
20	49	6	12	67.605	8.278	166.37	72.13	90.6

Vosges — Sample: SU 93-7

ζ = 113.49 ± 1.8 — Dated mineral: zircon

Irrad. code : BS-17 Rho_d: 3.3982 — Dosimeter glass: CN1

Grid unit: 60.4 μm^2 N_d: 1605

Cryst	N_s	N_i	Area	Rho_s	Rho_i	Age [Ma]	σ	U [ppm]
1	125	11	12	172.461	15.177	215.48	68.07	177.75
2	75	8	6	206.954	22.075	178.29	66.52	258.54
3	90	7	8	186.258	14.487	243.28	95.73	169.67
4	74	9	9	136.13	16.556	156.63	55.49	193.91
5	62	6	8	128.311	12.417	196.24	84.1	145.43
6	73	5	6	201.435	13.797	275.56	127.64	161.59
7	42	4	8	86.921	8.278	199.36	104.48	96.95
8	43	5	6	118.653	13.797	163.74	77.52	161.59
9	79	7	8	163.493	14.487	214.03	84.64	169.67
10	89	11	8	184.189	22.765	154.16	49.48	266.62
11	77	7	9	141.648	12.877	208.7	82.62	150.82
12	107	10	9	196.836	18.396	203.1	67.43	215.45

Vosges — Sample: SU 93-11

ζ = 113.49 ± 1.8 — Dated mineral: zircon

Irrad. code : BS-12 Rho_d: 3.9179 — Dosimeter glass: CN1

Grid unit: 60.4 μm^2 N_d: 1590

Cryst	N_s	N_i	Area	Rho_s	Rho_i	Age [Ma]	σ	U [ppm]
1	31	3	9	57.027	5.519	225.73	136.65	56.06
2	58	4	12	80.022	5.519	314.56	162.88	56.06
3	24	4	9	44.15	7.358	132.03	71.41	74.75
4	63	6	12	86.921	8.278	229.31	98.21	84.09
5	32	3	9	58.867	5.519	232.88	140.79	56.06
6	38	5	12	52.428	6.898	166.79	79.5	70.08

7	40	6	12	55.188	8.278	146.54	64.3	84.09
8	50	6	9	91.979	11.038	182.66	79.1	112.12
9	56	3	9	103.017	5.519	402.19	238.64	56.06
10	63	6	12	86.921	8.278	229.31	98.21	84.09
11	54	4	12	74.503	5.519	293.36	152.26	56.06
12	42	4	9	77.263	7.358	229.31	120.18	74.75
13	33	2	9	60.706	3.679	356.77	260.02	37.37
14	33	3	9	60.706	5.519	240.03	144.92	56.06
15	71	8	12	97.958	11.038	194.35	72.71	112.12
16	41	3	9	75.423	5.519	296.9	177.79	56.06
17	40	8	12	55.188	11.038	110.21	42.81	112.12
18	89	9	25	58.94	5.96	216.19	75.89	60.55
19	75	8	16	77.608	8.278	205.13	76.54	84.09
20	60	4	12	82.781	5.519	325.14	168.18	56.06

Vosges — Sample: SU 93-12

ζ = 113.49 $\pm$ 1.8 — Dated mineral: zircon

Irrad. code : BS-12 Rho_d: 4.4804 — Dosimeter glass: CN1

Grid unit: 60.4 μm^2 N_d: 1590

Cryst	N_s	N_i	Area	Rho_s	Rho_i	Age [Ma]	σ	U [ppm]
1	95	10	9	174.761	18.396	237.11	79.14	163.41
2	80	5	6	220.751	13.797	394.47	182.22	122.56
3	115	16	9	211.553	29.433	180.19	48.38	261.46
4	87	11	9	160.044	20.235	198.01	63.64	179.75
5	137	12	12	189.018	16.556	283.91	85.89	147.07
6	76	10	6	209.713	27.594	190.38	64.29	245.12
7	99	9	8	204.884	18.626	273.77	95.66	165.46
8	56	7	6	154.525	19.316	200.25	80.5	171.58
9	154	14	18	141.648	12.877	273.77	76.85	114.39
10	102	9	9	187.638	16.556	281.89	98.38	147.07
11	67	7	9	123.252	12.877	238.86	95.15	114.39
12	71	8	9	130.611	14.717	221.78	82.97	130.73
13	97	6	10	160.596	9.934	398.45	168.04	88.24
14	114	9	9	209.713	16.556	314.25	109.21	147.07
15	113	11	10	187.086	18.212	256.02	81.22	161.78
16	122	17	12	168.322	23.455	179.92	46.88	208.35
17	82	7	8	169.702	14.487	291.15	114.97	128.69
18	83	8	9	152.686	14.717	258.52	96.01	130.73
19	120	13	12	165.563	17.936	230.51	67.65	159.33
20	89	10	12	122.792	13.797	222.39	74.47	122.56

Vosges — Sample: SU 94-3

ζ = 113.49 $\pm$ 1.8 — Dated mineral: zircon

Irrad. code : BS-12 Rho_d: 3.7901 — Dosimeter glass: CN1

Grid unit: 60.4

μm^2 N_d: 1605

Cryst	N_s	N_i	Area	Rho_s	Rho_i	Age [Ma]	σ	U [ppm]
1	87	14	16	90.025	14.487	132.28	38.29	152.13
2	80	14	9	147.167	25.754	121.74	35.45	270.45

Vosges			Sample: SU 94-5					
ζ = 113.49 ± 1.8			Dated mineral: zircon					
Irrad. code : BS-12	Rho_d: 3.8054		Dosimeter glass: CN1					
Grid unit: 60.4 μm^2	N_d: 1590							
Cryst	N_s	N_i	Area	Rho_s	Rho_i	Age [Ma]	σ	U [ppm]
1	97	7	18	89.22	6.439	292.49	114.8	67.34
2	56	4	9	103.017	7.358	295.44	153.15	76.96
3	36	4	9	66.225	7.358	191.47	101.07	76.96
4	54	8	16	55.877	8.278	144.13	54.77	86.58
5	26	2	8	53.808	4.139	274.78	201.8	43.29
6	78	6	9	143.488	11.038	274.78	116.7	115.44
7	27	4	8	55.877	8.278	144.13	77.34	86.58
8	71	7	10	117.55	11.589	215.38	85.57	121.21
9	48	4	9	88.3	7.358	254.05	132.43	76.96
10	47	4	8	97.268	8.278	248.86	129.83	86.58

Vosges			Sample: SU 95-5					
ζ = 113.49 ± 1.8			Dated mineral: zircon					
Irrad. code : BS-12	Rho_d: 4.8179		Dosimeter glass: CN1					
Grid unit: 60.4 μm^2	N_d: 1590							
Cryst	N_s	N_i	Area	Rho_s	Rho_i	Age [Ma]	σ	U [ppm]
1	62	5	9	114.054	9.198	330.39	153.91	75.98
2	31	6	6	85.541	16.556	139.73	62.46	136.77
3	103	18	9	189.478	33.113	154.57	39.75	273.54
4	34	11	8	70.364	22.765	83.95	29.23	188.06
5	70	13	9	128.771	23.915	145.56	44.17	197.56
6	56	4	8	115.894	8.278	371.82	192.75	68.38
7	80	19	9	147.167	34.952	114.1	29.31	288.74
8	58	10	8	120.033	20.695	156.65	53.84	170.96
9	46	8	6	126.932	22.075	155.31	59.67	182.36
10	84	16	12	115.894	22.075	141.96	38.95	182.36
11	52	12	12	71.744	16.556	117.39	37.76	136.77
12	65	9	9	119.573	16.556	194.49	69.41	136.77
13	65	10	10	107.616	16.556	175.3	59.77	136.77
14	54	4	6	149.007	11.038	358.9	186.28	91.18
15	52	5	9	95.659	9.198	278.24	130.54	75.98
16	62	11	8	128.311	22.765	152.28	50.03	188.06

Vosges			Sample: SU 95-15					
ζ = 113.49 ± 1.8			Dated mineral: zircon					
Irrad. code : BS-12	Rho_d: 4.7054		Dosimeter glass: CN1					
Grid unit: 60.4 μm^2	N_d: 1590							
Cryst	N_s	N_i	Area	Rho_s	Rho_i	Age [Ma]	σ	U [ppm]
1	73	12	12	100.717	16.556	160.42	50.2	140.04
2	112	12	15	123.62	13.245	244.51	74.62	112.03
3	133	19	14	157.285	22.469	184.25	45.52	190.05
4	82	8	12	113.135	11.038	268.03	99.6	93.36
5	74	8	12	102.097	11.038	242.37	90.49	93.36
6	50	5	12	68.985	6.898	261.63	122.96	58.35
7	87	11	12	120.033	15.177	207.79	66.78	128.37
8	87	12	12	120.033	16.556	190.73	59.01	140.04

9	57	7	12	78.642	9.658	213.83	85.88	81.69
10	80	11	12	110.375	15.177	191.32	61.78	128.37
11	66	8	12	91.06	11.038	216.6	81.34	93.36
12	45	5	12	62.086	6.898	235.94	111.44	58.35
13	87	7	12	120.033	9.658	323.59	127.49	81.69
14	86	12	12	118.653	16.556	188.57	58.38	140.04
15	67	5	12	92.439	6.898	348.21	161.76	58.35
16	70	10	12	96.578	13.797	184.25	62.53	116.7
17	76	9	12	104.857	12.417	221.62	78.4	105.03
18	77	7	12	106.236	9.658	287.21	113.7	81.69
19	73	13	12	100.717	17.936	148.22	44.83	151.71
20	74	7	12	102.097	9.658	276.26	109.55	81.69

Vosges — Sample: SU 95-17

ζ = 113.49 $\pm$ 1.8 — Dated mineral: zircon

Irrad. code : BS-17 — Rho_d: 3.6595 — Dosimeter glass: CN1

Grid unit: 60.4 μm^2 — N_d: 1605

Cryst	N_s	N_i	Area	Rho_s	Rho_i	Age [Ma]	σ	U [ppm]
1	147	18	25	97.351	11.921	167.4	42.09	129.65
2	186	25	24	128.311	17.246	152.68	32.83	187.57
3	75	7	12	103.477	9.658	218.74	86.69	105.04
4	156	26	25	103.311	17.219	123.41	26.39	187.27
5	66	11	12	91.06	15.177	123.41	40.36	165.06
6	128	12	16	132.45	12.417	217.78	66.06	135.05
7	84	13	12	115.894	17.936	132.8	39.77	195.07
8	107	10	10	177.152	16.556	218.45	72.52	180.06
9	102	12	15	112.583	13.245	174.14	53.39	144.05
10	123	17	16	127.276	17.591	148.52	38.68	191.32
11	122	10	16	126.242	10.348	248.49	82.07	112.54
12	115	15	16	118.998	15.522	157.27	43.42	168.81
13	76	6	12	104.857	8.278	257.81	109.59	90.03
14	88	8	12	121.413	11.038	224.47	83.16	120.04
15	143	11	16	147.972	11.382	264.46	83.12	123.79
16	168	13	16	173.841	13.452	262.92	76.09	146.3
17	75	8	9	137.969	14.717	191.8	71.56	160.06
18	105	14	16	108.651	14.487	153.89	44.02	157.56
19	65	7	9	119.573	12.877	190	75.79	140.05
20	110	17	16	113.825	17.591	132.99	34.88	191.32

Vosges — Sample: SU 95-18

ζ = 113.49 $\pm$ 1.8 — Dated mineral: zircon

Irrad. code : BS-17 — Rho_d: 3.8554 — Dosimeter glass: CN1

Grid unit: 60.4 μm^2 — N_d: 1605

Cryst	N_s	N_i	Area	Rho_s	Rho_i	Age [Ma]	σ	U [ppm]
1	55	7	9	101.177	12.877	169.64	68.26	132.93
2	138	23	30	76.159	12.693	129.95	29.52	131.03
3	99	10	15	109.272	11.038	213.03	70.97	113.94
4	84	12	14	99.338	14.191	151.35	46.92	146.5
5	73	7	12	100.717	9.658	224.21	88.96	99.7
6	47	5	8	97.268	10.348	202.44	95.41	106.82
7	78	10	20	64.57	8.278	168.42	56.79	85.46
8	124	18	25	82.119	11.921	148.98	37.83	123.06

9	109	12	18	100.258	11.038	195.72	59.81	113.94
10	92	12	12	126.932	16.556	165.58	51.06	170.91
11	103	10	16	106.581	10.348	221.49	73.65	106.82
12	48	6	9	88.3	11.038	172.69	74.95	113.94
13	95	9	9	174.761	16.556	226.89	79.41	170.91
14	165	11	20	136.589	9.106	320.08	100.12	94
15	157	15	16	162.459	15.522	225.01	61.17	160.23
16	46	4	9	84.621	7.358	246.81	128.86	75.96
17	61	6	12	84.161	8.278	218.67	93.78	85.46
18	78	9	16	80.712	9.313	186.87	66.02	96.14
19	193	15	36	88.76	6.898	275.52	74.3	71.21
20	62	5	12	85.541	6.898	265.73	123.79	71.21

Vosges — Sample: SU 95-1
ζ = 113.49 $\pm$ 1.8 — Dated mineral: zircon
Irrad. code : BS-12 — Rho_d: 3.6292 — Dosimeter glass: CN1
Grid unit: 60.4 μm^2 — N_d: 1590

Cryst	N_s	N_i	Area	Rho_s	Rho_i	Age [Ma]	σ	U [ppm]
1	175	28	25	115.894	18.543	127.44	26.21	203.35
2	202	21	20	167.219	17.384	195.11	45.11	190.64
3	118	18	15	130.243	19.868	133.61	34.04	217.88
4	133	10	16	137.624	10.348	268.24	88.32	113.48
5	158	13	16	163.493	13.452	245.56	71.23	147.52
6	150	18	15	165.563	19.868	169.37	42.55	217.88
7	172	13	20	142.384	10.762	266.87	77.17	118.02
8	197	19	18	181.199	17.476	210.07	50.85	191.65
9	120	10	16	124.172	10.348	242.51	80.14	113.48
10	139	20	16	143.833	20.695	141.56	34.11	226.96
11	163	16	16	168.667	16.556	206.46	54.43	181.57
12	159	12	16	164.528	12.417	267.25	80.4	136.17
13	155	19	16	160.389	19.661	165.85	40.61	215.61
14	148	17	16	153.146	17.591	176.84	45.59	192.91
15	150	12	16	155.215	12.417	252.42	76.09	136.17
16	169	18	16	174.876	18.626	190.51	47.57	204.26
17	206	12	16	213.162	12.417	344.18	102.72	136.17
18	140	19	16	144.868	19.661	149.99	36.94	215.61
19	102	10	16	105.546	10.348	206.71	68.77	113.48

Vosges — Sample: SU 95-20
ζ = 113.49 $\pm$ 1.8 — Dated mineral: zircon
Irrad. code : BS-17 — Rho_d: 3.3329 — Dosimeter glass: CN1
Grid unit: 60.4 μm^2 — N_d: 1605

Cryst	N_s	N_i	Area	Rho_s	Rho_i	Age [Ma]	σ	U [ppm]
1	68	10	6	187.638	27.594	127.34	43.29	329.51
2	199	18	25	131.788	11.921	205.77	51.01	142.35

Vosges — Sample: SU 96-1
ζ = 113.49 $\pm$ 1.8 — Dated mineral: zircon
Irrad. code : BS-17 — Rho_d: 3.5289 — Dosimeter glass: CN1
Grid unit: 60.4 μm^2 — N_d: 1605

Cryst	N_s	N_i	Area	Rho_s	Rho_i	Age [Ma]	σ	U [ppm]
1	74	7	8	153.146	14.487	208.29	82.6	163.39
2	122	17	8	252.483	35.182	142.13	37.03	396.79
3	34	5	4	140.728	20.695	134.75	64.66	233.41
4	35	3	6	96.578	8.278	229.49	138.22	93.36
5	104	13	12	143.488	17.936	158.24	46.78	202.29
6	76	10	9	139.809	18.396	150.42	50.79	207.47
7	148	14	16	153.146	14.487	208.29	58.57	163.39
8	46	5	6	126.932	13.797	181.64	85.7	155.61
9	94	9	8	194.536	18.626	205.83	72.08	210.07

Vosges — Sample: SU 96-2

ζ = 113.49 ± 1.8 — Dated mineral: zircon

Irrad. code : BS-17 — Rho_d: 3.7248 — Dosimeter glass: CN1

Grid unit: 60.4 μm^2 — N_d: 1605

Cryst	N_s	N_i	Area	Rho_s	Rho_i	Age [Ma]	σ	U [ppm]
1	93	8	12	128.311	11.038	241.14	89.13	117.94
2	111	12	10	183.775	19.868	192.61	58.81	212.29
3	95	12	9	174.761	22.075	165.19	50.85	235.87
4	77	10	9	141.648	18.396	160.73	54.24	196.56
5	165	13	25	109.272	8.609	262.84	76.11	91.99
6	41	7	9	75.423	12.877	122.63	50.28	137.59
7	84	6	12	115.894	8.278	289.32	122.56	88.45
8	111	16	12	153.146	22.075	144.99	39.01	235.87
9	109	8	9	200.515	14.717	281.74	103.54	157.25
10	78	7	12	107.616	9.658	231.32	91.53	103.2
11	180	18	15	198.675	19.868	207.97	51.78	212.29
12	70	6	12	96.578	8.278	241.99	103.19	88.45
13	108	10	12	149.007	13.797	224.32	74.45	147.42
14	139	15	16	143.833	15.522	192.95	52.75	165.85
15	86	9	12	118.653	12.417	198.87	69.92	132.68
16	135	12	12	186.258	16.556	233.5	70.68	176.91
17	58	5	10	96.026	8.278	240.63	112.38	88.45
18	174	14	24	120.033	9.658	257.48	71.93	103.2

Vosges — Sample: SU 96-4

ζ = 113.49 ± 1.8 — Dated mineral: zircon

Irrad. code : BS-12 — Rho_d: 4.4804 — Dosimeter glass: CN1

Grid unit: 60.4 μm^2 — N_d: 1590

Cryst	N_s	N_i	Area	Rho_s	Rho_i	Age [Ma]	σ	U [ppm]
1	29	5	6	80.022	13.797	145.8	70.73	122.56
2	40	8	6	110.375	22.075	125.88	48.9	196.1
3	74	5	12	102.097	6.898	365.7	169.33	61.28
4	52	4	8	107.616	8.278	322.32	167.52	73.54
5	90	6	12	124.172	8.278	370.51	156.61	73.54
6	44	9	8	91.06	18.626	123.11	45.19	165.46
7	69	4	9	126.932	7.358	424.29	218.57	65.37
8	56	5	9	103.017	9.198	278.64	130.32	81.71
9	76	11	18	69.904	10.118	173.31	56.14	89.88
10	78	7	9	143.488	12.877	277.25	109.7	114.39
11	83	14	9	152.686	25.754	148.99	43.27	228.78

12	96	8	9	176.6	14.717	298.09	110.05	130.73
13	78	7	9	143.488	12.877	277.25	109.7	114.39
14	49	5	9	90.14	9.198	244.46	115	81.71
15	88	8	12	121.413	11.038	273.77	101.42	98.05
16	91	9	12	125.552	12.417	252.07	88.4	110.3
17	136	14	16	140.728	14.487	242.36	68.41	128.69
18	105	12	21	82.781	9.461	218.71	66.96	84.04
19	170	11	28	100.52	6.504	381.41	119.2	57.78

Vosges — Sample: SU 96-5

ζ = 113.49 $\pm$ 1.8 — Dated mineral: zircon

Irrad. code : BS-12 — Rho_d: 4.8742 — Dosimeter glass: CN1

Grid unit: 60.4 μm^2 — N_d: 1590

Cryst	N_s	N_i	Area	Rho_s	Rho_i	Age [Ma]	σ	U [ppm]
1	56	8	12	77.263	11.038	190.76	72.32	90.13
2	59	11	10	97.682	18.212	146.67	48.37	148.71
3	34	5	8	70.364	10.348	185.39	88.97	84.49
4	76	8	10	125.828	13.245	257.54	96.03	108.15
5	59	8	10	97.682	13.245	200.82	75.9	108.15
6	77	12	12	106.236	16.556	175.08	54.58	135.19
7	45	6	10	74.503	9.934	204.17	88.94	81.11
8	32	4	12	44.15	5.519	217.56	115.56	45.06
9	58	6	12	80.022	8.278	261.97	112.61	67.59
10	21	5	12	28.974	6.898	115.13	57.39	56.33
11	30	4	8	62.086	8.278	204.17	108.85	67.59
12	59	8	12	81.402	11.038	200.82	75.9	90.13
13	30	3	9	55.188	5.519	270.82	164.18	45.06
14	35	5	10	57.947	8.278	190.76	91.38	67.59
15	43	5	10	71.192	8.278	233.58	110.58	67.59
16	47	7	8	97.268	14.487	183.08	74.37	118.29
17	35	4	8	72.434	8.278	237.58	125.59	67.59
18	62	6	9	114.054	11.038	279.65	119.85	90.13
19	41	5	8	84.851	10.348	222.9	105.8	84.49
20	36	10	12	49.669	13.797	98.81	35.44	112.66

Vosges — Sample: SU 97-2

ζ = 113.49 $\pm$ 1.8 — Dated mineral: zircon

Irrad. code : BS-12 — Rho_d: 3.8617 — Dosimeter glass: CN1

Grid unit: 60.4 μm^2 — N_d: 1590

Cryst	N_s	N_i	Area	Rho_s	Rho_i	Age [Ma]	σ	U [ppm]
1	41	4	8	84.851	8.278	220.79	115.84	85.32
2	36	3	12	49.669	4.139	257.74	155.07	42.66
3	52	4	12	71.744	5.519	278.76	144.88	56.88
4	51	11	12	70.364	15.177	100.81	33.65	156.42
5	28	3	9	51.508	5.519	201.35	122.46	56.88
6	48	5	9	88.3	9.198	207.01	97.47	94.8
7	49	6	9	90.14	11.038	176.52	76.53	113.76
8	29	3	12	40.011	4.139	208.42	126.55	42.66
9	51	7	8	105.546	14.487	157.71	63.74	149.31
10	40	3	9	73.584	5.519	285.75	171.26	56.88
11	39	3	12	53.808	4.139	278.76	167.22	42.66
12	68	8	10	112.583	13.245	183.62	68.85	136.51

13	74	8	9	136.13	14.717	199.58	74.51	151.68
14	48	3	12	66.225	4.139	341.41	203.43	42.66
15	53	6	9	97.498	11.038	190.72	82.34	113.76
16	51	9	12	70.364	12.417	122.99	44.62	127.98
17	65	8	12	89.68	11.038	175.63	66.01	113.76
18	34	3	9	62.546	5.519	243.69	146.95	56.88
19	60	6	9	110.375	11.038	215.49	92.49	113.76
20	52	7	8	107.616	14.487	160.76	64.9	149.31

2. Zircon and apatite FT data from outcrop samples collected along two EW transects in the Black Forest and the Vosges

The interpretation of the data is given in Chapter III of the thesis.

Black Forest		Sample: ZTG-0-06
ζ = 345.69 ± 8.75		Dated mineral: apatite
Irrad. code: BS-19	Rho_d: 8.1934	Dosimeter glass: CN5
Grid unit: 63.03	N_d: 3578	

Cryst	N_s	N_i	Area	Rho_s	Rho_i	Age [Ma]	σ	U [ppm]
1	15	55	25	9.519	34.904	38.51	11.28	51.84
2	56	124	42	21.154	46.841	63.64	10.43	69.57
3	8	47	16	7.933	46.605	24.06	9.23	69.22
4	61	161	50	19.356	51.087	53.43	8.2	75.88
5	26	93	36	11.458	40.986	39.47	8.84	60.88
6	25	52	28	14.166	29.464	67.73	16.61	43.76
7	34	88	21	25.687	66.484	54.49	11.13	98.75
8	15	25	16	14.874	24.79	84.42	27.69	36.82
9	60	136	42	22.665	51.374	62.18	9.82	76.31
10	10	11	16	9.916	10.908	127.48	55.83	16.2
11	39	76	20	30.938	60.289	72.27	14.4	89.55
12	17	120	36	7.492	52.885	20.03	5.23	78.55
13	108	332	60	28.558	87.789	45.9	5.27	130.4
14	36	63	32	17.849	31.235	80.42	16.98	46.39
15	25	104	50	7.933	33	33.95	7.63	49.02
16	44	82	36	19.391	36.138	75.55	14.3	53.68
17	44	103	36	19.391	45.393	60.22	11	67.42
18	56	127	49	18.132	41.121	62.15	10.15	61.08
19	78	144	36	34.375	63.462	76.26	10.97	94.26
20	30	141	36	13.221	62.14	30.06	6.11	92.3

Confined track lengths:

9.0687	8.7403	12.3019		10.3503		14.6454			
14.1041		11.8933		14.197	9.9958		9.0332		
9.6906		12.6798		6.4961	6.785		11.1477		
9.3647	11.4515		11.775	13.2192		4.7144			
10.0748		11.874	8.6834	13.6023		11.5074			
12.2904		13.4263		13.3648		6.7906		15.4984	
9.3243	14.4737		14.6885		12.5014			14.4081	
13.3443		13.0576		9.5047	11.094		13.6798		
15.3314		14.5063		9.9958	12.7873			11.1035	

11.1178	10.4284	11.6786	9.3473	11.9643
12.6358	10.43	9.774	13.5842	14.9675
12.1187	10.5001	6.0787	14.1224	9.7518
10.4616	9.3311	12.6298	8.9226	12.3618
6.637	7.1659	12.5398	13.6741	13.0698
5.032	11.6817	12.2556	10.5524	7.9247
9.851	12.1543	10.9184	9.8027	12.0149
12.6612	13.2506	14.5283	13.8333	10.5418
8.8177	8.9408	10.179	9.6291	10.6954
13.5324	10.6439	13.8934	9.5789	12.6044
9.5688	13.6148	9.445	12.1397	11.2293

Black Forest		Sample: ZTG-0-07
ζ = 345.69 $\pm$ 8.75		Dated mineral: apatite
Irrad. code: BS-19	Rho_d: 8.8388	Dosimeter glass: CN5
Grid unit: 63.03	N_d: 3578	

Cryst	N_s	N_i	Area	Rho_s	Rho_i	Age [Ma]	σ	U [ppm]
1	21	28	25	13.327	17.769	113.57	32.97	24.47
2	4	12	16	3.966	11.899	50.72	29.33	16.38
3	8	29	25	5.077	18.404	42.01	16.82	25.34
4	9	18	25	5.712	11.423	75.94	31.09	15.73
5	12	82	25	7.615	52.039	22.32	6.93	71.65
6	8	50	36	3.526	22.035	24.4	9.32	30.34
7	10	31	24	6.611	20.493	49.09	17.92	28.22
8	16	47	60	4.231	12.428	51.8	15.08	17.11
9	5	21	16	4.958	20.823	36.27	18.08	28.67
10	3	17	25	1.904	10.789	26.9	16.87	14.85
11	8	20	25	5.077	12.692	60.82	25.51	17.48
12	33	81	60	8.726	21.418	61.94	12.93	29.49
13	13	20	25	8.25	12.692	98.55	35.24	17.48
14	12	67	50	3.808	21.26	27.3	8.6	29.27
15	11	42	30	5.817	22.212	39.89	13.56	30.58
16	50	112	60	13.221	29.616	67.84	11.72	40.78
17	33	95	80	6.545	18.84	52.85	10.8	25.94
18	17	42	36	7.492	18.51	61.54	17.79	25.49
19	24	48	60	6.346	12.692	75.94	19.12	17.48
20	12	24	50	3.808	7.615	75.94	26.95	10.49

Confined track lengths:

11.3491	15.8793	9.0063	13.716	11.1527
12.8624	8.7087	9.0209	12.1477	10.2317
13.75	11.8196	13.8157	13.8735	13.1165
7.4403	6.9438	6.9438	11.7816	10.9062
5.2792	8.5556	8.1069	10.3819	16.0382
12.7769	13.1655	13.8171	7.2426	14.0413
10.286	11.059	7.7473	11.036	8.8719
13.0532	9.8938	4.6898	11.5989	8.8674
5.6527	14.4279	11.0032	5.2433	11.3372
13.6035	7.4968	9.5533	8.8349	10.5472
12.3729	9.3276	4.3035	11.5737	10.5416
9.203	10.9242	8.8647	11.762	13.3528
12.194	9.8328	12.4938	8.4423	12.4757

7.4311	9.5533	13.0677	9.4669	12.4719
4.0864	8.5479	12.1076	8.8033	14.0206
9.0635	8.4347	14.4964	6.8673	15.1908
6.6127	15.7827	11.5565	13.8094	14.0164
8.3713	8.2349	7.8143	12.1617	5.7149
9.9674	7.5081	11.1375	10.3883	8.8881
7.0731	6.9319	14.9473	14.3753	11.9002

Black Forest — Sample: ZTG-0-08

ζ = 345.69 ± 8.75 — Dated mineral: apatite

Irrad. code: BS-19 — Rho_d: 7.548 — Dosimeter glass: CN5

Grid unit: 63.03 — N_d: 3578

Cryst	N_s	N_i	Area	Rho_s	Rho_i	Age [Ma]	σ	U [ppm]
1	22	29	24	14.543	19.171	98.22	27.93	30.91
2	15	25	25	9.519	15.865	77.81	25.52	25.58
3	20	47	36	8.814	20.713	55.28	14.85	33.4
4	36	50	28	20.398	28.331	93.26	20.58	45.68
5	18	23	24	11.899	15.204	101.3	32.03	24.51
6	37	59	24	24.459	39.003	81.3	17.23	62.89
7	66	105	48	21.815	34.706	81.49	13.04	55.96
8	98	142	100	15.548	22.529	89.42	12.05	36.32
9	46	78	100	7.298	12.375	76.48	14.41	19.95
10	48	100	80	9.519	19.832	62.32	11.11	31.98
11	11	37	25	6.981	23.481	38.67	13.33	37.86
12	85	151	100	13.486	23.957	73.02	10.15	38.63
13	42	59	70	9.519	13.372	92.21	18.82	21.56
14	24	44	36	10.577	19.391	70.77	18.09	31.27
15	16	18	16	15.865	17.849	114.94	39.64	28.78
16	36	36	36	15.865	15.865	129.16	30.69	25.58
17	30	51	49	9.714	16.513	76.29	17.71	26.62
18	16	43	40	6.346	17.055	48.36	14.24	27.5
19	48	76	70	10.879	17.225	81.88	15.3	27.77
20	113	156	64	28.012	38.672	93.82	11.93	62.35

Confined track lengths:

12.9452	8.2555	15.4239	12.7112	10.7181
10.6246	13.3392	11.679	13.9867	13.4249
13.9671	14.1549	13.187	9.0585	13.9101
14.0874	15.5428	11.9091	11.0524	12.0807
14.7115	9.3151	11.7511	7.2138	13.0801
10.2502	14.4507	12.6889	13.8825	8.822
9.5876	13.1698	9.8718	8.3467	13.4212
13.566	9.8517	6.3219	9.3351	14.7403
14.3795	15.8298	9.7433	10.4718	13.0879
14.6454	12.8469	11.9997	12.8829	15.2251
9.2938	15.151	10.4157	9.4159	12.5458
9.7762	11.416	11.1254	12.99	13.0266
9.5384	12.8262	12.2751	11.6574	15.1978
8.0109	12.0578	10.8731	9.7719	9.2061
12.9156	15.0259	14.4711	9.0377	13.3344
14.1657	12.3096	7.9482	13.9324	6.2123
9.6065	10.0528	10.3862	8.9178	12.3851

7.3432	10.6538	13.566	12.0531	10.3004
8.258	13.6435	8.8068	11.4711	9.3795
14.3491	13.3851	11.5074	12.462	10.9112

Black Forest — Sample: ZTG-0-09

ζ = 345.69 ± 8.75 — Dated mineral: apatite

Irrad. code: BS-19 — Rho_d: 9.1615 — Dosimeter glass: CN5

Grid unit: 63.03 — N_d: 3578

Cryst	N_s	N_i	Area	Rho_s	Rho_i	Age [Ma]	σ	U [ppm]
1	23	11	16	22.807	10.908	322.88	118.77	14.49
2	10	17	25	6.346	10.789	92.48	36.96	14.33
3	19	26	50	6.029	8.25	114.69	34.79	10.96
4	13	12	25	8.25	7.615	169.31	67.97	10.12
5	11	15	36	4.848	6.611	115.09	45.82	8.78
6	13	13	36	5.729	5.729	156.44	61.54	7.61
7	13	9	30	6.875	4.76	224.77	97.7	6.32
8	5	13	25	3.173	8.25	60.62	31.95	10.96
9	8	16	36	3.526	7.051	78.69	34.16	9.37
10	135	434	100	21.418	68.856	49.07	5.06	91.47
11	9	25	49	2.914	8.095	56.76	22.13	10.75
12	3	20	36	1.322	8.814	23.71	14.7	11.71
13	4	17	36	1.763	7.492	37.15	20.68	9.95
14	6	8	50	1.904	2.538	117.68	63.66	3.37
15	6	30	80	1.19	5.95	31.59	14.16	7.9
16	14	24	49	4.533	7.771	91.72	30.97	10.32
17	7	22	36	3.085	9.696	50.19	21.83	12.88
18	15	28	24	9.916	18.51	84.28	27.09	24.59
19	20	36	80	3.966	7.139	87.38	24.51	9.48
20	11	55	100	1.745	8.726	31.59	10.48	11.59

Confined track lengths:

12.0961	11.3719	12.899	11.8056	12.8251
6.8909	14.1524	12.3876	8.1392	13.2051
11.7798	7.2562	8.777	9.914	15.0915
8.9112	8.7877	12.9326	12.9814	13.1691
2.5158	6.5356	15.1473	6.7526	11.998
8.0617	7.0921	12.4347	11.7966	11.4061
8.1479	7.5938	11.8978	11.4451	14.1582
11.177	8.1903	13.0185	14.4586	4.5705
4.8266	8.0118	9.4659	13.5219	5.7149
11.7147	14.4767	11.6841	13.6106	14.3015
8.9429	12.0131	9.0726	11.8595	12.1053
13.2442	10.3162	9.1105	6.8597	10.9804
12.0168	7.3287	7.5298	13.4212	11.679
7.4653	13.9156	14.5484	9.4816	11.5653
13.5062	7.9816	12.3129	13.1219	13.7022
14.2296	6.9282	11.2133	5.923	14.7148
15.2652	14.9711	9.6577	11.8406	10.6175
13.1865	9.4337	6.6992	14.0004	13.8631
6.2562	11.5416	9.801	9.9561	10.7036
10.2752	9.9388	11.6479	10.2363	9.9852

Black Forest		Sample: ZTG-0-13	
ζ = 345.69 ± 8.75		Dated mineral: apatite	
Irrad. code: BS-20	Rho_d: 7.0148	Dosimeter glass: CN5	
Grid unit: 63.03	N_d: 3215		

Cryst	N_s	N_i	Area	Rho_s	Rho_i	Age [Ma]	σ	U [ppm]
1	30	94	60	7.933	24.856	38.58	8.18	43.12
2	37	77	80	7.338	15.271	58	11.74	26.49
3	24	50	80	4.76	9.916	57.94	14.5	17.2
4	3	7	24	1.983	4.627	51.75	35.75	8.03
5	52	92	100	8.25	14.596	68.17	12.01	25.32
6	37	81	49	11.98	26.227	55.15	11.07	45.5
7	11	31	24	7.272	20.493	42.88	15.11	35.55
8	19	35	70	4.306	7.933	65.49	18.77	13.76
9	39	71	60	10.313	18.774	66.26	13.36	32.57
10	64	130	80	12.692	25.781	59.42	9.26	44.73
11	38	75	80	7.536	14.874	61.14	12.32	25.8
12	15	26	50	4.76	8.25	69.57	22.66	14.31
13	16	27	25	10.154	17.135	71.45	22.65	29.73
14	11	15	40	4.363	5.95	88.31	35.16	10.32
15	13	18	25	8.25	11.423	86.98	31.77	19.82
16	42	64	100	6.663	10.154	79.08	15.89	17.62
17	76	118	100	12.058	18.721	77.62	11.67	32.48
18	34	81	100	5.394	12.851	50.69	10.48	22.3
19	104	222	50	33	70.443	56.55	6.94	122.21
20	39	94	100	6.188	14.914	50.11	9.67	25.87

Confined track lengths:

7.7229	9.4878	9.6141	7.1014	11.6689
11.9042	12.5644	11.0609	5.6019	12.2904
13.0105	9.7157	10.6026	11.6111	13.3379
16.4158	12.2143	11.7075	9.9255	13.2931
12.8658	6.857	11.6077	9.3394	10.7313
10.7546	13.6936	13.0935	11.7315	12.3815
5.8075	15.114	3.8275	8.1363	6.7382
11.514	15.6567	11.8669	11.5361	10.7216
12.8094	10.7313	11.2394	9.165	13.2137
3.1045	13.0163	12.8807	11.5633	11.8905
14.0397	5.686	10.6636	12.9545	11.2202
4.423	13.9068	7.047	9.7091	11.3197
13.3613	14.9554	11.3097	11.5794	10.7335
14.4189	12.0508	9.3159	12.2149	12.7132
12.3555	14.2559	12.3404	6.568	11.4927
12.3148	8.6292	10.7588	12.7281	5.6472
12.2606	7.0051	11.8674	4.4209	11.9406
11.9137	12.5076	8.9453	12.7207	4.3694
8.8801	7.7786	8.0485	11.2337	10.35
11.1161	11.7884	10.7227	11.4009	10.4155

Black Forest		Sample: ZTG-0-14	
ζ = 345.69 ± 8.75		Dated mineral: apatite	
Irrad. code: BS-20	Rho_d: 9.064	Dosimeter glass: CN5	

Grid unit: 63.03 N_d: 3215

Cryst	N_s	N_i	Area	Rho_s	Rho_i	Age [Ma]	σ	U [ppm]
1	11	49	50	3.49	15.548	35.07	11.75	20.88
2	18	71	25	11.423	45.058	39.6	10.52	60.5
3	69	333	100	10.947	52.832	32.38	4.4	70.94
4	13	56	50	4.125	17.769	36.27	11.22	23.86
5	21	159	60	5.553	42.043	20.66	4.84	56.45
6	26	73	36	11.458	32.172	55.56	12.8	43.2
7	21	64	60	5.553	16.923	51.2	12.97	22.72
8	14	65	60	3.702	17.188	33.66	9.97	23.08
9	11	26	20	8.726	20.625	65.94	23.81	27.69
10	14	33	18	12.34	29.087	66.12	21.19	39.05
11	6	27	25	3.808	17.135	34.72	15.71	23.01
12	13	34	25	8.25	21.577	59.63	19.53	28.97
13	36	88	50	11.423	27.923	63.77	12.77	37.49
14	10	61	40	3.966	24.195	25.63	8.78	32.49
15	36	145	50	11.423	46.01	38.78	7.32	61.78
16	22	55	49	7.123	17.808	62.36	15.85	23.91
17	43	156	42	16.243	58.929	43.04	7.53	79.12
18	37	81	20	29.351	64.255	71.17	14.29	86.27
19	36	181	60	9.519	47.861	31.09	5.75	64.26
20	6	37	36	2.644	16.306	25.36	11.19	21.89

Confined track lengths:

7.9704	10.6146	12.3249	6.6241	11.3107
8.777	11.4663	11.0616	14.5816	6.9929
11.8184	9.0967	6.5622	11.3303	12.9623
12.4793	7.374	11.571	12.2606	12.2556
10.1446	6.6696	10.9718	9.158	12.779
11.4787	8.6032	15.9629	12.8074	11.5361
12.4906	15.4238	10.7605	12.5678	11.1576
12.5065	11.6355	12.1014	13.5367	
13.9853	13.7272	14.0634	6.6045	
11.2806	9.5441	14.27	13.5423	

Black Forest Sample: ZTG-0-15

$\zeta = 345.69 \pm 8.75$ Dated mineral: apatite

Irrad. code: BS-20 Rho_d: 10.0885 Dosimeter glass: CN5

Grid unit: 63.03 N_d: 3215

Cryst	N_s	N_i	Area	Rho_s	Rho_i	Age [Ma]	σ	U [ppm]
1	31	106	40	12.296	42.043	50.8	10.49	50.72
2	26	134	70	5.893	30.371	33.75	7.31	36.64
3	64	308	100	10.154	48.866	36.13	5.09	58.95
4	12	47	25	7.615	29.827	44.37	14.42	35.98
5	7	43	20	5.553	34.111	28.32	11.58	41.15
6	53	165	70	12.012	37.397	55.77	8.97	45.11
7	10	60	24	6.611	39.664	29	9.94	47.85
8	21	76	36	9.255	33.494	48	11.93	40.4
9	96	372	70	21.758	84.314	44.84	5.32	101.71
10	23	55	36	10.136	24.239	72.51	18.14	29.24
11	8	37	36	3.526	16.306	37.59	14.7	19.67
12	14	54	25	8.885	34.269	45.05	13.58	41.34

13	10	29	25	6.346	18.404	59.85	22.03	22.2
14	19	63	25	12.058	39.981	52.38	13.8	48.23
15	124	376	100	19.673	59.654	57.25	6.19	71.96
16	42	122	60	11.106	32.26	59.75	10.85	38.92
17	51	159	50	16.183	50.452	55.69	9.13	60.86
18	40	130	36	17.628	57.292	53.43	9.8	69.11
19	26	52	25	16.5	33	86.6	20.97	39.81
20	43	91	36	18.95	40.104	81.87	15.36	48.38

Confined track lengths:

12.0108	13.9148	12.5436	14.6654	10.8803
9.2641	12.7599	12.5909	11.0776	13.3957
10.5979	13.8694	13.8648	15.1953	11.1493
12.5347	12.9612	9.8172	11.1627	14.6168
12.9989	12.1327	14.626	10.2511	12.9743
9.3455	7.8793	14.25	10.9757	11.03
11.1466	11.5361	13.0568	14.4553	13.9696
6.7487	14.0231	11.4144	13.1799	11.364
15.3521	14.5393	9.5493	13.3535	10.2917
8.8413	13.9461	9.2745	14.1442	11.3688
13.4069	11.9665	12.0557	11.8841	13.1239
14.2475	9.8364	13.6134	11.7244	11.4548
15.7502	8.6989	12.5368	14.6338	12.4774
12.935	11.6841	13.3365	12.6416	10.6368
14.7731	13.2137	12.0617	5.9297	9.6205
12.9845	11.8645	15.5367	11.7606	12.6231
11.5148	11.0366	9.5614	14.601	8.5465
10.3635	11.297	10.8049	13.963	12.4182
11.6798	12.5468	12.1055	14.3716	12.6044
8.0602	14.0286	11.5877	11.5639	10.5228

Black Forest — Sample: ZTG-0-16

ζ = 345.69 ± 8.75 — Dated mineral: apatite

Irrad. code: BS-20 — Rho_d: 6.6733 — Dosimeter glass: CN5

Grid unit: 63.03 — N_d: 3215

Cryst	N_s	N_i	Area	Rho_s	Rho_i	Age [Ma]	σ	U [ppm]
1	58	114	25	36.808	72.347	58.42	9.59	131.94
2	171	334	100	27.13	52.991	58.78	5.82	96.64
3	40	86	36	17.628	37.901	53.43	10.36	69.12
4	63	160	60	16.659	42.308	45.26	6.87	77.16
5	26	94	36	11.458	41.426	31.83	7.12	75.55
6	111	328	80	22.013	65.048	38.92	4.44	118.63
7	58	122	100	9.202	19.356	54.6	8.87	35.3
8	80	221	40	31.731	87.657	41.62	5.58	159.86
9	42	110	49	13.599	35.616	43.89	8.08	64.95
10	79	191	36	34.816	84.175	47.53	6.53	153.51
11	27	82	40	10.709	32.524	37.87	8.48	59.31
12	62	147	36	27.324	64.784	48.47	7.49	118.15
13	52	129	36	22.917	56.851	46.33	7.74	103.68
14	25	87	25	15.865	55.212	33.06	7.57	100.69
15	41	92	50	13.01	29.192	51.2	9.74	53.24
16	87	152	50	27.606	48.231	65.68	9.06	87.96

17	48	165	36	21.154	72.717	33.47	5.58	132.61
18	29	44	25	18.404	27.923	75.58	18.23	50.92
19	112	396	100	17.769	62.827	32.54	3.62	114.58
20	40	97	36	17.628	42.749	47.39	9.02	77.96

Confined track lengths:

8.1912	8.8046	13.4738	9.3908	12.0803
13.1282	9.3473	14.1955	12.4182	13.492
9.4179	10.2476	12.5263	10.6075	14.1862
12.8545	11.2	14.3164	9.2099	9.372
12.4051	8.2486	4.5201	8.9811	12.1708
11.1836	14.6084	14.1282	12.4923	13.072
11.3053	3.971	8.1799	6.5395	12.6546
13.9588	11.5322	10.9873	11.4102	8.0517
11.7335	4.4491	12.5858	12.6416	8.7079
5.1065	4.2377	10.1697	9.1382	11.4959
8.173	10.1379	14.2733	10.834	13.4654
10.5371	4.1823	13.4894	13.5367	8.8605
11.034	6.4812	10.6441	10.5691	12.0944
13.9163	10.9965	12.8966	6.8359	12.5119
10.1732	8.6519	6.8218	10.3199	12.4421
6.7487	10.9598	8.3479	10.0805	14.7506
10.7282	10.0903	7.7634	4.4022	14.7705
8.421	13.7663	9.3858	13.2112	13.4807
9.2552	11.0912	9.9483	10.8809	12.1031
6.4219	10.0373	6.2713	12.7309	10.7386

Black Forest — Sample: ZTG-0-17

ζ = 345.69 ± 8.75 — Dated mineral: apatite

Irrad. code: BS-20 — Rho_d: 10.43 — Dosimeter glass: CN5

Grid unit: 63.03 — N_d: 3215

Cryst	N_s	N_i	Area	Rho_s	Rho_i	Age [Ma]	σ	U [ppm]
1	25	65	12	33.053	85.938	68.97	16.37	100.27
2	30	89	12	39.664	117.669	60.48	12.9	137.3
3	99	230	36	43.63	101.363	77.13	9.57	118.27
4	13	60	24	8.594	39.664	38.94	11.97	46.28
5	12	43	15	12.692	45.481	50.11	16.43	53.07
6	95	244	25	60.289	154.847	69.81	8.71	180.68
7	74	220	30	39.135	116.347	60.36	8.32	135.76
8	107	291	28	60.629	164.887	65.95	7.73	192.4
9	23	48	12	30.409	63.462	85.81	21.92	74.05
10	28	128	40	11.106	50.769	39.32	8.29	59.24
11	50	156	32	24.79	77.344	57.52	9.52	90.25
12	18	70	25	11.423	44.423	46.19	12.29	51.83
13	34	145	28	19.265	82.16	42.13	8.13	95.87
14	34	171	80	6.743	33.912	35.75	6.8	39.57
15	4	21	15	4.231	22.212	34.25	18.71	25.92
16	19	92	30	10.048	48.654	37.12	9.42	56.77
17	58	210	36	25.561	92.549	49.6	7.51	107.99
18	44	131	50	13.962	41.568	60.27	10.66	48.5
19	142	408	100	22.529	64.731	62.44	6.38	75.53
20	27	97	36	11.899	42.749	49.99	10.99	49.88

Confined track lengths:

7.1084	13.3344	13.3252	14.1036	14.5816
12.6156	14.5971	14.7213	15.3626	8.9281
9.127	12.0149	11.766	10.7675	9.103
8.2649	9.9786	10.8089	11.8774	7.8394
8.3589	13.8694	13.5841	12.7385	13.9328
13.6118	12.7853	12.6835	13.6181	13.9151
9.5812	16.3161	11.0471	12.5723	15.2032
9.6731	12.9434	11.5224	7.4431	6.627
11.483	7.0128	11.1728	9.5925	8.5512
10.5807	9.9899	8.1669	14.6922	10.9598
15.2634	10.9354	11.827	16.0852	11.0609
15.0453	12.8431	11.352	8.1113	11.755
15.7732	11.3107	13.1261	14.6499	15.2293
13.7046	12.9667	9.4159	9.451	15.0409
14.4409	13.7363	12.1228	11.4391	12.2858
12.4802	6.1758	14.4416	15.8154	12.679
14.1457	9.248	14.1417	11.1375	13.4605
13.864	12.3708	11.5089	8.4219	12.5042
11.9645	10.6541	12.4218	13.1309	9.6889
10.6112	6.4611	11.4373	12.9434	13.0422

Black Forest — Sample: ZTG-0-19

ζ = 345.69 ± 8.75 — Dated mineral: apatite

Irrad. code: BS-20 — Rho_d: 8.7224 — Dosimeter glass: CN5

Grid unit: 63.03 — N_d: 3215

Cryst	N_s	N_i	Area	Rho_s	Rho_i	Age [Ma]	σ	U [ppm]
1	16	38	16	15.865	37.68	63.17	18.93	52.57
2	25	60	36	11.018	26.442	62.51	15.01	36.89
3	39	99	36	17.188	43.63	59.12	11.32	60.88
4	30	98	36	13.221	43.189	45.99	9.7	60.26
5	34	94	36	14.984	41.426	54.3	11	57.8
6	43	135	36	18.95	59.495	47.84	8.51	83.01
7	9	34	20	7.139	26.971	39.78	14.96	37.63
8	13	51	25	8.25	32.366	38.32	11.96	45.16
9	23	58	25	14.596	36.808	59.51	14.78	51.36
10	81	261	100	12.851	41.409	46.62	6.1	57.78
11	19	48	36	8.373	21.154	59.4	16.2	29.52
12	6	52	36	2.644	22.917	17.37	7.51	31.97
13	28	99	36	12.34	43.63	42.5	9.19	60.88
14	28	99	36	12.34	43.63	42.5	9.19	60.88
15	37	111	36	16.306	48.919	50.06	9.63	68.25
16	30	120	36	13.221	52.885	37.58	7.76	73.79
17	31	110	36	13.662	48.478	42.35	8.71	67.64
18	31	73	40	12.296	28.954	63.71	13.8	40.4
19	61	73	24	40.325	48.257	124.76	21.98	67.33
20	55	157	36	24.239	69.191	52.6	8.4	96.54

Confined track lengths:

11.6154	10.069	9.8654	12.0086	7.1448
12.487	11.075	14.2939	15.0221	12.7873

9.6811	12.7301	10.1148	11.3053	10.2511
10.1085	12.2004	13.9691	8.0168	7.9399
11.9	16.0466	7.7131	12.2779	9.2702
9.1495	11.4731	5.7199	15.2448	6.5927
10.5941	8.4034	9.7743	7.7786	13.6148
11.571	11.6689	5.2917	10.0387	9.0819
9.0039	13.1978	8.9453	7.9882	9.0967
14.5216	7.9303	11.4299	14.4695	9.6682
9.0162	15.0146	8.4791	10.3484	14.9498
10.9371	7.2344	10.2545	8.9122	13.9853
13.1969	7.6161	6.5193	9.8263	13.6886
14.1404	11.001	10.7155	8.4526	10.0605
13.2627	12.1024	9.2376	11.3139	13.3965
12.5227	12.3334	10.5383	6.5135	11.641
10.3059	13.8299	12.6004	12.9304	9.8895
10.9974	9.7162	13.7093	13.1165	5.0694
15.2734	6.8218	9.8644	9.8971	11.5224
8.6649	13.0944	14.9081	11.2375	9.1268

Black Forest — Sample: ZTG-0-20

ζ = 345.69 ± 8.75 — Dated mineral: apatite

Irrad. code: BS-20 — Rho_d: 7.3564 — Dosimeter glass: CN5

Grid unit: 63.03 — N_d: 3215

Cryst	N_s	N_i	Area	Rho_s	Rho_i	Age [Ma]	σ	U [ppm]
1	4	36	16	3.966	35.697	14.11	7.45	59.06
2	9	89	36	3.966	39.223	12.85	4.51	64.89
3	9	69	9	15.865	121.635	16.56	5.89	201.23
4	4	25	16	3.966	24.79	20.31	10.96	41.01
5	4	13	16	3.966	12.891	39.01	22.33	21.33
6	6	37	25	3.808	23.481	20.59	9.08	38.85
7	20	137	36	8.814	60.377	18.54	4.47	99.88
8	12	124	36	5.288	54.648	12.29	3.74	90.41
9	40	167	100	6.346	26.495	30.38	5.43	43.83
10	5	25	16	4.958	24.79	25.38	12.46	41.01
11	5	33	20	3.966	26.178	19.24	9.25	43.31
12	33	200	60	8.726	52.885	20.95	3.99	87.49
13	16	112	50	5.077	35.539	18.14	4.88	58.79
14	9	87	49	2.914	28.169	13.14	4.62	46.6
15	10	76	36	4.407	33.494	16.71	5.64	55.41
16	9	48	25	5.712	30.462	23.8	8.68	50.39
17	6	42	36	2.644	18.51	18.14	7.94	30.62
18	17	60	28	9.633	33.997	35.93	9.93	56.24
19	5	25	25	3.173	15.865	25.38	12.46	26.25
20	31	167	49	10.037	54.072	23.56	4.66	89.45

Confined track lengths:

9.0259	10.8139	9.3647	6.0319	10.849
9.434	9.713	10.8646	15.4161	10.5114

Black Forest — Sample: ZTG-0-21

ζ = 345.69 ± 8.75 — Dated mineral: apatite

Irrad. code: BS-19	Rho_d: 10.4523	Dosimeter glass: CN5
Grid unit: 63.03	N_d: 3578	

Cryst	N_s	N_i	Area	Rho_s	Rho_i	Age [Ma]	σ	U [ppm]
1	6	66	20	4.76	52.356	16.4	7.01	60.96
2	6	59	20	4.76	46.803	18.35	7.88	54.49
3	5	54	100	0.793	8.567	16.71	7.83	9.98
4	4	28	40	1.587	11.106	25.76	13.79	12.93
5	5	32	16	4.958	31.731	28.17	13.57	36.95
6	14	34	16	13.882	33.714	73.96	23.59	39.25
7	9	48	50	2.856	15.231	33.79	12.32	17.73
8	8	53	30	4.231	28.029	27.21	10.35	32.64
9	8	120	60	2.115	31.731	12.03	4.41	36.95
10	2	11	25	1.269	6.981	32.76	25.21	8.13
11	5	47	36	2.204	20.713	19.19	9.05	24.12
12	5	29	35	2.266	13.146	31.07	15.08	15.31
13	3	15	16	2.975	14.874	36.03	22.81	17.32
14	3	45	16	2.975	44.622	12.03	7.18	51.95
15	13	138	35	5.893	62.555	17	4.96	72.84
16	16	375	50	5.077	118.991	7.7	1.98	138.55
17	44	112	49	14.247	36.264	70.59	12.74	42.22
18	6	18	15	6.346	19.039	59.94	28.32	22.17
19	25	320	100	3.966	50.769	14.1	2.96	59.11
20	12	45	16	11.899	44.622	48	15.66	51.95

Confined track lengths:

10.8156	6.2017	9.4647	9.9369	6.2381
9.2171	10.0577	7.6947	10.6441	8.7079
10.6707	10.6068	9.1897	7.9482	

Black Forest		Sample: ZTG-0-22
$\zeta = 345.69 \pm 8.75$		Dated mineral: apatite
Irrad. code: BS-19	Rho_d: 9.8069	Dosimeter glass: CN5
Grid unit: 63.03	N_d: 3578	

Cryst	N_s	N_i	Area	Rho_s	Rho_i	Age [Ma]	σ	U [ppm]
1	5	128	20	3.966	101.539	6.62	3.02	126.01
2	35	129	42	13.221	48.73	45.83	8.84	60.47
3	8	33	16	7.933	32.723	40.96	16.19	40.61
4	34	147	36	14.984	64.784	39.09	7.53	80.39
5	26	232	40	10.313	92.02	18.97	3.96	114.19
6	7	95	16	6.941	94.201	12.48	4.9	116.9
7	41	314	100	6.505	49.818	22.1	3.73	61.82
8	23	133	24	15.204	87.921	29.25	6.66	109.11
9	7	60	16	6.941	59.495	19.75	7.91	73.83
10	24	185	25	15.231	117.404	21.95	4.81	145.69
11	20	90	16	19.832	89.243	37.56	9.35	110.75
12	3	66	16	2.975	65.445	7.7	4.55	81.21
13	57	328	80	11.304	65.048	29.39	4.31	80.72
14	2	53	25	1.269	33.635	6.39	4.61	41.74
15	2	48	9	3.526	84.616	7.06	5.1	105.01
16	15	102	24	9.916	67.428	24.88	6.92	83.68
17	3	84	30	1.587	44.423	6.05	3.56	55.13
18	4	49	15	4.231	51.827	13.82	7.2	64.32

19	2	55	12	2.644	72.717	6.16	4.44	90.24
20	2	40	12	2.644	52.885	8.47	6.14	65.63

Confined track lengths:

8.2452	11.3214	11.5191	7.836	9.1348
15.6758	5.9962	12.7034	11.938	15.6661
11.8054	11.105	13.2579	11.3078	12.7991
9.6205	10.6326	13.0749	11.0641	12.0052

Black Forest — Sample: ZTG-0-23

ζ = 345.69 ± 8.75 — Dated mineral: apatite

Irrad. code: BS-19 — Rho_d: 10.1296 — Dosimeter glass: CN5

Grid unit: 63.03 — N_d: 3578

Cryst	N_s	N_i	Area	Rho_s	Rho_i	Age [Ma]	σ	U [ppm]
1	24	168	36	10.577	74.039	24.96	5.5	88.95
2	41	179	30	21.683	94.664	39.98	7.03	113.73
3	41	141	32	20.328	69.907	50.71	9.13	83.99
4	46	318	70	10.426	72.075	25.28	4.06	86.59
5	28	140	36	12.34	61.699	34.92	7.31	74.13
6	22	105	36	9.696	46.274	36.58	8.65	55.6
7	37	150	36	16.306	66.106	43.04	8.01	79.42
8	26	67	18	22.917	59.055	67.59	15.75	70.95
9	27	179	36	11.899	78.887	26.36	5.5	94.78
10	39	177	36	17.188	78.005	38.46	6.9	93.72
11	99	522	100	15.707	82.818	33.12	3.77	99.5
12	51	230	50	16.183	72.981	38.71	6.1	87.68
13	60	325	70	13.599	73.661	32.24	4.63	88.5
14	61	194	36	26.883	85.497	54.82	8.22	102.72
15	24	143	25	15.231	90.75	29.32	6.53	109.03
16	33	364	100	5.236	57.75	15.85	2.92	69.38
17	60	358	70	13.599	81.14	29.28	4.18	97.48
18	56	436	70	12.692	98.819	22.45	3.26	118.72
19	28	202	35	12.692	91.566	24.22	4.94	110.01
20	23	142	25	14.596	90.116	28.3	6.42	108.27

Confined track lengths:

3.3012	8.9848	12.0474	15.0767	14.0493
13.9853	8.796	14.8018	13.7211	14.8704
12.6865	6.7151	11.0776	10.6139	13.8563
10.9639	13.4516	14.5114	9.8632	11.1303
9.8704	13.9664	14.5289	11.3877	10.5147
13.562	9.2378	14.6576	14.1629	12.9408
10.3199	11.9972	14.8031	11.2183	16.0811
13.0662	13.2698	11.4633	13.5681	15.1978
10.6332	9.5325	12.2712	10.5091	16.1937
9.8328	8.9724	14.0569	13.3046	8.7684
10.547	10.1223	13.7874	12.4728	11.8196
9.111	14.6994	9.6928	12.7873	13.7478
8.7979	14.0639	10.8612	11.8828	14.448
9.9674	11.7678	15.0685	13.1095	10.3236
10.7859	13.209	11.9738	14.9918	9.0614

14.8394	9.7801	10.9093	11.9279	15.6758
13.5588	14.1224	8.2652	11.037	10.9253
10.4499	13.8181	12.8966	11.4682	15.628
13.0937	10.9563	13.0512	10.6068	13.2579
13.5827	7.397	13.6042	13.9507	14.4154

Black Forest — Sample: ZTG-0-06
ζ = 113.49 ± 1.8 — Dated mineral: zircon
Irrad. code: BS-17 — Rho_d: 4.5086 — Dosimeter glass: CN1
Grid unit: 24.4 — N_d: 1605

Cryst	N_s	N_i	Area	Rho_s	Rho_i	Age [Ma]	σ	U [ppm]
1	151	8	24	257.855	13.661	465.67	169.5	120.6
2	114	9	25	186.885	14.754	316.18	109.87	130.24
3	160	8	25	262.295	13.115	492.39	178.98	115.77
4	81	8	25	132.787	13.115	253.97	94.42	115.77
5	55	6	25	90.164	9.836	230.36	99.27	86.83
6	71	13	18	161.658	29.599	138.24	41.9	261.29
7	54	4	12	184.426	13.661	336.45	174.63	120.6
8	79	8	16	202.357	20.492	247.82	92.24	180.89
9	32	4	12	109.29	13.661	201.49	107.02	120.6
10	72	6	25	118.033	9.836	299.92	127.75	86.83
11	116	5	18	264.117	11.384	567.79	259.88	100.5
12	54	3	15	147.541	8.197	444.81	264.17	72.36
13	38	4	12	129.781	13.661	238.58	125.61	120.6
14	57	3	15	155.738	8.197	468.64	277.95	72.36
15	113	12	25	185.246	19.672	236.52	72.15	173.66
16	44	3	10	180.328	12.295	364.72	217.9	108.54
17	127	11	25	208.197	18.033	288.81	91.17	159.19
18	95	6	16	243.34	15.369	392.86	165.78	135.67
19	103	9	25	168.852	14.754	286.34	99.89	130.24
20	121	9	20	247.951	18.443	335.1	116.2	162.8

Black Forest — Sample: ZTG-0-07
ζ = 113.49 ± 1.8 — Dated mineral: zircon
Irrad. code: BS-17 — Rho_d: 4.182 — Dosimeter glass: CN1
Grid unit: 24.4 — N_d: 1605

Cryst	N_s	N_i	Area	Rho_s	Rho_i	Age [Ma]	σ	U [ppm]
1	39	3	15	106.557	8.197	301.35	180.77	78.01
2	75	14	16	192.111	35.861	125.89	36.84	341.29
3	45	3	6	307.377	20.492	346.48	206.86	195.02
4	66	6	10	270.492	24.59	255.89	109.37	234.02
5	72	5	12	245.902	17.077	332.97	154.31	162.52
6	110	6	20	225.41	12.295	421.01	176.94	117.01
7	78	7	15	213.115	19.126	259.15	102.54	182.02
8	56	4	12	191.257	13.661	323.95	167.93	130.01
9	56	4	15	153.005	10.929	323.95	167.93	104.01
10	52	6	15	142.077	16.393	202.45	87.49	156.02
11	57	4	12	194.672	13.661	329.59	170.76	130.01
12	55	5	12	187.842	17.077	255.89	119.77	162.52
13	102	8	16	261.27	20.492	295.68	108.91	195.02
14	72	6	12	245.902	20.492	278.66	118.69	195.02
15	115	8	20	235.656	16.393	332.41	121.94	156.02

16	25	3	12	85.383	10.246	194.78	119.15	97.51
17	78	7	24	133.197	11.954	259.15	102.54	113.76
18	69	5	18	157.104	11.384	319.44	148.24	108.34
19	162	13	24	276.639	22.199	289.14	83.79	211.27
20	101	6	18	229.964	13.661	387.58	163.26	130.01

Black Forest — Sample: ZTG-0-08

ζ = 113.49 $\pm$ 1.8 — Dated mineral: zircon

Irrad. code: BS-17 — Rho_d: 4.4432 — Dosimeter glass: CN1

Grid unit: 24.4 — N_d: 1605

Cryst	N_s	N_i	Area	Rho_s	Rho_i	Age [Ma]	σ	U [ppm]
1	58	4	16	148.566	10.246	355.6	184.13	91.78
2	131	8	36	149.135	9.107	400.18	146.22	81.58
3	56	4	9	255.009	18.215	343.66	178.15	163.16
4	59	5	18	134.335	11.384	290.85	135.75	101.98
5	114	14	40	116.803	14.344	202.1	57.55	128.49
6	49	5	16	125.512	12.807	242.47	114.06	114.72
7	87	6	12	297.131	20.492	355.6	150.46	183.56
8	30	5	12	102.459	17.077	149.53	72.37	152.96
9	55	5	15	150.273	13.661	271.54	127.09	122.37
10	65	6	16	166.496	15.369	267.51	114.41	137.67
11	87	14	24	148.566	23.907	154.81	44.81	214.15
12	64	6	25	104.918	9.836	263.48	112.76	88.11
13	25	2	12	85.383	6.831	307.7	226.3	61.19
14	31	3	16	79.406	7.684	255.41	154.61	68.83
15	92	10	25	150.82	16.393	227.88	76.18	146.84
16	19	2	12	64.891	6.831	235.18	174.97	61.19
17	66	4	25	108.197	6.557	403.14	207.93	58.74
18	29	3	12	99.044	10.246	239.23	145.26	91.78
19	40	4	9	182.149	18.215	247.32	129.9	163.16
20	39	3	18	88.798	6.831	319.71	191.78	61.19

Black Forest — Sample: ZTG 0-09

ζ = 113.49 $\pm$ 1.8 — Dated mineral: zircon

Irrad. code: BS-17 — Rho_d: 4.9004 — Dosimeter glass: CN1

Grid unit: 24.4 — N_d: 1605

Cryst	N_s	N_i	Area	Rho_s	Rho_i	Age [Ma]	σ	U [ppm]
1	64	7	16	163.934	17.93	249.35	99.54	145.63
2	158	13	35	185.012	15.222	329.4	95.54	123.63
3	79	5	9	359.745	22.769	425.03	196.41	184.92
4	49	10	9	223.133	45.537	134.84	46.96	369.84
5	109	9	12	372.268	30.738	328.28	114.27	249.65
6	65	7	12	221.995	23.907	253.17	100.99	194.17
7	79	8	9	359.745	36.43	268.91	100.09	295.88
8	64	5	9	291.439	22.769	346.45	161.2	184.92
9	84	15	12	286.885	51.23	153.87	43.37	416.08
10	154	17	18	350.638	38.707	247.1	63.57	314.37
11	45	3	12	153.689	10.246	404.17	241.3	83.22
12	75	9	6	512.295	61.475	227.66	80.59	499.29
13	126	13	21	245.902	25.371	264.04	77.31	206.06
14	63	6	8	322.746	30.738	285.56	122.3	249.65
15	44	4	8	225.41	20.492	298.85	156.32	166.43

16	53	5	18	120.674	11.384	288.22	135.11	92.46
17	74	6	10	303.279	24.59	334.15	142.18	199.72
18	119	10	20	243.852	20.492	322.69	106.67	166.43
19	112	18	30	153.005	24.59	170.74	43.65	199.72
20	59	9	9	268.67	40.984	179.76	64.55	332.86

Black Forest — Sample: ZTG-0-13

ζ = 113.49 ± 1.8 — Dated mineral: zircon

Irrad. code: BS-17 — Rho_d: 4.8351 — Dosimeter glass: CN1

Grid unit: 24.4 — N_d: 1605

Cryst	N_s	N_i	Area	Rho_s	Rho_i	Age [Ma]	σ	U [ppm]
1	76	13	12	259.563	44.399	158.44	47.78	365.47
2	90	23	20	184.426	47.131	106.48	25.08	387.96
3	71	22	10	290.984	90.164	87.94	21.62	742.18
4	143	41	15	390.71	112.022	94.99	17.06	922.11
5	131	13	15	357.923	35.519	270.71	79.13	292.37
6	119	19	20	243.852	38.934	169.59	42.2	320.49
7	108	22	9	491.803	100.182	133.3	31.43	824.65
8	124	35	12	423.497	119.536	96.48	18.69	983.95
9	39	27	5	319.672	221.311	39.51	9.96	1821.72
10	200	20	25	327.869	32.787	268.69	63.51	269.88
11	143	9	16	366.291	23.053	421.83	145.5	189.76
12	103	9	10	422.131	36.885	306.59	106.95	303.62
13	82	9	12	280.055	30.738	245.25	86.43	253.02
14	124	15	30	169.399	20.492	222.91	61.29	168.68
15	42	5	4	430.328	51.23	226.44	107.34	421.69
16	44	5	8	225.41	25.615	237.03	112.08	210.85
17	62	14	9	282.332	63.752	120.37	35.8	524.78
18	165	27	20	338.115	55.328	165.53	34.71	455.43
19	129	36	15	352.459	98.361	97.57	18.62	809.65
20	106	15	15	289.617	40.984	191.03	53	337.36

Black Forest — Sample: ZTG-0-14

ζ = 113.49 ± 1.8 — Dated mineral: zircon

Irrad. code: BS-17 — Rho_d: 4.5739 — Dosimeter glass: CN1

Grid unit: 24.4 — N_d: 1605

Cryst	N_s	N_i	Area	Rho_s	Rho_i	Age [Ma]	σ	U [ppm]
1	53	10	6	362.022	68.306	136.11	47.1	594.37
2	155	29	32	198.514	37.141	137.25	28.06	323.19
3	118	13	15	322.404	35.519	231.39	67.96	309.07
4	27	7	2	553.279	143.443	99.34	42.24	1248.17
5	20	4	4	204.918	40.984	128.48	70.48	356.62
6	33	9	4	338.115	92.213	94.47	35.64	802.4
7	19	5	2	389.344	102.459	97.88	49.28	891.55
8	58	12	6	396.175	81.967	124.24	39.57	713.24
9	31	8	6	211.749	54.645	99.8	39.69	475.49

Black Forest — Sample: ZTG-0-15

ζ = 113.49 ± 1.8 — Dated mineral: zircon

Irrad. code: BS-17 — Rho_d: 4.7698 — Dosimeter glass: CN1

Grid unit: 24.4 N_d: 1605

Cryst	N_s	N_i	Area	Rho_s	Rho_i	Age [Ma]	σ	U [ppm]
1	50	3	10	204.918	12.295	436.02	259.5	102.59
2	52	4	8	266.393	20.492	342.59	178.05	170.99
3	42	3	8	215.164	15.369	368.21	220.32	128.24
4	85	8	15	232.24	21.858	281.35	104.38	182.39
5	73	5	20	149.59	10.246	383.53	177.66	85.49
6	126	9	15	344.262	24.59	368.21	127.51	205.18
7	76	7	10	311.475	28.689	287.36	113.82	239.38
8	143	20	21	279.079	39.032	190.68	45.87	325.69
9	119	7	16	304.816	17.93	444.45	173.35	149.61
10	88	5	12	300.546	17.077	459.59	211.73	142.49
11	45	4	10	184.426	16.393	297.52	155.48	136.79
12	72	9	12	245.902	30.738	212.97	75.56	256.48
13	74	10	14	216.628	29.274	197.24	66.71	244.27
14	78	7	12	266.393	23.907	294.75	116.62	199.48
15	61	4	8	312.5	20.492	400.08	206.84	170.99
16	61	5	9	277.778	22.769	322.03	150.1	189.99
17	105	11	15	286.885	30.055	253.32	80.63	250.78
18	54	7	9	245.902	31.876	205.49	82.77	265.98
19	62	7	12	211.749	23.907	235.38	94.11	199.48
20	49	6	12	167.35	20.492	217.34	94.22	170.99

Black Forest Sample: ZTG-0-16

ζ = 113.49 ± 1.8 Dated mineral: zircon

Irrad. code: BS-17 Rho_d: 4.3126 Dosimeter glass: CN1

Grid unit: 24.4 N_d: 1605

Cryst	N_s	N_i	Area	Rho_s	Rho_i	Age [Ma]	σ	U [ppm]
1	37	3	6	252.732	20.492	294.97	177.28	189.11
2	60	4	8	307.377	20.492	357.01	184.66	189.11
3	140	8	24	239.071	13.661	414.63	151.22	126.08
4	41	4	6	280.055	27.322	246.08	129.11	252.15
5	76	6	12	259.563	20.492	302.75	128.7	189.11
6	40	5	8	204.918	25.615	192.86	91.66	236.39
7	52	5	12	177.596	17.077	249.61	117.11	157.6
8	50	7	8	256.148	35.861	172.47	69.79	330.95
9	37	4	4	379.098	40.984	222.48	117.28	378.23
10	75	6	9	341.53	27.322	298.86	127.1	252.15
11	61	4	12	208.333	13.661	362.79	187.56	126.08
12	27	3	6	184.426	20.492	216.57	131.95	189.11
13	52	3	6	355.191	20.492	410.81	244.23	189.11
14	86	10	12	293.716	34.153	207.1	69.46	315.19

Black Forest Sample: ZTG-0-17

ζ = 113.49 ± 1.8 Dated mineral: zircon

Irrad. code: BS-17 Rho_d: 3.6595 Dosimeter glass: CN1

Grid unit: 24.4 N_d: 1605

Cryst	N_s	N_i	Area	Rho_s	Rho_i	Age [Ma]	σ	U [ppm]
1	31	2	9	141.166	9.107	314.09	229.34	99.05
2	139	18	16	356.045	46.107	158.4	39.95	501.45
3	101	10	12	344.945	34.153	206.4	68.69	371.44

4	118	12	16	302.254	30.738	201.03	61.2	334.3
5	172	12	18	391.621	27.322	290.98	87.3	297.15
6	183	11	20	375	22.541	336.53	104.95	245.15
7	74	6	8	379.098	30.738	251.16	106.87	334.3
8	365	27	40	373.975	27.664	274.78	55.4	300.87
9	69	5	12	235.656	17.077	280.38	130.12	185.72
10	110	6	12	375.683	20.492	369.89	155.46	222.86
11	64	9	20	131.148	18.443	146	52.16	200.58
12	103	12	9	469.035	54.645	175.82	53.88	594.31
13	106	7	9	482.696	31.876	307.03	120.16	346.68
14	52	6	9	236.794	27.322	177.5	76.71	297.15
15	68	5	9	309.654	22.769	276.4	128.34	247.63
16	119	8	12	406.421	27.322	301.72	110.56	297.15
17	89	10	16	227.971	25.615	182.22	61.01	278.58
18	67	5	16	171.619	12.807	272.42	126.55	139.29
19	95	8	12	324.454	27.322	241.99	89.37	297.15
20	89	6	9	405.282	27.322	300.89	127.22	297.15

Black Forest — Sample: ZTG-0-19

ζ = 113.49 $\pm$ 1.8 — Dated mineral: zircon

Irrad. code: BS-17 — Rho_d: 4.7045 — Dosimeter glass: CN1

Grid unit: 24.4 — N_d: 1605

Cryst	N_s	N_i	Area	Rho_s	Rho_i	Age [Ma]	σ	U [ppm]
1	83	6	15	226.776	16.393	359.1	152.18	138.69
2	31	2	15	84.699	5.464	401.05	292.83	46.23
3	35	5	5	286.885	40.984	184.21	88.24	346.72
4	110	14	30	150.273	19.126	206.41	58.89	161.8
5	73	16	20	149.59	32.787	120.66	33.5	277.38
6	80	6	48	68.306	5.123	346.46	147.01	43.34
7	30	3	9	136.612	13.661	261.58	158.58	115.57
8	59	5	10	241.803	20.492	307.55	143.54	173.36
9	76	9	21	148.322	17.564	221.58	78.38	148.59
10	32	3	12	109.29	10.246	278.64	168.45	86.68
11	61	6	18	138.889	13.661	265.85	114.02	115.57
12	107	10	40	109.631	10.246	279.5	92.79	86.68
13	67	6	24	114.413	10.246	291.41	124.48	86.68
14	88	9	18	200.364	20.492	255.88	89.87	173.36
15	128	7	50	104.918	5.738	470.55	183.18	48.54
16	194	14	100	79.508	5.738	359.7	100.11	48.54
17	31	3	10	127.049	12.295	270.12	163.52	104.02

Black Forest — Sample: ZTG-0-20

ζ = 113.49 $\pm$ 1.8 — Dated mineral: zircon

Irrad. code: BS-17 — Rho_d: 4.6392 — Dosimeter glass: CN1

Grid unit: 24.4 — N_d: 1605

Cryst	N_s	N_i	Area	Rho_s	Rho_i	Age [Ma]	σ	U [ppm]
1	54	4	6	368.852	27.322	345.94	179.55	234.4
2	147	18	25	240.984	29.508	211.48	53.18	253.15
3	77	4	8	394.467	20.492	487.83	250.58	175.8
4	50	5	9	227.687	22.769	258.02	121.26	195.33
5	62	8	15	169.399	21.858	200.86	75.69	187.52
6	171	9	18	389.344	20.492	481.72	165.36	175.8

7	108	8	9	491.803	36.43	345.94	127.17	312.53
8	57	5	9	259.563	22.769	293.33	137.09	195.33
9	92	4	16	235.656	10.246	578.71	296.07	87.9
10	18	4	4	184.426	40.984	117.39	64.98	351.6
11	136	20	20	278.689	40.984	176.57	42.61	351.6
12	89	9	18	202.641	20.492	255.21	89.59	175.8
13	56	4	8	286.885	20.492	358.4	185.79	175.8
14	131	7	12	447.404	23.907	474.74	184.7	205.1
15	77	10	6	525.956	68.306	199.58	67.35	586
16	71	6	6	484.973	40.984	304.22	129.65	351.6
17	35	5	12	119.536	17.077	181.69	87.03	146.5

Black Forest — Sample: ZTG-0-21

ζ = 113.49 $\pm$ 1.8 — Dated mineral: zircon

Irrad. code: BS-17 — Rho_d: 4.0514 — Dosimeter glass: CN1

Grid unit: 24.4 — N_d: 1605

Cryst	N_s	N_i	Area	Rho_s	Rho_i	Age [Ma]	σ	U [ppm]
1	57	3	9	259.563	13.661	422.64	250.66	134.2
2	130	8	30	177.596	10.929	363.16	132.72	107.36
3	70	4	9	318.761	18.215	390.26	200.96	178.94
4	58	8	10	237.705	32.787	164.56	62.25	322.09
5	48	10	12	163.934	34.153	109.42	38.17	335.51
6	30	5	8	153.689	25.615	136.48	66.05	251.63
7	61	7	12	208.333	23.907	197.29	78.95	234.86
8	90	17	18	204.918	38.707	120.58	32.09	380.25
9	69	8	12	235.656	27.322	195.3	73.17	268.41
10	48	4	9	218.579	18.215	270.14	140.81	178.94
11	89	9	18	202.641	20.492	223.43	78.43	201.31
12	43	11	8	220.287	56.352	89.25	30.27	553.59
13	22	2	6	150.273	13.661	248.05	183.35	134.2
14	36	4	8	184.426	20.492	203.66	107.5	201.31
15	50	4	8	256.148	20.492	281.15	146.33	201.31
16	17	3	4	174.18	30.738	128.98	80.86	301.96
17	44	5	9	200.364	22.769	199.2	94.19	223.67
18	28	3	8	143.443	15.369	211.08	128.38	150.98
19	15	3	6	102.459	20.492	113.94	72.14	201.31
20	85	7	16	217.725	17.93	273.28	107.76	176.14

Black Forest — Sample: ZTG-0-22

ζ = 113.49 $\pm$ 1.8 — Dated mineral: zircon

Irrad. code: BS-17 — Rho_d: 3.9207 — Dosimeter glass: CN1

Grid unit: 24.4 — N_d: 1605

Cryst	N_s	N_i	Area	Rho_s	Rho_i	Age [Ma]	σ	U [ppm]
1	124	10	16	317.623	25.615	270.14	89.16	260.02
2	54	11	6	368.852	75.137	108.3	35.97	762.73
3	39	4	9	177.596	18.215	213.35	112.19	184.9
4	26	2	4	266.393	20.492	282.92	207.78	208.02
5	64	5	9	291.439	22.769	278.66	129.66	231.13
6	53	10	5	434.426	81.967	116.85	40.43	832.07
7	71	6	9	323.315	27.322	258.03	109.97	277.36
8	152	16	20	311.475	32.787	207.97	55	332.83
9	54	4	8	276.639	20.492	293.56	152.37	208.02

10	41	4	6	280.055	27.322	224.1	117.58	277.36
11	59	6	6	403.005	40.984	215.14	92.41	416.03
12	33	3	4	338.115	30.738	240.2	145.02	312.03
13	40	5	5	327.869	40.984	175.57	83.44	416.03
14	64	9	9	291.439	40.984	156.3	55.83	416.03
15	144	10	25	236.066	16.393	312.66	102.67	166.41
16	48	6	12	163.934	20.492	175.57	76.2	208.02
17	70	9	12	239.071	30.738	170.76	60.68	312.03
18	37	8	8	189.549	40.984	102.08	39.92	416.03
19	71	13	18	161.658	29.599	120.38	36.49	300.47
20	25	2	4	256.148	20.492	272.27	200.24	208.02

Black Forest — Sample: ZTG-0-23

ζ = 113.49 $\pm$ 1.8 — Dated mineral: zircon

Irrad. code: BS-17 — Rho_d: 3.986 — Dosimeter glass: CN1

Grid unit: 24.4 — N_d: 1605

Cryst	N_s	N_i	Area	Rho_s	Rho_i	Age [Ma]	σ	U [ppm]
1	151	12	24	257.855	20.492	278.51	83.94	204.61
2	66	11	12	225.41	37.568	134.3	43.92	375.12
3	86	9	16	220.287	23.053	212.59	74.74	230.19
4	68	7	10	278.689	28.689	216.06	86	286.45
5	59	5	9	268.67	22.769	261.52	122.06	227.34
6	148	17	24	252.732	29.03	193.97	50	289.86
7	117	12	15	319.672	32.787	216.84	66.04	327.38
8	114	15	24	194.672	25.615	169.65	46.87	255.76
9	86	6	16	220.287	15.369	316.31	133.89	153.46
10	98	8	12	334.699	27.322	271.29	100.08	272.81
11	73	8	15	199.454	21.858	203.16	75.9	218.25
12	68	6	12	232.24	20.492	251.38	107.31	204.61
13	59	4	15	161.202	10.929	325.28	168.34	109.13
14	106	16	16	271.516	40.984	148.13	39.97	409.22
15	79	6	16	202.357	15.369	291.14	123.59	153.46
16	48	7	9	218.579	31.876	153.26	62.17	318.28
17	38	3	8	194.672	15.369	280.32	168.31	153.46
18	33	4	12	112.705	13.661	183.95	97.54	136.41
19	106	9	16	271.516	23.053	261.04	90.96	230.19
20	68	17	16	174.18	43.545	89.85	24.51	434.8

Vosges — Sample: ZTG-1-01

ζ = 345.69 $\pm$ 8.75 — Dated mineral: apatite

Irrad. code: BS-38 — Rho_d: 10.9368 — Dosimeter glass: CN5

Grid unit: 63.03 — N_d: 3690

Cryst	N_s	N_i	Area	Rho_s	Rho_i	Age [Ma]	σ	U [ppm]
1	64	260	25	40.616	165.001	46.37	6.62	183.61
2	42	194	49	13.599	62.814	40.8	7.05	69.9
3	16	100	20	12.692	79.327	30.18	8.18	88.27
4	19	111	36	8.373	48.919	32.28	8.07	54.43
5	40	172	36	17.628	75.802	43.81	7.8	84.35
6	35	156	25	22.212	99	42.27	8.01	110.16
7	37	236	40	14.676	93.606	29.57	5.3	104.16
8	16	54	20	12.692	42.837	55.77	15.96	47.67
9	47	212	40	18.642	84.087	41.77	6.85	93.57

10	35	241	36	15.425	106.21	27.4	5.02	118.19
11	51	194	25	32.366	123.116	49.5	7.93	137
12	81	249	36	35.697	109.736	61.2	8.04	122.11
13	67	239	30	35.433	126.395	52.78	7.47	140.65
14	46	281	36	20.273	123.839	30.87	5	137.8
15	16	232	40	6.346	92.02	13.02	3.39	102.4
16	68	209	35	30.824	94.739	61.21	8.74	105.42
17	58	234	36	25.561	103.125	46.69	6.99	114.75
18	26	122	20	20.625	96.779	40.16	8.76	107.69
19	34	150	24	22.476	99.159	42.71	8.21	110.34
20	17	114	36	7.492	50.241	28.13	7.36	55.91

Confined track lengths:

11.2668	13.328	11.5467	13.1935	14.0352
7.6532	9.0843	10.3261	12.3527	14.7418
8.5058	12.8	9.7839	15.3626	13.431
11.2034	13.7031	11.0974	11.9911	13.2322
10.8625	10.1679	14.0433	9.5464	11.5841
9.5917	11.775	11.9293	10.1864	9.8251
10.9804	12.1444	11.9635	11.5339	13.5451
11.3607	11.7495	13.6106	11.7942	12.0257
12.5639	11.0163	8.1034	11.1016	13.7134
9.8646	12.1446	10.879	9.7859	13.6144
11.0931	8.7087	11.3247	11.2419	14.3373
10.8566	10.7651	14.5037	12.7873	12.3196
12.2927	13.1397	15.4899	10.5264	13.0386
9.2888	13.2255	13.2522	10.1148	10.6651
10.6332	10.66	10.1288	14.4185	15.8842
10.5383	13.2807	9.774	11.1101	10.9101
10.9929	12.7019	16.0531	9.1216	11.8643
11.9777	10.5383	10.6574	9.8818	14.5037
10.9688	12.3509	11.8555	11.0912	13.2335
6.5884	9.173	12.7723	11.1768	12.757

Vosges — Sample: ZTG-1-02

ζ = 345.69 $\pm$ 8.75 — Dated mineral: apatite

Irrad. code: BS-38 — Rho_d: 8.9958 — Dosimeter glass: CN5

Grid unit: 63.03 — N_d: 3690

Cryst	N_s	N_i	Area	Rho_s	Rho_i	Age [Ma]	σ	U [ppm]
1	10	95	70	2.266	21.532	16.35	5.46	29.13
2	51	224	35	23.118	101.539	35.3	5.58	137.37
3	27	85	20	21.418	67.428	49.2	10.97	91.22
4	35	152	36	15.425	66.988	35.7	6.78	90.62
5	29	128	36	12.781	56.411	35.13	7.3	76.32
6	62	256	50	19.673	81.231	37.55	5.43	109.89
7	27	139	24	17.849	91.887	30.13	6.4	124.31
8	19	115	25	12.058	72.981	25.64	6.4	98.73
9	48	192	40	19.039	76.154	38.76	6.36	103.03
10	49	179	36	21.595	78.887	42.42	6.96	106.72
11	17	52	20	13.486	41.25	50.63	14.23	55.81
12	24	121	36	10.577	53.326	30.77	6.94	72.14
13	21	120	16	20.823	118.991	27.15	6.47	160.98

14	37	87	24	24.459	57.512	65.79	13.06	77.81
15	37	142	35	16.772	64.368	40.39	7.55	87.08
16	70	205	35	31.731	92.926	52.88	7.49	125.72
17	57	204	36	25.12	89.904	43.3	6.62	121.63
18	26	73	20	20.625	57.909	55.14	12.7	78.34
19	17	104	20	13.486	82.5	25.37	6.68	111.61
20	16	60	15	16.923	63.462	41.33	11.7	85.85

Confined track lengths:

8.7939	12.1135	15.5454	12.6828	11.1493
15.3655	12.0068	13.716	13.0935	13.4941
13.0974	12.53	13.6195	13.0619	13.1476
12.7335	8.6347	13.1892	14.7616	10.4073
14.1404	8.0953	11.7566	13.2892	12.7335
14.2873	12.4376	15.1179	8.8762	13.7683
10.098	12.0451	11.692	14.9484	13.5564
12.8618	13.3204	11.4781	13.4584	15.1717
12.9222	12.2789	11.143	12.3984	11.8714
11.343	12.8	11.5621	12.9277	13.9522
15.0631	11.5322	11.4974	14.4566	12.8939
12.3111	14.8851	13.9463	12.7731	13.7272
11.5142	11.3939	13.1799	11.827	13.6941
13.9095	13.0119	12.0932	14.597	11.8452
9.382	9.0697	11.5351	12.3817	9.0843
9.508	11.4249	10.7078	13.4409	13.7139
9.7157	13.2963	10.2766	11.2612	13.4064
11.9066	12.6201	12.9747	14.2559	14.4489
13.6292	15.2102	12.3952	12.2281	13.0003
10.82	12.6201	13.0141	14.8972	9.1845

Vosges — Sample: ZTG-1-03

ζ = 345.69 $\pm$ 8.75 — Dated mineral: apatite

Irrad. code: BS-38 — Rho_d: 11.6426 — Dosimeter glass: CN5

Grid unit: 63.03 — N_d: 3690

Cryst	N_s	N_i	Area	Rho_s	Rho_i	Age [Ma]	σ	U [ppm]
1	8	28	25	5.077	17.769	57.24	23.01	18.57
2	33	103	30	17.452	54.471	64.15	12.98	56.94
3	130	440	70	29.464	99.726	59.18	6.17	104.24
4	35	159	28	19.832	90.093	44.15	8.35	94.17
5	76	318	49	24.608	102.964	47.92	6.29	107.63
6	50	192	25	31.731	121.847	52.19	8.44	127.37
7	91	489	70	20.625	110.832	37.34	4.41	115.85
8	129	615	100	20.466	97.573	42.07	4.27	101.99
9	19	87	25	12.058	55.212	43.8	11.17	57.71
10	23	82	25	14.596	52.039	56.2	13.37	54.4
11	22	133	25	13.962	84.404	33.2	7.71	88.23
12	19	105	36	8.373	46.274	36.31	9.12	48.37
13	40	167	24	26.442	110.397	48.02	8.58	115.4
14	84	282	70	19.039	63.915	59.67	7.63	66.81
15	182	688	80	36.094	136.443	53.02	4.7	142.62
16	63	236	49	20.398	76.413	53.5	7.76	79.87
17	34	184	36	14.984	81.09	37.08	7.01	84.76

18	19	79	30	10.048	41.779	48.22	12.41	43.67
19	40	139	28	22.665	78.761	57.65	10.49	82.33
20	76	370	60	20.096	97.837	41.2	5.34	102.27

Confined track lengths:

11.1652	13.8245	11.9738	11.3445	11.8756
12.5933	13.1234	10.9757	11.8136	11.3646
4.5368	12.7309	12.3939	12.2219	14.2168
12.5967	12.6298	13.8621	11.5418	14.2083
12.7398	8.7268	12.3249	14.0164	13.4631
13.1654	11.2268	12.5787	13.8417	10.9507
11.7467	8.9911	9.7557	10.2366	11.9645
14.9136	14.5008	11.6604	13.9345	9.5851
9.8039	13.5848	13.3011	11.312	11.8883
7.3714	12.0421	15.7028	13.8239	10.321
13.9107	12.2381	13.8502	12.7184	13.4305
7.0078	12.5466	13.1632	13.5135	14.3721
12.8	10.4749	12.9705	13.8171	13.4486
11.7982	11.3763	13.8776	13.9563	15.7637
12.5042	12.9158	14.8851	12.9492	12.5212
14.7213	13.4738	12.89	14.0071	12.9623
12.7924	10.969	10.7282	15.5481	8.4532
14.2028	12.1164	12.1601	14.4008	10.4248
13.8883	12.383	13.2399	15.4984	11.5228
10.3443	12.8735	12.8558	12.0149	13.3186

Vosges — Sample: ZTG-1-04

ζ = 345.69 ± 8.75 — Dated mineral: apatite

Irrad. code: BS-38 — Rho_d: 10.5838 — Dosimeter glass: CN5

Grid unit: 63.03 — N_d: 3690

Cryst	N_s	N_i	Area	Rho_s	Rho_i	Age [Ma]	σ	U [ppm]
1	13	70	49	4.209	22.665	33.88	10.28	26.06
2	27	101	64	6.693	25.038	48.72	10.66	28.79
3	39	135	28	22.098	76.494	52.63	9.7	87.96
4	15	38	20	11.899	30.144	71.81	22	34.66
5	35	163	100	5.553	25.861	39.16	7.39	29.74
6	12	66	36	5.288	29.087	33.18	10.46	33.45
7	12	69	32	5.95	34.21	31.74	9.97	39.34
8	12	55	24	7.933	36.358	39.79	12.73	41.81
9	9	47	35	4.08	21.305	34.94	12.75	24.5
10	9	69	30	4.76	36.491	23.82	8.47	41.96
11	22	45	30	11.635	23.798	88.82	23.26	27.36
12	28	70	50	8.885	22.212	72.76	16.42	25.54
13	17	58	36	7.492	25.561	53.4	14.81	29.39
14	10	42	25	6.346	26.654	43.41	15.33	30.65
15	8	55	30	4.231	29.087	26.55	10.08	33.45
16	15	53	36	6.611	23.357	51.57	15.16	26.86
17	7	53	30	3.702	28.029	24.12	9.73	32.23
18	14	45	36	6.17	19.832	56.66	17.42	22.8
19	13	39	25	8.25	24.75	60.69	19.52	28.46
20	12	54	36	5.288	23.798	40.52	12.99	27.36

Confined track lengths:

13.431	13.5604	12.99	11.8555	12.5136
14.9283	12.021	8.9598	11.397	10.0312
9.5117	11.6511	14.5743	9.0486	12.4395
10.8824	14.5232	8.1392	8.7347	12.5933
10.5273	14.3669	11.0931	9.7653	11.1137
10.2317	11.1889	10.1713	11.6331	10.5369
13.7761	11.8212	15.3964	9.2971	11.2337
6.8649	10.2575	9.7375	14.073	9.4382
10.3849	7.2004	13.1906	10.5371	9.4257
12.8251	6.6074	9.3707	8.9903	13.8017
9.6877	11.9	11.2343	12.7932	13.0888
11.4119	8.3297	11.3445	9.9783	7.6507
8.4524	9.7467	7.1448	7.6828	8.9724
8.2194	8.3758	6.9605	11.7806	11.3091
11.8046	10.4248	8.8844	13.5006	14.2939
13.3591	15.7634	11.0974	14.0197	11.9706
11.1895	10.1372	13.2255	12.4855	9.9958
13.2791	12.9727	12.7762	15.8167	12.5136
11.6239	7.6947	13.9184	12.3801	11.7678
13.3909	13.2934	8.9732	12.7132	8.7087

Vosges — Sample: ZTG-1-07

ζ = 345.69 ± 8.75 — Dated mineral: apatite

Irrad. code: BS-38 — Rho_d: 11.2896 — Dosimeter glass: CN5

Grid unit: 63.03 — N_d: 3690

Cryst	N_s	N_i	Area	Rho_s	Rho_i	Age [Ma]	σ	U [ppm]
1	4	33	25	2.538	20.942	23.61	12.52	22.58
2	12	42	30	6.346	22.212	55.51	18.25	23.94
3	10	30	36	4.407	13.221	64.72	23.71	14.25
4	6	28	20	4.76	22.212	41.68	18.79	23.94
5	12	81	20	9.519	64.255	28.84	8.96	69.27
6	24	93	49	7.771	30.112	50.16	11.58	32.46
7	15	51	30	7.933	26.971	57.14	16.87	29.07
8	7	42	16	6.941	41.647	32.44	13.28	44.89
9	14	77	49	4.533	24.931	35.38	10.34	26.88
10	27	153	100	4.284	24.274	34.34	7.24	26.17
11	12	75	32	5.95	37.185	31.15	9.73	40.08
12	15	51	20	11.899	40.457	57.14	16.87	43.61
13	6	30	20	4.76	23.798	38.91	17.44	25.65
14	11	104	25	6.981	66	20.61	6.56	71.15
15	7	39	25	4.442	24.75	34.93	14.38	26.68
16	15	110	60	3.966	29.087	26.55	7.35	31.35
17	12	45	28	6.799	25.498	51.83	16.91	27.49
18	12	87	25	7.615	55.212	26.86	8.31	59.52
19	8	59	36	3.526	26.002	26.4	9.98	28.03
20	7	62	36	3.085	27.324	21.99	8.79	29.45

Confined track lengths:

14.1504	16.1131	13.3285	7.1847	14.3175
13.5888	11.9097	11.2169	8.1557	11.4051

12.3996	13.7541	12.0068	11.6493	12.2529
12.5263	12.8006	10.7465	11.7395	11.03
10.6983	12.6337	8.8242	11.1703	10.7005
11.0797	6.1486	9.7011	13.1261	12.6038
10.5818	13.8442	10.5383	13.3731	14.4318
9.5688	7.7131	14.1969	15.3535	8.1727
10.9339	12.5336	13.1711	9.6811	10.882
10.9639	13.6527	6.9848	13.7855	13.033
9.6087	8.4264	13.3492	10.9432	12.7279
11.3578	11.4908	14.4964	10.7868	8.9661
11.397	9.7991	13.8912	14.9498	9.5276
12.2606	15.0605	11.1347	10.6441	12.5368
10.0166	11.6103	7.6825	14.8146	11.4645
12.6982	9.5688	12.6313	10.7493	13.858
11.298	9.8205	12.2726	9.5298	12.0196
13.9739	12.021	10.5418	10.3217	12.462
15.5269	8.1779	12.1756	12.6651	15.7593
11.5469	11.5829	9.8364	8.6519	14.1506

Vosges — Sample: ZTG-1-08

ζ = 345.69 ± 8.75 — Dated mineral: apatite

Irrad. code: BS-38 — Rho_d: 10.7603 — Dosimeter glass: CN5

Grid unit: 63.03 — N_d: 3690

Cryst	N_s	N_i	Area	Rho_s	Rho_i	Age [Ma]	σ	U [ppm]
1	12	31	36	5.288	13.662	71.6	24.44	15.45
2	37	106	32	18.344	52.554	64.6	12.49	59.44
3	31	81	49	10.037	26.227	70.79	15.1	29.66
4	28	89	36	12.34	39.223	58.25	12.74	44.36
5	31	80	25	19.673	50.769	71.67	15.32	57.42
6	26	72	25	16.5	45.693	66.81	15.42	51.68
7	55	130	49	17.808	42.092	78.21	12.8	47.61
8	53	104	80	10.511	20.625	94.09	16.13	23.33
9	95	240	100	15.072	38.077	73.2	9.14	43.07
10	23	46	25	14.596	29.192	92.33	23.74	33.02
11	32	101	49	10.361	32.702	58.66	12.03	36.99
12	34	72	24	22.476	47.596	87.23	18.34	53.83
13	28	80	36	12.34	35.257	64.77	14.36	39.88
14	29	101	25	18.404	64.096	53.18	11.32	72.49
15	12	41	20	9.519	32.524	54.21	17.87	36.79
16	14	34	16	13.882	33.714	76.13	24.28	38.13
17	11	55	24	7.272	36.358	37.09	12.3	41.12
18	62	171	36	27.324	75.361	67.08	10.15	85.23
19	47	84	25	29.827	53.308	103.23	19.06	60.29
20	13	29	25	8.25	18.404	82.84	27.76	20.82

Confined track lengths:

8.9976	12.1694	15.5572	15.4479	15.4614
9.158	10.1774	12.427	11.4243	14.0686
13.1892	14.7148	10.8722	9.571	7.2383
7.577	13.8938	15.0309	12.0384	8.2999
10.2315	15.6945	10.4302	11.1889	10.1351
10.1588	11.2152	13.7608	13.9273	8.7877

14.4638	12.9501	12.9509	13.4863	14.1265
10.204	12.833	13.2308	10.9112	11.5737
14.0963	12.4378	12.8438	13.4409	14.0206
12.3175	11.0984	9.6828	12.8519	9.127
7.5264	11.199	11.4102	10.437	8.4255
9.8364	14.7634	12.9049	10.5512	11.7204
14.9397	13.4315	15.9461	12.427	12.1357
10.7075	13.6994	9.5986	11.9724	12.1374
12.5624	14.3905	13.8157	10.7675	12.4106
13.262	12.7457	11.7099	12.8851	11.8567
14.3871	14.3598	12.8265	11.655	8.8044
12.5984	9.1358	10.9302	12.3508	11.55
13.9842	11.6446	10.9804	12.819	12.5639
12.2344	14.648	10.5919	12.9727	12.679

Vosges — Sample: ZTG-1-09

ζ = 345.69 $\pm$ 8.75 — Dated mineral: apatite

Irrad. code: BS-38 — Rho_d: 10.2309 — Dosimeter glass: CN5

Grid unit: 63.03 — N_d: 3690

Cryst	N_s	N_i	Area	Rho_s	Rho_i	Age [Ma]	σ	U [ppm]
1	27	158	36	11.899	69.632	30.15	6.34	82.83
2	87	276	40	34.507	109.472	55.5	7.03	130.22
3	59	146	25	37.442	92.654	71.07	11.17	110.22
4	48	163	25	30.462	103.443	51.87	8.66	123.05
5	30	76	50	9.519	24.116	69.43	15.12	28.69
6	11	56	36	4.848	24.68	34.64	11.47	29.36
7	21	46	36	9.255	20.273	80.23	21.27	24.11
8	14	53	24	9.255	35.036	46.54	14.06	41.68
9	24	86	49	7.771	27.846	49.16	11.45	33.12
10	14	40	24	9.255	26.442	61.6	19.22	31.45
11	26	93	36	11.458	40.986	49.25	11.03	48.75
12	45	159	70	10.199	36.037	49.85	8.55	42.87
13	24	69	24	15.865	45.613	61.22	14.62	54.26
14	29	71	16	28.756	70.403	71.83	15.98	83.75
15	33	108	50	10.471	34.269	53.81	10.83	40.76
16	31	82	36	13.662	36.138	66.51	14.17	42.99
17	59	255	100	9.361	40.457	40.79	6.02	48.12
18	13	90	36	5.729	39.664	25.49	7.6	47.18
19	30	90	30	15.865	47.596	58.68	12.5	56.62
20	31	110	40	12.296	43.63	49.64	10.21	51.9

Confined track lengths:

11.2015	14.378	10.1456	14.4812	10.7544
12.5181	9.372	12.8131	8.8196	8.7444
10.24	13.2863	10.6771	12.0961	10.8698
7.3484	8.678	9.0835	9.9404	9.2613
14.9541	13.8258	11.8166	8.2726	10.8566
13.7764	12.9361	10.1827	11.0223	10.3059
8.6837	9.593	9.914	12.8636	8.4838
9.9774	11.2343	10.9242	10.2059	10.8233
7.7853	10.1681	11.4061	13.9826	11.8044
8.8434	12.6932	11.8901	12.8403	10.6698

7.2835	10.6397	13.5346	8.2948	13.002
13.9151	8.7382	9.5441	12.0639	11.2337
9.6709	11.2404	12.1648	8.6245	10.9811
8.3693	11.0025	11.105	9.677	10.1052
9.1784	10.8357	11.0212	11.4959	11.8535
10.1204	9.2816	9.3442	7.0931	9.8395
10.6397	10.2697	9.0988	14.0364	11.4515
11.5714	13.5212	9.451	8.4816	9.7847
10.1435	11.4959	13.1578	11.0914	13.053
10.8989	11.5224	11.7566	9.1657	15.6962

Vosges — Sample: ZTG-1-10

ζ = 345.69 ± 8.75 — Dated mineral: apatite

Irrad. code: BS-38 — Rho_d: 10.0545 — Dosimeter glass: CN5

Grid unit: 63.03 — N_d: 3690

Cryst	N_s	N_i	Area	Rho_s	Rho_i	Age [Ma]	σ	U [ppm]
1	15	60	60	3.966	15.865	43.3	12.57	19.2
2	19	77	49	6.152	24.931	42.74	11.02	30.18
3	13	22	16	12.891	21.815	101.88	35.77	26.4
4	14	35	32	6.941	17.353	69.14	21.96	21
5	10	30	25	6.346	19.039	57.67	21.13	23.04
6	27	29	25	17.135	18.404	159.8	43.01	22.28
7	15	52	36	6.611	22.917	49.94	14.71	27.74
8	5	38	25	3.173	24.116	22.83	10.88	29.19
9	13	43	49	4.209	13.923	52.33	16.64	16.85
10	54	220	100	8.567	34.904	42.52	6.58	42.25
11	12	47	36	5.288	20.713	44.22	14.36	25.07
12	8	39	36	3.526	17.188	35.55	13.84	20.8
13	13	57	35	5.893	25.838	39.51	12.2	31.27
14	14	21	36	6.17	9.255	114.83	39.77	11.2
15	15	33	20	11.899	26.178	78.51	24.56	31.69
16	13	38	28	7.366	21.532	59.18	19.1	26.06
17	11	32	25	6.981	20.308	59.46	20.86	24.58
18	14	25	24	9.255	16.527	96.59	32.38	20
19	21	30	49	6.799	9.714	120.52	34.48	11.76
20	5	27	20	3.966	21.418	32.1	15.66	25.92

Confined track lengths:

10.6733	11.6833	8.9882	10.5687	12.4349
10.6627	10.4562	9.1333	11.4762	8.8418
10.5091	11.1226	11.9309	12.9749	9.9433
7.2004	11.6111	15.1647	11.5629	9.8364
9.5337	8.3921	13.7647	12.9131	8.8817
12.0068	14.2442	10.0528	11.589	5.7182
9.5008	9.2877	12.0854	8.7468	8.4791
14.1551	11.2265	12.8118	10.2833	14.7257
12.3678	9.2222	9.0726	10.1679	13.2294
9.2768	10.1725	12.1461	12.0225	12.3952
7.8619	10.0615	14.748	11.0827	9.4302
11.3422	13.2769	10.5818	10.486	11.5105
7.1719	7.0574	10.1062	11.7576	12.5436
6.3271	9.0752	7.1508	9.8654	11.5433

8.4727	13.74	7.2462	7.1781	9.6731
14.3015	13.8836	11.2442	12.5263	12.0325
10.7122	10.2683	12.1172	10.1588	12.5149
10.0312	8.8215	12.1399	12.1694	10.3564
8.213	9.8627	8.7008	8.2314	8.9958
11.034	12.5453	10.9768	12.8646	10.8198

Vosges — Sample: ZTG-1-22

ζ = 345.69 $\pm$ 8.75 — Dated mineral: apatite

Irrad. code: BS-34 — Rho_d: 9.9577 — Dosimeter glass: CN5

Grid unit: 63.03 — N_d: 1660

Cryst	N_s	N_i	Area	Rho_s	Rho_i	Age [Ma]	σ	U [ppm]
1	29	219	70	6.573	49.636	22.75	4.57	60.66
2	24	168	100	3.808	26.654	24.54	5.42	32.58
3	7	64	50	2.221	20.308	18.8	7.51	24.82
4	10	65	49	3.238	21.046	26.42	9.02	25.72
5	5	71	50	1.587	22.529	12.11	5.62	27.53
6	9	90	60	2.38	23.798	17.19	6.04	29.09
7	18	168	100	2.856	26.654	18.41	4.61	32.58
8	4	15	16	3.966	14.874	45.73	25.79	18.18
9	12	95	70	2.72	21.532	21.7	6.69	26.32
10	17	70	48	5.619	23.137	41.66	11.36	28.28
11	61	188	100	9.678	29.827	55.6	8.42	36.45
12	22	133	100	3.49	21.101	28.41	6.61	25.79
13	8	17	16	7.933	16.857	80.49	34.63	20.6
14	6	32	21	4.533	24.176	32.19	14.37	29.55
15	12	184	70	2.72	41.703	11.22	3.36	50.97
16	17	139	36	7.492	61.258	21.02	5.45	74.87
17	4	38	36	1.763	16.747	18.09	9.53	20.47
18	10	77	60	2.644	20.361	22.31	7.54	24.88
19	8	47	36	3.526	20.713	29.23	11.23	25.32
20	6	31	25	3.808	19.673	33.23	14.87	24.04

Confined track lengths:

12.5669	12.6546	13.864	15.8607	13.2171
9.3394	12.0225	13.1842	10.101	7.7741
11.0616	10.7667	9.0374	11.9285	10.2232
14.4689	11.775	8.9226	11.676	12.8006
14.1132	13.0179	14.0392	13.4731	14.512
10.213	10.6894	13.0179	10.1027	13.4486
10.3087	10.6397	10.0992	13.7029	13.793
8.3309	13.3331	13.8812	10.9845	13.9219
9.2745	14.1384	13.2121	13.6236	12.7335
10.0641	15.5305	12.0813	14.5042	11.6315
14.8241	14.5011	8.3758	14.8128	8.8626
11.9974	14.2898	11.5142	10.8783	9.4247
11.5525	15.1173	9.9219	10.0837	9.3949
12.8545	14.7761	8.4755	8.9811	12.1446
11.5714	12.4772	12.2812	11.4104	11.1025
16.2951	12.7512	10.1718	8.127	12.8851
13.6687	11.0351	13.1935	9.2115	9.1845
11.2806	10.0378	15.4684	9.4846	14.4803

12.7969	13.8163	13.6054	12.7398	13.7211
14.3795	14.1862	16.0943	13.9463	11.7576

Vosges		Sample: ZTG-1-23
ζ = 345.69 ± 8.75		Dated mineral: apatite
Irrad. code: BS-34	Rho_d: 9.7017	Dosimeter glass: CN5
Grid unit: 63.03	N_d: 1660	

Cryst	N_s	N_i	Area	Rho_s	Rho_i	Age [Ma]	σ	U [ppm]
1	23	107	80	4.561	21.22	35.94	8.36	26.62
2	20	51	50	6.346	16.183	65.43	17.42	20.3
3	8	18	25	5.077	11.423	74.1	31.6	14.33
4	22	86	64	5.454	21.319	42.76	10.33	26.74
5	15	85	70	3.4	19.265	29.52	8.33	24.17
6	8	68	50	2.538	21.577	19.7	7.4	27.07
7	35	135	100	5.553	21.418	43.33	8.36	26.87
8	5	44	42	1.889	16.621	19.03	9	20.85
9	17	46	50	5.394	14.596	61.68	17.64	18.31
10	10	39	36	4.407	17.188	42.85	15.27	21.56
11	13	27	32	6.445	13.386	80.24	27.23	16.79
12	75	309	100	11.899	49.024	40.57	5.42	61.5
13	17	70	60	4.495	18.51	40.6	11.07	23.22
14	13	74	24	8.594	48.919	29.39	8.9	61.36
15	18	44	40	7.139	17.452	68.24	19.24	21.89
16	6	59	50	1.904	18.721	17.03	7.32	23.48
17	11	77	49	3.562	24.931	23.91	7.75	31.27
18	17	70	60	4.495	18.51	40.6	11.07	23.22
19	15	43	25	9.519	27.289	58.23	17.58	34.23
20	15	62	49	4.857	20.075	40.44	11.72	25.18

Confined track lengths:

13.7966	12.2379	12.2358	9.5878	13.0886
11.7495	12.0304	10.7181	12.8019	11.3673
13.6259	12.83	10.8609	14.5644	12.9814
11.7131	14.5633	11.5841	11.7752	14.2028
11.985	11.0882	15.2833	12.4277	8.7347
13.0272	11.8302	12.6982	10.8235	12.1357
11.449	15.3964	11.1832	11.0545	11.7083
10.7577	11.3414	10.0699	12.2843	14.7937
15.7085	14.8451	14.0917	11.9018	12.2591
10.0312	14.0586	13.1016	12.4364	13.5514
11.4711	14.1212	15.8413	11.7495	16.1533
11.2978	13.4815	13.1131	14.3491	12.2298
12.996	12.2981	16.2918	12.4376	11.245
13.5004	8.9482	11.2536	12.7095	15.6072
12.271	11.6239	15.0781	12.4516	12.1037
12.3048	13.7143	12.4944	10.0029	12.5172
14.7169	15.3583	13.7486	12.8195	9.8532
9.8205	15.2794	13.481	11.6304	14.8217
12.8999	14.8704	14.058	13.2465	9.382
12.0035	12.8144	13.09	11.1534	15.0032

Vosges		Sample: ZTG-1-24	
ζ = 345.69 ± 8.75		Dated mineral: apatite	
Irrad. code: BS-37	Rho_d: 12.4856	Dosimeter glass: CN5	
Grid unit: 63.03	N_d: 3882		

Cryst	N_s	N_i	Area	Rho_s	Rho_i	Age [Ma]	σ	U [ppm]
1	7	30	20	5.553	23.798	50.16	21.11	23.2
2	22	39	32	10.908	19.336	120.6	32.36	18.85
3	11	23	15	11.635	24.327	102.39	37.66	23.71
4	22	51	32	10.908	25.286	92.43	23.74	24.65
5	20	61	12	26.442	80.649	70.37	18.25	78.61
6	16	54	36	7.051	23.798	63.63	18.21	23.2
7	23	36	28	13.032	20.398	136.42	36.65	19.88
8	26	72	64	6.445	17.849	77.46	17.88	17.4
9	18	90	50	5.712	28.558	43.02	11.18	27.84
10	18	44	24	11.899	29.087	87.69	24.67	28.35
11	23	82	49	7.447	26.55	60.25	14.33	25.88
12	46	115	100	7.298	18.245	85.75	15.18	17.78
13	24	73	50	7.615	23.164	70.56	16.74	22.58
14	68	232	36	29.968	102.244	62.95	8.88	99.66
15	15	42	25	9.519	26.654	76.62	23.16	25.98
16	77	159	100	12.216	25.226	103.67	14.73	24.59
17	22	59	24	14.543	39.003	79.97	20.12	38.02
18	26	77	25	16.5	48.866	72.46	16.58	47.63
19	24	79	50	7.615	25.067	65.23	15.33	24.43
20	36	151	100	5.712	23.957	51.25	9.63	23.35

Confined track lengths:

10.7386	8.2363	13.4764	11.0684	10.1941
12.1778	13.328	12.4671	10.3464	6.6767
10.1825	10.8383	11.8643	7.6532	13.5229
11.9424	13.3294	13.2826	11.3078	8.2888
13.0944	9.7653	10.9458	12.8997	8.8794
9.8078	13.1476	8.2512	10.3744	11.9972
11.5039	4.2177	12.0985	11.5132	11.1184
9.2399	6.5265	9.2135	7.4782	12.7512
10.3108	11.4005	10.0312	5.032	10.9371
12.5573	10.6352	10.1456	8.1938	10.7544
12.8094	7.5081	12.1125	9.3908	13.4878
11.2141	7.7146	11.2719	12.252	14.2688
8.4356	8.478	14.4558	9.6087	11.2394
8.6696	8.4546	9.8625	11.7918	15.6859
14.4097	10.1686	8.2053	12.6313	15.144
11.2721	12.1669	11.0216	7.3589	11.8406
10.8548	11.7395	10.0483	6.7063	10.458
14.5027	12.2991	13.7709	9.8328	11.5617
12.5607	9.8244	8.5614	7.6112	9.2099
14.4845	8.4616	11.2677	5.607	13.1568

Vosges		Sample: ZTG-1-25	
ζ = 345.69 ± 8.75		Dated mineral: apatite	
Irrad. code: BS-37	Rho_d: 12.1892	Dosimeter glass: CN5	
Grid unit: 63.03	N_d: 3882		

Cryst	N_s	N_i	Area	Rho_s	Rho_i	Age [Ma]	σ	U [ppm]
1	14	40	25	8.885	25.385	73.32	22.87	25.34
2	22	50	18	19.391	44.071	92.04	23.71	44
3	22	115	50	6.981	36.491	40.18	9.43	36.43
4	15	22	20	11.899	17.452	142.07	47.76	17.42
5	10	34	25	6.346	21.577	61.67	22.26	21.54
6	9	43	25	5.712	27.289	43.95	16.16	27.25
7	14	46	20	11.106	36.491	63.8	19.57	36.43
8	65	214	50	20.625	67.904	63.68	9.22	67.8
9	46	173	50	14.596	54.894	55.78	9.4	54.81
10	15	43	24	9.916	28.426	73.08	22.02	28.38
11	25	74	10	39.664	117.404	70.79	16.51	117.22
12	19	95	70	4.306	21.532	42	10.63	21.5
13	10	31	25	6.346	19.673	67.61	24.67	19.64
14	7	21	9	12.34	37.019	69.85	30.56	36.96
15	61	445	100	9.678	70.601	28.82	4.03	70.49
16	8	29	20	6.346	23.005	57.86	23.17	22.97
17	7	21	18	6.17	18.51	69.85	30.56	18.48
18	17	39	16	16.857	38.672	91.19	26.64	38.61
19	22	76	36	9.696	33.494	60.7	14.81	33.44
20	8	28	25	5.077	17.769	59.92	24.09	17.74

Confined track lengths:

10.1699	14.6737	7.6972	11.2806	10.7412
7.7786	14.4975	10.5711	10.7313	10.3846
12.9268	8.2954	10.8305	10.1806	10.0408
10.9235	9.1413	11.5224	12.3249	9.4659
14.4566	8.7786	9.6425	12.6246	13.0884
12.2541	7.6037	9.0726	9.8938	15.3257
10.1574	9.9852	10.297	11.8196	14.4108
9.9197	10.3108	13.5493	9.3518	9.914
12.5046	12.6446	6.8635	9.0272	9.7586
13.9617	13.8703	6.6925	13.0801	10.1509
9.165	8.6606	9.5651	10.2621	13.6936
8.5685	12.0813	9.058	7.6828	9.7149
9.2888	7.6316	14.7347	7.3865	12.9863
10.116	14.4873	8.8517	13.2197	10.969
8.242	8.0929	8.2145	12.2072	12.2895
12.0367	12.2126	11.0306	9.4129	9.0986
8.5894	11.4391	13.8858	13.5592	11.6525
11.3345	8.7635	12.2975	11.8406	8.8812
14.3844	9.6474	13.3379	7.9837	6.9002
13.027	11.8716	7.4681	13.7005	7.4997

Vosges — Sample: ZTG-1-26

ζ = 345.69 ± 8.75 — Dated mineral: apatite

Irrad. code: BS-37 — Rho_d: 11.8929 — Dosimeter glass: CN5

Grid unit: 63.03 — N_d: 3882

Cryst	N_s	N_i	Area	Rho_s	Rho_i	Age [Ma]	σ	U [ppm]
1	45	57	32	22.311	28.26	160.28	32.32	28.92
2	25	88	16	24.79	87.26	58.14	13.29	89.29
3	16	35	12	21.154	46.274	93.29	28.29	47.35

4	17	84	20	13.486	66.635	41.47	11.1	68.19
5	8	21	20	6.346	16.659	77.84	32.42	17.05
6	11	29	16	10.908	28.756	77.5	27.54	29.43
7	28	71	36	12.34	31.29	80.56	18.14	32.02
8	22	58	20	17.452	46.01	77.5	19.54	47.08
9	18	104	25	11.423	66	35.48	9.12	67.54
10	54	225	49	17.484	72.852	49.15	7.59	74.55
11	22	41	25	13.962	26.019	109.37	29.09	26.63
12	40	132	30	21.154	69.808	61.99	11.34	71.43
13	59	137	36	26.002	60.377	87.92	13.94	61.78
14	39	146	16	38.672	144.772	54.68	9.99	148.15
15	18	26	15	19.039	27.5	140.76	43.37	28.14
16	103	313	36	45.393	137.941	67.29	7.91	141.16
17	35	70	32	17.353	34.706	101.97	21.33	35.51
18	12	56	20	9.519	44.423	43.9	14.03	45.46
19	14	78	18	12.34	68.75	36.79	10.74	70.35
20	15	48	12	19.832	63.462	63.92	19	64.94

Confined track lengths:

11.4803	9.5293	12.4142
8.2729	8.5025	10.3484
11.4748	10.2991	9.6828
11.5617	10.6538	8.7713
9.2847	11.4373	10.3364
15.3261	12.0803	10.1648
9.9404	6.2017	14.7681
7.3996	12.83	10.4411
9.5204	11.3906	12.6835
10.4988	9.6867	8.6862
9.327	7.0881	8.234
8.6957	7.3213	10.2068
10.6041	10.9173	11.9911
6.3688	9.7615	11.7244
6.7358	8.4364	10.1941
5.3502	9.2511	9.6477
9.6877	11.0641	10.305
10.7894	10.9166	13.9184
7.6828	11.3488	12.367
10.668	12.2712	10.2513
11.6525	8.1687	10.4866
11.9665	9.8826	8.3082
9.2748	10.2241	12.0155
7.8466	12.2556	10.5584
8.0288	11.4649	10.7227
7.843	10.2936	8.1987
10.1762	11.8835	11.8196
11.9635	8.2652	7.6112
11.9822	7.0604	
6.516	9.0322	
9.4896	13.2042	
8.7127	13.5257	
7.8167	9.4809	
8.931	13.7347	
11.4119	12.3067	
8.1534	7.4659	

Vosges			Sample: ZTG-1-27				
ζ = 345.69 ± 8.75			Dated mineral: apatite				
Irrad. code: BS-38	Rho_d: 9.7016		Dosimeter glass: CN5				
Grid unit: 63.03	N_d: 3690						
Cryst	N_s	N_i	Area	Rho_s	Rho_i	Age [Ma]	σ	U [ppm]
1	32	115	42	12.088	43.441	46.49	9.4	54.49
2	40	93	36	17.628	40.986	71.72	13.73	51.41
3	17	43	15	17.981	45.481	65.96	19	57.05
4	32	87	42	12.088	32.864	61.38	12.83	41.23
5	26	107	25	16.5	67.904	40.62	8.97	85.18
6	14	48	49	4.533	15.542	48.72	14.87	19.5
7	22	108	20	17.452	85.673	34.07	8.04	107.47
8	13	34	24	8.594	22.476	63.8	20.89	28.19
9	15	52	24	9.916	34.375	48.19	14.2	43.12
10	21	98	24	13.882	64.784	35.83	8.68	81.27
11	17	38	25	10.789	24.116	74.58	21.88	30.25
12	20	57	20	15.865	45.217	58.57	15.32	56.72
13	27	79	25	17.135	50.135	57.06	12.84	62.89
14	30	65	25	19.039	41.25	76.93	17.14	51.75
15	12	33	20	9.519	26.178	60.69	20.54	32.84
16	19	37	48	6.28	12.23	85.54	24.28	15.34
17	37	86	25	23.481	54.577	71.74	14.27	68.46
18	20	39	32	9.916	19.336	85.42	23.64	24.26
19	31	52	20	24.591	41.25	99.2	22.71	51.75
20	26	42	25	16.5	26.654	102.98	25.89	33.44

Confined track lengths:

10.6352	12.0013	14.2442	11.7113	11.6142
7.8044	12.075	12.2606	13.057	12.7864
11.0454	9.8854	10.8904	10.8294	8.0999
10.1425	8.2004	11.8172	8.2409	15.8537
10.8698	10.5854	12.2062	9.8205	11.8613
11.924	8.7936	14.1118	7.7293	13.234
13.9801	11.6479	11.5663	10.2513	11.5236
12.2975	11.082	11.8716	14.0555	12.007
13.9534	12.4577	12.8431	14.0407	
11.5867	8.9432	11.5721	13.5917	
11.0537	8.7705	14.8203	9.4806	
10.8748	10.8049	11.772	14.5257	
14.8394	13.3294	9.4077	13.6195	
12.1351	12.1055	13.4465	8.7856	
9.1825	11.2769	13.0154	11.9471	
13.0422	10.3758	12.2101	14.39	
14.9208	10.8522	13.408	10.022	
12.0052	9.7011	10.3703	13.8012	
11.4051	12.9479	11.5361	10.4718	
12.6397	14.3598	10.8581	11.8631	
13.849	13.769	9.6906	10.201	
11.4299	12.3662	11.8182	12.4944	
13.1018	15.9482	13.6905	9.774	

Vosges — Sample: ZTG-1-01
ζ = 113.49 ± 1.8 — Dated mineral: zircon
Irrad. code: BS-39 — Rho_d: 4.0071 — Dosimeter glass: CN1
Grid unit: 24.4 — N_d: 1660

Cryst	N_s	N_i	Area	Rho_s	Rho_i	Age [Ma]	σ	U [ppm]
1	189	17	18	430.328	38.707	247.97	63.2	384.45
2	36	5	9	163.934	22.769	161.67	77.3	226.15
3	47	7	4	481.557	71.721	150.89	61.29	712.36
4	46	9	6	314.208	61.475	115.18	42.12	610.6

Vosges — Sample: ZTG-1-02
ζ = 113.49 ± 1.8 — Dated mineral: zircon
Irrad. code: BS-39 — Rho_d: 4.1157 — Dosimeter glass: CN1
Grid unit: 24.4 — N_d: 1660

Cryst	N_s	N_i	Area	Rho_s	Rho_i	Age [Ma]	σ	U [ppm]
1	41	4	6	280.055	27.322	235.05	123.31	264.22
2	78	5	9	355.191	22.769	354.41	163.82	220.18
3	67	4	9	305.1	18.215	379.78	195.79	176.14
4	66	7	6	450.82	47.814	216.52	86.3	462.38
5	61	7	12	208.333	23.907	200.37	80.17	231.19
6	24	4	4	245.902	40.984	138.63	74.98	396.32
7	60	5	9	273.224	22.769	274.33	127.95	220.18
8	42	9	3	573.77	122.951	108.08	39.82	1188.97
9	103	8	12	351.776	27.322	293.89	108.21	264.22
10	75	12	6	512.295	81.967	144.34	45.07	792.65
11	42	3	3	573.77	40.984	318.94	190.83	396.32
12	41	5	5	336.066	40.984	188.72	89.57	396.32
13	48	14	4	491.803	143.443	79.58	24.28	1387.13
14	40	9	10	163.934	36.885	102.97	38.11	356.69
15	63	4	4	645.492	40.984	357.72	184.75	396.32
16	44	3	4	450.82	30.738	333.74	199.39	297.24
17	120	10	16	307.377	25.615	274.33	90.65	247.7

Vosges — Sample: ZTG-1-03
ζ = 113.49 ± 1.8 — Dated mineral: zircon
Irrad. code: BS-39 — Rho_d: 4.1002 — Dosimeter glass: CN1
Grid unit: 24.4 — N_d: 1660

Cryst	N_s	N_i	Area	Rho_s	Rho_i	Age [Ma]	σ	U [ppm]
1	64	7	15	174.863	19.126	209.29	83.54	185.65
2	64	12	8	327.869	61.475	122.91	38.83	596.73
3	24	3	3	327.869	40.984	183.5	112.5	397.82
4	38	11	6	259.563	75.137	79.88	27.45	729.34
5	56	10	4	573.77	102.459	128.99	44.44	994.55
6	135	12	16	345.799	30.738	256.57	77.65	298.37
7	87	12	9	396.175	54.645	166.51	51.51	530.43
8	74	6	15	202.186	16.393	280.75	119.45	159.13
9	56	9	4	573.77	92.213	143.17	51.58	895.1
10	63	10	6	430.328	68.306	144.94	49.52	663.04
11	58	10	9	264.117	45.537	133.55	45.9	442.02
12	48	11	9	218.579	50.091	100.74	33.8	486.23
13	14	2	3	191.257	27.322	160.84	121.68	265.21

14	128	15	16	327.869	38.422	195.55	53.67	372.96
15	91	11	8	466.189	56.352	189.66	60.8	547

Vosges — Sample: ZTG-1-07
ζ = 113.49 ± 1.8 — Dated mineral: zircon
Irrad. code: BS-39 — Rho_d: 3.976 — Dosimeter glass: CN1
Grid unit: 24.4 — N_d: 1660

Cryst	N_s	N_i	Area	Rho_s	Rho_i	Age [Ma]	σ	U [ppm]
1	63	8	4	645.492	81.967	175.27	65.98	820.5
2	27	4	3	368.852	54.645	150.52	80.76	547
3	98	11	8	502.049	56.352	197.94	63.21	564.09
4	26	3	4	266.393	30.738	192.63	117.59	307.69
5	86	13	8	440.574	66.598	147.55	44.12	666.65
6	110	11	10	450.82	45.082	221.76	70.43	451.27

Vosges — Sample: ZTG-1-08
ζ = 113.49 ± 1.8 — Dated mineral: zircon
Irrad. code: BS-39 — Rho_d: 4.0692 — Dosimeter glass: CN1
Grid unit: 24.4 — N_d: 1660

Cryst	N_s	N_i	Area	Rho_s	Rho_i	Age [Ma]	σ	U [ppm]
1	38	3	4	389.344	30.738	286.04	171.74	300.64
2	63	5	4	645.492	51.23	284.57	132.48	501.07
3	61	5	4	625	51.23	275.72	128.51	501.07
4	74	5	4	758.197	51.23	332.99	154.17	501.07
5	49	3	6	334.699	20.492	366.53	218.26	200.43
6	41	3	4	420.082	30.738	308.09	184.49	300.64
7	53	8	6	362.022	54.645	151.19	57.52	534.47
8	45	7	4	461.066	71.721	146.76	59.78	701.49
9	42	4	4	430.328	40.984	238	124.73	400.85
10	25	8	4	256.148	81.967	71.76	29.22	801.7
11	78	8	6	532.787	54.645	221.29	82.41	534.47
12	33	3	3	450.82	40.984	249.12	150.4	400.85
13	50	4	4	512.295	40.984	282.36	146.95	400.85
14	29	2	4	297.131	20.492	326.41	238.82	200.43
15	57	7	4	584.016	71.721	185.33	74.42	701.49
16	27	2	4	276.639	20.492	304.42	223.27	200.43
17	38	4	4	389.344	40.984	215.71	113.57	400.85
18	83	10	8	425.205	51.23	188.86	63.46	501.07
19	29	4	4	297.131	40.984	165.27	88.28	400.85
20	85	6	6	580.601	40.984	319.09	135.11	400.85

Vosges — Sample: ZTG-1-09
ζ = 113.49 ± 1.8 — Dated mineral: zircon
Irrad. code: BS-39 — Rho_d: 3.9916 — Dosimeter glass: CN1
Grid unit: 24.4 — N_d: 1660

Cryst	N_s	N_i	Area	Rho_s	Rho_i	Age [Ma]	σ	U [ppm]
1	16	2	4	163.934	20.492	178.7	134.13	204.32
2	24	3	2	491.803	61.475	178.7	109.56	612.97
3	53	5	6	362.022	34.153	235.73	110.5	340.54
4	58	9	12	198.087	30.738	144.34	51.88	306.48
5	59	7	4	604.508	71.721	188.14	75.41	715.13

6	33	5	4	338.115	51.23	147.79	71.05	510.81
7	50	6	4	512.295	61.475	186.04	80.56	612.97
8	51	4	4	522.541	40.984	282.51	146.92	408.65
9	32	5	4	327.869	51.23	143.36	69.06	510.81
10	57	5	4	584.016	51.23	253.18	118.32	510.81
11	42	6	4	430.328	61.475	156.63	68.51	612.97
12	45	6	6	307.377	40.984	167.68	73.04	408.65
13	79	11	9	359.745	50.091	160.65	51.91	499.46
14	42	5	2	860.656	102.459	187.51	88.88	1021.61
15	74	9	6	505.464	61.475	183.6	65.04	612.97
16	32	5	4	327.869	51.23	143.36	69.06	510.81
17	54	8	12	184.426	27.322	151.1	57.41	272.43
18	103	10	8	527.664	51.23	229.18	76.2	510.81
19	10	2	2	204.918	40.984	112.27	87.02	408.65
20	55	7	6	375.683	47.814	175.55	70.64	476.75

Vosges — Sample: ZTG-1-10
ζ = 113.49 ± 1.8 — Dated mineral: zircon
Irrad. code: BS-39 — Rho_d: 4.1468 — Dosimeter glass: CN1
Grid unit: 24.4 — N_d: 1660

Cryst	N_s	N_i	Area	Rho_s	Rho_i	Age [Ma]	σ	U [ppm]
1	17	2	2	348.361	40.984	196.97	147.36	393.35
2	85	7	6	580.601	47.814	279.58	110.24	458.91
3	23	3	2	471.311	61.475	177.93	109.34	590.03
4	84	7	4	860.656	71.721	276.36	109.02	688.36
5	60	8	6	409.836	54.645	174.11	65.73	524.47
6	46	3	3	628.415	40.984	351.07	209.45	393.35
7	44	6	9	200.364	27.322	170.29	74.28	262.23

Vosges — Sample: ZTG-1-23
ζ = 113.49 ± 1.8 — Dated mineral: zircon
Irrad. code: BS-32 — Rho_d: 4.38 — Dosimeter glass: CN1
Grid unit: 24.4 — N_d: 1503

Cryst	N_s	N_i	Area	Rho_s	Rho_i	Age [Ma]	σ	U [ppm]
1	64	7	5	524.59	57.377	223.33	89.16	521.37
2	107	14	12	365.437	47.814	187.21	53.51	434.48
3	38	3	2	778.689	61.475	307.38	184.57	558.61
4	33	8	4	338.115	81.967	101.72	40.2	744.82
5	48	12	4	491.803	122.951	98.66	31.98	1117.22
6	92	5	10	377.049	20.492	441.83	203.33	186.2
7	52	5	4	532.787	51.23	253.44	118.91	465.51
8	53	4	6	362.022	27.322	321.18	166.83	248.27
9	77	15	8	394.467	76.844	126.34	35.86	698.27
10	64	7	5	524.59	57.377	223.33	89.16	521.37
11	99	8	9	450.82	36.43	300.46	110.81	331.03

Vosges — Sample: ZTG-1-24
ζ = 113.49 ± 1.8 — Dated mineral: zircon
Irrad. code: BS-32 — Rho_d: 4.36 — Dosimeter glass: CN1
Grid unit: 24.4 — N_d: 1503

Cryst	N_s	N_i	Area	Rho_s	Rho_i	Age [Ma]	σ	U [ppm]
1	27	3	2	553.279	61.475	218.91	133.39	561.17
2	26	5	3	355.191	68.306	127.39	62.32	623.53
3	92	7	4	942.623	71.721	317.23	124.75	654.7
4	64	5	5	524.59	40.984	309.15	143.86	374.12

Vosges — Sample: ZTG-1-25
$\zeta = 113.49 \pm 1.8$ — Dated mineral: zircon
Irrad. code: BS-39 — Rho_d: 4.0847 — Dosimeter glass: CN1
Grid unit: 24.4 — N_d: 1660

Cryst	N_s	N_i	Area	Rho_s	Rho_i	Age [Ma]	σ	U [ppm]
1	117	16	15	319.672	43.716	167.3	44.86	425.95
2	64	7	4	655.738	71.721	208.51	83.23	698.83
3	18	2	2	368.852	40.984	205.3	153.14	399.33
4	79	8	4	809.426	81.967	224.92	83.71	798.66
5	77	11	6	525.956	75.137	160.24	51.86	732.11
6	19	4	3	259.563	54.645	109.17	60.14	532.44
7	13	2	2	266.393	40.984	148.93	113.2	399.33
8	48	8	6	327.869	54.645	137.59	52.7	532.44
9	131	14	9	596.539	63.752	213.32	60.3	621.18
10	43	5	4	440.574	51.23	196.32	92.94	499.16
11	28	4	2	573.77	81.967	160.24	85.78	798.66

Vosges — Sample: ZTG-1-27
$\zeta = 113.49 \pm 1.8$ — Dated mineral: zircon
Irrad. code: BS-32 — Rho_d: 4.1313 — Dosimeter glass: CN1
Grid unit: 24.4 — N_d: 1503

Cryst	N_s	N_i	Area	Rho_s	Rho_i	Age [Ma]	σ	U [ppm]
1	24	4	3	327.869	54.645	139.15	75.27	526.44
2	40	5	6	273.224	34.153	184.87	87.87	329.02
3	26	4	3	355.191	54.645	150.61	81.02	526.44
4	84	5	8	430.328	25.615	382.28	176.36	246.77
5	45	8	6	307.377	54.645	130.54	50.24	526.44
6	40	3	3	546.448	40.984	305.23	182.95	394.83
7	80	5	6	546.448	34.153	364.58	168.43	329.02
8	40	4	4	409.836	40.984	230.27	120.95	394.83
9	35	3	3	478.142	40.984	267.86	161.34	394.83
10	52	6	5	426.23	49.18	200.04	86.46	473.79
11	18	2	2	368.852	40.984	207.61	154.87	394.83
12	33	4	3	450.82	54.645	190.56	101.05	526.44
13	14	2	2	286.885	40.984	162.05	122.59	394.83
14	19	2	2	389.344	40.984	218.95	162.9	394.83
15	74	7	8	379.098	35.861	243.18	96.44	345.47
16	64	5	4	655.738	51.23	293.3	136.48	493.53
17	52	5	6	355.191	34.153	239.31	112.28	329.02
18	31	6	4	317.623	61.475	120	53.64	592.24
19	42	6	4	430.328	61.475	162.05	70.89	592.24
20	23	2	2	471.311	40.984	264.11	194.87	394.83

3. Zircon and apatite FT data of four borehole samples from northern Switzerland

These data are interpreted in Chapter IV of the thesis.

Kaisten — Sample: Kai1
ζ = 113.49 ± 1.8 — Dated mineral: zircon
Irrad. code: BS-28 — Rho_d: 3.9378 — Dosimeter glass: CN1
Grid unit: 24.4 μm^2 — N_d: 1587

Cryst	N_s	N_i	Area	Rho_s	Rho_i	Age [Ma]	σ	U [ppm]
1	105	11	20	215.164	22.541	209.84	66.79	227.83
2	208	14	36	236.794	15.938	323.72	89.9	161.09
3	160	11	21	312.256	21.468	317.09	99.29	216.98
4	126	17	25	206.557	27.869	163.52	42.53	281.68
5	47	3	6	321.038	20.492	340.9	203.25	207.11
6	75	5	16	192.111	12.807	326.75	151.23	129.45
7	43	7	6	293.716	47.814	135.82	55.5	483.27
8	66	6	9	300.546	27.322	241.23	103.11	276.15
9	68	4	9	309.654	18.215	369.09	190.21	184.1
10	187	14	40	191.598	14.344	291.76	81.31	144.98
11	71	4	9	323.315	18.215	384.9	198.13	184.1
12	59	4	16	151.127	10.246	321.44	166.35	103.56
13	50	7	15	136.612	19.126	157.66	63.8	193.31
14	72	11	16	184.426	28.176	144.62	47.01	284.78
15	83	7	12	283.47	23.907	259.65	102.48	241.63
16	109	14	12	372.268	47.814	171.67	49	483.27
17	51	6	9	232.24	27.322	187.19	80.98	276.15
18	116	6	12	396.175	20.492	418.14	175.51	207.11
19	58	6	16	148.566	15.369	212.46	91.33	155.34
20	58	5	8	297.131	25.615	254.13	118.69	258.89

Kaisten — Sample: Kai4
ζ = 113.49 ± 1.8 — Dated mineral: zircon
Irrad. code: BS-28 — Rho_d: 3.884 — Dosimeter glass: CN1
Grid unit: 24.4 μm^2 — N_d: 1587

Cryst	N_s	N_i	Area	Rho_s	Rho_i	Age [Ma]	σ	U [ppm]
1	44	5	9	200.364	22.769	191.09	90.36	233.31
2	79	11	10	323.77	45.082	156.37	50.54	461.96
3	163	10	25	267.213	16.393	349.59	114.36	167.99
4	56	7	9	255.009	31.876	173.95	69.93	326.64
5	124	8	20	254.098	16.393	332.87	121.83	167.99
6	105	12	16	268.955	30.738	190.02	58.18	314.97
7	60	5	16	153.689	12.807	259.2	120.89	131.24
8	65	4	25	106.557	6.557	348.55	179.86	67.19
9	74	12	16	189.549	30.738	134.5	42.05	314.97
10	28	3	9	127.505	13.661	202.49	123.16	139.99
11	58	6	12	198.087	20.492	209.61	90.1	209.98
12	66	6	16	169.057	15.369	237.99	101.72	157.49
13	82	8	25	134.426	13.115	222.04	82.51	134.39
14	73	9	9	332.423	40.984	176.33	62.52	419.97
15	114	10	24	194.672	17.077	246.48	81.62	174.99
16	48	3	12	163.934	10.246	343.33	204.58	104.99
17	102	11	25	167.213	18.033	201.2	64.13	184.78
18	102	10	12	348.361	34.153	220.97	73.52	349.97

19	85	5	15	232.24	13.661	364.19	167.94	139.99
20	108	7	15	295.082	19.126	331.38	129.62	195.98

Riniken — Sample: Rin1
ζ = 113.49 ± 1.8 — Dated mineral: zircon
Irrad. code: BS-28 — Rho_d: 4.1889 — Dosimeter glass: CN1
Grid unit: 24.4 μm^2 — N_d: 1587

Cryst	N_s	N_i	Area	Rho_s	Rho_i	Age [Ma]	σ	U [ppm]
1	148	12	12	505.464	40.984	286.69	86.47	389.4
2	181	11	20	370.902	22.541	379.72	118.45	214.17
3	187	11	20	383.197	22.541	391.93	122.15	214.17
4	133	10	16	340.676	25.615	308.63	101.61	243.37
5	160	8	16	409.836	20.492	458.69	166.73	194.7
6	168	11	25	275.41	18.033	353.18	110.42	171.33
7	203	13	30	277.322	17.76	360.88	103.8	168.74
8	116	9	16	297.131	23.053	299.31	103.95	219.04
9	62	6	12	211.749	20.492	241.06	103.31	194.7
10	217	17	25	355.738	27.869	296.49	75.19	264.79
11	218	20	25	357.377	32.787	254.02	59.83	311.52
12	94	12	16	240.779	30.738	183.56	56.53	292.05
13	113	11	16	289.447	28.176	239.67	76.03	267.71
14	192	21	25	314.754	34.426	213.74	49.54	327.09
15	144	13	16	368.852	33.299	258.06	75.13	316.39
16	119	11	16	304.816	28.176	252.15	79.81	267.71
17	202	22	25	331.148	36.066	214.64	48.61	342.67
18	90	6	12	307.377	20.492	347.04	146.69	194.7
19	143	9	15	390.71	24.59	367.03	126.6	233.64
20	95	9	9	432.605	40.984	246.14	86.16	389.4

Riniken — Sample: Rin2
ζ = 113.49 ± 1.8 — Dated mineral: zircon
Irrad. code: BS-28 — Rho_d: 4.153 — Dosimeter glass: CN1
Grid unit: 24.4 μm^2 — N_d: 1587

Cryst	N_s	N_i	Area	Rho_s	Rho_i	Age [Ma]	σ	U [ppm]
1	564	65	100	231.148	26.639	201.31	27.04	255.3
2	940	100	100	385.246	40.984	217.8	23.8	392.76
3	94	6	12	321.038	20.492	359.02	151.55	196.38
4	178	11	36	202.641	12.523	370.49	115.63	120.01
5	468	37	36	532.787	42.122	291.39	50.51	403.67
6	69	9	9	314.208	40.984	178.19	63.37	392.76
7	122	14	16	312.5	35.861	202.16	57.36	343.67
8	249	21	25	408.197	34.426	273.54	62.69	329.92
9	36	3	5	295.082	24.59	276.77	166.52	235.66
10	74	11	12	252.732	37.568	156.62	50.82	360.03
11	165	18	16	422.643	46.107	212.48	53.12	441.86
12	335	22	36	381.375	25.046	349.22	77.56	240.02
13	105	11	10	430.328	45.082	221.11	70.38	432.04
14	200	16	16	512.295	40.984	288.05	75.32	392.76
15	257	26	25	421.311	42.623	228.83	47.58	408.47
16	289	28	25	473.77	45.902	238.76	47.79	439.9
17	63	10	12	215.164	34.153	146.78	50.15	327.3
18	150	12	18	341.53	27.322	288.05	86.84	261.84

19	77	14	16	197.234	35.861	128.33	37.48	343.67
20	217	19	20	444.672	38.934	263.68	63.57	373.13

Riniken — Sample: Rin3

ζ = 113.49 ± 1.8 — Dated mineral: zircon

Irrad. code: BS-28 — Rho_d: 4.1172 — Dosimeter glass: CN1

Grid unit: 24.4 μm^2 — N_d: 1587

Cryst	N_s	N_i	Area	Rho_s	Rho_i	Age [Ma]	σ	U [ppm]
1	158	11	25	259.016	18.033	327.14	102.47	174.32
2	40	4	5	327.869	32.787	229.5	120.54	316.94
3	55	5	9	250.455	22.769	252	117.95	220.1
4	145	12	16	371.414	30.738	276.3	83.4	297.13
5	243	22	28	355.679	32.201	253.02	56.83	311.28
6	165	22	20	338.115	45.082	172.88	39.57	435.8
7	84	9	10	344.262	36.885	214.45	75.48	356.56
8	110	12	16	281.762	30.738	210.68	64.35	297.13
9	152	14	16	389.344	35.861	248.79	69.88	346.66
10	128	6	12	437.158	20.492	480.08	201.04	198.09
11	128	12	15	349.727	32.787	244.51	74.17	316.94
12	142	11	18	323.315	25.046	294.75	92.66	242.11
13	98	10	12	334.699	34.153	224.99	74.99	330.15
14	62	4	6	423.497	27.322	352.32	182.06	264.12
15	75	11	9	341.53	50.091	157.36	51.02	484.22
16	51	4	8	261.27	20.492	291.2	151.45	198.09
17	117	12	16	299.693	30.738	223.86	68.18	297.13
18	69	11	8	353.484	56.352	144.91	47.24	544.75
19	110	7	12	375.683	23.907	357.06	139.59	231.1
20	197	18	30	269.126	24.59	250.75	62.19	237.71

Riniken — Sample: Rin4

ζ = 113.49 ± 1.8 — Dated mineral: zircon

Irrad. code: BS-28 — Rho_d: 4.0813 — Dosimeter glass: CN1

Grid unit: 24.4 μm^2 — N_d: 1587

Cryst	N_s	N_i	Area	Rho_s	Rho_i	Age [Ma]	σ	U [ppm]
1	77	5	12	262.978	17.077	347.14	160.54	166.53
2	70	4	12	239.071	13.661	393.06	202.4	133.22
3	115	16	15	314.208	43.716	164.34	44.12	426.31
4	99	6	12	338.115	20.492	371.23	156.47	199.83
5	53	4	6	362.022	27.322	299.78	155.7	266.44
6	197	17	24	336.407	29.03	262.94	66.92	283.1
7	241	18	40	246.926	18.443	302.85	74.54	179.85
8	122	10	21	238.095	19.516	276.53	91.33	190.32
9	97	12	12	331.284	40.984	184.54	56.74	399.66
10	134	11	25	219.672	18.033	276.12	86.99	175.85
11	137	10	16	350.922	25.615	309.72	101.87	249.79
12	152	6	50	124.59	4.918	561.52	234.31	47.96
13	229	18	40	234.631	18.443	288.1	71.04	179.85
14	185	14	24	315.915	23.907	298.99	83.35	233.14
15	81	7	12	276.639	23.907	262.57	103.73	233.14
16	98	9	10	401.639	36.885	247.37	86.47	359.7
17	46	4	8	235.656	20.492	260.98	136.26	199.83
18	72	4	10	295.082	16.393	403.94	207.85	159.87

19	166	16	15	453.552	43.716	235.91	62.15	426.31
20	82	7	20	168.033	14.344	265.74	104.94	139.88

Riniken — Sample: Rin5

ζ = 113.49 $\pm$ 1.8 — Dated mineral: zircon

Irrad. code: BS-28 — Rho_d: 4.0454 — Dosimeter glass: CN1

Grid unit: 24.4 μm^2 — N_d: 1587

Cryst	N_s	N_i	Area	Rho_s	Rho_i	Age [Ma]	σ	U [ppm]
1	94	7	9	428.051	31.876	301.12	118.31	313.61
2	75	5	8	384.221	25.615	335.45	155.26	252.01
3	65	6	6	443.989	40.984	244.01	104.36	403.21
4	54	5	6	368.852	34.153	243.27	113.95	336.01
5	151	12	16	386.783	30.738	282.57	85.17	302.41
6	139	7	21	271.272	13.661	440.44	171.11	134.4
7	41	7	8	210.041	35.861	133.07	54.56	352.81
8	68	8	8	348.361	40.984	192.23	72.08	403.21
9	90	5	9	409.836	22.769	400.5	184.4	224.01
10	68	7	12	232.24	23.907	219.23	87.26	235.21
11	130	11	16	332.992	28.176	265.74	83.82	277.21
12	192	15	25	314.754	24.59	287.33	77.5	241.93
13	72	6	16	184.426	15.369	269.74	114.9	151.2
14	70	7	8	358.607	35.861	225.56	89.67	352.81
15	62	5	6	423.497	34.153	278.54	129.76	336.01
16	66	6	16	169.057	15.369	247.69	105.87	151.2
17	56	5	6	382.514	34.153	252.11	117.91	336.01
18	45	5	8	230.533	25.615	203.36	96.05	252.01
19	69	6	9	314.208	27.322	258.73	110.39	268.81
20	65	6	10	266.393	24.59	244.01	104.36	241.93

Leuggern — Sample: Leu1

ζ = 113.49 $\pm$ 1.8 — Dated mineral: zircon

Irrad. code: BS-32 — Rho_d: 4.3679 — Dosimeter glass: CN1

Grid unit: 24.4 μm^2 — N_d: 1503

Cryst	N_s	N_i	Area	Rho_s	Rho_i	Age [Ma]	σ	U [ppm]
1	117	14	12	399.59	47.814	203.88	57.99	435.68
2	95	7	12	324.454	23.907	327.89	128.8	217.84
3	65	9	9	295.993	40.984	176.57	63.03	373.44
4	146	10	16	373.975	25.615	352.08	115.58	233.4
5	73	5	12	249.317	17.077	352.08	163.11	155.6
6	47	3	6	321.038	20.492	377.06	224.83	186.72
7	137	12	16	350.922	30.738	276.93	83.79	280.08
8	142	10	9	646.63	45.537	342.68	112.6	414.93
9	185	21	25	303.279	34.426	214.73	49.87	313.69
10	191	21	20	391.393	43.033	221.58	51.38	392.11
11	69	9	15	188.525	24.59	187.28	66.61	224.06
12	62	9	9	282.332	40.984	168.52	60.33	373.44
13	85	8	10	348.361	32.787	258.11	95.77	298.75
14	199	19	30	271.858	25.956	254.51	61.6	236.51
15	56	4	9	255.009	18.215	337.98	175.22	165.97
16	102	9	9	464.481	40.984	274.96	95.97	373.44
17	73	8	6	498.634	54.645	222.29	83.06	497.92
18	75	13	10	307.377	53.279	141.43	42.71	485.47

19	100	12	15	273.224	32.787	203.31	62.42	298.75
20	158	13	25	259.016	21.311	294.41	85.42	194.19

Leuggern — Sample: Leu3

ζ = 113.49 ± 1.8 — Dated mineral: zircon

Irrad. code: BS-32 — Rho_d: 4.3117 — Dosimeter glass: CN1

Grid unit: 24.4 μm^2 — N_d: 1503

Cryst	N_s	N_i	Area	Rho_s	Rho_i	Age [Ma]	σ	U [ppm]
1	81	9	25	132.787	14.754	216.52	76.36	136.19
2	64	7	14	187.354	20.492	219.9	87.8	189.15
3	131	11	16	335.553	28.176	284.98	89.88	260.09
4	76	8	12	259.563	27.322	228.34	85.15	252.2
5	51	5	6	348.361	34.153	244.85	114.98	315.26
6	155	12	25	254.098	19.672	308.53	92.92	181.59
7	96	5	9	437.158	22.769	453.43	208.45	210.17
8	82	10	16	210.041	25.615	197.57	66.45	236.44
9	31	3	8	158.811	15.369	247.99	150.13	141.87
10	54	5	12	184.426	17.077	258.97	121.31	157.63
11	46	4	9	209.472	18.215	275.4	143.8	168.14
12	51	6	12	174.18	20.492	204.68	88.56	189.15
13	76	4	16	194.672	10.246	448.87	230.67	94.58
14	69	7	16	176.742	17.93	236.77	94.19	165.51
15	41	5	9	186.703	22.769	197.57	93.78	210.17
16	30	5	9	136.612	22.769	145.15	70.25	210.17
17	69	5	12	235.656	17.077	329.1	152.74	157.63
18	92	8	16	235.656	20.492	275.4	101.86	189.15
19	182	14	25	298.361	22.951	310.47	86.62	211.85
20	29	4	9	132.058	18.215	174.99	93.48	168.14

Leuggern — Sample: Leu4

ζ = 113.49 ± 1.8 — Dated mineral: zircon

Irrad. code: BS-32 — Rho_d: 4.2554 — Dosimeter glass: CN1

Grid unit: 24.4 μm^2 — N_d: 1503

Cryst	N_s	N_i	Area	Rho_s	Rho_i	Age [Ma]	σ	U [ppm]
1	53	4	15	144.809	10.929	312.26	162.19	102.22
2	76	8	16	194.672	20.492	225.41	84.06	191.66
3	34	5	6	232.24	34.153	162.15	77.82	319.43
4	99	8	12	338.115	27.322	292.1	107.73	255.54
5	79	7	16	202.357	17.93	266.92	105.57	167.7
6	53	5	6	362.022	34.153	251.01	117.68	319.43
7	72	6	9	327.869	27.322	283.44	120.75	255.54
8	50	6	10	204.918	24.59	198.15	85.82	229.99
9	90	9	9	409.836	40.984	237.06	83.19	383.31
10	13	2	4	133.197	20.492	155.08	117.88	191.66
11	26	2	6	177.596	13.661	306.51	225.11	127.77
12	74	8	16	189.549	20.492	219.58	81.99	191.66
13	33	5	6	225.41	34.153	157.43	75.7	319.43
14	95	8	12	324.454	27.322	280.55	103.63	255.54
15	77	7	16	197.234	17.93	260.29	103.06	167.7
16	56	5	6	382.514	34.153	264.93	123.92	319.43
17	77	6	9	350.638	27.322	302.67	128.62	255.54
18	93	11	16	238.217	28.176	200.99	64.37	263.53

19	26	2	8	133.197	10.246	306.51	225.11	95.83
20	49	5	6	334.699	34.153	232.4	109.33	319.43

Siblingen — Sample: Sib1
ζ = 113.49 ± 1.8 — Dated mineral: zircon
Irrad. code: BS-28 — Rho_d: 4.0096 — Dosimeter glass: CN1
Grid unit: 24.4 μm^2 — N_d: 1587

Cryst	N_s	N_i	Area	Rho_s	Rho_i	Age [Ma]	σ	U [ppm]
1	74	9	12	252.732	30.738	184.41	65.33	305.11
2	55	4	9	250.455	18.215	305.49	158.46	180.8
3	79	9	12	269.809	30.738	196.68	69.44	305.11
4	147	21	15	401.639	57.377	157.33	37	569.53
5	126	22	12	430.328	75.137	129.01	30.05	745.82
6	94	13	10	385.246	53.279	162.45	48.31	528.85
7	53	6	9	241.348	27.322	197.91	85.45	271.21
8	68	5	9	309.654	22.769	302.24	140.33	226.01
9	265	13	25	434.426	21.311	447.88	127.92	211.54
10	135	12	12	461.066	40.984	251.01	75.98	406.81
11	48	4	10	196.721	16.393	267.41	139.39	162.72
12	60	4	6	409.836	27.322	332.56	172.02	271.21
13	157	26	15	428.962	71.038	135.95	29.07	705.14
14	95	6	9	432.605	27.322	350.54	147.92	271.21
15	114	9	10	467.213	36.885	281.94	97.98	366.13
16	64	10	6	437.158	68.306	144	49.15	678.02
17	129	7	12	440.574	23.907	406.22	158.11	237.31
18	237	11	30	323.77	15.027	472.47	146.4	149.16
19	49	7	10	200.82	28.689	157.33	63.74	284.77
20	54	5	6	368.852	34.153	241.16	112.96	339.01

Siblingen — Sample: Sib2
ζ = 113.49 ± 1.8 — Dated mineral: zircon
Irrad. code: BS-28 — Rho_d: 3.9916 — Dosimeter glass: CN1
Grid unit: 24.4 μm^2 — N_d: 1587

Cryst	N_s	N_i	Area	Rho_s	Rho_i	Age [Ma]	σ	U [ppm]
1	29	3	6	198.087	20.492	215.32	130.74	204.32
2	36	3	4	368.852	30.738	266.23	160.18	306.48
3	51	6	5	418.033	49.18	189.71	82.07	490.37
4	58	6	6	396.175	40.984	215.32	92.56	408.65
5	99	10	6	676.23	68.306	220.43	73.43	681.08
6	56	5	12	191.257	17.077	248.82	116.37	170.27
7	45	5	5	368.852	40.984	200.7	94.8	408.65
8	47	4	4	481.557	40.984	260.79	136.05	408.65
9	57	10	12	194.672	34.153	127.83	43.99	340.54
10	37	3	4	379.098	30.738	273.47	164.37	306.48
11	12	1	4	122.951	10.246	266.23	277.21	102.16
12	34	5	8	174.18	25.615	152.21	73.04	255.4
13	95	13	8	486.68	66.598	163.43	48.57	664.05
14	151	12	20	309.426	24.59	278.9	84.06	245.19
15	37	6	4	379.098	61.475	138.19	60.95	612.97
16	58	8	6	396.175	54.645	162.16	61.35	544.86
17	43	7	6	293.716	47.814	137.66	56.25	476.75
18	26	3	4	266.393	30.738	193.37	118.05	306.48

19	62	5	9	282.332	22.769	274.92	128.07	227.03
20	33	3	4	338.115	30.738	244.46	147.59	306.48

Siblingen — Sample: Sib3
ζ = 113.49 ± 1.8 — Dated mineral: zircon
Irrad. code: BS-28 — Rho_d: 3.9737 — Dosimeter glass: CN1
Grid unit: 24.4 μm^2 — N_d: 1587

Cryst	N_s	N_i	Area	Rho_s	Rho_i	Age [Ma]	σ	U [ppm]
1	84	6	12	286.885	20.492	308.2	130.56	205.24
2	40	4	5	327.869	32.787	221.63	116.41	328.39
3	100	7	12	341.53	23.907	314.34	123.25	239.45
4	43	4	4	440.574	40.984	237.95	124.59	410.49
5	67	8	12	228.825	27.322	186.13	69.84	273.66
6	155	13	15	423.497	35.519	263.4	76.46	355.75
7	57	5	6	389.344	34.153	252.06	117.8	342.07
8	56	4	6	382.514	27.322	308.2	159.77	273.66
9	28	3	6	191.257	20.492	207.09	125.96	205.24
10	40	3	5	327.869	24.59	293.85	176.12	246.29
11	109	15	15	297.814	40.984	161.81	44.82	410.49
12	64	5	6	437.158	34.153	282.35	131.38	342.07
13	33	6	5	270.492	49.18	122.84	54.64	492.58
14	168	14	36	191.257	15.938	265.06	74.15	159.63
15	70	5	6	478.142	34.153	308.2	142.96	342.07
16	69	6	6	471.311	40.984	254.23	108.47	410.49
17	56	6	9	255.009	27.322	207.09	89.17	273.66
18	73	7	9	332.423	31.876	230.96	91.64	319.27
19	72	8	6	491.803	54.645	199.81	74.7	547.31
20	67	5	6	457.65	34.153	295.29	137.18	342.07

Siblingen — Sample: Sib4
ζ = 113.49 ± 1.8 — Dated mineral: zircon
Irrad. code: BS-28 — Rho_d: 3.9558 — Dosimeter glass: CN1
Grid unit: 24.4 μm^2 — N_d: 1587

Cryst	N_s	N_i	Area	Rho_s	Rho_i	Age [Ma]	σ	U [ppm]
1	58	7	8	297.131	35.861	183.36	73.57	360.8
2	91	9	10	372.951	36.885	223.06	78.23	371.11
3	199	21	25	326.23	34.426	209.28	48.42	346.37
4	75	7	9	341.53	31.876	236.13	93.58	320.71
5	92	13	9	418.944	59.199	156.93	46.73	595.61
6	76	17	8	389.344	87.09	99.58	26.88	876.23
7	57	8	6	389.344	54.645	157.98	59.83	549.79
8	112	15	10	459.016	61.475	165.46	45.76	618.51
9	57	4	6	389.344	27.322	312.19	161.74	274.9
10	55	8	8	281.762	40.984	152.51	57.88	412.34
11	54	12	8	276.639	61.475	100.23	32.13	618.51
12	97	9	10	397.541	36.885	237.5	83.06	371.11
13	93	11	16	238.217	28.176	187.04	59.89	283.49
14	121	8	14	354.215	23.419	330.88	121.19	235.62
15	47	4	6	321.038	27.322	258.5	134.86	274.9
16	101	16	16	258.709	40.984	140.16	37.94	412.34
17	71	5	6	484.973	34.153	311.12	144.25	343.62
18	120	15	12	409.836	51.23	177.12	48.79	515.43

19	44	9	6	300.546	61.475	108.82	39.94	618.51
20	91	6	9	414.39	27.322	331.76	140.18	274.9

Kaisten — Sample: Kai1

ζ = 345.69 $\pm$ 8.75 — Dated mineral: apatite

Irrad. code: BS-29 — Rho_d: 10.7677 — Dosimeter glass: CN5

Grid unit: 63.0 μm^2 — N_d: 4250

Cryst	N_s	N_i	Area	Rho_s	Rho_i	Age [Ma]	σ	U [ppm]
1	36	218	49	11.656	70.585	30.66	5.59	79.78
2	18	80	50	5.712	25.385	41.74	10.96	28.69
3	15	92	49	4.857	29.788	30.27	8.48	33.67
4	35	207	49	11.332	67.023	31.39	5.81	75.75
5	19	83	64	4.71	20.576	42.46	10.87	23.26
6	26	121	64	6.445	29.996	39.87	8.7	33.9
7	34	200	49	11.009	64.757	31.56	5.93	73.19
8	38	134	64	9.42	33.218	52.56	9.79	37.54
9	64	168	100	10.154	26.654	70.51	10.57	30.13
10	14	64	36	6.17	28.205	40.58	12.03	31.88
11	26	90	70	5.893	20.398	53.54	12.03	23.05
12	15	37	36	6.611	16.306	75.01	23.07	18.43
13	24	93	80	4.76	18.444	47.85	11.05	20.85
14	30	89	36	13.221	39.223	62.43	13.31	44.33
15	42	130	100	6.663	20.625	59.85	10.77	23.31
16	43	151	100	6.822	23.957	52.78	9.26	27.08
17	20	72	36	8.814	31.731	51.49	13.1	35.86
18	36	134	70	8.159	30.371	49.81	9.47	34.33
19	18	96	36	7.933	42.308	34.8	9	47.82
20	67	331	100	10.63	52.515	37.56	5.15	59.35

Confined track lengths:

9.8378	9.6467	12.8251	10.8433	7.814
11.6614	9.8364	9.6877	8.6095	10.5416
9.5812	11.374	5.9659	10.8194	10.0453
7.4228	12.5468	6.4611	11.5255	9.7902
11.2595	10.286	10.101	11.397	10.4988
10.1073	6.7777	12.8048	9.2419	11.819
8.2041	8.1154	8.3093	9.2314	9.72
12.2699	11.3445	11.828	10.4101	12.679
11.7509	9.301	10.0861	10.73	8.307
11.2141	12.6308	10.0295	13.0801	8.2168
12.4421	15.172	11.5148	8.384	9.6604
13.3614	10.3233	10.8294	8.7014	12.3025
11.0974	10.3999	12.3111	10.9112	9.0497
12.245	11.7495	11.6152	10.8228	13.2051
13.3851	9.9205	12.1053	10.8646	13.5219
10.4073	10.418	9.4039	10.6397	11.4044
7.0078	11.3868	8.6666	9.4337	11.4185
9.2399	14.1864	12.8997	10.9931	9.4965
11.642	10.5801	13.8258	12.1543	10.0147
11.9487	11.0609	10.6574	6.9767	10.0987

Kaisten		Sample: Kai2
ζ = 345.69 ± 8.75		Dated mineral: apatite
Irrad. code: BS-29	Rho_d: 10.4812	Dosimeter glass: CN5
Grid unit: 63.0 μm^2	N_d: 4250	

Cryst	N_s	N_i	Area	Rho_s	Rho_i	Age [Ma]	σ	U [ppm]
1	11	47	25	6.981	29.827	42.26	14.21	34.63
2	54	170	100	8.567	26.971	57.29	9.11	31.32
3	70	131	49	22.665	42.416	96.08	14.51	49.25
4	27	38	36	11.899	16.747	127.45	32.3	19.45
5	51	152	49	16.513	49.215	60.5	9.95	57.15
6	41	163	49	13.275	52.777	45.41	8.05	61.28
7	41	112	36	18.069	49.359	65.98	12.2	57.31
8	42	149	49	13.599	48.244	50.86	9.01	56.02
9	20	74	36	8.814	32.612	48.78	12.38	37.87
10	112	329	100	17.769	52.197	61.38	6.96	60.61
11	42	124	36	18.51	54.648	61.07	11.05	63.45
12	39	80	36	17.188	35.257	87.72	17.33	40.94
13	35	120	36	15.425	52.885	52.62	10.23	61.41
14	62	208	64	15.37	51.563	53.78	7.94	59.87
15	61	219	64	15.122	54.29	50.26	7.43	63.04
16	53	197	64	13.139	48.836	48.56	7.65	56.7
17	127	460	100	20.149	72.981	49.82	5.21	84.74
18	45	124	36	19.832	54.648	65.41	11.55	63.45
19	43	252	49	13.923	81.594	30.84	5.17	94.74
20	64	228	80	12.692	45.217	50.65	7.32	52.5

Confined track lengths:

11.2419	9.0624	10.2218	9.6166	7.618
10.757	10.969	10.3728	9.301	10.5167
13.5132	13.3648	11.7351	14.3603	12.6313
12.3349	11.5932	11.7702	11.8841	10.3281
9.8701	9.914	10.0823	9.3667	11.617
12.341	12.1008	13.1234	7.1922	12.2866
9.9485	12.1834	11.5469	10.2979	9.9067
10.728	13.873	13.6587	10.3027	11.421
9.7554	15.2632	10.2952	12.4501	12.3639
8.4236	8.8857	9.8704	11.2668	12.3056
9.7641	8.7576	9.4382	10.9507	13.4631
5.4857	10.8036	12.8497	9.6811	10.0631
12.2286	7.6993	10.9787	10.9184	10.2033
8.0412	8.9059	10.9412	13.738	12.8851
9.6555	6.6181	12.7249	11.1713	11.1313
10.1699	9.0332	12.2356	9.5276	12.4469
9.8395	8.4264	9.4669	12.6476	9.1688
11.4935	11.6833	10.4994	9.3768	11.9667
9.6425	10.9998	11.0797	11.2337	12.2779
9.6342	10.2089	9.7084	13.2085	9.8704

Kaisten		Sample: Kai3
ζ = 345.69 ± 8.75		Dated mineral: apatite
Irrad. code: BS-29	Rho_d: 10.1947	Dosimeter glass: CN5
Grid unit: 63.0 μm^2	N_d: 4250	

Cryst	N_s	N_i	Area	Rho_s	Rho_i	Age [Ma]	σ	U [ppm]
1	109	292	70	24.705	66.182	65.44	7.6	79
2	33	52	25	20.942	33	110.87	24.89	39.39
3	33	82	30	17.452	43.366	70.53	14.69	51.77
4	125	284	100	19.832	45.058	77.09	8.58	53.79
5	149	344	100	23.64	54.577	75.88	7.77	65.15
6	157	429	100	24.909	68.063	64.17	6.28	81.25
7	49	107	25	31.096	67.904	80.19	14.04	81.06
8	84	196	60	22.212	51.827	75.08	10.04	61.87
9	146	319	100	23.164	50.611	80.15	8.35	60.42
10	36	52	25	22.846	33	120.85	26.45	39.39
11	66	122	36	29.087	53.766	94.63	14.73	64.18
12	56	111	49	18.132	35.94	88.29	14.71	42.9
13	27	57	25	17.135	36.173	82.93	19.53	43.18
14	24	63	25	15.231	39.981	66.78	16.14	47.73
15	37	62	25	23.481	39.346	104.31	21.89	46.97
16	47	88	25	29.827	55.846	93.43	17.1	66.67
17	61	135	36	26.883	59.495	79.13	12.43	71.02
18	49	114	25	31.096	72.347	75.3	13.05	86.36
19	87	207	100	13.803	32.842	73.64	9.66	39.2
20	29	111	50	9.202	35.221	45.87	9.66	42.05

Confined track lengths:

10.9397	9.7489	11.679	10.3053	11.4451
10.8418	10.3539	12.2651	6.5873	11.1239
11.8645	11.0469	9.7991	10.497	11.5449
14.1083	8.1078	12.2564	8.4616	10.213
7.1263	10.9656	9.9757	12.931	11.6446
11.4711	10.2114	10.2389	11.843	12.5148
10.0823	11.0539	10.079	10.693	11.7942
11.7766	12.1979	10.9656	12.1397	11.4457
12.0108	12.6352	10.305	11.0422	10.8156
10.6972	12.7512	10.9581	9.5917	12.0961
10.0182	12.7368	12.6582	11.7678	10.7405
13.8517	13.1325	12.1636	12.7651	11.0094
11.6525	11.1286	10.8287	13.8294	14.9927
10.9078	11.037	11.6817	12.9523	12.4089
13.0125	10.2199	9.8378	9.3637	15.291
12.5149	11.6883	11.3407	13.4009	12.1232
10.7735	10.5416	11.0486	11.8196	12.4364
13.9609	11.5877	10.6021	10.6192	10.0163
12.5328	10.1342	12.1172	12.8734	13.9487
9.4527	12.1834	10.4646	12.3508	11.2337

Kaisten — Sample: Kai4

ζ = 345.69 ± 8.75 — Dated mineral: apatite

Irrad. code: BS-29 — Rho_d: 9.9082 — Dosimeter glass: CN5

Grid unit: 63.0 μm^2 — N_d: 4250

Cryst	N_s	N_i	Area	Rho_s	Rho_i	Age [Ma]	σ	U [ppm]
1	31	59	100	4.918	9.361	89.36	20	11.5
2	41	80	100	6.505	12.692	87.18	16.94	15.59
3	44	85	100	6.981	13.486	88.05	16.56	16.56

4	40	86	100	6.346	13.644	79.17	15.33	16.76
5	11	21	49	3.562	6.799	89.09	33.26	8.35
6	19	31	60	5.024	8.197	104.12	30.49	10.07
7	20	57	100	3.173	9.043	59.81	15.65	11.11
8	14	41	49	4.533	13.275	58.21	18.1	16.31
9	20	48	100	3.173	7.615	70.97	19	9.35
10	19	67	70	4.306	15.186	48.38	12.66	18.65
11	19	39	80	3.768	7.734	82.9	23.32	9.5
12	11	16	49	3.562	5.181	116.68	45.83	6.36
13	29	53	50	9.202	16.817	93.03	21.66	20.66
14	15	18	49	4.857	5.828	141.16	49.53	7.16
15	17	24	80	3.371	4.76	120.18	38.26	5.85
16	9	25	50	2.856	7.933	61.36	23.92	9.74
17	38	46	70	8.613	10.426	139.94	30.96	12.81
18	15	29	36	6.611	12.781	87.98	28.1	15.7
19	7	12	36	3.085	5.288	99.13	47.24	6.5
20	44	73	100	6.981	11.582	102.41	19.78	14.23

Confined track lengths:

11.2419	13.4015	13.7951	11.6077	9.9205
12.0233	10.8959	13.1808	13.4126	13.3625
11.1971	11.2114	9.4669	11.4051	12.1055
10.8438	11.0661	9.8517	13.6851	14.3598
12.5813	12.7969	12.2927	10.7982	12.5933
10.9787	10.0971	12.4961	9.2419	9.6819
11.299	12.4011	10.5163	12.0969	10.7588
11.8326	13.2206	13.9101	12.4376	9.5848
10.6872	11.4826	11.6604	11.5074	12.8545
9.0611	13.3174	11.0336	9.0562	11.6679
12.8251	9.445	13.7956	13.2647	12.5136
13.1234	10.3108	7.9288	12.8844	9.7411
12.5768	12.4666	13.412	14.4489	10.849
7.1912	11.2771	11.4185	13.1822	8.2948
15.0154	9.6124	11.2442	10.6665	13.7683
11.6136	11.3937	8.969	14.8572	10.6627
12.0068	10.5812	7.8838	12.4762	13.5514
12.2841	10.4587	11.3355	10.849	13.1589
9.6974	13.1503	12.6522	11.5361	10.3087
12.5999	9.111	14.1279	9.1536	11.5694

Riniken — Sample: Rin1

ζ = 345.69 $\pm$ 8.75 — Dated mineral: apatite

Irrad. code: BS-29 — Rho_d: 13.9192 — Dosimeter glass: CN5

Grid unit: 63.0 μm^2 — N_d: 4250

Cryst	N_s	N_i	Area	Rho_s	Rho_i	Age [Ma]	σ	U [ppm]
1	63	195	16	24.033	74.387	77.26	11.43	65.04
2	81	248	16	30.899	94.604	78.1	10.26	82.72
3	66	257	40	10.071	39.215	61.49	8.68	34.29
4	131	267	30	26.652	54.321	116.97	12.95	47.49
5	41	192	12	20.854	97.656	51.17	8.93	85.38
6	38	225	25	9.277	54.932	40.5	7.2	48.03
7	33	237	21	9.591	68.883	33.41	6.29	60.23

8	29	95	30	5.9	19.328	73.03	15.64	16.9
9	28	147	25	6.836	35.889	45.66	9.51	31.38
10	32	199	24	8.138	50.608	38.57	7.43	44.25
11	58	168	16	22.125	64.087	82.53	12.8	56.03
12	44	163	24	11.19	41.453	64.62	11.14	36.24
13	34	124	18	11.529	42.046	65.63	12.85	36.76
14	30	82	20	9.155	25.024	87.42	18.83	21.88
15	52	236	16	19.836	90.027	52.79	8.24	78.71
16	26	60	6	26.449	61.035	103.42	24.47	53.36
17	9	83	12	4.578	42.216	26.04	9.17	36.91
18	43	145	36	7.29	24.584	70.95	12.5	21.49
19	8	60	15	3.255	24.414	32	12.08	21.35
20	18	80	16	6.866	30.518	53.91	14.15	26.68

Confined track lengths:

9.666	7.1164	9.6114	8.3045	13.8836
9.8107	11.7186	7.8754	6.7487	9.7278
9.8654	11.4009	9.1017	7.7146	12.2281
6.6696	7.2903	10.275	13.9265	11.0827
7.5336	10.0041	11.0609	6.9794	11.6932
4.6443	7.4735	9.8646	11.6954	12.4455
5.5016	7.9339	9.4099	10.0241	5.8326
8.8325	8.3896	10.689	11.7864	9.0165
12.1694	9.553	9.2245	8.1014	8.9112
11.0814	10.0568	12.8535	8.6761	9.0778
11.0616	10.5506	10.2766	8.7552	11.2097
11.3038	4.6928	10.8233	8.9072	9.2143
7.2822	5.9962	10.0312	7.0454	10.3962
7.2383	11.4484	10.7807	5.0226	10.9716
7.9196	9.6087	8.6215	12.245	10.5901
12.051	12.7969	10.8418	6.8218	10.5434
9.2796	4.8898	9.4916	8.1822	8.9945
8.3241	7.833	5.6839	9.9067	5.7663
12.5044	10.7498	8.4034	10.6877	10.0542
9.2222	10.9787	4.099	6.9554	8.726

Riniken — Sample: Rin2

ζ = 345.69 ± 8.75 — Dated mineral: apatite

Irrad. code: BS-29 — Rho_d: 13.0597 — Dosimeter glass: CN5

Grid unit: 63.0 μm^2 — N_d: 4250

Cryst	N_s	N_i	Area	Rho_s	Rho_i	Age [Ma]	σ	U [ppm]
1	47	309	25	11.475	75.439	34.24	5.46	70.3
2	139	430	25	33.936	104.98	72.56	7.4	97.83
3	47	244	16	17.929	93.079	43.33	7.02	86.74
4	64	356	24	16.276	90.535	40.45	5.62	84.37
5	173	660	100	10.559	40.283	58.9	5.32	37.54
6	66	186	16	25.177	70.953	79.6	11.65	66.12
7	52	140	25	12.695	34.18	83.3	13.75	31.85
8	94	326	36	15.937	55.271	64.76	7.82	51.51
9	33	122	18	11.19	41.368	60.77	12.06	38.55
10	70	274	36	11.868	46.455	57.41	7.87	43.29
11	17	110	16	6.485	41.962	34.79	9.13	39.1

12	84	300	24	21.362	76.294	62.9	7.98	71.1
13	102	407	36	17.293	69.004	56.32	6.46	64.3
14	116	505	25	28.32	123.291	51.64	5.53	114.89
15	348	1250	100	21.24	76.294	62.54	4.22	71.1
16	507	1820	100	30.945	111.084	62.58	3.65	103.52
17	45	240	12	22.888	122.07	42.19	6.97	113.75
18	76	360	25	18.555	87.891	47.48	6.16	81.9
19	26	79	24	6.612	20.091	73.87	16.84	18.72
20	397	1240	100	24.231	75.684	71.87	4.66	70.53

Confined track lengths:

10.7113	8.2314	10.4499	9.6418	9.8646
12.9019	9.0272	9.0999	9.6828	13.2963
11.8907	7.3394	9.2388	11.7113	10.6857
10.693	6.4153	5.6539	11.874	10.1232
8.1148	8.2271	10.5192	10.693	11.231
8.4616	8.2948	10.5147	8.6379	10.5472
10.8305	8.6119	9.6425	8.6891	11.9665
9.9331	10.3576	10.7807	11.5737	11.1905
10.6432	7.9277	8.7979	11.2652	7.0931
9.0939	7.6504	10.0305	4.9887	7.2838
11.4051	4.2182	13.4878	10.1718	13.4141
8.6948	9.3969	13.0814	4.7527	10.0076
5.4964	11.3563	9.8747	5.1268	9.2626
5.0857	9.6887	7.24	8.8503	10.5961
8.6957	8.2888	7.1084	8.8442	10.7553
7.4085	8.9643	10.0528	8.2512	10.9563
4.9259	9.1472	7.1824	7.627	7.5414
7.9657	8.8676	9.0502	7.6507	13.2313
9.5085	8.7317	4.399	5.1005	7.4453
10.1379	14.1924	7.7497	8.9606	13.6741

Riniken — Sample: Rin3

ζ = 345.69 $\pm$ 8.75 — Dated mineral: apatite

Irrad. code: BS-29 — Rho_d: 12.7732 — Dosimeter glass: CN5

Grid unit: 63.0 μm^2 — N_d: 4250

Cryst	N_s	N_i	Area	Rho_s	Rho_i	Age [Ma]	σ	U [ppm]
1	43	139	25	10.498	33.936	67.94	12.02	32.33
2	76	257	24	19.328	65.358	64.96	8.7	62.27
3	23	94	16	8.774	35.858	53.8	12.62	34.16
4	84	273	36	14.242	46.285	67.58	8.67	44.1
5	302	920	60	30.721	93.587	72.07	5.23	89.17
6	57	175	16	21.744	66.757	71.51	11.11	63.6
7	37	117	15	15.055	47.607	69.44	13.26	45.36
8	66	260	20	20.142	79.346	55.8	7.87	75.6
9	112	420	25	27.344	102.539	58.61	6.47	97.7
10	43	94	16	16.403	35.858	100.21	18.69	34.16
11	166	661	36	28.144	112.067	55.21	5.06	106.78
12	69	173	24	17.548	43.996	87.46	12.72	41.92
13	53	195	24	13.479	49.591	59.73	9.42	47.25
14	50	197	24	12.716	50.1	55.79	8.99	47.73
15	65	201	16	24.796	76.675	71	10.35	73.05

16	65	245	25	15.869	59.814	58.31	8.32	56.99
17	47	248	36	7.968	42.046	41.71	6.75	40.06
18	49	220	25	11.963	53.711	48.99	7.87	51.17
19	52	160	16	19.836	61.035	71.36	11.58	58.15
20	45	165	25	10.986	40.283	59.93	10.23	38.38

Confined track lengths:

9.7157	12.0176	12.2031	10.7313	8.4816
9.5456	5.6288	10.3853	12.8447	7.2253
9.9852	10.6474	11.7662	7.1491	8.8812
9.7198	9.0021	8.6707	10.2573	9.1105
11.2652	9.5533	12.1694	11.8595	7.9303
9.165	7.0614	9.5258	10.8809	10.4427
9.9698	13.4064	13.33	11.1031	9.7653
8.9945	10.3935	11.9546	9.3442	11.0334
12.4618	10.6275	11.0148	9.7518	9.3523
10.8646	7.1425	10.3464	10.1372	10.4012
10.5167	10.8228	8.9112	10.8418	9.5708
7.9005	10.3903	9.4159	9.382	12.0052
8.1223	10.5398	10.1864	10.2979	11.3374
10.3546	10.5908	7.761	6.416	12.3401
8.9152	9.8155	5.2662	7.3557	10.4284
9.6582	8.3297	6.6426	9.6269	11.0967
11.5418	9.4119	11.3207	5.3819	10.7546
11.3756	8.9769	10.7438	10.4071	8.9453
11.7576	8.2176	10.2538	11.3503	10.0302
10.7754	10.3655	5.9607	11.1184	9.8241

Riniken — Sample: Rin4

ζ = 345.69 $\pm$ 8.75 — Dated mineral: apatite

Irrad. code: BS-29 — Rho_d: 12.2002 — Dosimeter glass: CN5

Grid unit: 63.0 μm^2 — N_d: 4250

Cryst	N_s	N_i	Area	Rho_s	Rho_i	Age [Ma]	σ	U [ppm]
1	35	135	15	14.242	54.932	54.44	10.45	54.8
2	41	170	25	10.01	41.504	50.66	8.94	41.4
3	100	354	60	10.173	36.011	59.3	6.94	35.92
4	47	170	21	13.66	49.409	58.04	9.72	49.29
5	62	189	16	23.651	72.098	68.81	10.27	71.92
6	44	192	25	10.742	46.875	48.15	8.17	46.76
7	50	107	12	25.431	54.423	97.79	17	54.29
8	79	230	18	26.788	77.989	72.03	9.63	77.8
9	54	124	25	13.184	30.273	91.18	15.11	30.2
10	113	445	100	6.897	27.161	53.33	5.84	27.09
11	91	238	25	22.217	58.105	80.13	10.16	57.96
12	52	187	36	8.816	31.704	58.37	9.31	31.63
13	38	115	25	9.277	28.076	69.31	13.13	28.01
14	26	97	15	10.579	39.469	56.28	12.54	39.37
15	30	120	25	7.324	29.297	52.5	10.83	29.22
16	63	276	25	15.381	67.383	47.96	6.84	67.22
17	32	161	25	7.813	39.307	41.78	8.18	39.21
18	71	174	25	17.334	42.48	85.48	12.3	42.38
19	29	109	16	11.063	41.58	55.86	11.79	41.48

20	23	70	15	9.359	28.483	68.92	16.69	28.41

Confined track lengths:

7.4912	6.0861	10.5149	9.0016	8.9469
8.4914	10.6368	11.7752	10.5418	11.1016
9.8133	9.559	10.5905	13.2094	11.0135
8.7317	6.3264	6.8649	11.4274	9.3475
12.754	10.8331	8.7993	11.7608	11.2217
13.5785	10.2019	10.5881	8.0179	11.4028
11.9359	8.8156	11.1551	10.4107	10.6414
8.5721	10.4302	10.0605	9.7709	11.2
11.82	7.0574	13.2308	15.1904	15.2875
8.8844	9.8895	9.3151	8.224	9.2427
8.9302	8.4311	9.5147	9.3402	10.3683
8.3402	7.3358	14.7294	10.7392	10.1085
8.1069	7.9184	10.0076	10.7999	10.116
9.3134	7.2514	11.2183	9.9331	12.0451
10.7735	10.5801	7.947	9.7709	11.5721
12.1543	10.4706	13.6527	9.4407	10.0474
11.2131	10.1588	11.4639	12.8735	10.6379
10.3921	10.2326	8.552	8.4185	11.3355
12.9268	10.1681	11.9382	10.9008	11.5565
12.252	10.6698	8.7403	6.9251	12.2087

Riniken — Sample: Rin5

ζ = 345.69 $\pm$ 8.75 — Dated mineral: apatite

Irrad. code: BS-29 — Rho_d: 11.3407 — Dosimeter glass: CN5

Grid unit: 63.0 μm^2 — N_d: 4250

Cryst	N_s	N_i	Area	Rho_s	Rho_i	Age [Ma]	σ	U [ppm]
1	34	40	16	12.97	15.259	164.5	38.68	16.37
2	16	74	25	3.906	18.066	42.24	11.71	19.39
3	27	57	20	8.24	17.395	92.19	21.71	18.67
4	93	210	25	22.705	51.27	86.23	11.04	55.02
5	45	104	25	10.986	25.391	84.26	15.24	27.25
6	68	232	16	25.94	88.501	57.2	8.07	94.97
7	71	248	25	17.334	60.547	55.88	7.7	64.97
8	58	156	16	22.125	59.509	72.47	11.35	63.86
9	32	76	25	7.813	18.555	82.01	17.45	19.91
10	75	320	25	18.311	78.125	45.78	6.03	83.84
11	256	760	50	31.25	92.773	65.69	5.13	99.56
12	53	209	25	12.939	51.025	49.52	7.76	54.76
13	51	132	16	19.455	50.354	75.29	12.61	54.04
14	146	281	36	24.753	47.641	101.05	10.73	51.13
15	80	224	20	24.414	68.359	69.63	9.3	73.36
16	37	121	16	14.114	46.158	59.66	11.35	49.53
17	37	89	16	14.114	33.951	80.98	16.02	36.43
18	25	68	20	7.629	20.752	71.67	16.9	22.27
19	41	105	16	15.64	40.054	76.09	14.19	42.98
20	79	200	25	19.287	48.828	76.97	10.48	52.4

Confined track lengths:

11.6055	12.9164	9.9693	4.339	11.1239
11.1667	8.8046	9.571	11.5306	11.0614
12.444	11.7564	8.9292	12.2656	10.4562
6.2381	12.4484	11.4896	12.9569	9.8164
9.0544	8.2546	11.4781	9.1348	11.7622
10.5228	9.0812	9.9975	11.6883	10.0558
10.6574	6.0772	10.1383	10.3071	12.4089
8.0707	9.2427	10.834	10.1957	9.6291
9.0147	11.1279	11.5867	8.9976	9.8133
7.5586	12.4034	9.9464	9.878	8.7936
9.8328	14.2269	10.6397	6.6216	8.7684
7.6603	10.0783	7.5573	10.4555	10.7787
10.7616	12.4247	9.496	7.586	9.1505
9.7373	9.7702	11.3777	6.2453	10.1774
10.8872	10.6228	12.4567	10.6059	11.4639
9.6308	13.0814	11.5224	11.0693	9.0999
10.512	10.7313	12.4421	12.3134	9.0895
13.6416	12.3134	9.8316	12.0086	9.4047
9.9295	9.4938	9.2102	8.1171	9.438
9.3101	11.4102	9.3969	9.5285	10.5436

Leuggern — Sample: Leu1

ζ = 345.69 $\pm$ 8.75 — Dated mineral: apatite

Irrad. code: BS-34 — Rho_d: 11.2374 — Dosimeter glass: CN5

Grid unit: 63.0 μm^2 — N_d: 1660

Cryst	N_s	N_i	Area	Rho_s	Rho_i	Age [Ma]	σ	U [ppm]
1	8	143	50	2.538	45.375	10.86	3.96	49.14
2	27	124	49	8.742	40.149	42.15	9.07	43.48
3	18	197	40	7.139	78.137	17.72	4.41	84.62
4	15	146	30	7.933	77.212	19.92	5.45	83.62
5	27	88	60	7.139	23.269	59.32	13.22	25.2
6	52	479	70	11.786	108.565	21.05	3.16	117.57
7	4	31	20	3.173	24.591	25.01	13.32	26.63
8	24	143	30	12.692	75.625	32.52	7.26	81.9
9	16	155	30	8.462	81.972	20.02	5.3	88.77
10	69	520	70	15.639	117.858	25.72	3.42	127.64
11	13	137	30	6.875	72.452	18.4	5.38	78.47
12	11	113	49	3.562	36.588	18.88	6	39.62
13	12	139	24	7.933	91.887	16.75	5.07	99.51
14	33	365	50	10.471	115.818	17.54	3.25	125.43
15	24	118	60	6.346	31.202	39.38	8.93	33.79
16	18	134	40	7.139	53.149	26.04	6.6	57.56
17	16	139	50	5.077	44.106	22.32	5.94	47.77
18	13	67	30	6.875	35.433	37.58	11.47	38.37
19	7	97	20	5.553	76.947	14	5.5	83.33
20	18	128	36	7.933	56.411	27.26	6.93	61.09

Confined track lengths:

11.2015	11.2538	7.2004	8.4838	13.5604
10.3921	11.2802	8.234	10.5818	14.5674
9.7118	9.8359	11.9645	9.7974	9.0439
9.9485	8.3696	12.729	9.9143	10.9484

10.3053	14.922	10.6972	11.8326	9.5496
7.6006	14.1462	13.734	16.1482	7.725
13.3034	11.3022	10.5718	11.1667	12.2327
10.2545	12.2143	11.8853	12.1685	13.1578
10.8198	9.5799	9.3032	12.1791	10.4064
11.4342	8.0412	9.7653	12.2841	11.3091
12.3822	8.9756	8.2145	15.2012	12.8131
9.9568	8.8791	10.6806	13.9649	11.3821
11.0641	10.5042	10.9639	11.5989	10.1104
12.9572	5.032	10.4994	11.1642	11.5255
10.338	8.8626	13.0038	12.3096	12.0944
9.8902	13.2769	15.8234	8.5851	11.7395
15.2688	16.0983	11.455	11.6679	11.0507
13.4212	11.9392	14.9711	11.1506	11.297
13.67	12.5044	6.3238	8.4042	12.6293
13.2428	12.4423	12.8234	12.0776	10.5091

Leuggern — Sample: Leu2

ζ = 345.69 $\pm$ 8.75 — Dated mineral: apatite

Irrad. code: BS-38 — Rho_d: 11.4661 — Dosimeter glass: CN5

Grid unit: 63.0 μm^2 — N_d: 3690

Cryst	N_s	N_i	Area	Rho_s	Rho_i	Age [Ma]	σ	U [ppm]
1	3	15	10	4.76	23.798	39.52	25.02	25.26
2	8	40	28	4.533	22.665	39.52	15.35	24.06
3	5	21	20	3.966	16.659	47.02	23.44	17.68
4	6	13	16	5.95	12.891	90.83	44.91	13.68
5	6	30	16	5.95	29.748	39.52	17.71	31.57
6	11	60	50	3.49	19.039	36.23	11.93	20.21
7	18	83	50	5.712	26.337	42.84	11.21	27.95
8	12	70	36	5.288	30.85	33.89	10.64	32.74
9	13	49	50	4.125	15.548	52.37	16.41	16.5
10	7	33	36	3.085	14.543	41.9	17.48	15.44
11	5	38	36	2.204	16.747	26.02	12.41	17.77
12	6	39	24	3.966	25.781	30.42	13.37	27.36
13	4	33	28	2.266	18.699	23.98	12.72	19.85
14	5	34	24	3.305	22.476	29.08	13.96	23.86
15	3	15	16	2.975	14.874	39.52	25.02	15.79
16	5	20	16	4.958	19.832	49.36	24.72	21.05
17	5	29	36	2.204	12.781	34.08	16.53	13.57
18	7	92	60	1.851	24.327	15.06	5.92	25.82
19	5	62	49	1.619	20.075	15.96	7.44	21.31
20	7	81	36	3.085	35.697	17.1	6.76	37.89

Confined track lengths:

10.4073	15.7329	9.3243	8.7533	13.7486
10.969	12.899	9.9977	10.0474	
11.827	13.3699	8.2214	7.5047	
10.2695	11.8008	9.747	10.3498	
11.799	11.5761	13.9204	12.7064	

Leuggern — Sample: Leu3

ζ = 345.69 ± 8.75 Dated mineral: apatite
Irrad. code: BS-38 Rho_d: 9.1722 Dosimeter glass: CN5
Grid unit: 63.0 μm^2 N_d: 3690

Cryst	N_s	N_i	Area	Rho_s	Rho_i	Age [Ma]	σ	U [ppm]
1	21	33	25	13.327	20.942	100.11	28.11	27.79
2	29	56	40	11.502	22.212	81.58	18.83	29.47
3	38	82	40	15.072	32.524	73.05	14.5	43.15
4	38	102	50	12.058	32.366	58.79	11.31	42.94
5	50	143	60	13.221	37.813	55.2	9.22	50.17
6	87	156	60	23.005	41.25	87.81	12.05	54.73
7	28	88	42	10.577	33.242	50.25	11.01	44.11
8	13	41	24	8.594	27.103	50.07	16.01	35.96
9	24	54	36	10.577	23.798	70.08	17.32	31.58
10	27	48	36	11.899	21.154	88.57	21.47	28.07
11	61	140	40	24.195	55.529	68.71	10.74	73.68
12	14	30	25	8.885	19.039	73.56	23.91	25.26
13	23	51	25	14.596	32.366	71.1	17.99	42.94
14	23	42	36	10.136	18.51	86.24	22.52	24.56
15	27	54	24	17.849	35.697	78.79	18.72	47.36
16	39	89	50	12.375	28.241	69.1	13.43	37.47
17	22	46	36	9.696	20.273	75.38	19.67	26.9
18	33	86	28	18.699	48.73	60.55	12.53	64.66
19	111	295	100	17.611	46.803	59.38	6.85	62.1
20	19	45	35	8.613	20.398	66.59	18.33	27.07

Confined track lengths:

8.1479	10.0528	12.9408	12.3634	4.5306
10.2646	9.1536	10.6275	8.9321	11.7848
11.231	13.3699	10.5114	13.4631	7.4817
10.7113	12.5006	7.5984	9.8414	10.7966
4.7844	12.8528	12.7398	12.0233	10.0865
6.3895	10.3108	6.6127	10.1073	8.8794
7.5386	12.6774	8.2592	6.5626	10.6075
10.7528	10.7735	12.0821	8.4199	10.213
10.9114	11.1222	11.1371	9.0986	6.9401
9.1619	9.1927	6.4593	10.3628	10.1725
8.3198	10.4227	11.2821	8.6207	10.6713
10.5765	10.8496	9.4199	8.8314	9.6889
13.4305	8.4076	8.3535	9.8078	12.2535
9.249	11.0931	10.723	9.1102	9.5414
11.0812	7.3512	9.0063	9.0413	14.521
10.9662	10.4562	10.8331	10.7078	14.2754
12.1669	8.2812	12.1242	10.5383	11.2612
11.3678	11.6306	9.895	10.4643	12.0508
14.1537	8.8674	7.0199	10.6899	10.0823
12.4045	8.7008	10.7894	6.3219	11.2152

Leuggern Sample: Leu4
ζ = 345.69 ± 8.75 Dated mineral: apatite
Irrad. code: BS-38 Rho_d: 9.3487 Dosimeter glass: CN5
Grid unit: 63.0 μm^2 N_d: 3690

Cryst	N_s	N_i	Area	Rho_s	Rho_i	Age [Ma]	σ	U [ppm]

1	9	35	45	3.173	12.34	41.42	15.53	16.06
2	44	155	100	6.981	24.591	45.71	7.93	32.01
3	67	181	100	10.63	28.716	59.54	8.7	37.38
4	22	73	70	4.986	16.545	48.51	11.89	21.54
5	15	29	49	4.857	9.39	83.04	26.53	12.22
6	51	138	100	8.091	21.894	59.44	9.9	28.5
7	48	128	100	7.615	20.308	60.31	10.37	26.44
8	10	42	60	2.644	11.106	38.36	13.55	14.46
9	58	149	100	9.202	23.64	62.59	9.87	30.77
10	52	133	100	8.25	21.101	62.87	10.46	27.47
11	53	88	70	12.012	19.945	96.59	17.05	25.96
12	9	23	25	5.712	14.596	62.92	24.81	19
13	13	42	36	5.729	18.51	49.82	15.88	24.1
14	44	103	60	11.635	27.236	68.66	12.54	35.46
15	37	79	80	7.338	15.667	75.24	15.16	20.4
16	28	38	36	12.34	16.747	117.98	29.6	21.8
17	31	107	100	4.918	16.976	46.65	9.62	22.1
18	43	146	100	6.822	23.164	47.42	8.35	30.15
19	53	133	100	8.409	21.101	64.07	10.59	27.47
20	32	73	64	7.933	18.097	70.45	15.09	23.56

Confined track lengths:

9.5164	12.6783	12.5976	8.9099	9.8938
10.3197	11.5163	12.3065	15.7049	7.7583
10.8566	11.5279	8.0215	12.0666	7.7439
7.8466	7.6541	9.6675	9.7322	10.0107
8.5465	11.6992	10.2366	11.1375	9.0126
7.516	10.7577	9.6224	11.8406	10.9959
7.9017	7.8751	9.8078	10.5655	9.1309
11.2165	7.8586	10.7216	9.0697	10.7859
9.7025	9.7394	8.6978	10.6432	8.1756
10.5114	13.5151	11.1424	10.4749	11.8597
8.3479	8.0874	11.6477	10.0012	13.2255
7.6871	7.0681	8.8033	9.5819	13.0483
8.2194	12.5375	9.3737	9.6682	9.2809
10.9845	10.9101	8.6783	7.5882	10.4806
11.9103	9.7653	8.713	10.0453	7.3932
7.768	12.2971	10.9759	13.6665	11.5875
11.9714	7.044	10.7658	11.0216	9.7953
9.9958	12.4923	8.7338	10.8052	11.8008
12.2097	11.9026	10.3007	6.6302	8.3181
9.5256	8.9848	10.2793	6.9098	10.3108

Siblingen		Sample: Sib1
ζ = 345.69 $\pm$ 8.75		Dated mineral: apatite
Irrad. code: BS-29	Rho_d: 9.0487	Dosimeter glass: CN5
Grid unit: 63.0 μm^2	N_d: 4250	

Cryst	N_s	N_i	Area	Rho_s	Rho_i	Age [Ma]	σ	U [ppm]
1	28	102	25	17.769	64.731	42.79	9.22	87.06
2	36	140	36	15.865	61.699	40.09	7.59	82.98
3	16	63	25	10.154	39.981	39.6	11.15	53.77

4	21	98	36	9.255	43.189	33.43	8.1	58.09
5	26	92	16	25.781	91.226	44.05	9.87	122.69
6	35	111	16	34.706	110.067	49.13	9.63	148.03
7	37	139	80	7.338	27.566	41.5	7.77	37.08
8	27	52	25	17.135	33	80.7	19.29	44.38
9	9	33	25	5.712	20.942	42.51	16.04	28.17
10	98	360	100	15.548	57.116	42.44	5	76.82
11	23	68	25	14.596	43.154	52.68	12.8	58.04
12	51	126	36	22.476	55.529	63	10.62	74.68
13	14	47	25	8.885	29.827	46.42	14.2	40.12
14	25	53	25	15.865	33.635	73.36	17.93	45.24
15	34	99	30	17.981	52.356	53.49	10.75	70.42
16	12	35	16	11.899	34.706	53.4	17.93	46.68
17	9	25	9	15.865	44.071	56.06	21.86	59.27
18	10	38	16	9.916	37.68	41.03	14.63	50.68
19	14	69	25	8.885	43.789	31.66	9.33	58.89
20	17	50	25	10.789	31.731	52.96	14.95	42.68

Confined track lengths:

11.7083	9.6224	10.5807	6.483	8.6125
12.99	8.1649	13.1912	6.7568	13.5541
11.4867	7.1319	10.9931	9.3273	8.6576
11.2141	12.4395	11.5191	13.7046	14.4108
11.6315	9.828	12.5751	10.2842	8.5754
9.5523	12.5051	12.5119	10.43	11.1246
11.0146	11.1239	8.4501	14.013	
14.2291	10.6698	14.2003	10.2142	

Siblingen — Sample: Sib3

ζ = 345.69 ± 8.75 — Dated mineral: apatite

Irrad. code: BS-29 — Rho_d: 8.4757 — Dosimeter glass: CN5

Grid unit: 63.0 μm^2 — N_d: 4250

Cryst	N_s	N_i	Area	Rho_s	Rho_i	Age [Ma]	σ	U [ppm]
1	24	120	25	15.231	76.154	29.23	6.59	109.35
2	15	50	20	11.899	39.664	43.8	12.96	56.95
3	84	153	25	53.308	97.097	79.93	11.11	139.42
4	15	51	20	11.899	40.457	42.94	12.68	58.09
5	18	31	20	14.279	24.591	84.51	25.17	35.31
6	50	97	25	31.731	61.558	75.08	13.26	88.39
7	18	37	25	11.423	23.481	70.88	20.48	33.72
8	25	64	25	15.865	40.616	56.97	13.54	58.32
9	37	82	25	23.481	52.039	65.77	13.17	74.72
10	36	82	36	15.865	36.138	64	12.93	51.89
11	28	65	25	17.769	41.25	62.8	14.32	59.23
12	40	69	16	39.664	68.42	84.37	16.95	98.24
13	29	63	16	28.756	62.47	67.09	15.18	89.7
14	38	133	36	16.747	58.614	41.72	7.77	84.16
15	31	85	16	30.739	84.285	53.21	11.27	121.02
16	15	51	16	14.874	50.571	42.94	12.68	72.61
17	17	29	16	16.857	28.756	85.31	26.18	41.29
18	37	94	25	23.481	59.654	57.41	11.27	85.66
19	61	104	36	26.883	45.834	85.36	14	65.81

20	39	118	40	15.469	46.803	48.24	9.02	67.2

Confined track lengths:

12.729	10.213	9.6033	8.5611	13.2682
10.4071	9.6205	11.0417	7.4225	8.5365
10.9432	11.9724	9.0905	7.9098	13.7194
4.7129	10.7675	7.2608	6.9554	12.8107
9.5678	13.3838	6.7452	12.3876	12.2317
11.3937	9.3235	11.7373	9.2938	12.1793
9.9509	10.5147	9.5799	9.9312	13.4029
10.4607	13.09	12.0912	9.7023	12.1685
8.48	15.9411	9.9596	10.1232	10.7335
11.6863	10.4562	11.7974	11.5025	13.1115
9.4089	11.0539	13.7971	7.6993	11.762
10.5096	10.7675	11.5214	10.8287	14.0049
10.4742	10.7999	10.428	11.3939	9.3996
11.3397	8.0014	9.4021	11.9676	10.6075
13.0025	9.3768	9.7331	10.8566	14.301
12.1685	12.1708	13.5924	10.2991	12.996
11.299	8.5743	13.5477	11.2802	9.2552
13.0206	10.2428	12.5091	14.7506	11.5142
8.5724	10.0276	10.021	9.9464	10.3375
7.2165	11.7884	8.5113	12.0617	9.4841

Siblingen — Sample: Sib4

ζ = 345.69 $\pm$ 8.75 — Dated mineral: apatite

Irrad. code: BS-29 — Rho_d: 8.1892 — Dosimeter glass: CN5

Grid unit: 63.0 μm^2 — N_d: 4250

Cryst	N_s	N_i	Area	Rho_s	Rho_i	Age [Ma]	σ	U [ppm]
1	14	20	12	18.51	26.442	98.33	34.39	39.3
2	17	57	16	16.857	56.521	42.08	11.69	84
3	34	53	16	33.714	52.554	90.17	19.99	78.1
4	46	61	12	60.818	80.649	105.87	20.91	119.85
5	27	30	25	17.135	19.039	126.15	33.67	28.29
6	51	71	16	50.571	70.403	100.88	18.76	104.63
7	19	30	9	33.494	52.885	89.03	26.24	78.59
8	28	79	20	22.212	62.669	49.97	11.09	93.13
9	14	28	9	24.68	49.359	70.39	23.13	73.35
10	18	46	12	23.798	60.818	55.15	15.42	90.38
11	18	55	16	17.849	54.538	46.16	12.61	81.05
12	8	39	9	14.103	68.75	28.97	11.28	102.17
13	23	51	15	24.327	53.943	63.52	16.06	80.16
14	33	49	16	32.723	48.588	94.63	21.49	72.21
15	13	24	18	11.458	21.154	76.22	26.34	31.44
16	51	84	16	50.571	83.294	85.37	15.36	123.78
17	45	58	9	79.327	102.244	108.9	21.87	151.95
18	37	40	16	36.689	39.664	129.62	29.81	58.94
19	27	42	9	47.596	74.039	90.36	22.45	110.03
20	8	9	16	7.933	8.924	124.61	60.66	13.26

Confined track lengths:

8.449
12.9539
10.2003
12.3678
11.1016
11.7998
10.8625
11.4951
9.8666
12.8785
9.4422
13.6241
12.9909
8.3297
5.169
14.0155
12.3716
8.6557
12.2327
10.8575

CURRICULUM VITAE

Zoltan Timar-Geng

Personal details

Date of birth: 23.01.1973
Place of birth: Carei / Romania
Nationality: German

Working address:
Geological-Paleontological Institute
University of Basel
Bernoullistrasse 32
CH-4056 Basel

Private address:
Oberer Kirchweg 19
D-79112 Freiburg

E-mail: zoltan.timar-geng@unibas.ch

Studies

Aug. 2000 – Febr. 2005	PhD in Geology: „Post-Variscan thermal evolution of the flanks of the southern Upper Rhine Graben: fission-track analyses and thermal modelling.“
Oct. 1995 – July 2000	Studying Geology at the Albert-Ludwigs-Universität Freiburg. „Diploma“ in Geology: „Strukturgeologische Untersuchungen im Leventina-Tal und kinematische Analyse von Quarztexturen aus dem Bereich der Deckengrenze zwischen Leventina- und Simano-Decke, Kanton Tessin, Schweiz“.

Practical training

March 1998 – April 1998	Hydro-Data, Ballrechten-Dottingen, Germany Hydrogeological investigations.
June 1997 – July 1997	Terratec, Heitersheim, Germany Geophysical services.